2015

Volcanic Stratigraphy and Lithogeochemistry of the Northern Section of the Lynn Lake Greenstone Belt: Implications for Regional Geodynamics and Metallogenesis

Michael W.P. Glendenning
University of Windsor

Volcanic Stratigraphy and Lithogeochemistry of the Northern Section of the Lynn Lake Greenstone Belt: Implications for Regional Geodynamics and Metallogenesis

By

Michael W.P. Glendenning Jr.

A Thesis
Submitted to the Faculty of Graduate Studies
through the Department of Earth and Environmental Sciences
in Partial Fulfillment of the Requirements for
the Degree of Master of Science
at the University of Windsor

Windsor, Ontario, Canada

2014

Volcanic Stratigraphy and Lithogeochemistry of the Northern Section of the Lynn Lake Greenstone Belt: Implications for Regional Geodynamics and Metallogenesis

by

Michael W.P. Glendenning Jr.

APPROVED BY:

_____

Dr. J. Gauld
Department of Chemistry and Biochemistry

_____

Dr. I. Samson
Department of Earth and Environmental Sciences

_____

Dr. J. E. Gagnon (Advisor)
Department of Earth and Environmental Sciences

_____

Dr. A. Polat (Advisor)
Department of Earth and Environmental Sciences

September 26, 2014

Author's Declaration of Originality

I hereby certify that I am the sole author of this thesis and that no part of this thesis has been published or submitted for publication.

I certify that, to the best of my knowledge, my thesis does not infringe upon anyone's copyright nor violate any proprietary rights and that any ideas, techniques, quotations, or any other material from the work of other people included in my thesis, published or otherwise, are fully acknowledged in accordance with the standard referencing practices. Furthermore, to the extent that I have included copyrighted material that surpasses the bounds of fair dealing within the meaning of the Canada Copyright Act, I certify that I have obtained a written permission from the copyright owner(s) to include such material(s) in my thesis and have included copies of such copyright clearances to my appendix.

I declare that this is a true copy of my thesis, including any final revisions, as approved by my thesis committee and the Graduate Studies office, and that this thesis has not been submitted for a higher degree to any other University or Institution.

“When you have eliminated the impossible, whatever remains, however improbable, must be the truth”

Sherlock Holmes, written by Arthur Conan Doyle Sr.

Abstract

The MacLellan Au-Ag deposit, located in the Paleoproterozoic Lynn Lake greenstone belt of the Trans-Hudson Orogen, Manitoba, is hosted by a package of plagioclase-amphibole, chlorite-amphibole, and quartz-plagioclase-biotite schists that are considered to be representative of the geodynamic evolution of the northern section of the Lynn Lake greenstone belt. A combination of field and petrographic observations and high-precision trace element chemistry have identified the protoliths to the host rock sequence as transitional aluminous basalt with subordinate picrite and biotite-altered aluminous basalt, respectively. The Th-Nb-La-REE systematics of these rocks are consistent with a rifted continental margin environment. Volcanic rocks with similar Th-Nb-La-REE systematics to those from the MacLellan host rock sequence have been identified throughout the Lynn Lake region. Therefore, it is proposed that the Lynn Lake greenstone belt represents a rifted continental margin and based on this revised geodynamic model, the mineral potential of the belt should be reassessed.

Acknowledgements

I wish to thank the following people for their support:

- Dr. Joel Gagnon for having both the time and the extreme patience to guide me down the arduous path of a researcher and for instilling in me the importance of both objectivity and excitement while on the long road to scientific discovery;
- Dr. Ali Polat for taking the time to pass on his genuine excitement for discovery, mentoring me in the finer points of applying geochemical techniques to geological problems, and for his unique way of leading you to answers through self-discovery;
- Peter Karelse for his incredible support, patience, and his genuine excitmenet in this project;
- Dr. Iain Samson for providing insights into metallogenic processes and for always providing thought provoking feedback;
- Dr. James Gauld for his patience and for agreeing to sit on my committee;
- Ben Lane for both his interest and assistance in Lynn Lake, despite his lack of hand-eye coordination (you know what you did);
- The support staff of Carlisle Goldfields who were always ready for a night on the lake after a long day despite always having to clean the fish;
- My colleagues from the Department of Earth and Environmental Sciences for providing an oft desired mental break; and,
- My wife and family for their support and their interest in this project.

Table of Contents

List of Figures

List of Appendicies

CHAPTER 1

INTRODUCTION

1.1. Overview

The host rock sequence to the MacLellan Au-Ag deposit, which is located approximately 8 km northeast of Lynn Lake, Manitoba (Fig. 1), has been interpreted by researchers (e.g., Fedikow and Gale, 1982; Fedikow, 1986, 1992; Zwanzig et al., 1999;Ma and Beaumont-Smith, 2000; Ma et al., 2001; Gale and McClenaghan, 2002; Park et al., 2002; Beaumont-Smith and Böhm, 2003; Gale, 2003; Beaumont-Smith and Böhm, 2004; Gale et al., 2004) to be characteristic of the tectonic evolution and metallogenic potential of the northern half of the Lynn Lake greenstone belt. Originally defined as a subaqueous, syngenetic, stratiform exhalative deposit by Fedikow and Gale (1982) and Fedikow (1986, 1992), the MacLellan deposit was reclassified as an epigenetic, vein-associated, deposit by Gagnon (1991) and Samson and Gagnon (1995) and subsequent work by Ma and Beaumont-Smith (2000) supported this interpretation. More recent local and regional studies (e.g., Zwanzig et al., 1999; Ma and Beaumont-Smith, 2001; Ma et al., 2001; Gale and McClenaghan, 2002; Park et al., 2002; Beaumont-Smith and Böhm, 2003; Gale, 2003; Beaumont-Smith and Böhm, 2004; Gale et al., 2004), however, employed the tectonic and metallogenic model for the MacLellan Au-Ag deposit of Fedikow and Gale (1982) and Fedikow (1986, 1992) when discussing the tectonic evolution and metallogenic potential of the northern portion of the Lynn Lake greenstone belt. The broader application of a model based on a syngenetic, exhalative interpretation of the host rock sequence to the MacLellan Au-Ag deposit (e.g., Fedikow

and Gale, 1982; Fedikow, 1986, 1992) to the Lynn Lake greenstone belt has resulted in contradictory regional- and deposit-scale tectonic and metallogenic interpretations for both the host rock sequence to the MacLellan deposit and the Lynn Lake greenstone belt.

To ascertain the tectonic evolution of the host rock sequence to the MacLellan deposit, and thereby make inferences about the metallogeny of the Lynn Lake greenstone belt, a detailed study of the host rock sequence to the MacLellan Au-Ag deposit was conducted. In order to identify the igneous protoliths and to determine the petrogenesis and geodynamic setting of the lithologies comprising the host rocks to the MacLellan Au-Ag deposit, this study included field mapping, core logging, petrographic observations, and whole rock major, minor, and trace element geochemical analyses of variably altered and metamorphosed rocks from the host rock sequence to the MacLellan Au-Ag deposit. The interpretations included in this study integrate published data from Gagnon (1991) and Fedikow (1992) and represent the most comprehensive petrogenetic and metallogenetic synthesis of a portion of the northern portion of the Lynn Lake greenstone belt conducted to date.

1.2. Background

The Lynn Lake greenstone belt is a supracrustal sequence comprising a diverse tectonostratigraphy of contaminated and juvenile volcanic rocks and epiclastic sedimentary rocks that are collectively assigned to the Wasekwan Group (Bateman, 1945), and younger, synkinematic, fluvial-alluvial molasse-type sedimentary rocks of the Sickle Group (Norman, 1933) covering approximately 7800 km^2. Recent regional mapping, and lithogeochemical and isotopic studies indicate that metavolcanic rocks of

the Lynn Lake greenstone belt can be subdivided into up to three different sections, of varying ages and isotopic affinities (Fig. 1): Northern, Southern, and New Fox (Zwanzig et al., 1999; Beaumont-Smith and Böhm, 2002).

The geology of the Northern section has been interpreted by Fedikow and Gale (1982) and Fedikow (1986, 1992) to be characterized by a laterally extensive and compositionally unique stratigraphic sequence referred to as the Agassiz Metallotect, which was identified through studies of the host rock sequence to the MacLellan Au-Ag deposit. The Agassiz Metallotect is interpreted to comprise a metamorphosed package of high Mg-Ni-Cr and high alumina basalts, biotite-rich mudstones and siltstones, and iron formation that were deposited in an exhalative oceanic setting (Fedikow and Gale, 1982; Fedikow, 1986; 1992). A second Au deposit (Farley Lake) has been interpreted by Fedikow (1992) as occurring along strike from the MacLellan deposit and hosted within the Agassiz Metallotect.

Fox and Johnston (1980) had previously defined the high Mg-Ni-Cr metabasalts as picrites based on field observations and a combination of select major and minor element analysis (e.g., high MgO and Ni contents). The studies of Fedikow and Gale (1982) and Fedikow (1986) relied on limited outcrop exposure, and lithogeochemical analyses lacking high field strength elements (e.g., Nb, Ta, V, Co, Sc, Pr, Er, Ho) to interpret the protoliths and tectonic setting of the Northern section. Fedikow (1992) presented the results of a geochemical study intended to address geochemical anomalies (e.g., similarities between high alumina metabasalts and biotite-rich metasedimentary rocks), and to determine the tectonic setting of the host rock sequence to the MacLellan Au-Ag deposit. Fedikow (1992) interpreted the high Mg-Ni-Cr metabasalts to be

chemically similar to picrites and identified that the high alumina metabasalts and the biotite-rich metasedimentary rock were chemically indifferent. This observation led Fedikow (1992) to interpret the chemical similarities between the high alumina metabasalts and biotite-rich metasedimentary rock as the result of intense hydrothermal alteration associated with an active seafloor hydrothermal system operating during the deposition and mineralization of the host rock sequence. Fedikow (1992) used Ti, Zr, Y data to interpret the sequence to represent an ocean island setting, however, field evidence was not presented to support a subaqueous setting (e.g., pillows, abyssal sediments), and trace element variations (e.g., light rare-earth element enrichment) that could be used to distinguish between specific intra-plate settings (e.g., ocean island basalts vs. continental flood basalts) was not presented.

Gagnon (1991) and Samson and Gagnon (1995), in a study of the character of mineralization comprising the main zone of the MacLellan Au-Ag deposit, divided the host rock sequence into four major lithologic types based on metamorphic mineral assemblages (e.g., chlorite-hornblende schist, plagioclase-hornblende schist, biotite-plagioclase schist, and chlorite-quartz schist). Gagnon (1991) identified the igneous and sedimentary protoliths to be picrites (chlorite-hornblende schists), calc-alkaline basalts (plagioclase-hornblende schists), clastic metasedimentary rocks (chlorite-quartz schists), and altered aluminous basalts (biotite-plagioclase schists). In contrast to previous studies (e.g., Fedikow and Gale, 1982; Fedikow, 1986, 1992), Gagnon (1991) and Samson and Gagnon (1995) interpreted the mineralization to be epigenetic in origin and associated with zones of high strain and multiple generations of mineralogically distinct veins. Moreover, Gagnon (1991) and Samson and Gagnon (1995) did not identify

metamorphosed iron formation or biotite-rich sandstones within the main zone sequence, both of which are indicator lithologies of the Agassiz Metallotect (e.g., Fedikow and Gale, 1982; Fedikow, 1986, 1992). A lack of trace element data meant that Gagnon (1991) was unable to determine the tectonic setting of the host rock sequence to the MacLellan deposit.

The Southern section is interpreted to comprise an early bimodal suite of metamorphosed tholeiitic and lesser calc-alkaline basalts and rhyolites, intercalated greywacke-mudstone turbidites, and a later calc-alkaline andesite suite, which were intruded by syntectonic granitoid plutons with dioritic, quartz dioritic, tonalitic and granodioritic compositions, and minor gabbroic dykes (Peck and Smith, 1989; Zwanzig et al., 1999; Jones et al., 2006). Peck and Smith (1989) applied a combination of field observations and geochemical techniques to characterize the tectonic setting of the Southern section as an active continental margin or continental volcanic arc. Jones et al. (2006), in contrast with Peck and Smith (1989), interpreted the host rocks to the Burnt Timber deposit (Fig. 1), which is hosted by the Southern section, to represent a juvenile island arc using a combination of field observations and geochemical and isotopic analyses. The trace element data presented by Jones et al. (2006), however, do not exhibit the trace element distributions that are representative of volcanic arcs (e.g., enrichments in light rare-earth elements and depletions in Nb, Zr, Ti, and Y) as outlined by Pearce (1983, 2008), Pearce and Peate (1995), and Woodhead et al., (1998).

The New Fox section of the Lynn Lake greenstone belt has previously been grouped with the Southern section because the two sequences are contiguous. Chemical data presented by Zwanzig et al., (1999) and interpretations made by Beaumont-Smith

and Böhm (2002), however, suggest that this sequence may represent a separate lithotectonic terrane. Previously, the New Fox section was interpreted by Gilbert et al. (1980) to comprise a platform of metamorphosed pyroxene-phyric basaltic flows and autoclastic breccia, which was subsequently intruded by mafic to felsic plutons, and was overlain by tuff, greywacke, and a turbidite unit. Outcrops of pillowed basalt were used by Gilbert et al. (1980) to interpret the area as a seafloor setting, however, a lack of high precision trace element data (e.g., Nb, Ta, V, Co, Sc, Pr, Er, Ho) made it impossible to distinguish between specific oceanic environments (e.g., mid-ocean ridge, intra-oceanic rift, oceanic volcanic arc, etc.).

Regional lithochemical studies have been limited to Syme (1985) and Zwanzig et al., (1999). The studies of Syme (1985) and Zwanzig et al., (1999) failed to integrate available field data (e.g., lithologic relationships and textures) or petrography into the interpreted chemical variations. As a result, Syme (1985) concluded that the tectonic setting of the Lynn Lake greenstone belt is comparable to a modern-day Marianas Island arc, while Zwanzig et al., (1999) interpreted the Lynn Lake greenstone belt to be the result of tectonically stacking rocks derived from an oceanic intra-arc rift (e.g., Northern section), an island arc (e.g., Southern section), and a second tectonic collage of unknown affinity (e.g., New Fox section) onto the Hearne Craton during terminal collision of the Manikewan Ocean between the Superior, Rae, and Hearne Cratons.

1.3. Study Objectives

The primary objective of this study is to determine the tectonic setting and geodynamic evolution of the portion of the Lynn Lake greenstone belt that hosts the MacLellan Au-Ag deposit, and to assess the significance of these findings for the tectonics and metallogeny of the region. This study integrates new field and petrographic observations, and whole-rock major, minor, and trace element geochemical data of the MacLellan Au-Ag deposit in order to:

1. Identify the igneous and sedimentary protoliths to the metamorphosed and altered host rock lithologies, and
2. Determine the petrogenesis and identify the tectonic environment of emplacement of the host rock sequence.

The secondary objective of this study is to construct a geodynamic model to speculate on the most favourable environments for metallic mineral deposit formation, which can be used to develop a conceptual framework to guide future exploration activities in the Lynn Lake greenstone belt. This study incorporates new field and petrographic observations, whole rock major, minor, and trace element geochemical data from the MacLellan Au-Ag deposit as well as the Burnt Timber and Farley Lake deposits (Fig. 1.2), and integrates the results of previous investigations (e.g., Peck, 1986; Zwanzig et al., 1999; Jones, 2005; Beaumont-Smith, 2008) on the Lynn Lake greenstone belt in order to:

1. Determine the geodynamic evolution of the area, and
2. Make inferences about the metallic mineral deposits potential.

1.4. Thesis Structure

The thesis consists of two main data chapters, which are presented in manuscript format. Chapter 1 is the introduction to the thesis. Chapter 2 presents field relationships, petrographic observations, and high precision major, minor, and trace element geochemical data of the host rock sequence to the MacLellan deposit, which were used to identify igneous and sedimentary protoliths to the metamorphosed and altered host rocks and to understand the primary magmatic geochemical signatures. Detailed fieldwork and petrographic observations together with whole-rock geochemical data indicate that the host rock sequence comprises primarily picritic and high alumina transitional basalts, which erupted in a near-continental intra-plate environment. These rocks were subsequently overlain by calc-alkaline andesites and high-Mg andesites, which were derived from a continental arc environment. Chapter 3 presents high precision major, minor, and trace element geochemical data from the MacLellan, Burnt Timber, and Farley Lake deposits. Data from this study were integrated with data from Peck (1986), Peck and Smith (1989), Zwanzig et al., (1999), Jones (2005), Jones et al., (2006), and Beaumont-Smith (2007), which were used to identify igneous protoliths to the metamorphosed altered metavolcanics of the Lynn Lake greenstone belt and to understand the primary magmatic signatures. Whole-rock geochemical data and available fieldwork and petrographic observations indicate that the Lynn Lake greenstone belt is representative of a rifted continental margin, likely along the Hearne Craton boundary. These metavolcanic rocks were intruded by gabbroic, tonalitic, and granitic plutons and subsequently overlain by a calc-alkaline basaltic andesite-andesite suite with subordinate high-magnesium andesites. The final series of tectonomagmatic events

involve the terminal closure of the Manikewan Ocean accompanied by the intrusion of the Wathaman-Chipewyan-Baldock batholiths and peak metamorphic conditions.

Chapter 4 presents a summary of the study.

1.5. References

Beaumont-Smith, C.J., 2008. Geochemistry data for the Lynn Lake greenstone belt, Manitoba (NTS 64C11-16); Manitoba Science, Technology, Energy and Mines, Mantoba Geological Survey, Open File OF2007-1, 5 p. + Appendix.

Beaumont-Smith, C.J., and Böhm, C.O., 2002. Structural analysis and geochronological studies in the Lynn Lake greenstone belt and its gold-bearing shear zones (NTS 64C10, 11, 12, 14, 15 and 16), Manitoba; *in* Report of Activities 2002, Manitoba Industry, Trade and Mines, Manitoba Geological Survey, 159-170.

Beaumont-Smith, C.J., and Böhm, C.O., 2003. Tectonic evolution and gold metallogeny of the Lynn Lake greenstone belt, Manitoba (NTS 64C10, 11, 12, 14, 15, and 16). *In* Report of Activities 2003, Manitoba Industry, Trade and Mines, Manitoba Geological Survey, 39-49.

Beaumont-Smith, C.J., and Böhm, C.O., 2004. Structural analsysis of the Lynn lake greenstone belt, Manitoba (NTS 64C10, 11, 12, 14, 15, and 16). *In* Report of Activities 2004, Manitoba Industry, Economic Development and Mines, Manitoba Geological Survey, 55-68.

Fedikow, M.A.F., 1986. Geology of the Agassiz Stratabound Au-Ag Deposit, Lynn Lake Manitoba. Manitoba Energy and Mines, Geological Services Branch, Open File Report OF85-5, 80 p. Fedikow, M.A.F., 1992. Rock geochemical studies at the MacLellan Au-Ag deposit, Lynn Lake, Manitoba. Manitoba Energy and Mines, Geological Services Branch, Economic Geology Report ER91-1, 237 p.

Fedikow, M.A.F., 1992. Rock geochemical alteration studies at the MacLellan Au-Ag deposit, Lynn Lake, Manitoba. Manitoba Energy and Mines, Geological Services, Economic geology Report ER92-1, 237 p.

Fedikow, M.A.F., and Gale, G.H., 1982. Mineral deposit studies in the Lynn Lake area. *In* Report of Field Activities 1982. Manitoba Energy and Mines, Mineral Resources Division, 44-55.

Gagnon, J.E., 1991. Geology, geochemistry, and genesis of the Proterozoic MacLellan Au-Ag deposit, Lynn Lake greenstone belt, Manitoba. Unpublished M.Sc. thesis, University of Windsor, 275 p.

Gale, G.H., 2003. Rare earth element studies of soils and vegetation over the MacBride Lake massive sulphide deposit and the MacLellan mine Rainbow gold zone, Lynn Lake area, Manitoba (NTS 64C15 and 64B12); *in* Report of Activities 2003, Manitoba Industry, Economic Development and Mines, Manitoba Geological Survey, 50.

Gale, G.H., and McClenaghan, S.H., 2002. Determining residual mineral potential using europium anomalies in the Ruttan and Lynn Lake areas, Manitoba; *in* Report of Activities 2002, Manitoba Industry, Trade and Mines, Manitoba Geological Survey, 205-208.

Gale G.H., Pawliw, P., and Hill, G.T., 2004. Enzyme Leach^{SM} and Terrasol Leach^{SM} studies of soils at the MacLellan Au-Ag deposit, Lynn Lake, Manitoba (NTS 64C15); *in* Report of Activities 2004, Manitoba Industry, Economic Development and Mines, Manitoba Geological Survey, 92-103.

Gilbert, H.P., Syme, E.C., and Zwanzig, H.V., 1980. Geology of the metavolcanic and volcaniclastic metasedimentary rocks in the Lynn Lake area; Manitoba Energy and Mines, Geological Services, Geological Paper GP80-1, 118 p.

Jones, R.L., 2005. Geology of the shear-hosted Burnt Timber deposit, Lynn Lake, northern Manitoba. Unpublished M.Sc. thesis, Laurentian University, 80 p.

Jones, L.R., Lafrance, B., and Beaumont-Smith, C.J., 2006. Structural controls on gold mineralization at the Burnt Timber mine in the Lynn Lake greenstone belt, Trans-Hudson Orogen, Manitoba. Exploration and Mining Geology, 15, 89-100.

Ma, G., Beaumont-Smith, C.J., and Lentz, D.R., 2000. Preliminary structural analysis of the Agassiz Metallotect near the MacLellan and Dot Lake gold deposits, Lynn lake greenstone belt (parts of NTS 64C/14, /15); *in* Report of Activities 2000, Manitoba Industry, Trade and Mines, Manitoba Geological Survey, p. 51-56.

Ma, G., and Beaumont-Smith, C.J., 2001. Stratigraphic and structural mapping of the Agassiz Metallotect near Lynn Lake, Lynn Lake greenstone belt (parts of NTS 64C/15, /15); *in* Report of Activities 2001, Manitoba Industry, Trade and Mines, Manitoba Geological Survey, 86-93.

Norman, G.W.H., 1933. Granville Lake district, northern Manitoba. Geological Survey of Canada Summary Report Part C, 23-41.

Park, A.F., Beaumont-Smith, C.J., and Lentz, D.R., 2002. Structure and Stratigraphy in the Agassiz Metallotect, Lynn Lake greenstone belt (NTS 64C14 and 64C15), Manitoba; *in* Report of Activities 2002, Manitoba industry, Trade and mines, Manitoba Geological Survey, 171-186.

Pearce, J.A., 1983. Role of the sub-continental lithosphere in magma genesis at active continental margins. *In* Hawkesworth, C.J., and Norry, M.J. (Eds.). Continental basalts and mantle xenoliths. Shiva, Nantwich, England, 230-249.

Pearce, J.A., 2008. Geochemical fingerprinting of oceanic basalts with applications to ophiolite classification and the search for Archean oceanic crust. Lithos 100, 14-48.

Pearce, J.A., and Peate, D.W., 1995. Tectonic implications of the composition of volcanic arc magmas . Earth and Planetary Sciences Annual Reviews 23, 251-285.

Peck, D.C., 1986. The geology and geochemistry of the Cartwright Lake area: Lynn Lake greenstone belt, northwestern Manitoba. Unpublished M.Sc. Thesis, University of Windsor, 270 p.

Peck, D.C., and Smith, T.E., 1989. The geology and geochemistry of an early-Proterozoic volcanic arc association at Cartwright Lake Lynn Lake greenstone belt, Northwestern Manitoba. Canadian Journal of Earth Sciences 26, 716-736.

Samson, I.M., and Gagnon, J.E., 1995. Episodic fluid infiltration and genesis of the Proterozoic MacLellan Au-Ag deposit, Lynn Lake greenstone belt, Manitoba. Exploration and Mining Geology 4-1, 33-50.

Syme, E.C., 1985. Geochemistry of metavolcanic rocks in the Lynn lake belt; Manitoba Energy Mines, Geological Servies, Geological Report GR84-1.

Woodhead, J.D., Eggins, S.M., and Johnson, R.W., 1998. Magma genesis in the New Britain island arc: further insights into the melting and mass transfer processes. Journal of Petrology 39, 1641-1668.

Zwanzig, H.V., Syme, E.C., and Gilbert, H.P., 1999. Updated trace element geochemistry of ca. 1.9 Ga metavolcanic rocks in the Paleoproterozoic Lynn Lake Belt; Manitoba Industry, Trade and Mines, Geological Servies, Open File Report OF99-13, 48p. Plus map and diskette.

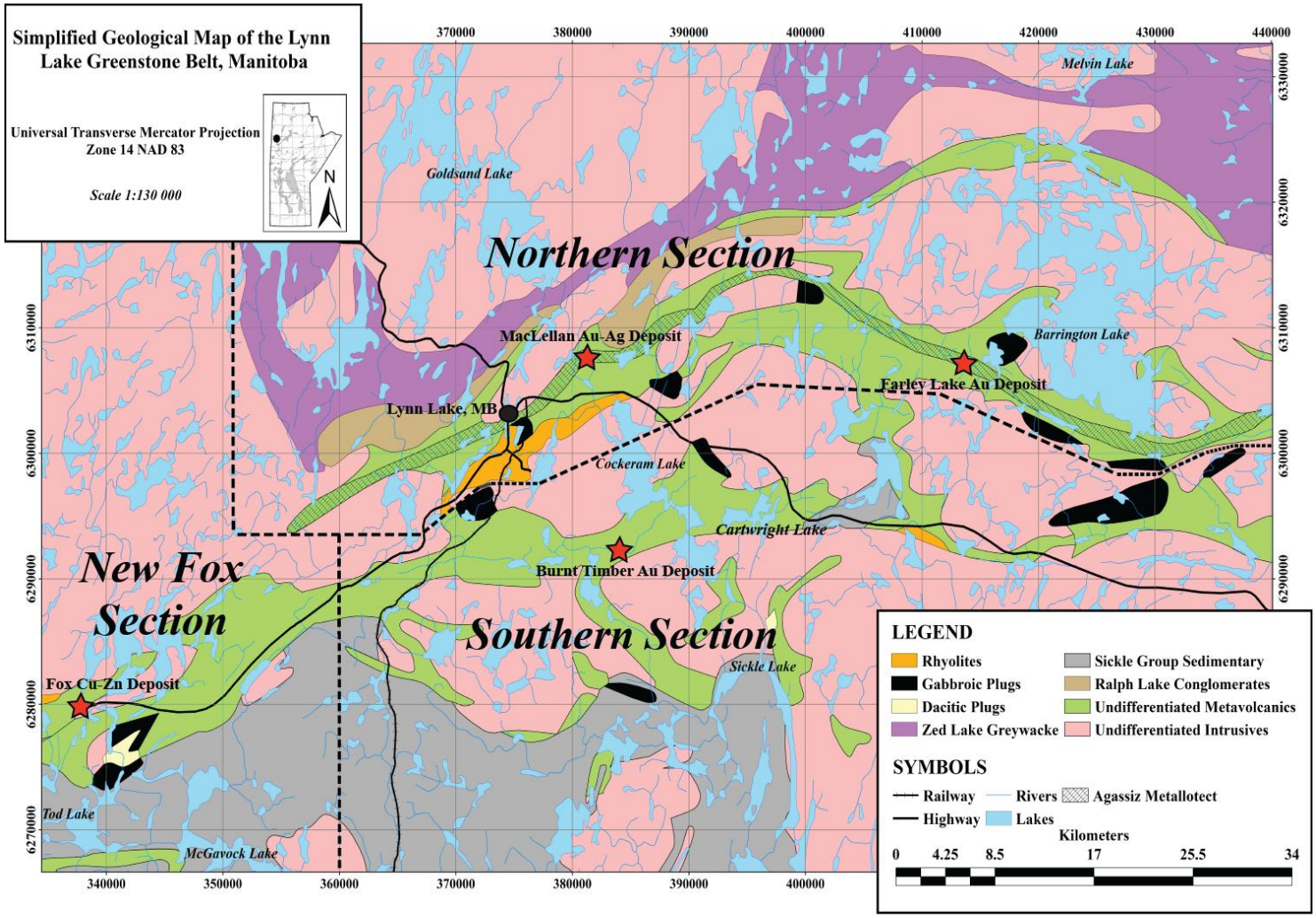

Figure 1.1 - Simplified geological map of the Lynn Lake greenstone belt. The study area is located roughly 8 km northeast of the town of Lynn Lake.

CHAPTER 2

The host rocks to the MacLellan Au-Ag deposit, Lynn Lake, Manitoba: evidence for mantle plume and continental lithosphere interaction during the Paleoproterozoic Trans-Hudson Orogen

2.1. Introduction

The MacLellan Au-Ag deposit, which is situated within the northern section of the Paleoproterozoic Lynn Lake greenstone belt, has a current resource that is estimated at approximately 2 million ounces Au equivalent at an average grade of 1.90 g/t Au (Gagnon et al., 2013). This significant resource is hosted within a supracrustral sequence that comprises ultramafic to mafic metavolcanic rocks that were interpreted to be compositionally distinct and to have significant mineral deposit potential (i.e., the 'Agassiz Metallotect') (Fedikow, 1986). Despite their implied geologic and economic significance, these rocks have only received limited study since discovery of the MacLellan deposit in 1946. The majority of these studies have focused on characterization or genesis of the Au-Ag mineralization (e.g., Koo, 1976; Fox and Johnston, 1980; Fedikow and Gale, 1982; Augsten et al., 1985; Fedikow, 1986, 1992; Samson and Gagnon, 1995; Samson et al., 1999) with little to no consideration given to the geochemistry, petrogenesis, and geodynamic setting of the host rock sequence. To date, Gagnon (1991) and Fedikow (1992) are the only studies to attempt to identify the igneous protoliths and tectonic setting of the host rock sequence to the MacLellan Au-Ag deposit. The conclusions of Gagnon (1991) and Fedikow (1992), however, were

developed using a combination of incomplete trace element and high field strength element data and reconnaissance-level field observations.

A geochemical study by Zwanzig et al., (1999), using samples and field observations from previous reconnaissance-level regional studies (Gilbert et al., 1980; Gilbert, 1993), proposed what is the currently accepted geodynamic model for the Lynn Lake greenstone belt. Through the application of high-precision trace element geochemistry, Zwanzig et al. (1999) proposed that the northern section of the Lynn Lake greenstone belt is a combination of subaqueous depleted volcanic arc tholeiites and extension-related enriched basalts (i.e., rift basalts), which were interpreted to be highly favourable targets for volcanogenic massive sulphide (VMS) deposits (Zwanzig et al., 1999). Despite approximately 40 years of prospecting, a single, significant VMS deposit has yet to be identified in the northern section of the Lynn Lake greenstone belt and the deposits that have been discovered (i.e., MacLellan Au-Ag, Farley Lake Au deposits) are inconsistent with emplacement in a VMS environment. Therefore, the geodynamic model proposed by Zwanzig et al., (1999) has been ineffective at predicting the type and location of mineral deposits (i.e., metallogeny) within the belt.

The lack of detailed field relationship, petrographic, and geochemical data has made it impossible to determine the igneous protoliths and petrogenesis of the host rocks to the MacLellan Au-Ag deposit, as well as to develop a regional geodynamic model and to reliably predict the mineral deposit potential (i.e., types and localities) of the Lynn Lake greenstone belt as a whole. In this study, the results of large scale, outcrop mapping, core logging, petrographic analysis, and major, minor and trace element geochemical analysis for 54 samples are reported from the host rock sequence to the

MacLellan Au-Ag deposit and from elsewhere in the Lynn Lake greenstone belt in order to identify the igneous protoliths and to determine the petrogenesis and geodynamic setting of the host rock sequence.

2.2. Regional Geology

The Lynn Lake greenstone belt is located in the central portion of the Reindeer Collisional Zone of the Trans-Hudson Orogen, and is bordered by the Kisseynew Gneiss Belt to the south, and the Wathaman-Chipewyan-Baldock Batholith and the Tonalite-Migmatite Complex to the north. By global standards, the Lynn Lake greenstone belt is significant, measuring approximately 150 km long by 50 km wide with the metavolcanic rocks covering an estimated area of approximately 1200 km^2. These rocks comprise a diverse tectonostratigraphy of what have been interpreted to be metamorphosed, contaminated and juvenile volcanic and epiclastic sedimentary rocks that are collectively assigned to the Wasekwan Group (Bateman, 1945), and younger, syn-kinematic, fluvial-alluvial molasse-type sedimentary rocks of the Sickle Group (Norman, 1933). Until 1999, the Lynn Lake greenstone belt had been subdivided into two subordinate greenstone belts (i.e., Northern and Southern) separated by a series of felsic plutons associated with the Wathaman-Chipewyan-Baldock Batholith. More recent regional mapping and geochemical data indicate, however, that the Lynn Lake greenstone belt can be subdivided into three different sections, of varying ages and geochemical affinities (i.e., Northern, Southern, and New Fox sections) (Zwanzig et al., 1999; Beaumont-Smith and Böhm, 2002) (Fig. 2.1). Patterns of regional deformation and metamorphism can be locally complex, however, metamorphic grade typically ranges between upper greenschist and upper amphibolite facies, with the greatest proportion of rocks in the belt

exhibiting middle amphibolite facies equilibrium mineral assemblages (Milligan, 1960; Gilbert et al., 1980). For brevity, the prefix 'meta' is implied throughout the following text.

The Northern section consists of what have been interpreted to be circa 1910 to 1890 Ma submarine, tholeiitic, mafic volcanic and volcaniclastic rocks, with lesser, circa 1890 Ma rhyolite and banded iron formation (Gilbert et al., 1980; Zwanzig et al., 1999; Beaumont-Smith and Böhm, 2002). The Southern section consists of an early, bimodal suite of predominantly tholeiitic with lesser calc-alkaline basalt and rhyolite that are intercalated with greywacke-mudstone turbidites, and a later calc-alkaline basalt/basaltic andesite/andesite suite, which were subsequently intruded by syn-tectonic plutons comprising diorite, quartz diorite, tonalite and granodiorite, and minor grabbroic dykes (Peck and Smith, 1989; Zwanzig et al., 1999). The New Fox section had been considered to be the western extension of the Southern section because these two rock sequences are contiguous. The New Fox section constitutes a platform of pyroxene-phyric basaltic flows and autoclastic breccia, which were intruded by mafic to felsic plutons and subsequently overlain by tuff, greywacke, and a turbidite unit (Gilbert et al., 1980; Syme, 1985). Minor iron formation and clastic sedimentary units occur in places throughout the Lynn Lake greenstone belt (Milligan, 1960; McRitchie, 1974; Gilbert et al., 1980).

The volcanic rocks of the Lynn Lake greenstone belt have been interpreted to be the products of a collage of subaqueous volcanic environments including oceanic volcanic arcs (Milligan, 1960; Syme, 1985; Baldwin et al., 1987; Lewry et al., 1987; Van Schmus et al., 1987; Zwanzig et al., 1999; Jones et al., 2006), ocean islands (Fedikow, 1992), intra-arc rifts (Zwanzig et al., 1999), and mid-ocean ridges (Zwanzig et al., 1999).

Peck and Smith (1989), however, proposed that the volcanic rocks in the Cartwright Lake area of the Southern section represent an active continental margin or continental volcanic arc. Furthermore, the geochemistry of Sickle Group rocks (e.g., Zwanzig, 1990), Pb-Pb isotope systematics of feldspars from rhyolitic and gabbroic rocks (Jurkowski, 1999), and Sm-Nd isotope systematics of rhyolites and diorites (Beaumont-Smith and Böhm, 2004) from the Lynn Lake region all support the presence of continental lithosphere in the Lynn Lake region during the formation of the Lynn Lake greenstone belt.

The precise ages of Lynn Lake greenstone belt volcanic rocks have not been determined, however, they have been constrained by the ages of surrounding felsic volcanics (e.g., rhyolites), as well as mafic and felsic plutons. The volcanic rocks of the Northern section have estimated U-Pb ages ranging from 1910 to 1886 Ma (Baldwin et al., 1987; Beaumont-Smith and Böhm, 2003), and the volcanic rocks from the Southern section have estimated U-Pb ages ranging from 1856 to 1842 Ma (Beaumont-Smith and Böhm, 2003). Furthermore, U-Pb dating of gabbroic plugs and dioritic, granitic, granodioritic, and tonalitic stocks from the Lynn Lake region suggests that at least five major magmatic events occurred between 1910 and 1831 Ma (Appendix A).

Four regional tectonostructural events have been identified in the Lynn Lake greenstone belt and are summarized in Appendix B.

2.3. Local Geology

The surficial geology of the MacLellan deposit was originally described by G. G. Suffel in 1947 for Noranda Mines Limited, and the mineralization was subsequently

described during an exploration program in 1956 by A. S. Dawson of Agassiz Mines Limited (Milligan, 1960). Various aspects of the deposit geology, mineralization, mineralogy, and genesis have been presented in Koo (1976), Fox and Johnston (1980), Fedikow and Gale (1982), Augsten (1985), Fedikow, (1986, 1992), and Samson and Gagnon (1995). The paucity of local outcrop required that these studies rely almost exclusively on drill core when interpreting the geologic relationships of the host rock sequence; with the exception of Samson and Gagnon (1995), which, in addition to using drill core, included underground mapping along the 370 m conveyer drift and sampling within operating stopes.

The host rock sequence to the MacLellan Au-Ag deposit defines a laterally-extensive feature that has been referred to as the Agassiz Metallotect (Fedikow, 1986). This sequence is interpreted to comprise interbedded, high Mg-Ni-Cr basalts or picrites, siliceous and biotite-rich, locally sulphidic siltstones, and oxide, sulphide, and silicate facies iron formation, all of which are sandwiched between thick layers of fragmental, aluminous basalt (Fedikow, 1986, 1992) (Fig. 2.2). In metamorphic terms, the host rock sequence to the MacLellan Au-Ag deposit is a northeast striking (045°E), north-dipping, sub-vertical (82°N) package of plagioclase-amphibole, quartz-plagioclase-biotite, and chlorite-amphibole schists (after Fedikow and Gale, 1982). The sulphidic siltstones and ultramafic rocks of this package were interpreted to represent an auriferous exhalative horizon (Fedikow and Gale, 1982; Fedikow, 1986); however, the study of Gagnon (1991) and Samson and Gagnon (1995) proposed that mineralization is vein-associated and identified two distinct, variably deformed, auriferous vein sets with associated wallrock alteration (principally silicification and biotitization).

Polyphase deformation and regional greenschist to amphibolite facies metamorphism have obliterated the primary textural and mineralogical characteristics of the host rocks, leaving the overall stratigraphic facing direction unknown. Locally, the host rock sequence has undergone several stages of syn- and post-volcanic alteration resulting in calc-silicate or potassic metasomatism, silicification, quartz veins, and carbonatization (Fedikow and Gale, 1982; Fedikow, 1986, 1992; Samson and Gagnon, 1995). The precise age of metamorphism is unknown.

2.4. Methods

2.4.1. Sample Collection

Due to the lack of outcrops and intense weathering and alteration associated with mineralization in the study area, representative fresh and least altered samples were collected at previously exposed outcrops located east of the MacLellan Au-Ag deposit (Fig. 2.3) via channel and chip sampling at the time of mapping of these outcrops. Additional samples were also collected from drill cores obtained from both within and outside of the mineralized zones of the MacLellan Au-Ag deposit (Fig. 2.3). Drill core samples record variable intensities of hydrothermal alteration, preserving none of the original mineralogy or textures, with the exception of some samples of plagioclase-amphibole schist, which contain relict plagioclase phenocrysts. Following the guidelines of Polat and Hofmann (2003), samples were identified as physically altered if they contained significant secondary (i.e., cross cutting) assemblages of quartz, calcite, or epidote. Global positioning system (GPS) readings for sample locations and sample depths, where applicable, are provided in Appendix C.

2.4.2. Chemical Analysis

Lithogeochemical analyses were performed by Activation Laboratories Ltd. (ACTLabs) of Ancaster, Ontario, Canada. Major element contents of the rocks, reported as weight percent oxides, were determined using a Thermo Jarrell-Ash ENVIRO II inductively coupled plasma optical emission spectrometer (ICP-OES). The samples were mixed with a flux of lithium metaborate and lithium tetraborate, and fused at 1000 °C in an induction furnace. Upon cooling, the beads were rapidly digested in a solution of 5% HNO_3 containing an internal standard, and mixed continuously until complete dissolution occurred. Minor and trace element contents of the samples, reported as parts per million (ppm), were determined using a Perkin Elmer SCIEX ELAN 6000 inductively coupled plasma mass spectrometer (ICP-MS). Loss on ignition (LOI) was determined by measuring weight loss upon heating to 1100 $^{\circ}$C over a three-hour period. The analytical precision is estimated to be better than 6% for trace elements and 3% for major elements (Young, 2002). Following the guidelines of Polat and Hofmann (2003), samples were labelled as chemically altered and were not included in the petrogenetic interpretation if they had a combined Ce/Ce* anomaly greater than 1.10 or less than 0.90, and an LOI of greater than 3.0 wt.%. Samples with an LOI of greater than 3.0 wt.% and a negligible Ce/Ce* anomaly, however, were included in the petrogenetic interpretation if inter-element trends and ratios remained consistent between least altered and altered equivalents.

2.5. Results

2.5.1. Field Observations and Petrography

Based on observations from drill core and outcrops, the host rock sequence to the MacLellan Au-Ag deposit consists of three dominant lithologies and one minor lithology. These are, in decreasing order of abundance: plagioclase-amphibole schist, chlorite-amphibole schist, quartz-plagioclase-biotite schist, and subordinate amphibole schist. Two large outcrops (Figs. 2.5 and 2.6) to the east of the MacLellan Au-Ag deposit (i.e., Eastern Outcrops 1 and 2) contain units of chlorite-amphibole, quartz-plagioclase-biotite, and amphibole schist; as well as four minor lithologies: 1) pods of amphobilite that occur within outcrops of amphibole schist; 2) quartz-amphibole schist; 3) magnetite-chert iron formation situated between units of chlorite-amphibole schist and quartz-amphibole schist; and, 4) amphibolite dykes that cross-cut outcrops of quartz-amphibole schist.

Plagioclase-amphibole Schist

In outcrop, plagioclase-amphibole schist occurs as several tens of metres thick, continuous layers, which can be traced along strike lengths of up to approximately 4 km. These rocks are medium- to fine-grained, dark blue to black blue, granoblastic to weakly foliated, and contain porphyroclasts (i.e., blastophenocrysts) of plagioclase set in a groundmass of blue-black hornblende and quartz (Fig. 2.6a). Hornblende comprises 50 to 60% of the rock, exhibits a penetrative foliation, as indicated by a mutual extinction in cross-polarized light, and occurs as hypidioblastic to idioblastic lathes, blades, and rhombohedra that range in size from 0.5 mm to 1 cm in length (Fig. 2.6b). Plagioclase exhibits albite twinning, comprises 35 to 45% of the rock, and occurs as granular,

hypidioblastic to idioblastic laths or xenoblastic, sub-rounded to ovoid grains that range in size from 0.5 mm to 6 cm. Quartz comprises up to 5% of the plagioclase-amphibole schist. It is fine-grained, around 0.1 mm in size, xenoblastic to hypidioblastic, and exhibits undulose extinction, indicating lattice strain (Fig. 2.6b). Accessory minerals include biotite, sercite, garnet, actinolite, calcite, magnetite, ilmenite, pyrite, and pyrrhotite.

Chlorite-amphibole Schist

Units of chlorite-amphibole schist occur within the host rock sequence to the MacLellan Au-Ag deposit as 2 m wide and 3 to 5 m long, irregularly-shaped, lensoidal pods (i.e., boudins), which have an apparent thickness of no more than a few metres (Fig. 2.6c). These rocks are medium- to fine-grained, dark green to black green, strongly foliated, and are dominated by green to blue-green hornblende, which comprises 60 to 90% of the rock. Hornblende is foliated and occurs as hypidioblastic to idioblastic laths, blades, and rhombohedra that range in size from 1 to 4 mm with straight to sutured grain boundaries (Fig. 2.6d). Hornblende crystals occur within a groundmass comprising chlorite, plagioclase, magnetite, and ilmenite. Chlorite comprises 5 to 15% of chlorite-amphibole schist, is fine-grained, up to 0.25 mm in size, xenoblastic, foliated and exibits a colourless to faint-green pleochroism, indicating that it is clinochlore (Fig. 2.6d). Outside of the host rock sequence, units of amphibole-chlorite schist occur continuously over at least 1 km as approximately 30 cm to tens of metres thick layers that are intercalated with quartz-plagioclase-biotite schist (Fig. 2.6e). These rocks are fine- to very fine-grained, light green, and are dominated by green to light-green chlorite, which constitutes nearly 100% of the rock. Chlorite is strongly foliated and occurs as

hyidioblastic to idioblastic lathes and blades that average 0.1 mm in size. Accessory minerals include actinolite, magnetite, ilmenite, titanite, pyrite, pyrrhotite, quartz, and calcite.

Quartz-plagioclase-biotite Schist

Units of quartz-plagioclase-biotite schist occur within the host rock sequence as discontinuous lenses or 1 to 5 m thick layers intercalated with chlorite-amphibole schist that can be traced between outcrops up to 200 m apart (Fig. 2.6e). These rocks are fine-grained, blue to light blue, strongly foliated, and comprise red-brown biotite (~ 40%), plagioclase (~ 35%), and quartz (up to 25%). In outcrop, these rocks are light brown to light gray in colour. Biotite imparts a foliation and occurs as hypidioblastic to idioblastic lathes and blades that range in size from 0.5 mm to 1 cm (Fig. 2.6f). Plagioclase exhibits albite twinning, and occurs as granular hypidioblastic to idioblastic laths or xenoblastic sub-rounded to ovoid grains that range in size from 0.5 mm to 1 cm (Fig. 2.6f), and is commonly replaced by quartz. Quartz is fine-grained, approximately 0.1 mm in size, xenoblastic to hypidioblastic, and exhibits undulose extinction (Fig. 2.6f). Accessory minerals include sericite, calcite, magnetite, ilmenite, pyrite, and pyrrhotite.

Amphibole Schist

Amphibole schist was identified in one outcrop as a several metres thick, discontinuous layer. In drill core, units of amphibole schist are observed as small, discordant lenses that are up to 2 m thick. These rocks are medium-grained, dark blue to black blue, granoblastic to weakly foliated and comprise blue-black hornblende with subordinate plagioclase and quartz (Fig. 2.7a). Hornblende comprises approximately 70

to 80% of the rock, exhibits a penetrative foliation, as indicated by mutual extinction in cross-polarized light, and occurs as hypidioblastic to idioblastic lathes, blades, and rhombohedra that range in size from 0.5 mm to 1.5 cm in length (Fig. 2.7b). In places, hornblende has been partially replaced by chlorite. Plagioclase exhibits albite twinning, comprises approximately 10 to 20% of the rock, and occurs as hypidioblastic to idioblastic laths or blades that range in size from 0.5 mm to 1 cm (Fig. 2.7b). In places, it has been partially replaced by biotite or sericite. Quartz comprises less than 9% of amphibole schist. It is fine-grained, approximately 0.1 mm in size, xenoblastic to hypidioblastic, and exhibits undulose extinction (Fig. 2.7b). Accessory minerals include actinolite, tremolite, biotite, garnet, sericite, calcite, magnetite, ilmenite, pyrite, and pyrrhotite.

Amphibolite

Amphibolite occurs as 1 m wide and 3 to 6 m long, irregularly-shaped lensoidal pods within units of amphibole schist, which have apparent thicknesses of no greater than a few metres (Fig. 2.7c). These rocks are granoblastic, medium-grained, and are dominated by blue-black hornblende, which comprises 90 to 95% of the rock. Hornblende exhibits a penetrative foliation, as indicated by mutual extinction in cross-polarized light (Fig. 2.7d). Grains occur as hypidioblastic to idioblastic laths, blades, and rhombohedra that range in size from 1 mm to 1 cm with straight to sutured grain boundaries. Chlorite comprises 5 to 10% of the rock (Fig. 2.7d), is fine-grained, up to 0.25 mm in size, xenoblastic and foliated. Accessory minerals include actinolite and quartz.

Quartz-amphibole Schist

Units of quartz-amphibole schist occur as several tens of metres thick, continuous layers, which can be traced along strike lengths of approximately 500 m (Fig. 2.7e). These rocks occur stratigraphically below a 2 to 3 m thick magnetite-chert iron formation unit comprising 5 to 10 cm thick, alternating layers of chert and iron oxides (i.e, magnetite and hematite). Units of quartz-amphibole schist are fine-grained, black-green in colour, granoblastic to weakly foliated, and dominated by fine-grained hornblende (60%), quartz (25%), and biotite (15%). Hornblende occurs as hypidioblastic to idioblastic laths, blades, and rhombohedra that range in size from 1 mm to 1 cm with straight to sutured grain boundaries (Fig. 2.7f). Quartz is fine-grained, hypidioblastic to xenoblastic with an average size of 0.2 mm (Fig. 2.7f). Biotite imparts a foliation and occurs as hypidioblastic to idioblastic lathes and blades that have an average size less than 0.2 mm (Fig. 2.7f). Accessory minerals include chlorite, actinolite, and calcite.

Amphibolite Dykes

Amphibolite dykes are approximately 1 m wide, with an apparent thickness greater than 5 m, and are observed obliquely cross-cutting units of quartz-amphibole schist at Eastern Outcrop 2 (samples LL13-17 and LL13-19) and 3 (LL13-23), approximately 600 m apart (Fig. 2.7g). These rocks are coarse-grained, dark green, granoblastic, and composed almost entirely of hornblende (~ 95%) with minor quartz (< 5%) (Fig. 2.7h). Hornblende occurs as hypidioblastic lathes and blades or acicular lathes, which range in size from 0.5 mm to 1.5 cm. Grain boundaries are irregular due to xenoblastic quartz replacing hornblende (Fig. 2.7h).

Accessory Minerals

The various occurrences of accessory (i.e., magnetite, ilmenite, pyrite, and pyrrhotite) and alteration (i.e., quartz, calcite, actinolite, chlorite, and sericite) minerals are described below with their corresponding lithologies and ordered based on their relative abundance.

Magnetite, ilmenite, pyrite, and pyrrhotite are common accessory minerals (< 1%) in units of plagioclase-amphibole, chlorite-amphibole, quartz-plagioclase-biotite, and amphibole schist, but can reach up to 20% in pervasively altered and mineralized equivalents. Magnetite, pyrrhotite, and pyrite occur primarily as disseminated hypidioblastic to idioblastic straight crystals or as xenoblastic irregular grains between 0.1 and 0.8 mm in size. Ilmenite occurs as foliated, bladed to acicular crystals or is observed mantling grains of magnetite. Titanite has only been identified in a few samples of quartz-plagioclase-biotite schist, where it was observed mantling ilmenite, which occurs as pseudomorphs after magnetite.

Biotite was observed in all of the above lithologies, except quartz-plagioclase-biotite schist where it is a major constituent, occurring as fine-grained, red-brown to brown, hypidioblastic to xenoblastic (rarely idioblastic) lathes or tabular grains that average between 0.1 to 0.4 mm in size. Biotite is most commonly observed replacing plagioclase or hornblende along cleavage planes and less commonly as inclusions within plagioclase.

Calcite was only identified in pervasively altered and mineralized units of plagioclase-amphibole, chlorite-amphibole, and quartz-plagioclase-biotite schist from

drill cores recovered from the MacLellan Au-Ag deposit. Calcite occurs as colourless, fine- to medium-grained xenoblastic to hypidioblastic crystals ranging in size from 0.1 mm to 0.5 mm. Rarely is calcite observed as idioblastic rhombohedral crystals up to 0.5 mm in size, with distinct simple or lamellar twinning, and a distinct rhombohedral cleavage.

Actinolite occurs in amphibolite and within units of chlorite-amphibole, plagioclase-amphibole, quartz-amphibole, and amphibole schist as fine- to medium-grained hypidioblastic to idioblastic lathes with straight to sutured boundaries. Actinolite crystals are commonly green to blue-green in colour, average between 0.5 mm to 1 cm in length, and are commonly observed replacing hornblende along grain boundaries, fractures, cleavages, and less commonly as inclusions within hornblende.

Chlorite was observed in samples of amphibolite and within units of chlorite-amphibole schist as foliated, fine-grained xenoblastic to acicular lathes up to 0.25 mm in size, which are colourless with a faint-green pleochroism, indicating that it is clinochlore. Chlorite is only observed where it has replaced hornblende at grain boundaries and along fractures and cleavage planes.

Sericite was observed in units of plagioclase-amphibole and quartz-plagioclase-biotite schist. Sericite crystals occur as fine-grained xenoblastic grains, less than 0.1 mm in size, commonly within plagioclase as inclusions and less commonly along cleavage planes or within fractures.

Garnet occurs rarely in samples of amphibole schist and plagioclase-amphibole schist as hypidioblastic to idioblastic, dodecahedral to sub-ovoid poikiloblasts up to 1 cm in diameter, which contain quartz inclusions set in a groundmass of quartz and biotite.

Tremolite has only been observed in a single sample of amphibole schist, occuring as hypidioblastic to xenoblastic grains, approximately 1 cm in length, with sutured grain boundaries. These crystals are colourless with a vibrant birefringence, which is indicative of tremolite.

2.5.2. Geochemical Analyses

The results of the major element oxide analyses were recalculated to a 100 wt. % anhydrous basis for comparison purposes. The chondrite and primitive mantle reservoir compositions used for normalization purposes are those of Sun and McDonough (1989) and Hofmann (1988), respectively. Europium (Eu/Eu*), Ce (Ce/Ce*), Nb (Nb/Nb*), Ti (Ti/Ti*), and Zr (Zr/Zr*) anomalies were calculated with respect to the concentrations of the neighbouring immobile elements, following the method of Taylor and McLennan (1985).

Plagioclase-amphibole Schist

Plagioclase-amphibole schist is characterized by variable SiO_2 (38.83 to 65.40 wt.%), MgO (1.70 to 7.26 wt.%), Fe_2O_3 (7.52 to 13.47 wt.%), TiO_2 (0. 60 to 1.19 wt.%), CaO (2.36 to 14.46 wt.%), K_2O (0.19 to 5.73 wt.%), and Na_2O (0.77 to 4.26 wt.%) and relatively high Al_2O_3 (13.66 to 21.63 wt.%) contents. These rocks also have relatively low Ni (20 to 50 ppm), Cr (20 to 120 ppm), Co (19 to 103 ppm), and Sc (19 to 37 ppm) abundances, and variable Mg-numbers (32 to 57) and V (75 to 327 ppm) abundances.

One exception is sample MG11-037, which has high Ni (1020 ppm) and Cr (1350 ppm) and low MgO (2.87 wt.%) contents. Sample MG11-037 has an LOI of 4.77 wt.%, contains a significant amount of hypidioblastic to xenoblastic calcite (5 to 10%) and chlorite (5 to 10%), which are after plagioclase and hornblende, respectively. Plagioclase-amphibole schist displays variable Al_2O_3/TiO_2 (14.3 to 30.2), Ti/Zr (58 to 232), and Zr/Y (2.3 to 5.1) ratios.

Plagioclase-amphibole schist has the following characteristics on chondrite- and primitive mantle-normalized trace element diagrams (Figs. 2.8a and 2.8b): 1) negligible to moderately enriched LREE (La/Sm_{CN} = 1.0 to 1.8; La/Yb_{CN} = 1.3 to 3.3) and moderately enriched HREE (Gd/Yb_{CN} = 1.1 to 1.7) patterns; 2) slightly negative to moderately positive Eu anomalies (Eu/Eu* = 0.9 to 1.4); 3) Ce anomalies (Ce/Ce* = 1.0 to 1.1) are absent; 4) moderately negative to slightly positive Nb anomalies (Nb/Nb* = 0.50 to 1.16), 5) negative to slightly positive Zr anomalies (Zr/Zr*= 0.64 to 1.12), and 6) slightly negative to moderately positive Ti anomalies (Ti/Ti* = 0.71 to 1.53).

Chlorite-amphibole Schist

Chlorite-amphibole schist is characterized by relatively high MgO (10.87 to 19.86 wt.%) and Fe_2O_3 (13.30 to 16.76 wt.%); moderate to low Al_2O_3 (5.54 to 12.04 wt.%), TiO_2 (0.89 to 1.56 wt.%), and CaO (4.73 to 12.54 wt.%); and variable but relatively low Na_2O (0.17 to 1.48 wt.%) and K_2O (0.04 to 2.01 wt.%) contents. Samples of chlorite-amphibole schist also have relatively high Ni (340 to 930 ppm) and Cr (920 to 1500 ppm) contents; high Mg-numbers (60 to 74); variable concentrations of V (162 to 307 ppm),

Co (49 to 85 ppm), and Sc (19 to 32 ppm); and display variable Al_2O_3/TiO_2 (6.2 to 7.7), Ti/Zr (95 to 109), and Zr/Y (5.1 to 7.1) ratios.

On primitive mantle- and chondrite-normalized trace element diagrams (Figs. 2.8c and 2.8d), samples of chlorite-amphibole schist are characterized by: 1) moderately enriched LREE (La/Sm_{CN} = 1.38 to 1.82; La/Yb_{CN} = 2.57 to 5.14) and moderately enriched HREE (Gd/Yb_{CN} = 1.48 to 2.32) patterns; 2) slightly negative to slightly positive Eu anomalies (Eu/Eu* = 0.82 to 1.14); 3) minor positive Ce anomalies (Ce/Ce* = 1.02 to 1.09); 4) slightly negative to slightly positive Nb anomalies (Nb/Nb* = 0.84 to 1.11), negative to slightly positive Zr anomalies (Zr/Zr* = 0.62 to 1.12), and positive Ti (Ti/Ti* = 1.05 to 1.88) anomalies.

Quartz-plagioclase-biotite Schist

Quartz-plagioclase-biotite schist is characterized by variable abundances of SiO_2 (48.48 to 60.18 wt.%), Al_2O_3 (14.60 to 21.09 wt.%), TiO_2 (0.61 to 0.89 wt.%), Fe_2O_3 (7.54 to 12.98 wt.%), MgO (1.96 to 6.63 wt.%), Na_2O (0.27 to 3.23 wt.%), K_2O (1.53 to 6.39 wt.%), and CaO (1.74 to 14.46 wt.%). Similar to samples of plagioclase-amphibole schist, these rocks are also characterized by low Ni (20 to 60 ppm), Cr (20 to 90 ppm), Co (15 to 44 ppm), Sc (18 to 29 ppm); variable V (114 to 253 ppm) abundances and Mg-numbers (30 to 60); however, they exhibit relatively restricted Al_2O_3/TiO_2 (18.5 to 27.4), Ti/Zr (95 to 145), and Zr/Y (2.9 to 4.2) ratios.

On chondrite- and primitive mantle-normalized trace element diagrams (Figs. 2.8e and 2.8f), samples of quartz-plagioclase-biotite schist have the following characteristics: 1) moderately enriched LREE (La/Sm_{CN} = 1.2 to 1.6; La/Yb_{CN} = 1.2 to 3.2) and slightly

depleted to moderately enriched HREE (Gd/Yb_{CN} = 0.9 to 1.7) patterns; 2) slightly negative to moderately positive Eu anomalies (Eu/Eu* = 0.8 to 1.4); 3); negligible Ce anomalies (Ce/Ce* = 1.0 to 1.1); 4) slightly negative to negligible Nb anomalies (Nb/Nb* = 0.79 to 1.02), negative Zr anomalies (Zr/Zr* = 0.71 to 0.90), and negligible to moderately positive Ti anomalies (Ti/Ti* = 1.00 to 1.36).

Amphibole Schist

Amphibole schist is characterized by variable SiO_2 (46.22 to 77.07 wt.%), MgO (1.57 to 7.02 wt.%), Fe_2O_3 (4.25 to 32.54 wt.%), TiO_2 (0.33 to 0.87 wt.%), CaO (1.37 to 9.22 wt.%), K_2O (0.52 to 4.33 wt.%), and Na_2O (0.25 to 2.65 wt.%) contents, and moderate to relatively high Al_2O_3 (7.91 to 18.16 wt.%) contents. Samples of amphibole schist have relatively low Ni (20 to 170 ppm), Cr (30 to 620 ppm), Co (9 to 51 ppm), Sc (11 to 25 ppm) contents, variable Mg-numbers (13 to 52) and V (51 to 144 ppm) contents, and variable Al_2O_3/TiO_2 (19.4 to 30.4), Ti/Zr (26 to 65), and Zr/Y (2.7 to 8.9) ratios.

On primitive mantle- and chondrite-normalized trace element diagrams (Figs. 2.9a and 2.9b), units of amphibole schist exhibit the following: 1) enriched LREE (La/Sm_{CN} = 1.94 to 2.75; La/Yb_{CN} = 3.29 to 8.07) and slightly to moderately enriched HREE (Gd/Yb_{CN} = 1.10 to 2.38) patterns; 2) moderately negative to weak positive Eu anomalies (Eu/Eu* = 0.53 to 1.08); 3) weak positive Ce anomalies (Ce/Ce*=1.02 to 1.10); (4) strongly negative Nb anomalies (Nb/Nb* = 0.22 to 0.50), negative to weak positive Zr anomalies (Zr/Zr* = 0.61 to 1.04), and negative to weak positive Ti anomalies (Ti/Ti* = 0.29 to 1.17).

Amphibolite

Amphibolite pods are characterized by relatively high MgO (11.61 to 12.19 wt.%), Fe_2O_3 (8.67 to 10.55 wt.%), Ni (310 to 330 ppm), Cr (730 to 960 ppm), and Mg-numbers (70 to 73); moderate Al_2O_3 (13.00 to 13.71 wt.%), TiO_2 (0.68 to 0.81 wt.%), and CaO (10.60 to 12.10 wt.%) contents; and low Na_2O (0.68 to 1.20 wt.%) and K_2O (0.29 to 0.44 wt.%) contents. Amphibolite is also characterized by relatively narrow ranges of V (132 to 161 ppm), Co (31 to 45 ppm), and Sc (21 to 26 ppm) concentrations, and Al_2O_3/TiO_2 (16.1 to 20.3), Ti/Zr (31 to 36), and Zr/Y (8.6 to 8.7) ratios.

On primitive mantle- and chondrite-normalized trace element diagrams (Figs. 2.9c and 2.9d), amphibolite pods are characterized by: 1) strongly enriched LREE (La/Sm_{CN} = 2.93 to 3.07; La/Yb_{CN} = 15.77 to 16.18) and enriched HREE (Gd/Yb_{CN} = 2.75 to 2.90) patterns; 2) moderately negative to weak positive Eu anomalies (Eu/Eu* = 0.69 to 1.07); 3) weak positive Ce anomalies (Ce/Ce* = 1.03 to 1.07); 4) strong negative Nb anomalies (Nb/Nb* = 0.32 to 0.35), negative Zr anomalies (Zr/Zr* = 0.58 to 0.94), and moderately negative Ti anomalies (Ti/Ti*=0.63 to 0.73).

Quartz-amphibole Schist

Quartz-amphibole schist is characterized by variable SiO_2 (49.29 to 58.59 wt.%), MgO (0.91 to 6.72 wt.%), Fe_2O_3 (11.15 to 13.03 wt.%), TiO_2 (1.46 to 1.94 wt.%), CaO (5.06 to 9.25 wt.%), K_2O (0.21 to 2.48 wt.%), and Na_2O (2.10 to 4.03 wt.%), and moderate to high Al_2O_3 (15.09 to 18.83 wt.%) contents. These rocks also have relatively low Ni (20 to 100 ppm), Cr (20 to 100 ppm), Co (14 to 63 ppm), and Sc (23 to 30 ppm)

abundances, variable Mg-numbers (14 to 51), and V (45-314 ppm) contents, and variable Al_2O_3/TiO_2 (8.2 to 12.9), Ti/Zr (38 to 102), and Zr/Y (6.2 to 10.0) ratios.

On chondrite- and primitive mantle-normalized trace element diagrams (Figs. 2.9e and 2.9f), units of quartz-amphibole schist have the following characteristics: 1) strongly enriched LREE (La/Sm_{CN} = 1.81 to 3.06; La/Yb_{CN} = 5.15 to 8.99) and moderately to strongly enriched HREE (Gd/Yb_{CN} = 1.42 to 2.12) patterns; 2) negligible Eu anomalies (Eu/Eu* = 0.97 to 1.06); 3) negligible Ce anomalies (Ce/Ce* = 0.96 to 1.02); 4) weak negative to weak positive Nb anomalies (Nb/Nb* = 0.93 to 1.14), weak negative to weak positive Zr anomalies (Zr/Zr* = 0.90 to 1.17), and weak negative to strong positive Ti anomalies (Ti/Ti* = 0.75 to 1.65).

Amphibolite Dykes

Amphibolite dykes are characterized by variable SiO_2 (45.85 to 51.57 wt.%), MgO (4.42 to 7.94 wt.%), Fe_2O_3 (12.64 to 14.38 wt.%), TiO_2 (0.57 to 0.94 wt.%), CaO (7.90 to 8.86 wt.%), K_2O (0.25 to 1.98 wt.%), and Na_2O (2.21 to 3.63 wt.%), and relatively high Al_2O_3 (17.35 to 19.32 wt.%) contents. These rocks also have relatively low Ni (40 to 70 ppm), Cr (60 to 90 ppm), Co (34 to 52 ppm), Sc (34 to 44 ppm) contents, and variable Mg-numbers (41 to 55) and V (176 to 317 ppm) contents. Two distinct clusters of samples (Groups 1 and 2) can be distinguished based on their REE fractionation and Nb anomalies.

Group 1 Amphibolite Dykes

On chondrite- and primitive mantle-normalized trace element diagrams (Figs. 2.9g and 2.9h), Group 1 amphibolite dykes are characterized by: 1) moderately to

strongly enriched LREE (La/Sm_{CN} = 1.57 to 1.99; La/Yb_{CN} = 1.91 to 4.58) and negligible to strongly enriched HREE (Gd/Yb_{CN} = 0.97 to 1.80) patterns; 2) weak negative to negligible positive Eu anomalies (Eu/Eu* = 0.74 to 1.05); 3) negligible Ce anomalies (Ce/Ce* = 0.97 to 1.010); 4) negligible to weak positive Nb anomalies (Nb/Nb* = 0.99 to 1.21), negative Zr anomalies (Zr/Zr* = 0.60 to 0.92), and weak negative to strong positive Ti anomalies (Ti/Ti* = 0.78 to 2.66).

Group 2 Amphibolite Dykes

One sample (i.e., LL13-17) represents the second amphibolite dyke group and is differentiated from the other group by positive fractionation of REE and moderately negative Nb anomalies (Nb/Nb*= 0.58). On chondrite- and primitive mantle-normalized trace element diagrams, sample LL13-17 has the following characteristics (Figs. 2.9g and 2.9h): 1) slightly enriched LREE (La/Sm_{CN} = 1.19; La/Yb_{CN} = 1.77) and HREE (Gd/Yb_{CN} = 1.20) patterns; 2) moderately positive Eu anomalies (Eu/Eu* = 1.38); 3) slightly negative Ce anomalies (Ce/Ce* = 0.95); 4) slightly negative Zr anomalies (Zr/Zr* = 0.79), and moderately positive Ti anomalies (Ti/Ti* = 1.32).

2.6. Discussion

2.6.1. Whole Rock Alteration

Patterns of deformation, alteration, and metamorphism in the Lynn Lake greenstone belt can be locally complex; however, regional metamorphic grade typically ranges between upper greenschist and upper amphibolite facies, with the greatest proportion of rocks exhibiting middle amphibolite facies equilibrium mineral assemblages (Milligan, 1960; Gilbert et al., 1980). Research in Archean greenstone

terranes (i.e., Winchester and Floyd, 1977; Dostal et al., 1980; Kerrich and Fyfe, 1981; Polat and Hofmann, 2003) has shown that, under amphibolite-facies metamorphic conditions, HFSE typically remain immobile; however, Fedikow (1992) implied that a period of intense hydrothermal activity in the vicinity of the MacLellan deposit resulted in HFSE mobility, which imprinted the chemical characteristics of the aluminous basalts onto what were interpreted to be biotite-rich clastic sedimentary rocks. Therefore, it is important to assess the potential effects of post-magmatic and post-metamorphic alteration on the geochemistry of least altered and altered samples from the MacLellan host rock sequence before undertaking igneous protolith identification and tectonic classification.

Plagioclase-amphibole schist, chlorite-amphibole schist, quartz-plagioclase-biotite schist, quartz-amphibole schist, amphibolite, amphibole schist, and amphibolite dykes comprise metamorphic mineral assemblages that include hornblende + albite + quartz and secondary mineral assemblages that include actinolite + chlorite + biotite + quartz + calcite. The metamorphic mineral assemblages are consistent with lower amphibolite metamorphic grade (North American Geologic-Map Data Model Science Language Technical Team, 2004); however, the replacement of hornblende by a combination of actinolite and chlorite along grain boundaries, fractures, and cleavage planes are interpreted to be the result of retrograde greenschist metamorphism of the original metamorphic assemblage.

Biotite is observed replacing hornblende and plagioclase at grain boundaries, fractures, cleavages, and rarely as inclusions that are interpreted to be the result of potassic metasomatism, rather than regional metamorphism. Similarly, quartz and calcite

are observed replacing the primary assemblages in pervasively altered samples and are interpreted to represent a combination of silicification and carbonatization.

Large ion lithophile elements (LILE) are expected to be mobile under most metamorphic conditions, but HFSE and transitional metals are expected to be immobile under similar conditions (Winchester and Floyd, 1977; Dostal et al., 1980; Kerrich and Fyfe, 1981; Polat and Hofmann, 2003). Concentrations of LILE, SiO_2, and CaO display large variations in fine-grained amphibolite, plagioclase-phyric amphibolite, medium-grained amphibolite, coarse-grained amphibolite dykes, biotite-plagioclase schist, and amphibole-chlorite schist for given MgO and Yb contents (Figs. 2.10 and 2.11), reflecting the mobility of the LILE, SiO_2, and CaO; which is consistent with potassic metasomatism, carbonatization, and silicification. The majority of samples display good correlation between HFSE and MgO or Yb (Figs. 2.10 and 2.11) on binary diagrams (Sun and McDonough, 1989). Similarly, all samples display coherent primitive mantle- and chondrite-normalized patterns, indicating that these elements were also relatively immobile during regional metamorphism and post-metamorphic alteration. These results suggest that, with respect to most non-LILE elements, the primary magmatic chemistry of the rocks has been largely preserved, which enables use of HFSE in classification of igneous protoliths and in determining the petrogenesis and geodynamic origin of the host rock sequence to the MacLellan Au-Ag deposit.

2.6.2. Protolith Classification and Origin of Quartz-plagioclase-biotite Schist

Despite multiple studies (e.g., Fox and Johnston, 1980; Fedikow, 1986, 1992; Gagnon, 1991), consensus has not been reached concerning the igneous protoliths to the

host rock sequence of the MacLellan Au-Ag deposit. Samples of plagioclase-amphibole schist and amphibolite dykes have Mg-numbers ranging from 32 to 57, and Zr/Y ratios ranging from 2.3 to 5.1, which are close to the range of Zr/Y ratios of modern tholeiitic basalts (2.0 to 4.5) (Barrett and MacLean, 1994). Samples containing an average aluminum content greater than 17 wt.% plot in the subalkaline basalt field on the Nb/Y vs. Zr/TiO_2 diagram (Fig. 2.12a), and trend from the tholeiitic to transitional field of the Yb vs. La magma series diagram (Fig. 2.12b); consistent with a transitional aluminous basalt classification. These results suggest that plagioclase-amphibole schist is the extrusive equivalent to the amphibolite dykes identified in Eastern Outcrops 1 and 2. Samples of amphibole schist consistently plot in the andesite field on the Nb/Y vs. Zr/TiO_2 diagram (Fig. 2.12a), and plot primarily in the calc-alkaline field on the Yb vs. La magma series diagram (Fig. 2.12b); consistent with a calc-alkaline andesite classification. Samples of quartz-amphibole schist plot in the field for alkaline basalts on the Nb/Y vs. Zr/TiO_2 diagram (Fig. 2.12a), plot within the calc-alkaline field of Yb vs. La magma series diagram (Fig. 2.12b), and have elevated HFSE contents; consistent with an alkaline basalt classification. Samples of chlorite-amphibole schist consistently plot in the picrite field of the $[Al_2O_3]$ vs. $[TiO_2]$ discrimination diagram (Fig. 2.13) and within the transitional field of the Yb vs. La magma series diagram (Fig. 2.12b); consistent with a picrite classification. Samples of amphibolite plot between the Ti-enriched and Al-undepleted komatiite fields of the $[Al_2O_3]$ vs. $[TiO_2]$ discrimination diagram (Fig. 2.13) and within the calc-alkaline field of the Yb vs. La magma series diagram (Fig. 2.12b); however, they have none of the primary characteristics that define a komatiite (cf., Kerr and Arndt, 2001). Rather, these samples display higher MgO (11.58 to 12.19 wt.%), Ni

(310 to 330 ppm), and Cr (730 to 960 ppm) contents and Mg-numbers (70 to 73) relative to 'normal' andesites and plot in the andesite field of the Nb/Y vs. Zr/TiO_2 discrimination diagram (Fig. 2.12a). Accordingly, these samples are best classified as calc-alkaline high-magnesian andesites (cf. McCarron and Smellie, 1998).

The origin of quartz-plagioclase-biotite schist is controversial, because it has been interpreted to be the primary metaliferous unit that is characteristic of the Agassiz Metallotect (Fedikow and Gale, 1982; Fedikow, 1986, 1992). Fedikow and Gale (1982) and Fedikow (1986) interpreted the intercalated quartz-plagioclase-biotite schist and picrites to represent an Au-bearing, syngenetic, exhalative ore horizon that characterized the mineralized zones within the MacLellan deposit. Alternatively, Gagnon (1991) suggested that the quartz-plagioclase-biotite schist may be biotite-altered basalt and interpreted the Au mineralization to be epigenetic in nature and associated with deformed quartz and sulphide mineral veins and associated alteration. Fedikow (1992) argued that the observed chemical similarities between the aluminous basalts and quartz-plagioclase-biotite schist to be the result of intense hydrothermal alteration associated with mineralization of the primary ore horizon. The results from this study (Figs. 2.10 and 2.11), however, show that the majority of the HFSE and transition metals were immobile when compared to both MgO and Yb contents indicating that, despite the interpretations of Fedikow (1992), the rocks retain their original magmatic chemistry.

Accordingly, the ratios of these trace elements can be used to determine the origin of the quartz-plagioclase-biotite schist. Compared to the aluminous basalt (i.e., plagioclase-amphibole schist), samples of quartz-plagioclase-biotite schist have similar REE patterns (Figs. 2.8a, b, e, and f), and similar TiO_2 and HREE concentrations for a

given MgO or Yb (Figs. 2.12 and 2.13) content. In addition, these rocks have comparable Zr/Ti, Nb/Y, Gd/Yb_{CN}, Zr/Sc, and Th/Sc ratios to aluminous basalt. Alternatively, the isocon method (after Grant, 1985, 2005) can be used to quantify metasomatism between unaltered and altered equivalants (e.g., to determine if quartz-plagioclase-biotite schist is the altered equivalent of aluminous basalt). Comparing the major and trace element chemistry of ten samples of quartz-plagioclase-biotite schist with ten samples of aluminous basalt on an isocon diagram shows two important characteristics (Fig. 2.14): 1) assuming constant mass, there are negligible enrichments or depletions in many of the elements that are considered immobile under most metamorphic conditions (Winchester and Floyd, 1977; Dostal et al., 1980; Kerrich and Fyfe, 1981; Polat and Hofmann, 2003); and 2) the only difference between quartz-plagioclase-biotite schist and aluminous basalt is an increase in some alkaline and alkaline earth metal content (e.g., Ba, Rb, K_2O) accompanied by decreases in Na_2O and Sr contents. Based on inter-element ratios and the results of the isocon analysis (Fig. 2.14), Nb/Y vs. Zr/TiO_2 (Fig. 2.12a), and Yb vs. La (Fig. 2.12b) diagrams, it is most likely that quartz-plagioclase-biotite schist is the altered equivalent of transitional aluminous basalts.

2.6.3. Depth of Partial Melting and Mantle Source Characteristics

HFSE distributions can be used to constrain the depths at which the magmas that produced the MacLellan deposit host rocks were produced and segregated from the mantle source. High pressure experimental studies show that a high-Mg (i.e., komatiitic) melt can be produced by a relatively low degree of partial melting of mantle at high pressure, or a relatively high degree of partial melting of mantle at lower pressure (Arndt,

2003; Herzberg, 1992; Wei et al., 1990). Irving and Frey (1978) noted that HREE distributions were significantly higher in garnet megacrysts compared to their host volcanic liquids of kimberlitic to rhyolitic composition and proposed that rocks forming within the garnet stability field will have fractionated HREE values as a result. The picrite and aluminous basalt that comprise the host rock sequence to the MacLellan Au-Ag deposit and the aluminous basalt dykes that intrude the alkaline basalt have slightly negative to moderately positive fractionated HREE (Gd/Yb_{CN} = 0.9 to 2.3) values, which may reflect a combination of melting at depths both within (> 90 km) and above (< 90 km) the garnet stability field. In contrast, large Gd/Yb_{CN} (1.10 to 2.90) and La/Yb_{CN} (3.29 to 16.18) ratios in the high-magnesium and calc-alkaline andesites are consistent with residual garnet in the source after melt extraction.

Pearce (1982, 2008) demonstrated that variations in Th/Yb vs. Nb(Ta)/Yb reflect a combination in degree of depletion or enrichment of the mantle source and fractional crystallization processes, and can be employed to further discriminate basalts from one another according to tectonic environment (i.e., convergent margin magmas vs. within-plate and spreading center basalts). On this diagram (Fig. 2.15), samples of picrite and aluminous basalt scatter between the contamination and within plate vectors, and the data trend, in terms of Ta/Th ratio, toward an enriched-mantle source. Alkaline basalt also scatters along the within plate vector, and the data extend in terms of Ta/Th ratio toward a more enriched source near the OIB location. Accordingly, aluminous basalt and picrite were derived from an enriched heterogenous mantle source, whereas alkaline basalt was derived from a source that is possibly depleted compared to modern OIB. Samples of calc-alkaline andesite plot on the boundary between continental and oceanic arcs, and

scatter along a trend that extends toward the lower crust value of Rudnick and Gao (2004). Samples of high-magnesium andesite plot in the continental arc field, near the upper crust value of Rudnick and Gao (2004).

The following geochemical characteristics suggest a petrogenetic link, through fractionation of a transitional parental magma, between basaltic rocks and picrite: 1) they all plot along the same fractionation trend in the transitional compositional field (Fig. 2.12b); 2) on MgO (Fig. 10) and Yb (Fig. 2.11) vs. incompatbible trace element diagrams; and 3) all samples, with the exception of a few outliers, display similar Th-Nb-La systematics (Figs. 2.8a to 2.8f).

2.6.4. Crustal Contamination

The tectonic environment of the host rock sequence to the MacLellan deposit has been interpreted to represent an intra-oceanic ridge (Fedikow and Gale, 1982; Fedikow, 1986), ocean island (Fedikow, 1992), or oceanic rift system (Zwanzig et al., 1999). Chemical modelling from the Cartwright Lake area (Peck and Smith, 1989), detailed mapping and major-element analyses from the Kisseynew Gneiss Belt (Zwanzig, 1990), Pb-Pb isotope analyses of feldspars from gabbroic stocks and rhyolitic flows in the northern Lynn Lake greenstone belt (Jurkowski, 1999), and Nd-Sm isotope analyses of samples of rhyolite and dacite from the Lynn Lake region (Beaumont-Smith and Böhm, 2004), however, provide a preponderance of evidence indicating contamination by continental crust of the plutonic and volcanic rocks that comprise the Lynn Lake greenstone belt. Therefore, it is pertinent to examine whether or not continental crust

contributed to the formation of the host rock sequence to the MacLellan Au-Ag deposit before considering any potential geodynamic models for the region.

The most reliable indicator of contamination by continental crust is the presence of a negative Nb anomaly on the primitive mantle-normalized trace element discrimination diagram, which is determined using Nb/Nb*, Nb/Th_{PM} and Nb/La_{PM} ratios (Nosova et al., 2010). This ratio in OIB, MORB, and continental tholeiites is close to 1, but decreases to 0.2 to 0.6 in strongly contaminated within-plate rocks (Nosova et al., 2010). For example, the Nb/La_{PM} is 0.22 to 0.56 in komatiites of the Vetreny Belt of Karelia (Puchtel et al., 1997), 0.15 to 0.25 in basic and ultrabasic rocks of the Bushveld province (Maier et al., 2000), while basalts of Etendeka are characterized by Nb/Nb* ratios between 0.25 and 0.9 (Thompson et al., 2007). The type of contaminant (e.g., upper crust or lower crust) can be deduced from the relative degree of REE fractionation in rocks with different degrees of contamination, the value of which is indicated by Nb/Nb*. The aluminous basalts and picrites show correlations of Nb/Nb* with La/Sm_{CN}, Nb/Th_{PM}, Nb/La_{PM} (Fig. 2.16) and La/Sm_{CN} with Nb/Th_{PM} and Nb/La_{PM} (Fig. 2.16), where samples trend toward the lower continental crust value; the average composition of which is characterized by Nb/Nb* of 0.55, La/Sm_{CN} of 1.84, Nb/Th_{PM} of 0.55, and Nb/La_{PM} of 0.62 (Rudnick and Gao, 2004). The high-magnesium and calc-alkaline andesites also show correlations of Nb/Nb* with La/Sm_{CN}, Nb/Th_{PM}, Nb/La_{PM} (Fig. 2.16) and La/Sm_{CN} with Nb/Th_{PM} and Nb/La_{PM} (Fig. 2.16), where samples trend toward the upper continental crust value; characterized by Nb/Nb* of 0.22, La/Sm_{CN} of 3.4, and Gd/Yb_{CN} of 1.7 (Rudnick and Gao, 2004).

Lassiter and DePaolo (1997) and Okamura et al., (2005) documented that La/Sm_{CN} correlated with La/Ta(Nb) (Fig. 2.17) where interaction of asthenospheric melts with continental crust or crustal melts had occurred, but not where asthenospheric melts had interacted with CLM. For samples obtained from the MacLellan volcanic rock sequence, the data trend between CLM and continental crust, extending toward the lower crust value of Rudnick and Gao (2004). Although Th-Nb-LREE systematics suggest contamination by sub-continental lithospheric mantle, contamination by continental crust cannot be ruled out given that subduction-modified lithospheric mantle and continental crust have similar trace element characteristics. Collectively, in the absence of radiogenic isotope data, it is possible that contamination of the MacLellan aluminous basalt and picrite by continental crust and subduction-metasomatized sub-continental lithospheric mantle are equally possible. Peck and Smith (1989), however, proposed that volcanic arc rocks of the Cartwright Lake area, which is situated in the southern section of the Lynn Lake greenstone belt, were erupted onto an already emplaced mafic platform making contamination through subduction-metasomatized sub-continental lithosphere unlikely.

2.6.5. Geodynamic Setting

The volcanic and associated rocks comprising and containing the MacLellan Au-Ag deposit and Agassiz Metallotect have been interpreted to represent an intra-oceanic ridge (Fedikow and Gale, 1982; Fedikow, 1986), ocean island (Fedikow, 1992), or oceanic rift system (Zwanzig et al., 1999); however, there is evidence that the volcanic rocks that occur within and in the vicinity of the MacLellan Au-Ag deposit have been contaminated by continental crust. There is no evidence that past studies (i.e., Fedikow

and Gale, 1982; Fedikow, 1986, 1992; Zwanzig et al., 1999) have even considered the possibility of crustally contaminated rocks occurring in the northern section of the Lynn Lake greenstone belt, rendering invalid the currently accepted regional geodynamic model of Zwanzig et al. (1999).

The volcanic rocks from the MacLellan area exhibit two distinct trends on the log-transformed IAB (island arc basalt)-MORB (mid-ocean ridge basalt)-CRB (continental rift basalt)+OIB (ocean island basalt) and IAB-OIB-CRB diagrams (Figs. 2.18a and 2.18b). Aluminous basalt, picrite, and alkaline basalt plot primarily within the MORB field with a few samples scattering into the CRB+OIB fields (Fig. 2.18a) and between the CRB and OIB fields (Fig. 2.18b). High magnesium and calc-alkaline andesites plot in the IAB field of the IAB-MORB-CRB+OIB (Fig. 2.18a) and IAB-OIB-CRB (Fig. 2.18b) diagrams. Alkaline basalt primarily cluster within the CRB+OIB (Fig. 2.18a) and CRB (Fig. 2.18b) fields.

The primitive mantle-normalized trace element trends observed for high-magnesium (Figs. 2.9c and 2.9d) and calc-alkaline andesites (Figs. 2.9a and 2.9b) are consistent with a volcanic arc setting (cf. Pearce and Peate, 1995; Woodhead et al., 1998; Pearce, 2008); however, the correlation of Nb/Nb* with La/Sm_{CN}, Nb/Th_{PM}, Nb/La_{PM} and La/Sm_{CN} with Nb/Th_{PM} and Nb/La_{PM}, is interpreted to be the result of contamination by upper crustal material, suggesting that these rocks formed in a continental volcanic arc setting.

Aluminous basalt and picrite show flat to E-MORB-style trends on chondrite- and primitive mantle-normalized diagrams (Figs. 2.8 and 2.9G, H). Data trends observed in

picrite and aluminous basalt in the MacLellan area are consistent with transitional rocks identified in Archean plume-derived oceanic plateau environments (Hollings and Kerrich, 2004; Young et al., 2006; Polat, 2009). In contrast, data trends observed in alkaline basalt are consistent with rocks common to an ocean island environment.

Though the composition of the picrite and aluminous basalt in the MacLellan area are consistent with emplacement in a plume-derived intra-oceanic plateau setting, the Nb-Th-La-REE systematic of these rocks are consistent with the contamination of the primary melt through the interaction of lower continental crust, continental lithospheric mantle, or a combination of the two, suggesting a near-continent setting. Kerrich et al. (2005) proposed that, because asthenospheric mantle plumes cannot melt beneath thick (greater than 200 km) continental lithosphere, they are "steered" to thinner margins where decompressional melting can occur at less than 150 km depth. The 3.51 Ga to 3.2 Ga basalt succession of the Pilbara Craton (Arndt et al., 2001), 3.0 Ga komatiite-basalt sequence of the North Caribou greenstone belt in the Superior Province (Hollings and Kerrich, 1999), volcanic rocks of the Taishan greenstone belt of the North China Craton (Polat et al., 2006), the Kambalda sequence of the Youanmi terrane in India (Said and Kerrich, 2010; Said et al., 2010), Sigegudda greenstone terrane of the Dharwar Craton (Said and Kerrich, 2010; Manikyamba et al., 2013), and the Kainuu Belt of the Fennoscandian Shield (Strand and Köykkä, 2012) preserve similar Nb-Th-La-REE systematics and are interpreted to be representative of a rifted continental margin setting. The presence of highly fractionated aluminous basalt ($MgO < 4$ wt.%; $Al_2O_3 > 17$ wt.%) suggests that this impinged mantle plume may have ponded either within or under the attenuated lithosphere. Cox (1980) proposed that dense picritic magmas pond within

deep sill complexes near the base of the crust (20 to 40 km depth). These sills provide an ideal environment for the fractionation of large volumes of magma within a comparatively restricted pressure range, and also one in which magmas are highly susceptible to crustal contamination (Patchett, 1980). Magmas from these lower sill complexes may feed directly to the surface via dykes, or they may pond again in higher level sill complexes, where further fractional crystallization and crustal contamination may occur before eruption. A similar model can be used to explain the formation of the aluminous basalt and picrite within the host rock sequence to the MacLellan Au-Ag deposit.

A three-stage evolutionary geodynamic model is proposed to explain the trace element characteristics of the host rock sequence to the MacLellan Au-Ag deposit. The first stage marks the initiation of rifting at a continental margin where the upwelling plume was contaminated by continental crust during redirection and ascent, with aluminous basalt and picrite erupting during this stage. In the second stage, oceanic crust is originated from an enriched upper mantle, close to present-day OIB. The third stage marks the development of an ocean-continent subduction system. Following the initiation of the ocean-continent subduction system at the cratonic margin, the mantle source for the calc-alkaline andesite and high-magnesium andesite was converted to a sub-arc mantle wedge. Hydrous fluids and/or melts originating from the subducted slab metasomatized the sub-arc mantle wedge, resulting in LREE-enriched and Nb-depleted normalized trace element patterns.

On the basis of field relationships, trace element data, and petrographic observations, the aluminous basalt and picrite that occur within the host rock sequence to

the MacLellan Au-Ag deposit are interpreted to be the products of a segment of Paleoproterozoic rifted continental margin that erupted in a near-continent environment.

2.7. Conclusions and Implications for Regional Geology

The following conclusions are drawn on the basis of field, petrographic, and geochemical characteristics of the Paleoproterozoic host rocks to the MacLellan Au-Ag deposit:

1. The host rock sequence to the MacLellan Au-Ag deposit is composed primarily of plagioclase-amphibole schist, quartz-plagioclase-biotite schist, and chlorite-amphibole schist. The igneous protoliths to the plagioclase-amphibole schist and chlorite-amphibole schist are transitional aluminous basalt and picrite, respectively. The quartz-plagioclase-biotite schist is interpreted, based on HFSE ratios, chondrite- and primitive mantle-normalized trends and the results of isocon analysis, to be the biotite-altered equivalent to transitional aluminous basalt.
2. Three volumetrically minor lithologies have been identified both within and in the vicinity the MacLellan Au-Ag deposit. These rocks are amphibole schist, pods of amphibolite that occur within outcrops of amphibole schist, and quartz-amphibole schist. The igneous protoliths to the amphibole schist and amphibolites are calc-alkaline andesite and high-Mg andesite, respectively. The igneous protolith to the quartz-amphibole schist is alkaline basalt.
3. Major and trace element data suggest a petrogenetic link, via a transitional differentiation trend, between the aluminous basalt and picrite. Calc-alkaline and high-Mg andesites have calc-alkaline affinity. In contrast, alkaline basalt has

distinct major and trace element characteristics, consistent with the existence of three distinct primary magma types.

4. The aluminous basalt and picrite display two different condrite-normalized REE patterns that result from partial melting at depths within (> 90 km) and outside of (< 90 km) the garnet stability field, respectively. Alkaline basalt, calc-alkaline andesite, and high-magnesium andesite display chondrite-normalized REE patterns that are consistent with a depth of partial melting within the garnet stability field (> 90 km).
5. The trace element systematics of aluminous basalt and picrite are consistent with a rifted continental margin geodynamic setting. Calc-alkaline andesite and high-magnesium andesite have trace element systematics consistent with a subduction zone geodynamic setting. Alkaline basalt has trace element systematics consistent with an ocean island geodynamic setting. On the basis of these geochemical characteristics, the northern Lynn Lake greenstone belt is interpreted to be a rifted continental margin that erupted in a near-continent setting.

The conclusions drawn from this study suggest that the northern section of the Lynn Lake greenstone belt has a complex geodynamic history as evidenced by the identification of three distinct primary magma types from within and the area around the MacLellan Au-Ag deposit. Isotope results from felsic volcanic and plutonic rocks of the northern section of the Lynn Lake greenstone belt indicate that crustal contamination has occurred (Jurkowski, 1999; Beaumont-Smith and Böhm, 2004), which is consistent with the interpretations of this study. Furthermore, the proposed geodynamic model for the

volcanic rocks comprising the northern section of the Lynn Lake greenstone belt is inconsistent with an exhalative origin for the Agassiz Metallotect.

2.8. References

Agrawal, S., Guevara, M., and Verma, S., 2008. Tectonic discrimination of basic and ultrabasic volcanic rocks through log-transformed ratios of immobile trace elements. International Geology Review 50, 1057-1079.

Arndt, N.T., 2003. Komatiites, kimberlites, and boninites. Journal of Geophysical Research: Solid Earth 108(B6), 2293.

Arndt, N.T., Bruzak, G., and Reischmann, T., 2001. The oldest continental and oceanic plateaus: geochemistry of basalts and komatiites of the Pilbara Craton, Australia. Geological Society of America Special Papers 352, 359-387.

Augsten, B.E.K., Thorpe, R.I., Harris, D.C., and Fedikow, M.A.F, 1986. Ore Geology of the Agassiz (MacLellan) Gold Deposit in the Lynn Lake Region, Manitoba. Canadian Mineralogist 24, 369-377.

Baldwin, D.A., Syme, E.C., Zwanzig, H.V., Gordon, T.M., Hunt, P.A., and Stevens, R.D., 1987. U-Pb zircon ages from the Lynn Lake and Rusty Lake metavolcanic belts, Manitoba: two ages of Proterozoic Magmatism. Canadian Journal of Earth Sciences 24, 1053-1063.

Bateman, J.D., 1945. McVeigh Lake area, Manitoba; Geological Survey of Canada Paper 45-14, 34 p.

Barrett, T.J., and MacLean, W.H., 1994. Chemostratigraphy and hydrothermal alteration in exploration for VHMS deposits in greenstones and younger volcanic rocks. In: Lentz, D.R. (Ed.). Alteration and alteration processes associated with ore-forming systems. St. John's: Geological Association of Canada. Short Course Notes 11, 433-467.

Beaumont-Smith, C.J., and Böhm, C.O., 2002. Structural analysis and geochronological studies in the Lynn Lake greenstone belt and its gold-bearing shear zones (NTS 64C10, 11, 12, 14, 15 and 16), Manitoba; *in* Report of Activities 2002, Manitoba Industry, Trade and Mines, Manitoba Geological Survey, 159-170.

Beaumont-Smith, C.J., and Böhm, C.O., 2003. Tectonic evolution and gold metallogeny of the Lynn Lake greenstone belt, Manitoba (NTS 64C10, 11, 12, 14, 15 and 16), Manitoba; *in* Report of Activities 2003, Manitoba Industry, Economic Development and Mines, Manitoba Geological Survey, 39-49.

Beaumont-Smith, C.J., and Böhm, C.O., 2004. Structural analysis of the Lynn Lake greenstone belt, Manitoba (NTS 64C10, 11, 12, 14, 15 and 16); *in* Report of Activities 2004, Manitoba Industry, Economic Development and Mines, Manitoba Geological Survey, 55-68.

Beaumont-Smith, C.J., Machado, N., Peck, D.C., 2006. New uranium-lead geochronology results from the Lynn Lake greenstone belt, Manitoba (NTS 64C11-16); Manitoba Science, Technology, Energy and Mines, Manitoba Geological Survey, Geoscientific Paper GP2006-1, 11 p.

Bickford, M.E., and Van Schmus, W.R., 1985. Preliminary U-Pb age data for the Trans-Hudsonian Orogen in northern Saskwatchewan; new and revised results. Miscellaneous Report – Saskatchewan Mineral Resources 85-4, 63-66.

Cox, K.C., 1980. A Model for Flood Basalt Vulcanism. Journal of Petrology 21(4), 629-650.

Donnelly K.E., Goldstein, S.L., Langmuir, C.H., Spiegelman, M., 2004. Origin of enriched ocean ridge basalts and implications for mantle dynamics. Earth and Planetary Science Letters 226, 347-366.

Dostal, J., Strong, D.F., and Jamieson, R.A., 1980. Trace element mobility in the mylonite zone within the ophiolite aureole, St. Anthony Complex, Newfoundland. Earth and Planetary Science Letters 49, 188-192.

Dudás, F.O., 1992. Petrogenetic evaluation of trace element discrimination diagrams. *In*: Batholomew, M.J., Hyndman, D.W., Mogk, D.W., and Mason, R. (Eds.). Basement Tectonics 8; Kluwer, Dodrecht, 93-127.

Fedikow, M.A.F., and Gale, G.H., 1982. Mineral deposit studies in the Lynn Lake area. *In* Manitoba Mineral Resources Division, Report of Field Activities, 44-54.

Fedikow, M.A.F., 1986. Geology of the Agassiz (MacLellan) Stratabound Au-Ag Deposit, Lynn Lake, Manitoba. Manitoba Energy and Mines, Geological Services Branch, Open File Report OF85-5, 80 p.

Fedikow, M.A.F., 1992. Rock geochemical alteration studies at the MacLellan Au-Ag deposit, Lynn Lake, Manitoba. Manitoba Energy and Mines, Geological Services, Economic geology Report ER92-1, 237 p.

Fox, J.S., and Johnston, W.G.Q., 1980. Komatiites, "boninites" and tholeiitic picrites in the central La Ronge metavolcanic belt, Saskatchewan and Manitoba, and their possible economic significance. Saskatchewan Department of Mineral Resources, Publication No. G-741-1-G-80, 51 p.

Gagnon, A., McKinnon, C., Tkaczuk, C., Burga, D., Puritch, E.J., McLaughlin, M., Bridson, P., Wenchang, N., and Yungang, W., 2013. Preliminary Economic Assessment for the MacLellan, Farley Lake, Burnt Timber, and Linkwood Properties, Lynn Lake Gold Camp, Manitoba. Effective December 2, 2013.

Gagnon, J.E., 1991. Geology, geochemistry, and genesis of the Proterozoic MacLellan Au-Ag Deposit, Lynn Lake greenstone belt, Manitoba. Unpublished M.Sc. thesis, University of Windsor, 275 p.

Gale, G.H., and McClenaghan, S.H., 2002. Determining residual mineral potential using europium anomalies in the Ruttan and Lynn Lake areas, Manitoba; *in* Report of Activities 2002, Manitoba Industry, Trade and Mines, Manitoba Geological Survey, 205-208.

Gale, G.H., 2003. Rare earth element studies of soils and vegetation over the MacBride Lake massive sulphide deposit and the MacLellan mine Rainbow gold zone, Lynn Lake area, Manitoba (NTS 64C15 and 64B12); *in* Report of Activities 2003, Manitoba Industry, Economic Development and Mines, Manitoba Geological Survey, 50.

Gale G.H., Pawliw, P., and Hill, G.T., 2004. Enzyme Leach^{SM} and Terrasol Leach^{SM} studies of soils at the MacLellan Au-Ag deposit, Lynn Lake, Manitoba (NTS 64C15); *in* Report of Activities 2004, Manitoba Industry, Economic Development and Mines, Manitoba Geological Survey, 92-103.

Gilbert, H.P., Syme, E.C., and Zwanzig, H.V., 1980. Geology of the metavolcanic and volcaniclastic metasedimentary rocks in the Lynn Lake area; Manitoba Energy and Mines, Geological Services, Geological Paper GP80-1, 118 p.

Gilbert, H.P., 1993. Geology of the Barrington Lake-Melvin Lake-Fraser Lake area. Manitoba Energy and Mines, Geological Report GR87-3, 97 p.

Grant, J.A., 1986. The isocon diagram-A simple solution to Gresens' equation for metasomatic alteration. Economic Geology 81, 1972-1982.

Grant, J.A., 2005. Isocon analysis: a brief review of the method of applications. Physics and Chemistry of the Earth 30(17-18), 997-1004.

Greene, A.R., Scoates, J.S., and Weis, D., 2008. Wrangellia flood basalts in Alaska: A record of plume-lithosphere interaction in a Late Triassic accreted oceanic plateau. Geochemistry, Geophysics, Geosystems 9(12), 1-34.

Hanski, E., Huhma, H., Rastas, P., and Kamenetsky, V.S., 2001. The Palaeoproterozoic Komatiite-Picrite Association of Finnish Lapland. Journal of Petrology 42(5), 855-876.

Herzberg, C., 1992. Depth and degree of melting of komatiite. Journal of Geophysical Research 97, 4521-4540.

Hofmann, A.W., 1988. Chemical differentiation of the Earth: the relationship between mantle, continental crust, and oceanic crust. Earth and Planetary Science Letters 90, 297-314.

Hollings, P., and Kerrich, R., 2004. Geochemical systematic of tholeiites from the 2.86 Ga Pickle Crow assemblage, northwestern Ontario: arc basalts with positive and negative Nb-Hf anomalies. Precambrian Research 134, 1-20.

Hunt, P.A., Zwanzig, H.V., Anonymous, 1990. Pre-Missi granitoid domes in the Puffy Lake area, Kisseynew gneiss belt, Manitoba. Geological Survey of Canada 89-02, 71-75.

Irving, A.J. and Frey, F.A., 1978. Distribution of trace elements between garnet megacrysts and host volcanic liquids of kimberlitic to rhyolitic composition. Geochimica et Cosmochimica Acta 42(6A), 771.

Jones, L.R., Lafrance, B., and Beaumont-Smith, C.J., 2006. Structural controls on gold mineralization at the Burnt Timber mine in the Lynn Lake greenstone belt, Trans-Hudson Orogen, Manitoba. Exploration and Mining Geology, 15, 89-100.

Jurkowski, J.S., 1999. Uranium-lead geochronology study of Lynn Lake greenstone belt, Manitoba. Unpublished M.Sc. thesis, University of Windsor, p.

Kerr, A.C., and Arndt, N.T., 2001. A note on the IUGS reclassification of the high-Mg and picritic volcanic rocks. Journal of Petrology 42(11), 2169-2171.

Kerrich, R., and Fyfe, W.S., 1981. The gold-carbonate association: Sources of CO2 fixation reactions in Archean lode deposits. Chemical Geology 33, 265-294.

Kerrich, R., Polat, A., Wyman, D., and Hollings, P., 1999a. Trace element systematic of Mg-, to Fe- tholeiitic basalt suites of the Superior Province: Implications for Archean mantle reservrois and greenstone belt genesis. Lithos 46, 163-187.

Kerrich, R., Wyman, D., Hollings, P., and Polat, A., 1999b. Variability of Nb/U and Th/La in 3.0 to 2.7 Ga Superior Province ocean plateau basalts: implications for the timing of continental growth and lithosphere recycling. Earth and Planetary Science Letters 168, 101-115.

Kerrich, R., Goldfarb, R., and Richard, J.P., 2005. Metallogenic Provinces in an evolving geodynamic framework. Economic Geology 100, 1097-1136.

Koo, J., 1976. Evaluation of massive sulphide environments in the Lynn Lake-Leaf Rapids region. Manitoba Mineral Resources Division, Report of Field Activties, 14-16.

Lassiter, J.C., and DePaolo, J., 1997. Plume/Lithosphere interaction in the generation of continental and oceanic flood basalts: chemical and isotopic constraints. Geophysical Monograph 100, 335-355.

Lewry, J.F., Macdonald, R., Livesey, C., Meyer, M., Van Schmus, R., and Bickford, M.E., 1987. U-Pb geochronology of accreted terranes in the Trans-Hudson Orogen, Northern Saskatchewan, Canada. *In* Pharoah, T.C., Beckinsale, R.D., and Rickard, D. (Eds.). Geochemistry and mineralization of Proterozoic Volcanic Suites, geological Society of London, Special Publication 33, 147-165.

Ma, G., Beaumont-Smith, C.J., and Lentz, D.R., 2000. Preliminary structural analysis of the Agassiz Metallotect near the MacLellan and Dot Lake gold deposits, Lynn lake greenstone belt (parts of NTS 64C/14, /15); *in* Report of Activities 2000, Manitoba Industry, Trade and Mines, Manitoba Geological Survey, p. 51-56.

Ma, G., and Beaumont-Smith, C.J., 2001. Stratigraphic and structural mapping of the Agassiz Metallotect near Lynn Lake, Lynn Lake greenstone belt (parts of NTS 64C/15, /15); *in* Report of Activities 2001, Manitoba Industry, Trade and Mines, Manitoba Geological Survey, 86-93.

Maier, W.D., Arndt, N.T., Curl, E.A., 2000. Progressive crustal contamination of the Bushveld Complex: evidence from Nd isotopic analyses of cumulate rocks. Contributions to Mineralogy and Petrology 140, 316-327.

Manikyamba, C., Kerrich, R., Polat, A., and Abhishek, S., 2013. Geochemistry to two stratigraphically-related ultramafic (komatiite) layers from the Neoarchean Sigegudda greenstone terrane, Western Dharwar Craton, India: Evidence for compositional diversity in Archean mantle plumes. Lithos 177, 120-135.

McCarron, J.J., and Smellie, J.L., 1998. Tectonic implication of fore-arc magmatism and generation of magnesian andesites. Journal of Geological Society of London 155, 269-280.

McRitchie, W.D., 1974. The Sickle-Wasekwan debate: a review. Manitoba Mines Branch, Geological Paper 1/74, 23 p.

Milligan, G.C., 1960. Geology of the Lynn Lake District. Manitoba Mines Branch, Publication 57-1, 317 p.

Norman, G.W.H., 1933. Graville Lake district, northern Manitoba. Geological Survey of Canada, Summary Report, Part C, 23-41.

Nosova, A.A., Sazonova, L.V., Gorozhanin, V.M., Kuz'menkova, O.F., Dubinina, E.O., 2010. Mesoproterozoic olivine gabbronorites of the Bashkirian anticlinorium, the South Urals: Parental melts and specifics of magma evolution. Petrology 18(1), 50-83.

Okamura, S., Arculus, R.J., Martynov, Y.A., 2005. Cenozoic Magmatism of the North-Eastern Eurasian Margin: The Role of Lithosphere Versus Asthenosphere. Journal of Petrology 46(2), 221-253.

Park, A.F., Beaumont-Smith, C.J., and Lentz, D.R., 2002. Structure and Stratigraphy in the Agassiz Metallotect, Lynn Lake greenstone belt (NTS 64C14 and 64C15), Manitoba; *in* Report of Activities 2002, Manitoba industry, Trade and mines, Manitoba Geological Survey, 171-186.

Patchett, P.J., 1980. Thermal effects of basalt on continental crust and crustal contamination of magmas. Nature 283, 559-561.

Pearce, J.A., 1982. Trace element characteristics of lavas from destructive plate boundaries. In: Thorpe, R.S. (Ed.). Andesites: Orogenic Andesites and Related Rocks. John Wiley & Sons, Chichester, 525-548.

Pearce, J.A., 1996. A user's guide to basalt discrimination diagrams. In: Wyman, D.A. (Ed.). Trace element geochemistry of volcanic rocks: applications for massive sulphide exploration. Geological Association of Canada, GAC Short Course Notes 12, 79-113.

Pearce, J.A., 2008. Geochemical fingerprinting of oceanic basalts with applications to ophiolite classification and the search for Archean oceanic crust. Lithos 100, 14-48.

Pearce, J.A., and Peate, D.W., 1995. Tectonic implications of the composition of volcanic arc magmas. Annual Reviews of Earth and Planetary Sciences 23, 251-285.

Peck, D.C., and Smith, T.E., 1989. The geology and geochemistry of an early-Proterozoic volcanic arc association at Cartwright Lake Lynn Lake greenstone belt, Northwestern Manitoba. Canadian Journal of Earth Sciences 26, 716-736.

Polat, A., 2009. The geochemistry of Neoarchean (ca. 2700 Ma) tholeiitic basalts, transitional to alkaline basalts, and gabbros, Wawa Subprovince, Canada: Implications for petrogenetic and geodynamic processes. Precambrian Research 168, 83-105.

Polat, A., Kerrich, R., and Wyman, D., 1998. The late Archean Schreiber-Hemlo and White River-Dayohessarah greenstone belts, Superior Province: collages of oceanic plateaus, oceanic arcs, and subduction-accretion complexes. Tectonophysics 289, 295-326.

Polat, A., and Hofmann, A.W., 2003. Alteration and geochemical patterns in the 3.7-3.8 Ga Isua greenstone belt, West Greenland. Precambrian Research 126, 197-218.

Polat A., Li, J., Fryer, B., Kusky, T., Gagnon, J., and Zhang, S., 2006. Geochemical characteristics of the Neoarchean (2800-2700 Ma) Taishan Greenstone Belt, North China Craton: Evidence for plume-craton interaction. Chemical Geology 230, 60-87.

Puchtel, I.S., Haase, K.M., Hofmann, A.W., Chauvel, C., Kulikov, V.S., Garbe-Schönberg, C.-D., Nemchin, A.A., 1997. Petrology and geochemistry of crustally contaminated komatiitic basalts from the Vetreny Belt, southeastern Baltic Shield: evidence for an early Proterozoic mantle plume beneath rifted Archean continental lithosphere. Geochim Cosmochim Acta 61, 1205-1222.

Ray, G.E., and Wanless, R.K., 1980. The ages of the Wathaman Batholith, Johnson River Granite and Peter Lake Complex and their geological relationships to the Wollaston, Peter Lake and Rottenstone Domains of northern Saskatchewan. Canadian Journal of Earth Sciences 17, 333-347.

Ross, P.-S., and Bédard, J.H., 2009. Magmatic affinity of modern and ancient subalkaline volcanic rocks determined from trace-element discriminant diagrams. Canadian Journal of Earth Sciences 46, 823-839.

Rudnick, R.L., and Gao, S., 2004. Composition of the Continental Crust. Treatise on Geochemistry 3, 1-64.

Said, N., and Kerrich, R., 2009. Geochemistry of coexisting depleted and enriched Paringa Basalts, in the 2.7 Ga Kalgoorlie Terrane, Yilgarn Craton, Western Australia: Evidence for a heterogeneous mantle plume event. Precambrian Research 174, 287-309.

Said, N., and Kerrich, R., 2010. Magnesian dyke suites of the 2.7 Ga Kambalda Sequence: Evidence for coeval melting of plume asthenosphere and metasomatised lithospheric mantle. Precambrian Research 180, 183-203.

Said, N., Kerrich, R., Groves, D.I., 2010. Geochemical systematics of Basalts of the Lower Basalt Unit, 2.7 Ga Kambalda Sequence: Plume Impingement at a Rifted Craton Margin. Lithos 115, 82-100.

Samson, I.M., and Gagnon, J.E., 1995. Episodic fluid infiltration and genesis of the Proterozoic MacLellan Au-Ag deposit, Lynn Lake greenstone belt, Manitoba. Exploration and Mining Geology 4-1, 33-50.

Samson, I.M., Blackburn, W.H., and Gagnon, J.E., 1999. Paragenesis and composition of amphibole and biotite in the MacLellan gold deposit, Lynn Lake greenstone belt, Manitoba, Canada. Canadian Mineralogist 37, 1405-1421.

Strand, K., and Köykkä, J., 2012. Early Paleoproterozoic rift volcanism in the eastern Fennoscandian Shield related to the breakup of the Kenorland supercontinent. Precambrian Research 214-215, 95-105.

Sun, S.S., and McDonough, W.F., 1989. Chemical and isotopic systematic of oceanic basalts: implications for mantle composition and processes. Geological Society of London, Special Publications 42, 313-345.

Syme, E.C., 1985. Geochemistry of metavolcanic rocks in the Lynn lake belt; Manitoba Energy Mines, Geological Servies, Geological Report GR84-1.

Taylor, S.R., and McLennan, S.M., 1985. The continental crust: Its composition and evolution. Blackwell, Oxford, 312 pp.

Thompson, R.N., Riches, A.J.V., Antoshechkina, P.M., Pearson, D.G., Nowell, G.M., Ottley, C.J., Dickin, A.P., Hards, V.L., Nguno, A.K., and Niku-Paavola, V., 2007. Origin of CFB Magmatism: Multi-tiered Intracrustal Picrite-Rhyolite Magmatic Plumbing at Spitzkoppe, Western Namibia, during Early Cretaceous Etendeka Magmatism. Journal of Petrology 48(6), 1119-1154.

Turek, A., Woodhead, J., and Zwaznig, H.V., 2000. U-Pb age of the gabbro and other plutons at Lynn Lake (part of NTS 64C); *in* Report of Activities 2000, Manitoba Industry, trade and Mines, Manitoba Geological Survey, p. 97-104.

Van Schmus, W.R., Bickford, M.E., Lewry, J.F., and Macdonald, R., 1987. U-Pb geochronology in the Trans-Hudson orogen, northern Saskatchewan Canada. Canadian Journal of Earth Sciences 24, 407-424.

Wei, K., Tronnes, R.G., and Scrafe, C.M., 1990. Phase relations of aluminum-undepleted and aluminum-depleted komatiites at pressures of 4-12 GPa. Journal of Geophysical Research 95, 15,817-15,827.

Winchester, J.A., and Floyd, P.A., 1977. Geochemical discrimination of different magma series and their differentiation products using immobile elements. Chemical Geology 20, 325-343.

Woodhead, J.D., Eggins, S.M., and Johnson, R.W., 1998. Magma genesis in the New Britain island arc: further insights into the melting and mass transfer processes. Journal of Petrology 39, 1641-1668.

Wyman, D., and Kerrich, R., 2009. Plume and Arc magmatism in the Abitibi Subprovince: implications for the origin of Archean Continental Lithospheric Mantle. Precambrian Research 168, 4-22.

Young, G.M., 2002. Geochemical investigation of a Neoproterozoic glacial unit: The Mineral Fork Formation in the Wasatch Range, Utah. Geological Society of America Bulletin 114, 387.399.

Young, M.D., McNicoll, V., Helmstaedt, H., Skulski, T., and Percival, J.A., 2006. Pickle Lake revisited: New structural, geochronological and geochemical constraints on greenstone belt assembly, western Superior Province, Canada. Canadian Journal of Earth Sciences 46, 821-847.

Zwanzig, H.V., 1990. Kisseynew gneiss belt in Manitoba: stratigraphy, structure and tectonic evolution. In: Lewry, J.F., and Stauffer, M.R. (Eds.). The Early Proterozoic Trans-Hudson Orogen of North America. Geological Asssociation of Canada, Special Paper 37, 95-120.

Zwanzig, H.V., Syme, E.C., and Gilbert, H.P., 1999. Updated trace element geochemistry of ca. 1.9 Ga metavolcanic rocks in the Paleoproterozoic Lynn Lake Belt; Manitoba Industry, Trade and Mines, Geological Servies, Open File Report OF99-13, 48p. Plus map and diskette.

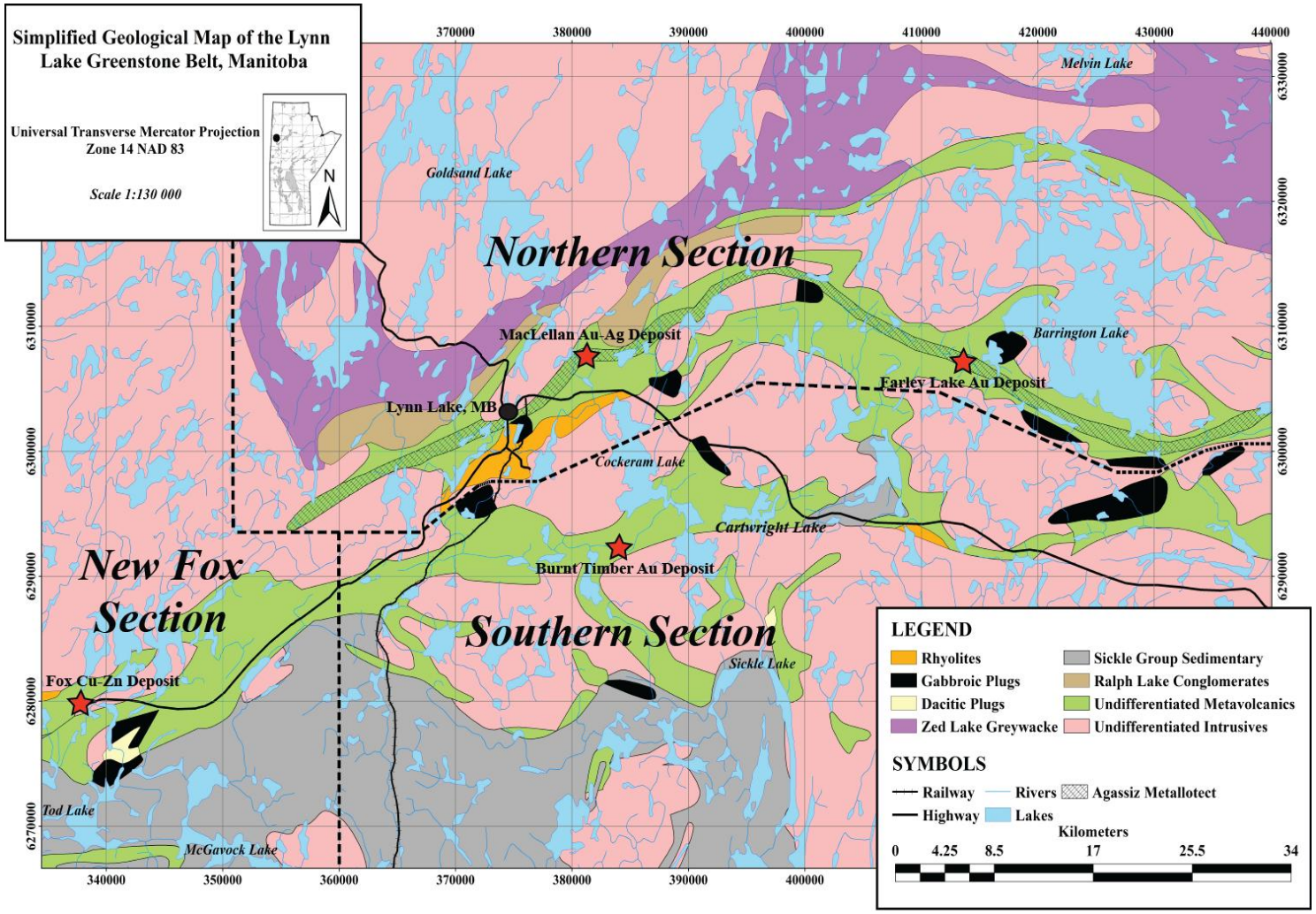

Figure 2.1 – Simplified regional geologic map of the Lynn Lake region showing the Agassiz Metallotect, MacLellan Au-Ag deposit, town of Lynn Lake, and greenstone belt subdivisions.

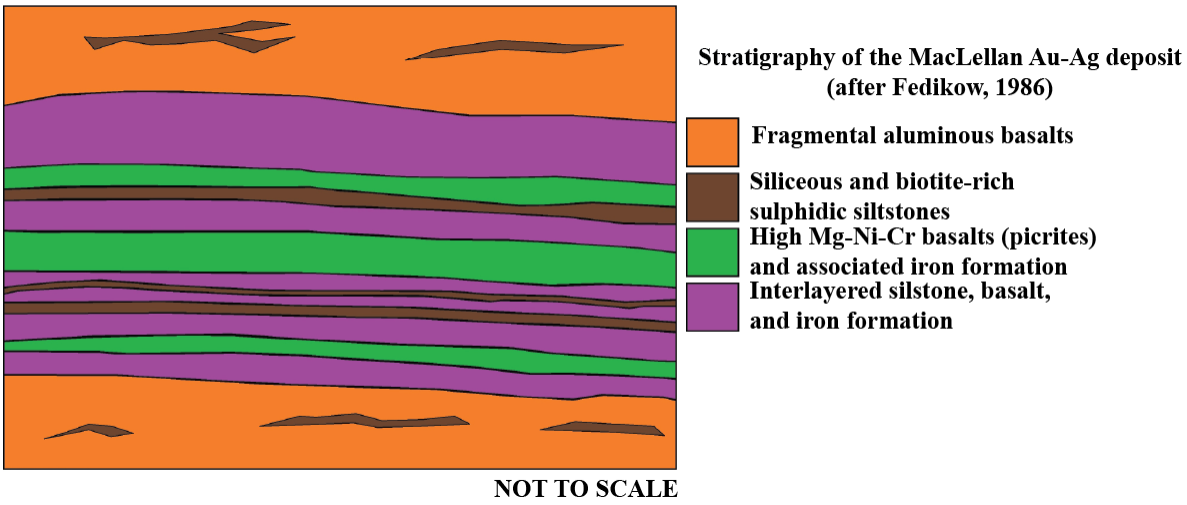

Figure 2.2 – Simplified stratigraphic cross-section of the MacLellan Au-Ag deposit/Agassiz Metallotect (after Fedikow, 1986).

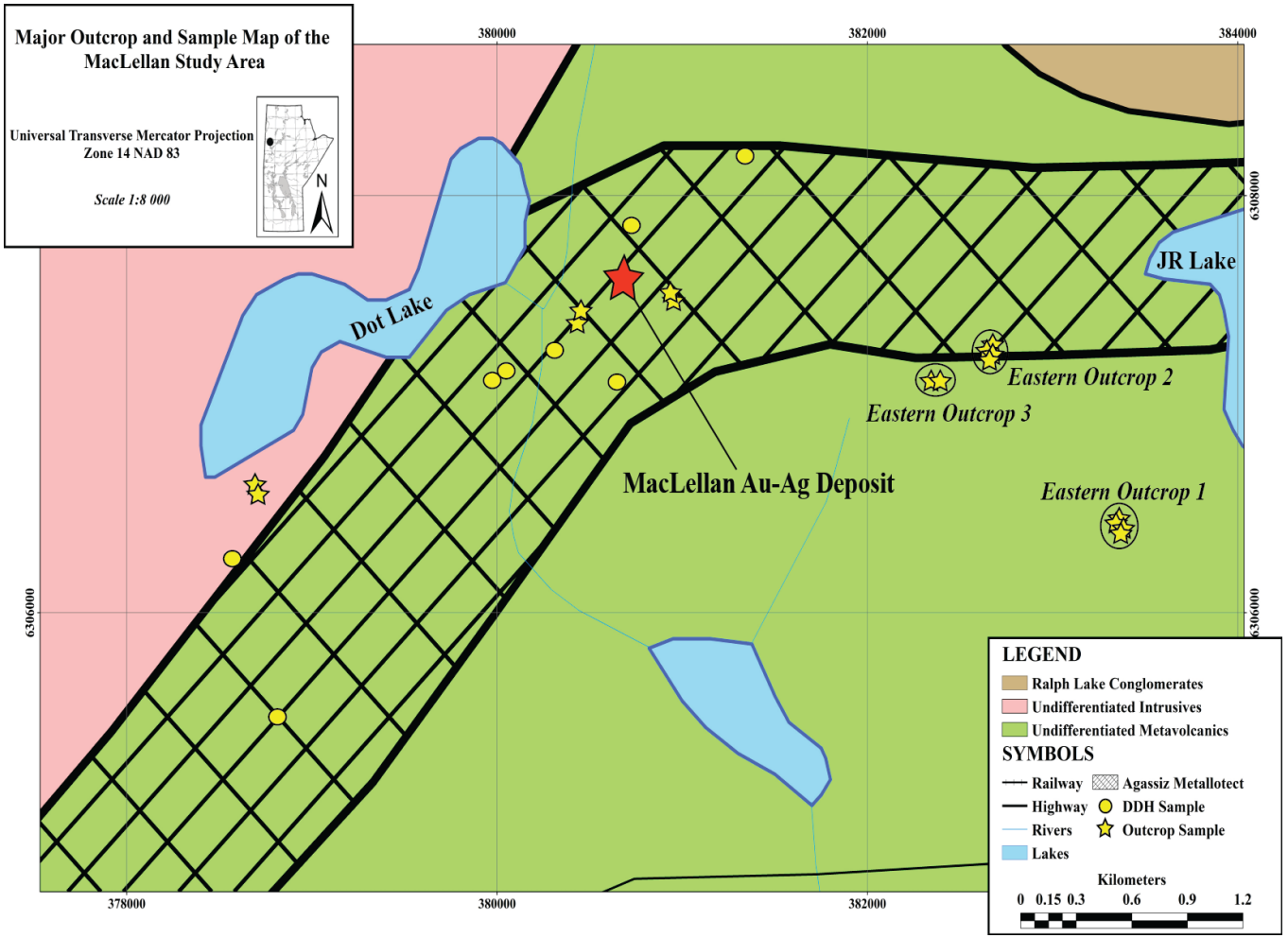

Figure 2.3 – Simplified geologic map of the area proximal to the MacLellan Au-Ag deposit showing position of large outcroppings (circles around samples), outcrop samples (yellow stars), and diamond drill-hole (DDH) samples (yellow circles).

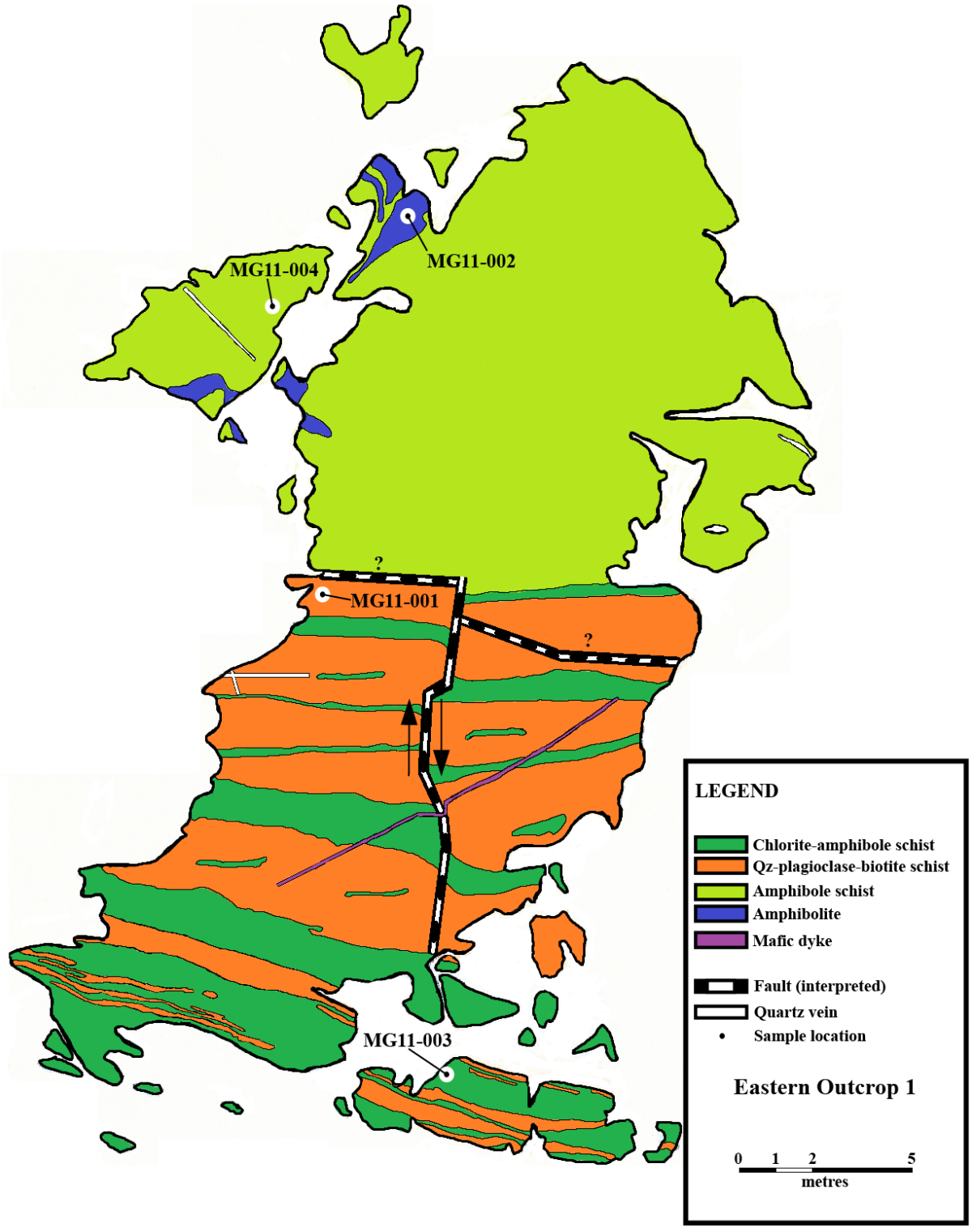

Figure 2.4 – Geologic map of Eastern Outcrop 1 showing approximate sample locations (black circle within white circle).

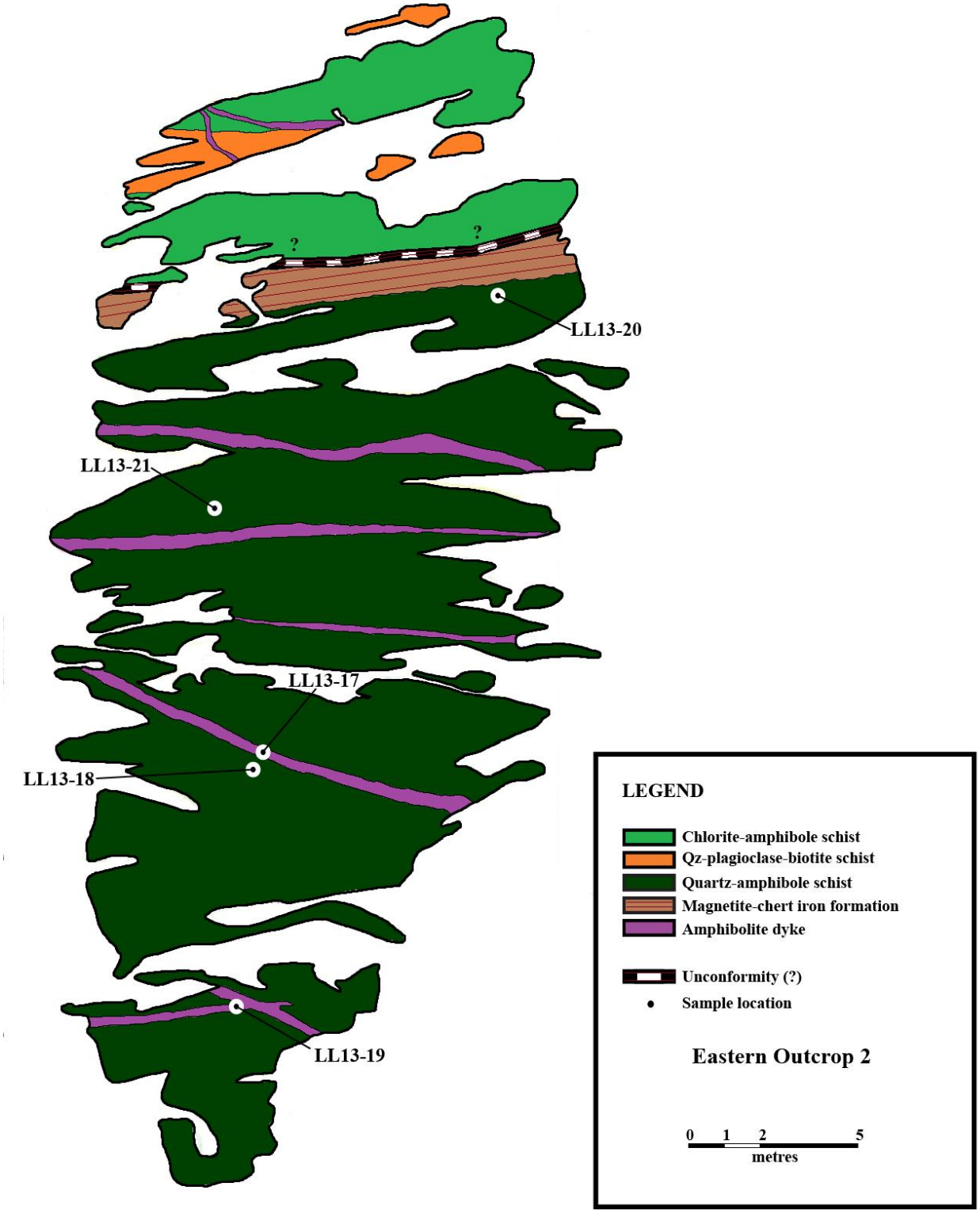

Figure 2.5 – Geologic map of Eastern Outcrop 2 showing approximate sample locations (black circle within white circle).

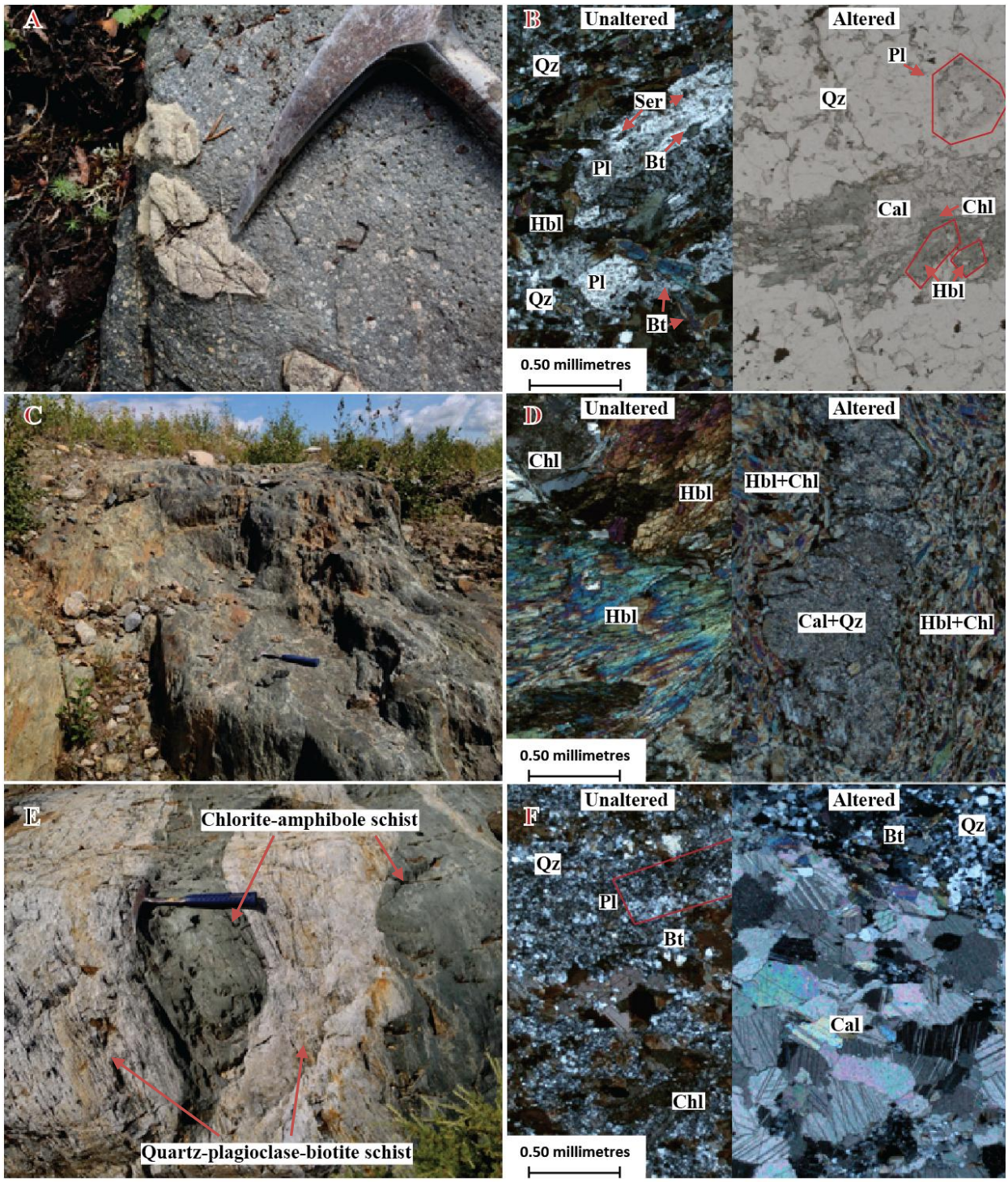
A
B
Unaltered
Qz
Ser
Pl
Bt
Hbl
Pl
Qz
Bt
0.50 millimetres
Altered
Pl
Qz
Cal
Chl
Hbl
C
D
Unaltered
Chl
Hbl
Hbl
0.50 millimetres
Altered
Hbl+Chl
Cal+Qz
Hbl+Chl
E
Chlorite-amphibole schist
Quartz-plagioclase-biotite schist
F
Unaltered
Qz
Pl
Bt
Chl
0.50 millimetres
Altered
Bt
Qz
Cal

Figure 2.6

Figure 2.6 – A) Field photograph proximal to the MacLellan Au-Ag deposit of an outcropping of plagioclasamphibolites-amphibole schist; B) Photomicrograph of an unaltered (crossed polarized light) and altered (plane polarized light) plagioclase-amphibole schist; C) Field photograph of an irregularly shaped pod of chlorite-amphibole schist; D) Photomicrograph of unaltered (crossed polarized light) and altered (crossed polarized light) chlorite-amphibole schist; E) Field photograph from Eastern Outcrop 1 of fine-grained, intercalated chlorite-amphibole and quartz-plagioclase-biotite schists; and, F) Photomicrograph of an unaltered (crossed polarized light) and altered (crossed polarized light) quartz-plagioclase-biotite schist.

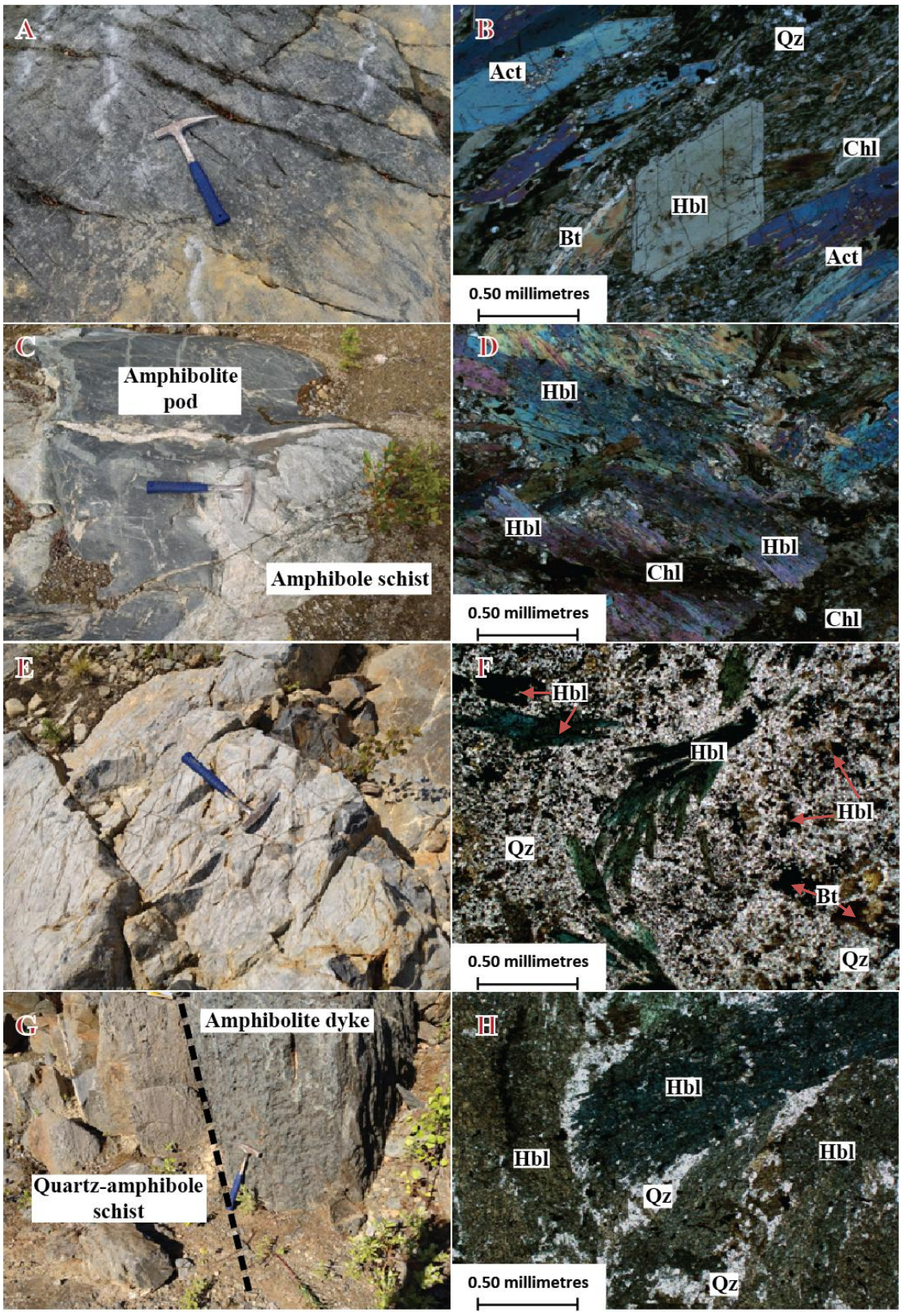
A
B
Act
Qz
Chl
Hbl
Bt
Act
0.50 millimetres
C
Amphibolite pod
Amphibole schist
D
Hbl
Hbl
Hbl
Chl
Chl
0.50 millimetres
E
F
Hbl
Hbl
Hbl
Qz
Bt
Qz
0.50 millimetres
G
Amphibolite dyke
Quartz-amphibole schist
H
Hbl
Hbl
Hbl
Qz
Qz
0.50 millimetres

Figure 2.7

Figure 2.7 – A) Field photograph from Eastern Outcrop 1 of an outcropping of amphibole schist; B) Photomicrograph of an amphibole schist under cross polarized light; C) Field photograph from Eastern Outcrop 1 of a large, irregularly shaped, lensoidal pod of amphibolite within an outcropping of amphibole schist; D) Photomicrograph of amphibolite under cross polarized light; E) Field photograph from Eastern Outcrop 2 of quartz-amphibole schist; F) Photomicrograph of quartz-amphibole schist under plane polarized light; G) Field photograph from Eastern Outcrop 2 of an amphibolite dyke obliquely cross-cutting an outcrop of quartz-amphibole schist; and, H) Photomicrograph of an amphibolite dyke under plane polarized light.

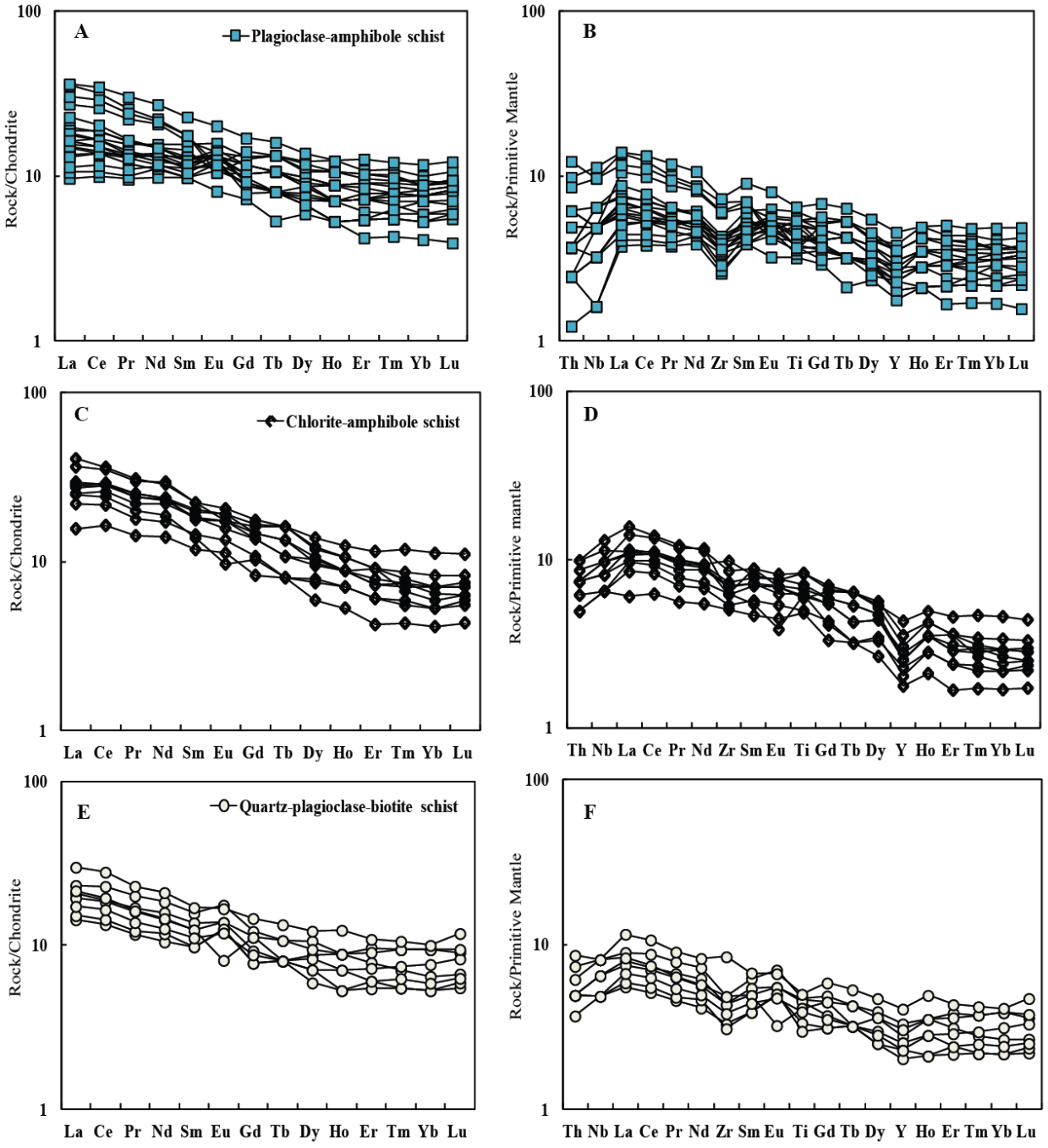

Figure 2.8 – Paired chondrite-normalized REE and primitive mantle-normalized multi-element diagrams for the plagioclase-amphibole schist (A and B), chlorite-amphibole schist (C and D), and quartz-plagioclase-biotite schist (E and F). Chondrite-normalizing values are from Sun and McDonough (1989) and primitive mantle-normalized values are from Hofmann (1988).

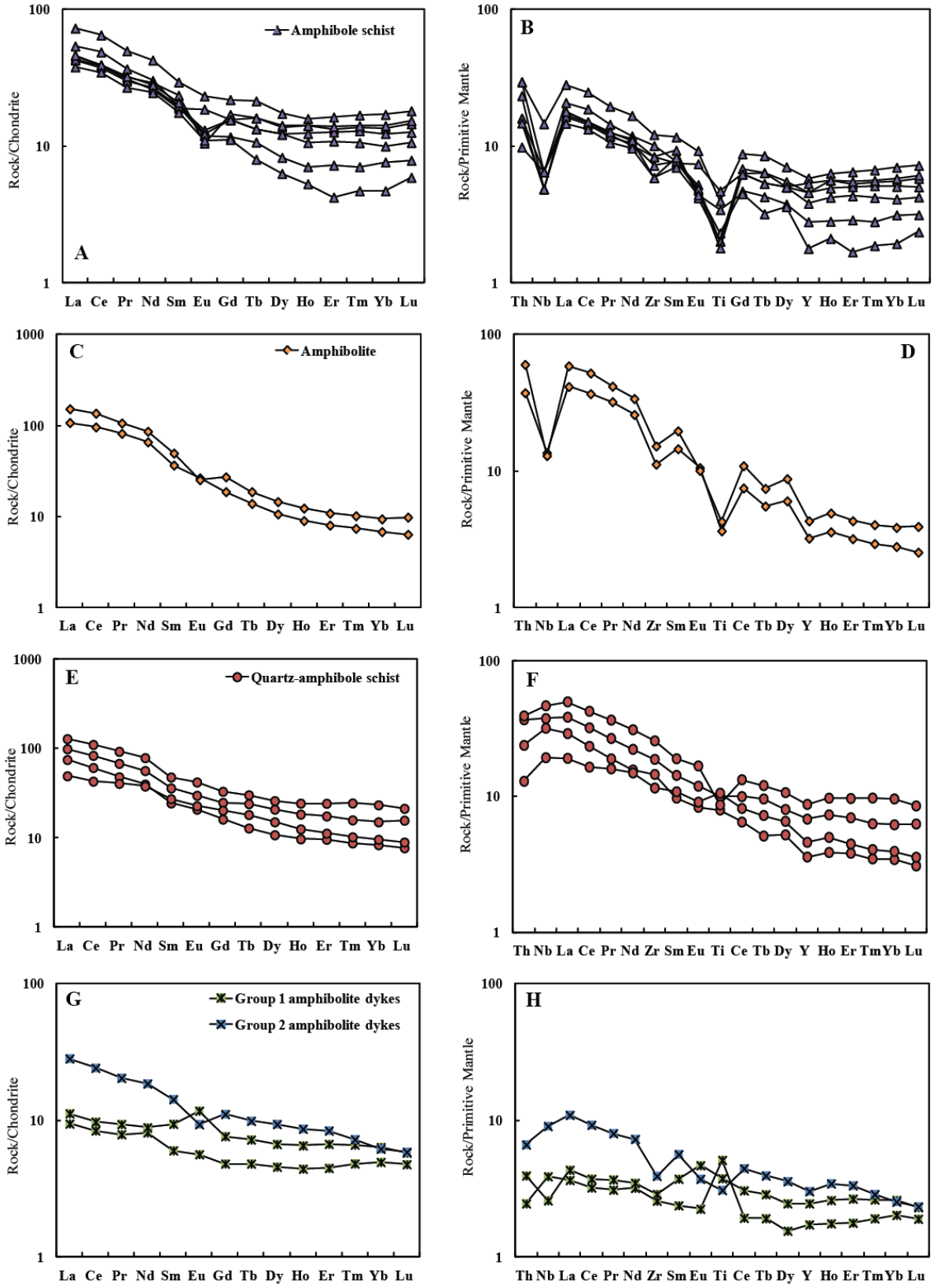
A
Amphibole schist
Rock/Chondrite
100
10
1
La Ce Pr Nd Sm Eu Gd Tb Dy Ho Er Tm Yb Lu
B
Rock/Primitive Mantle
Th Nb La Ce Pr Nd Zr Sm Eu Ti Gd Tb Dy Y Ho Er Tm Yb Lu
C
Amphibolite
1000
D
Th Nb La Ce Pr Nd Zr Sm Eu Ti Ce Tb Dy Y Ho Er Tm Yb Lu
E
Quartz-amphibole schist
F
G
Group 1 amphibolite dykes
Group 2 amphibolite dykes
H

Figure 2.9

Figure 2.9 – Paired chondrite-normalized REE and primitive mantle-normalized multi-element diagrams for the amphibole schist (A and B), amphibolite pods (C and D), quartz-amphibole schist (E and F), and amphibolite dykes (G and H). Chondrite-normalizing values are from Sun and McDonough (1989) and primitive mantle-normalized values are from Hofmann (1988).

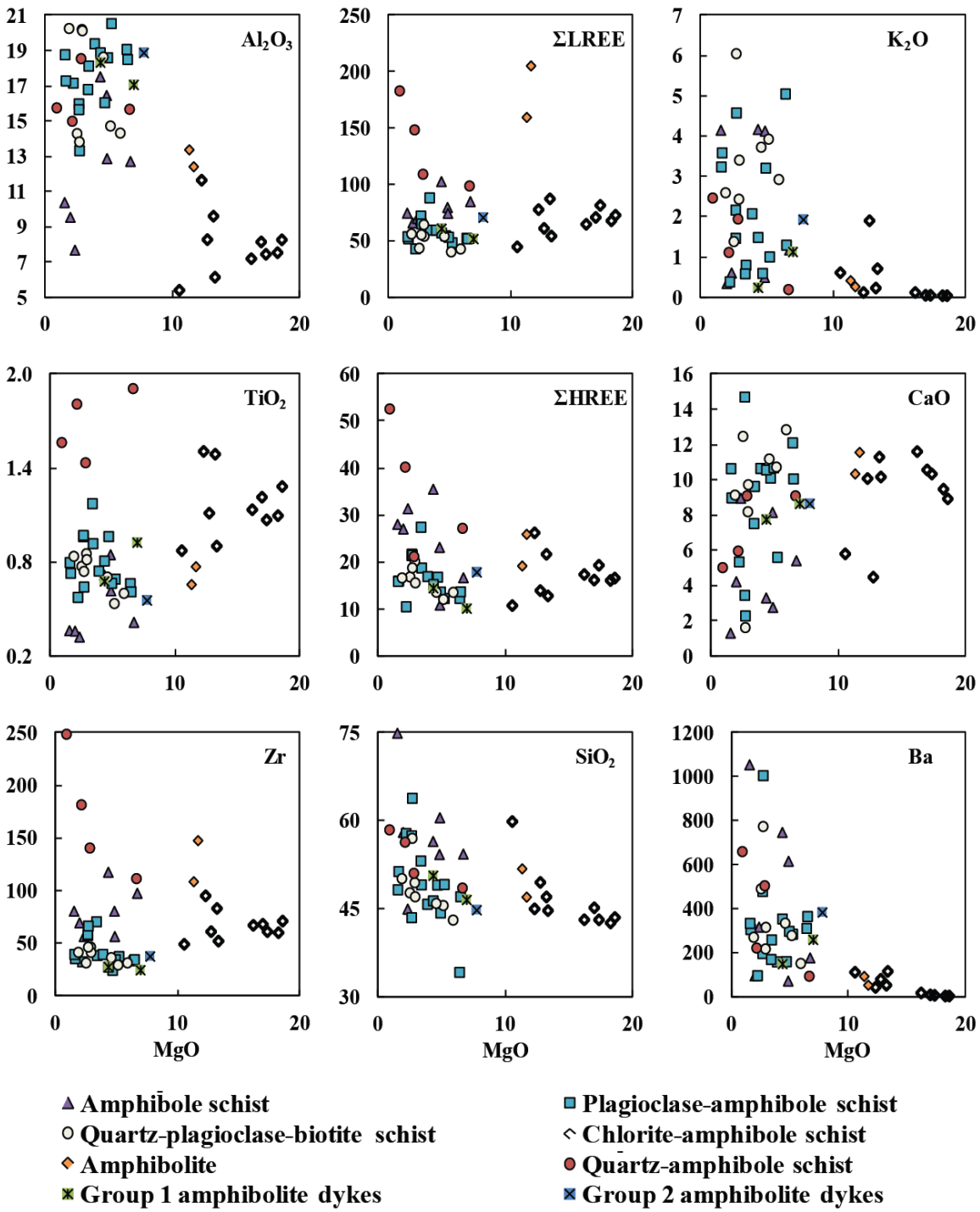
Al2O3
ΣLREE
K2O
TiO2
ΣHREE
CaO
Zr
SiO2
Ba
MgO
MgO
MgO
Amphibole schist
Plagioclase-amphibole schist
Quartz-plagioclase-biotite schist
Chlorite-amphibole schist
Amphibolite
Quartz-amphibole schist
Group 1 amphibolite dykes
Group 2 amphibolite dykes

Figure 2.10

Figure 2.10 – MgO (wt.%) versus Al_2O_3 (wt.%), TiO_2 (wt.%), Zr (ppm), ΣLREE, ΣHREE, SiO_2 (wt.%), K_2O (wt.%), CaO (wt.%), Ba (ppm) variation diagrams for amphibole schist, plagioclase-amphibole schist, quartz-plagioclase-biotite schist, chlorite-amphibole schist, amphibolite, quartz-amphibole schist, and amphibolite dykes, suggesting the relative immobility of these elements compared to MgO (wt.%). ΣLREE=Sc+La+Ce+Pr+Nd+Sm+Eu+Gd; ΣHREE=Y+Tb+Dy+Ho+Er+Tm+Yb+Lu.

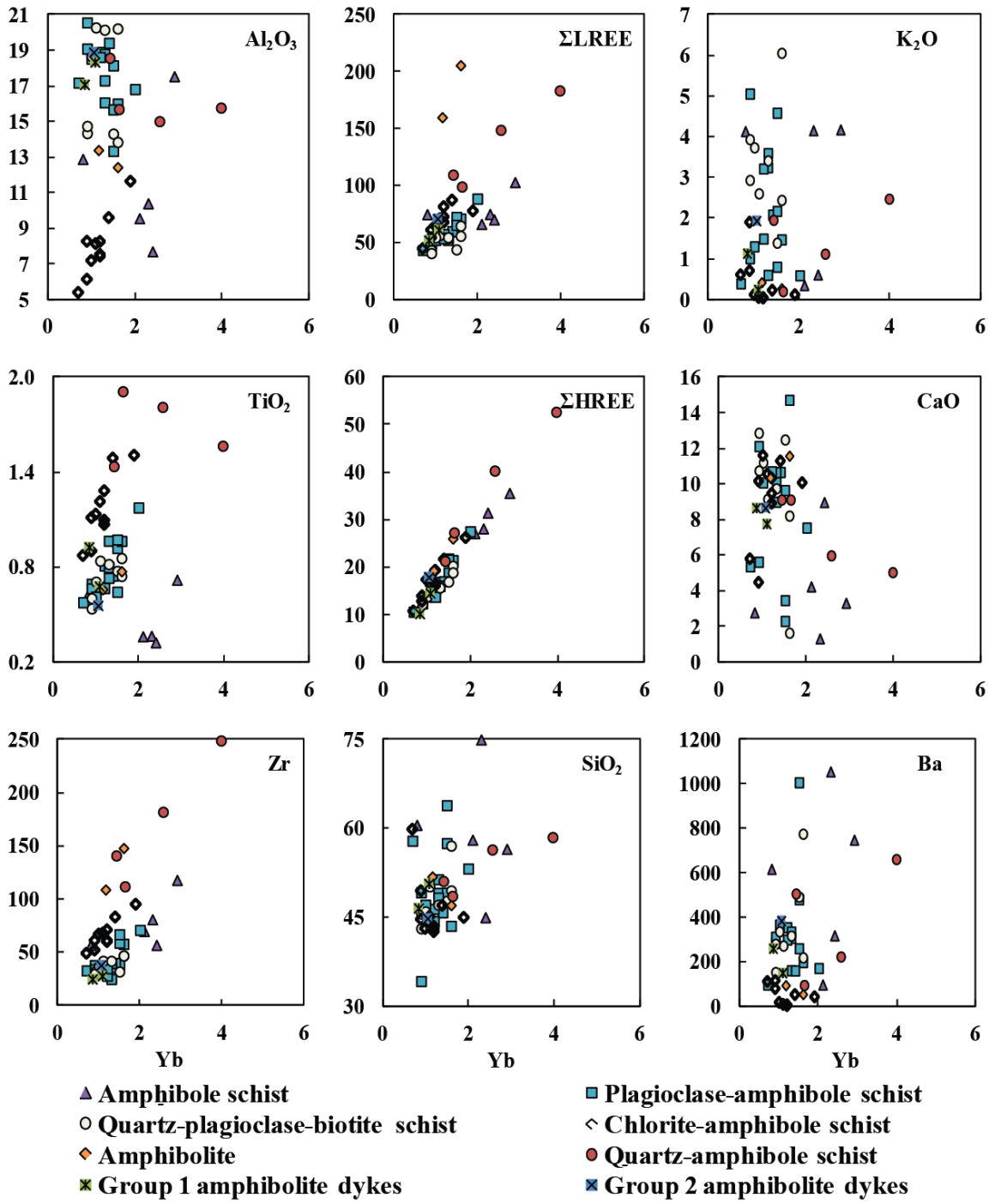
Al2O3
ΣLREE
K2O
TiO2
ΣHREE
CaO
Zr
SiO2
Ba
Yb
Amphibole schist
Plagioclase-amphibole schist
Quartz-plagioclase-biotite schist
Chlorite-amphibole schist
Amphibolite
Quartz-amphibole schist
Group 1 amphibolite dykes
Group 2 amphibolite dykes

Figure 2.11

Figure 2.11 – Yb (ppm) versus Al_2O_3 (wt.%), TiO_2 (wt.%), Zr (ppm), ΣLREE, ΣHREE, SiO_2 (wt.%), K_2O (wt.%), CaO (wt.%), Ba (ppm) variation diagrams for amphibole schist, plagioclase-amphibole schist, quartz-plagioclase-biotite schist, chlorite-amphibole schist, amphibolite, quartz-amphibole schist, and amphibolite dykes, suggesting the relative immobility of these elements compared to Yb (ppm). ΣLREE=Sc+La+Ce+Pr+Nd+Sm+Eu+Gd; ΣHREE=Y+Tb+Dy+Ho+Er+Tm+Yb+Lu.

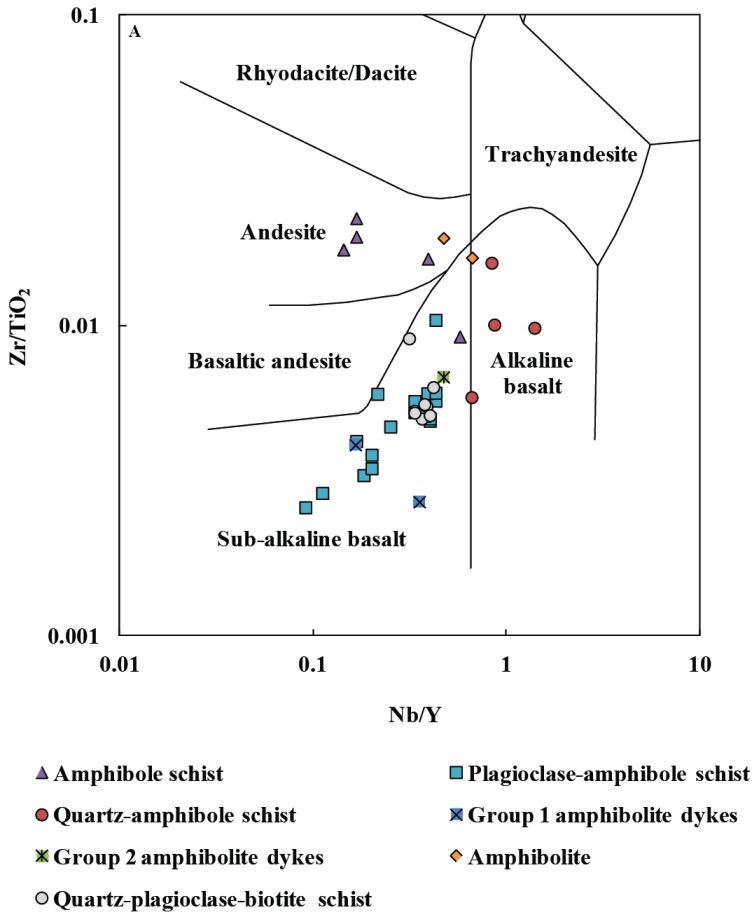

Figure 2.12a – Nb/Y versus Zr/TiO_2 discrimination diagram for the mafic volcanic rocks of the host rock sequence and area surrounding the MacLellan Au-Ag deposit. Compositional fields after Winchester and Floyd (1977).

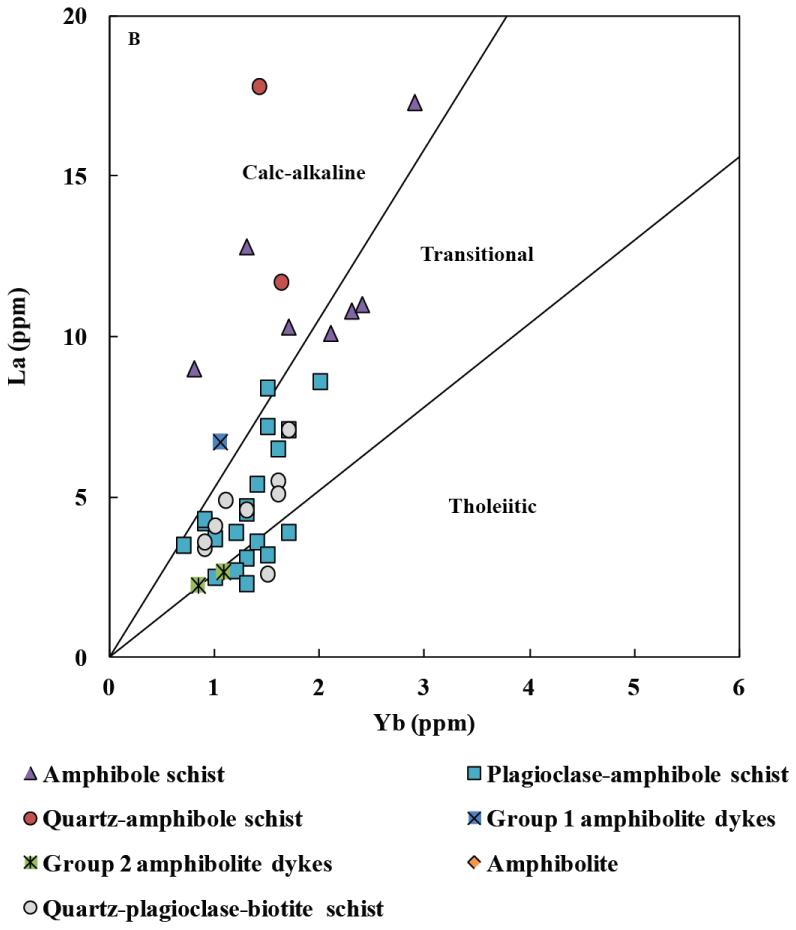

Figure 2.12b - Yb versus La magma series diagram for the mafic volcanic rocks of the host rock sequence and area surrounding the MacLellan Au-Ag deposit. Compositional fields after Ross and Bedard (2009).

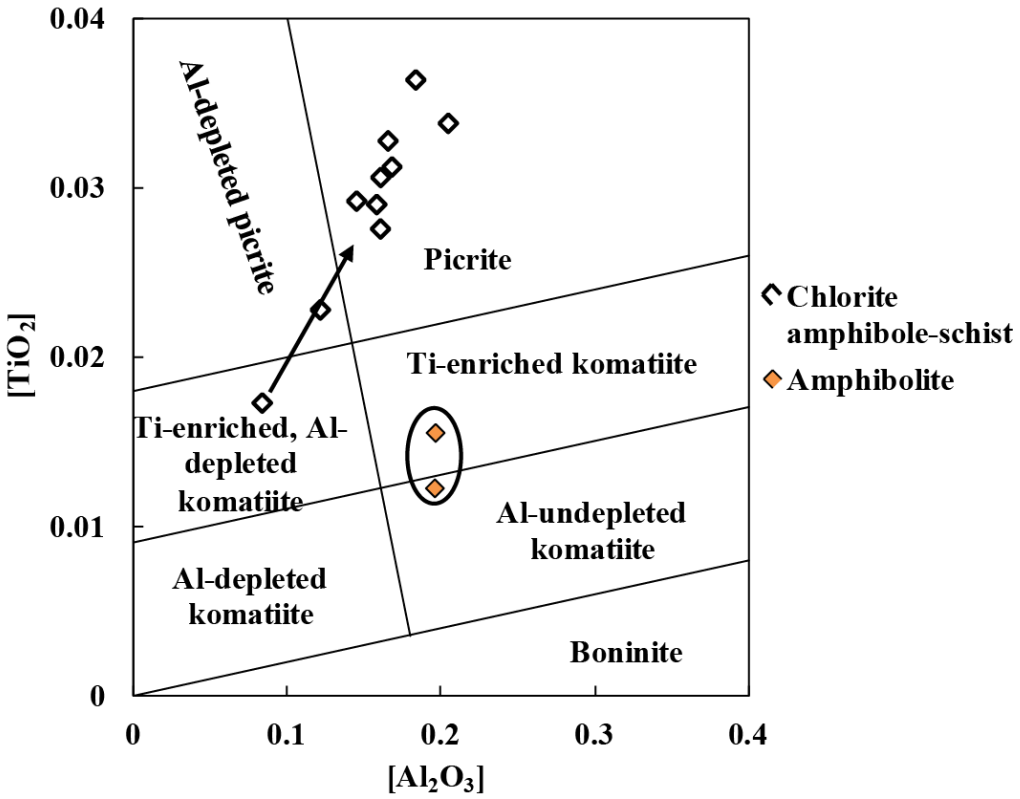

Figure 2.13 – $[Al_2O_3]$ versus $[TiO_2]$ mole proportion diagram for the ultramafic rocks from the host rock sequence and area surrounding the MacLellan Au-Ag deposit. $[Al_2O_3]$ and $[TiO_2]$ are molar compositions projected from olivine after Hanski et al., (2001). $[Al_2O_3] = Al_2O_3/(2/3\text{-}MgO\text{-}FeO)$ and $[TiO_2] = TiO_2/(2/3\text{-}MgO\text{-}FeO)$.

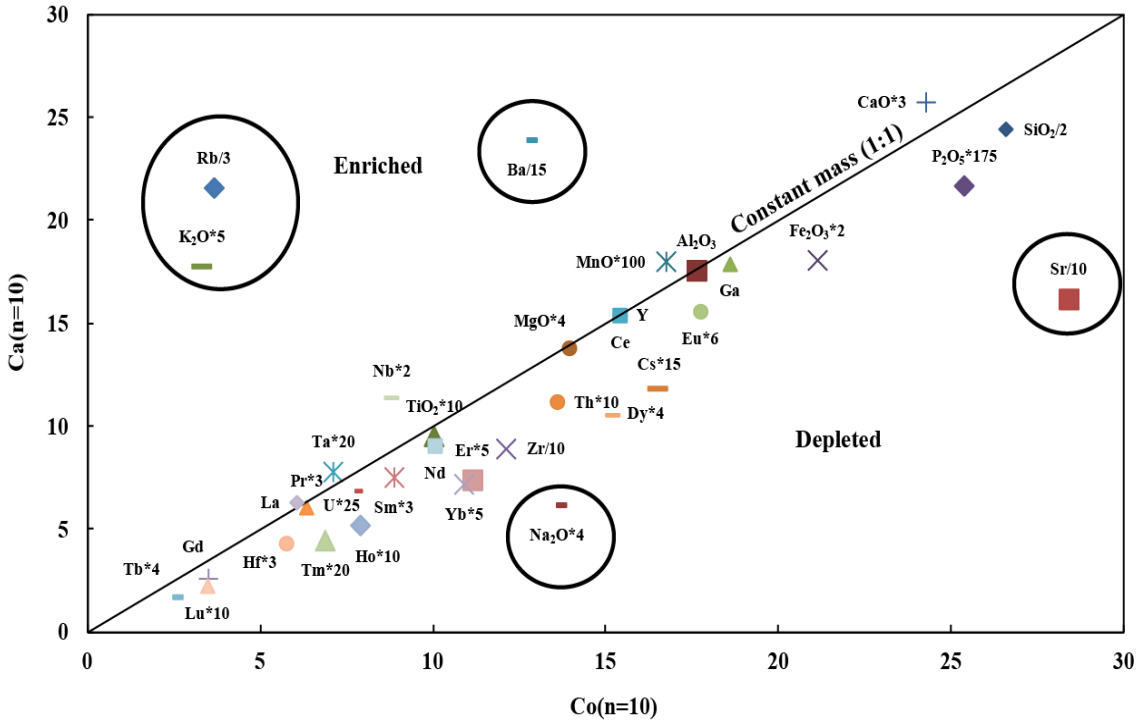

Figure 2.14 – Isocon diagram (method after Grant, 1986, 2008) comparing ten samples of plagioclase-amphibole schist (Co) with ten samples of quartz-plagioclase-biotite schist (Ca); assuming constant mass.

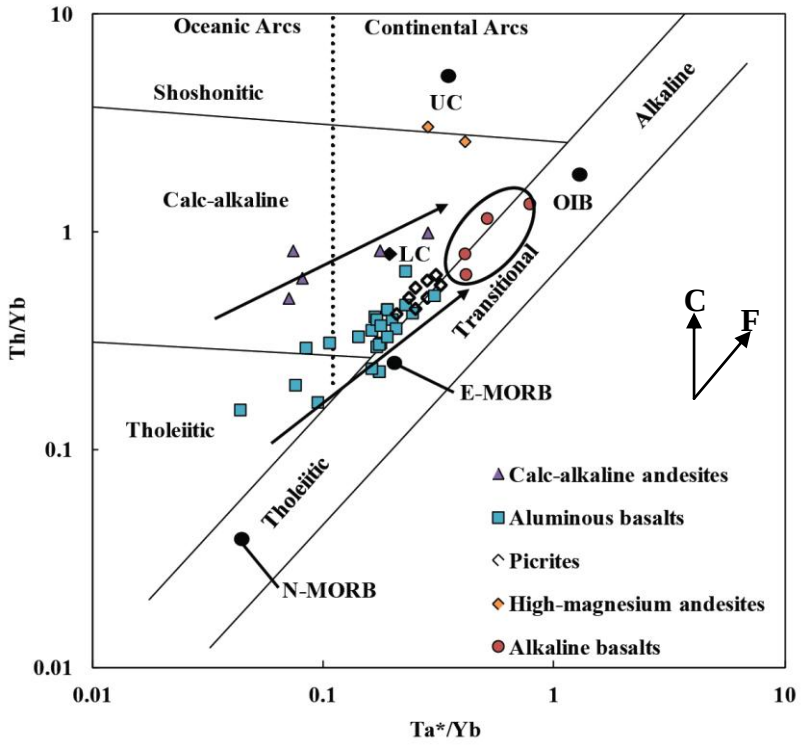

Figure 2.15 – Ta*/Yb versus Th/Yb petrogenetic variation diagram for the calc-alkaline andesites, aluminous basalts, picrites, high-magnesium andesites, and alkaline basalts. N-MORB, E-MORB, and OIB values are from Sun and McDonough, 1989. Upper crust (UC) and lower crust (LC) values are from Rudnick and Gao (2004). N-MORB: Normal Mid-ocean ridge basalt; E-MORB: Enriched Mid-ocean ridge basalts; OIB: Ocean island basalt. Adopted from Pearce (2008). Ta* = Nb/17.2. C: Crustal contamination vector; F: Within-plate fractionation vector.

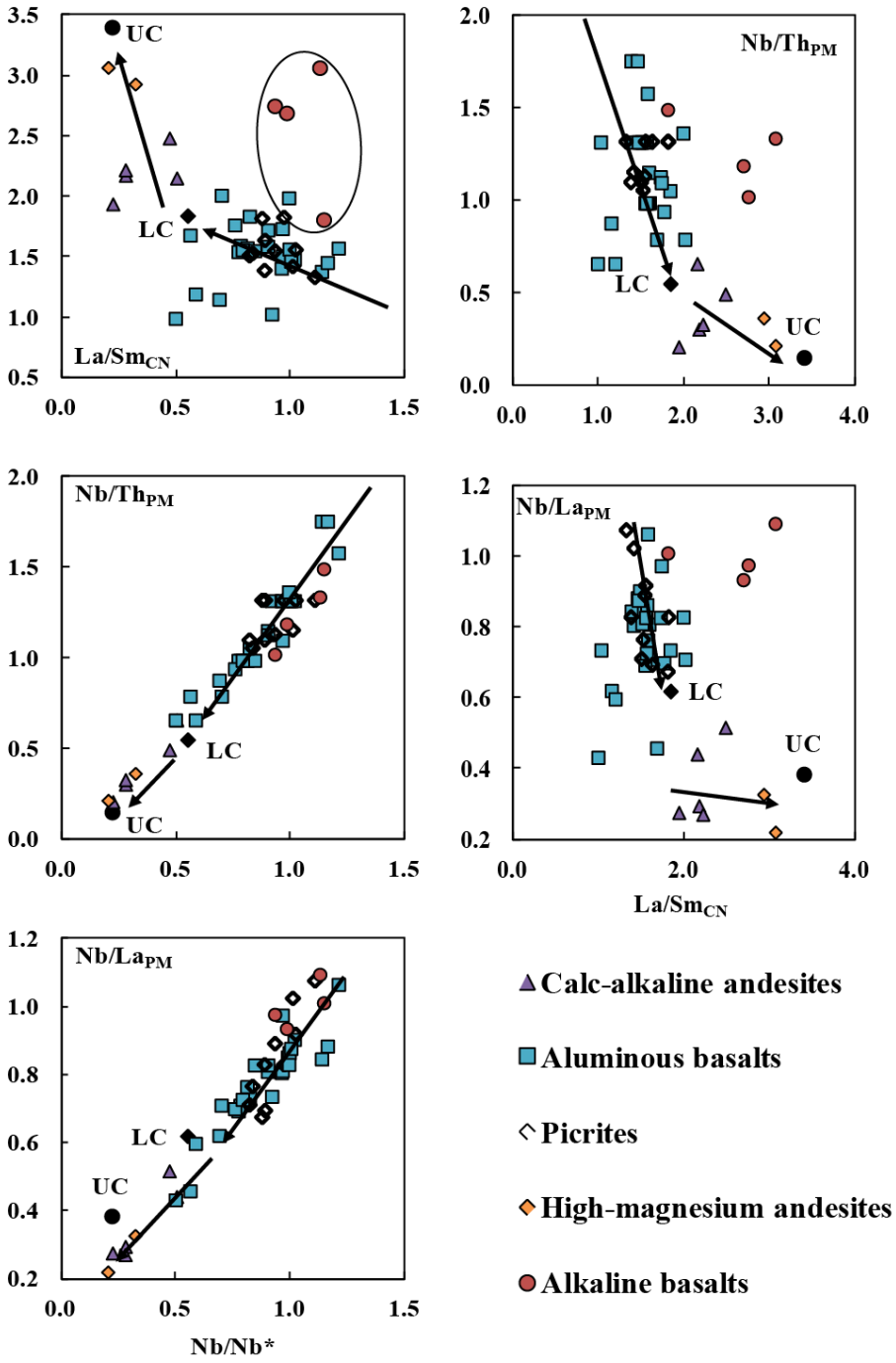
UC
LC
La/Sm$_{CN}$
Nb/Th$_{PM}$
LC
UC
Nb/Th$_{PM}$
LC
UC
Nb/La$_{PM}$
LC
UC
La/Sm$_{CN}$
Nb/La$_{PM}$
LC
UC
Nb/Nb*
Calc-alkaline andesites
Aluminous basalts
Picrites
High-magnesium andesites
Alkaline basalts

Figure 2.16

Figure 2.16 – Nb/Nb* versus La/Sm_{CN}, Nb/Th_{PM}, Nb/La_{PM}, and La/Sm_{CN} versus Nb/Th_{PM} and Nb/La_{PM} variation diagrams for calc-alkaline andesites, aluminous basalts picrites, high-magnesium andesites, and alkaline basalts. On these diagrams, calc-alkaline andesites and high-magnesium andesites trend between LC and UC values suggesting that these rocks were variably contaminated by continental crust during ascent. Aluminous basalts and picrites trend towards LC, indicative of LC or continental lithospheric mantle mixing. Alkaline basalts do not share the same trends suggesting that they were derived from an uncontaminated mantle source. Upper crust (UC) and lower crust (LC) values are from Rudnick and Gao (2004). PM: primitive mantle-normalized after Hofmann (1988); and, CN: chondrite-normalied after Sun and McDonough (1989).

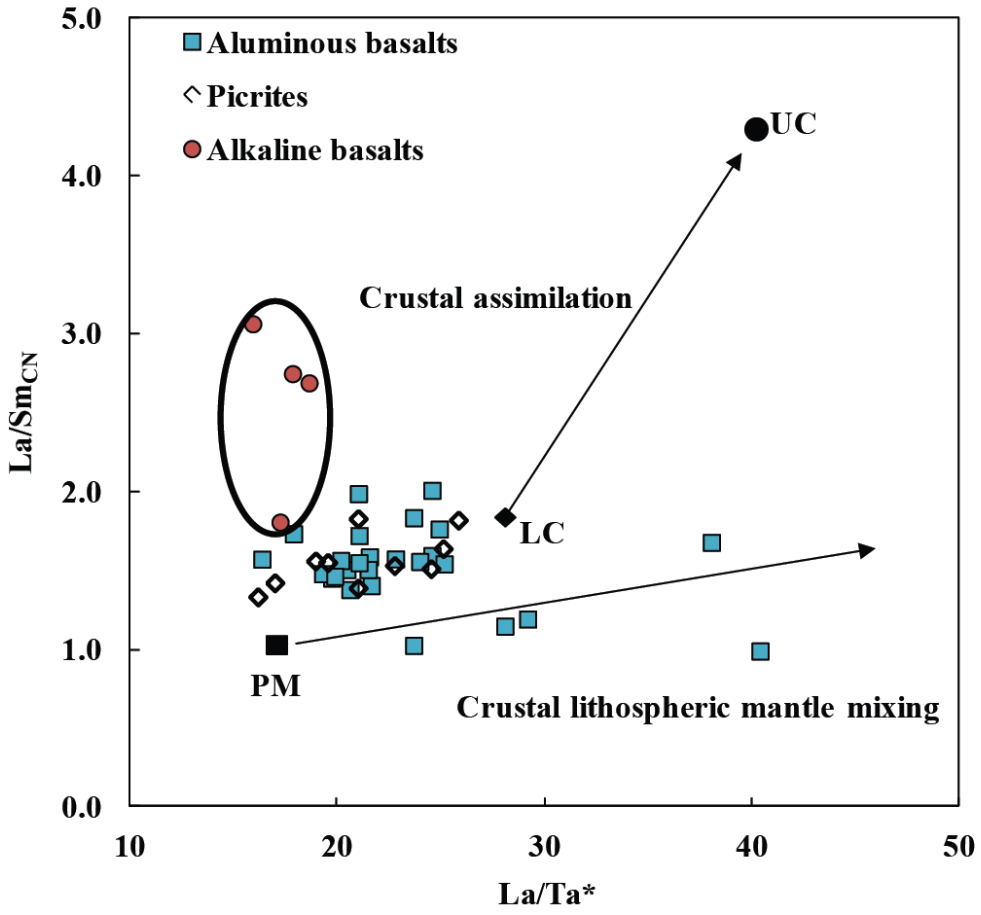

Figure 2.17 – La/Ta* versus La/Sm illustrating the different trends (arrows) for contamination of plume-derived liquids by continental crust as against continental lithospheric mantle (CLM). Aluminous basalts andpicrites plot along the CLM trend, which has been interpreted to be the result of an upwelling plume impinging along a Craton to a section of attenuated lithosphere. Samples of alkaline basalt do not plot along either trend suggesting that they represent a distinct source compared to the other plume-derived rocks. Upper crust (UC) and lower crust (LC) values are from Rudnick and Gao (2004). Vectors are from Lassiter and DePaolo (1997). Ta* = Nb/17.2.

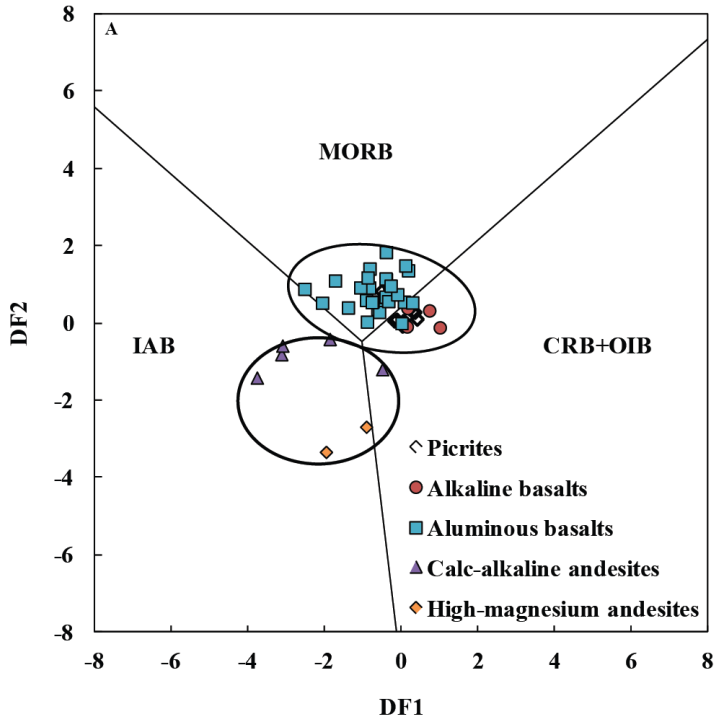

Figure 2.18a – Log-transformed immobile trace element tectonic discrimination diagrams, suggesting that the calc-alkaline andesites and high-magnesium andesites originated in a volcanic arc setting and that the aluminous basalts, picrites, and alkaline basalts, in a within-plate setting (adopted from Agrawal et al., 2008). The trend between the CRB+OIB and MORB fields and the CRB and OIB fields is attributed to the addition of crustal-derived components to more primitive plume-derived components. For diagram (A) DF1 = 0.3518 x ln(La/Th) + 0.6013 x ln(Sm/Th) - 1.345 x ln(Yb/Th) + 2.1056 x ln(Nb/Th) - 5.4763; DF2 = -0.305 x ln(La/Th) - 1.1801 x ln(Sm/Th) + 1.6189 x ln(Yb/Th) + 1.226 x ln(Nb/Th) - 0.9944. MORB: Mid-ocean ridge basalts; IAB: Island-arc basalts; CRB: Continental rift basalts; and, OIB: Ocean island basalts.

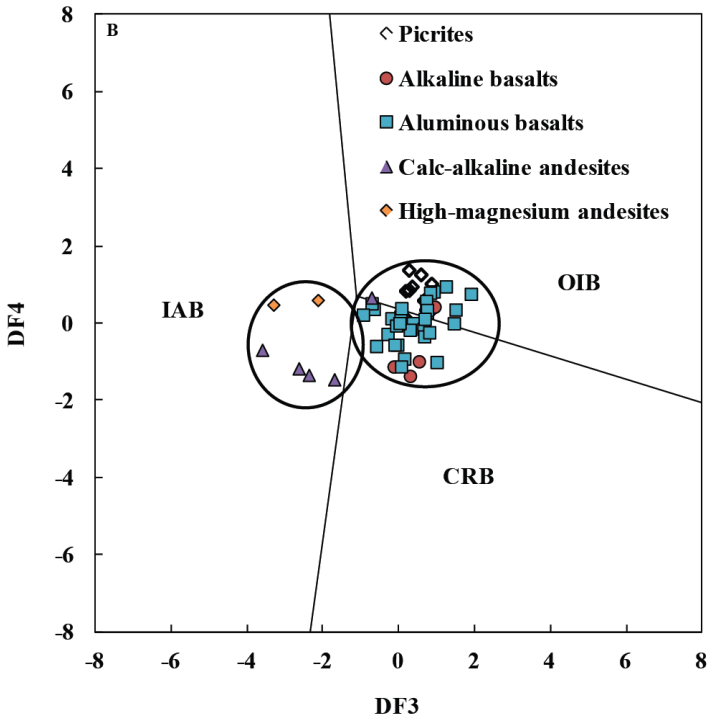

Figure 2.18b – Log-transformed immobile trace element tectonic discrimination diagrams, suggesting that the calc-alkaline andesites and high-magnesium andesites originated in a volcanic arc setting and that the aluminous basalts, picrites, and alkaline basalts, in a within-plate setting (adopted from Agrawal et al., 2008). For diagram (b) DF3 = 0.5533 x ln(La/Th) + 0.2173 x ln(Sm/Th) - 0.0969 x ln(Yb/Th) + 2.0454 x ln(Nb/Th) - 5.6305; DF4 = -2.4498 x ln(La/Th) + 4.8562 x ln(Sm/Th) - 2.124 x ln(Yb/Th) - 0.1567 x ln(Nb/Th) + 0.94. IAB: Island-arc basalts; CRB: Continental rift basalts; and, OIB: Ocean island basalts.

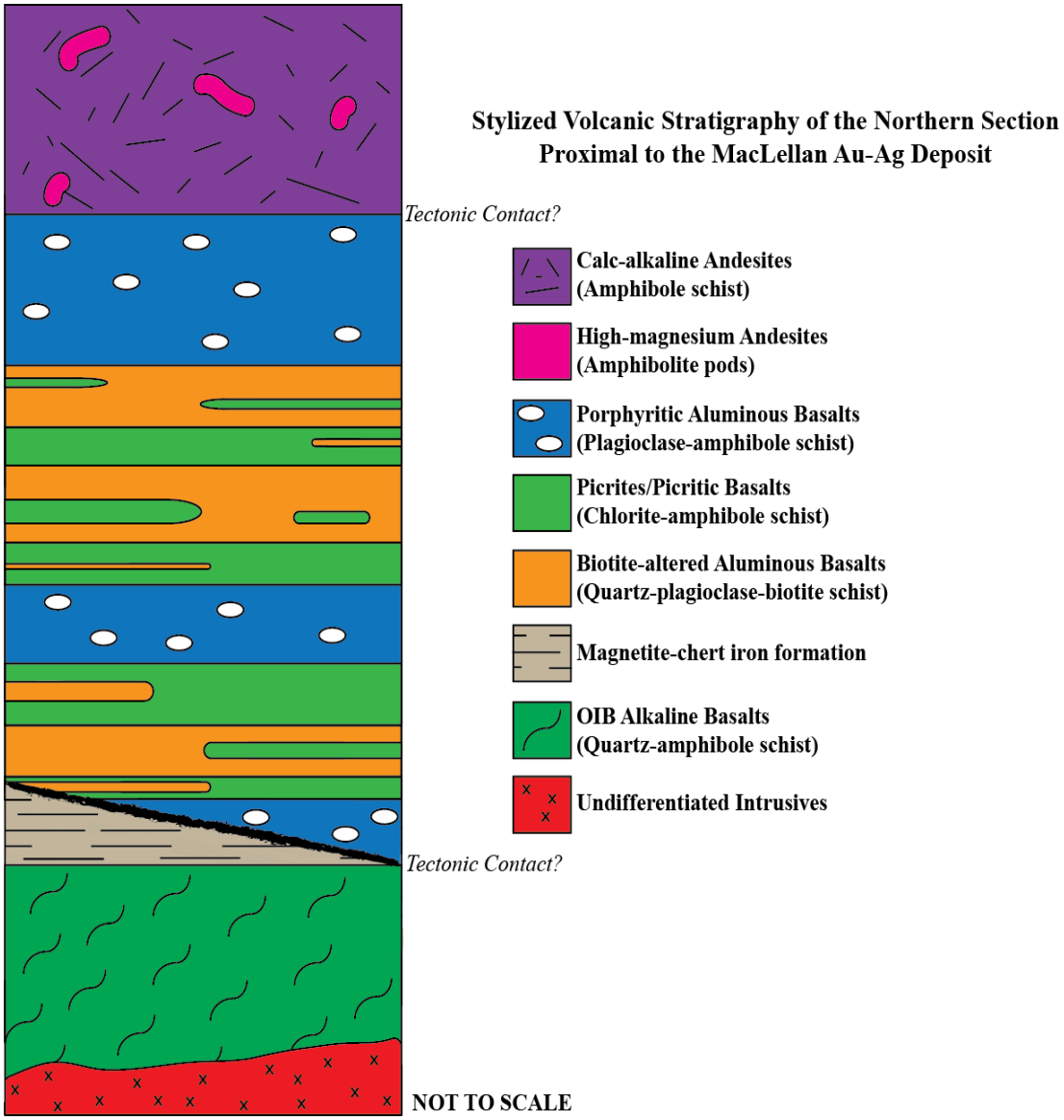

Figure 2.19 – Stylized stratigraphic section of the Northern section of the Lynn Lake greenstone belt proximal to the MacLellan Au-Ag deposit from north to south, based on field observations from this study and the regional structural observations of Gilbert (1980).

CHAPTER 3

Geochemistry of Paleoproterozoic ultramafic to intermediate metavolcanic rocks, Lynn Lake greenstone belt, Manitoba: implications for regional geodynamics, metallogeny, and the early (ca. ~ 1.9 Ga) history of the Trans-Hudson Orogen

3.1. Introduction

The Paleoproterozoic (ca. 1910 Ma) Lynn Lake greenstone belt hosts numerous significant gold deposits (e.g., MacLellan, Farley Lake, and Burnt Timber) and a number of potentially significant gold occurrences, which represent a total resource that is currently estimated at approximately 5 million ounces Au equivalent (Gagnon, et al., 2013). Despite the regional economic potential, there have been no comprehensive studies of the regional geodynamics and metallogeny of the Lynn Lake greenstone belt, making future greenfield exploration difficult to impossible. To date, there have only been six peer-reviewed publications on the geology of the Lynn Lake greenstone belt. These are studies of the U-Pb isotope ages of rhyolites in the northern portion of the Lynn Lake greenstone belt (Baldwin et al., 1987), character and genesis of mineralization within the MacLellan Au-Ag (Augsten et al., 1985; Samson and Gagnon, 1995; Samson et al., 1999) and Burnt Timber Au (Jones et al., 2006) deposits, and the geodynamics of the Cartwright Lake area (Peck and Smith, 1989).

The current tectonic model for the Lynn Lake greenstone belt, which was originally proposed by Zwanzig et al. (1999), did not consider the potential relationships between the geodynamics and metallogeny of the Lynn Lake greenstone belt in the context of all existing data, including geological and geochemical evidence (e.g., Peck

and Smith, 1989; Zwanzig, 1990) that supports a continental or near-continental tectonic setting for the Lynn Lake greenstone belt. For example, Peck and Smith (1989) suggest that the Lynn Lake greenstone belt contains a significant suite of continental volcanic arc-derived rocks, while other studies (e.g., Zwanzig, 1990; Beaumont-Smith and Böhm, 2004) and an unpublished M.Sc. thesis (e.g., Jurkowski, 1999) present geochemical (Zwanzig, 1990), U-Pb and Pb-Pb isotope (Jurkowski, 1999), and Nd-Sm isotope (Beaumont-Smith and Böhm, 2004) results that support a significant contribution of continental crust during formation of the metasedimentary, metavolcanic, and intrusive igneous rocks that comprise the majority of the Lynn Lake greenstone belt. Furthermore, a recent study of the host rocks to the MacLellan Au-Ag deposit (Chapter 2) suggests that the host rock sequence formed in a near-continent or continental environment, likely along a rifted continental margin.

Despite significant evidence to the contrary, the geodynamic model for the Lynn Lake greenstone belt proposes that the belt comprises a package of subaqueously erupted, chemically unrelated, juvenile to variably contaminated allochtonous terranes that became juxtaposed during terminal closure of the Manikewan Ocean (Zwanzig et al., 1999). In accordance with this model, the Lynn Lake region has been interpreted to have the potential to host significant volcanogenic massive sulphide (VMS) deposits (e.g., Syme, 1985; Zwanzig et al., 1999). Despite 40 years of prospecting, only one potential VMS deposit, the nature and genesis of which have been contentious (cf. Boyle, 1976; Norman, 1977; Lustig, 1979), has been discovered. All other significant mineral deposits discovered in the Lynn Lake greenstone belt to date (i.e., MacLellan, Farley Lake, and Burnt Timber) have the characteristics of vein hosted, intrusion associated, and orogenic

lode Au deposits, which are inconsistent with emplacement within an environment characteristic of a VMS-style of mineralization.

To date, the current model for the regional geodynamics and metallogeny of the Lynn Lake greenstone belt has been ineffective at predicting the type and location of mineral deposits within the belt. In this study, new geologic and geochemical data from several localities within the Lynn Lake greenstone belt are presented. This new information, along with data from previous published studies (i.e., Peck and Smith, 1989; Jones et al., 2006), unpublished M.Sc. theses (i.e., Peck, 1986; Jones, 2005; Chapter 2), and reports from the Manitoba Trades and Mines, Geological Services (i.e., Zwanzig et al., 1999; Beaumont-Smith, 2007), is used to develop a new geodynamic model for the formation of the Lynn Lake greenstone belt. This new model is used to develop a framework for metallogeny of the Lynn Lake greenstone belt, which can be used to guide future exploration activities.

3.2. Regional Geology

The Lynn Lake greenstone belt is located in the central portion of the Reindeer Collisional Zone of the Trans-Hudson Orogen, and is bordered by the Kisseynew Gneiss Belt to the south, and the Wathaman-Chipewyan-Baldock Batholith and the Tonalite-Migmatite Complex to the north. By global standards, the Lynn Lake greenstone belt is significant, measuring approximately 150 km long by 50 km wide, with the metavolcanic rocks covering an area of approximately 1200 km^2. These rocks comprise a diverse tectonostratigraphy of what have been interpreted to be metamorphosed, contaminated and juvenile volcanic and epiclastic sedimentary rocks that are collectively assigned to

the Wasekwan Group (Bateman, 1945), and younger, syn-kinematic, fluvial-alluvial molasse-type sedimentary rocks of the Sickle Group (Norman, 1933). Until 1999, the Lynn Lake greenstone belt had been subdivided into two subordinate greenstone belts (i.e., Northern and Southern) separated by a series of felsic plutons associated with the Wathaman-Chipewyan-Baldock Batholith. More recent regional mapping and geochemical data indicate, however, that the Lynn Lake greenstone belt can be subdivided into three different sections, of varying ages and geochemical affinities (i.e., Northern, Southern, and New Fox sections) (Zwanzig et al., 1999; Beaumont-Smith and Böhm, 2002) (Fig. 3.1). Patterns of regional deformation and metamorphism can be locally complex, however, metamorphic grade typically ranges between upper greenschist and upper amphibolite facies, with the greatest proportion of rocks in the belt exhibiting middle amphibolite facies equilibrium mineral assemblages (Milligan, 1960; Gilbert et al., 1980). For brevity, the prefix 'meta' is implied throughout the following text.

The Northern section consists of what have been interpreted to be circa 1910 to 1890 Ma submarine, tholeiitic, mafic volcanic and volcaniclastic rocks with lesser circa 1890 Ma rhyolite and banded iron formation (Gilbert et al., 1980; Zwanzig et al., 1999; Beaumont-Smith and Böhm, 2002) (Fig. 3.2a). The Southern section consists of an early, bimodal suite of predominantly tholeiitic with lesser calc-alkaline basalt and rhyolite that are intercalated with greywacke-mudstone turbidites, and a later calc-alkaline basalt/basaltic andesite/andesite suite, which were subsequently intruded by syn-tectonic plutons comprising diorite, quartz diorite, tonalite and granodiorite, and minor grabbroic dykes (Peck and Smith, 1989; Zwanzig et al., 1999) (Fig. 3.2b). The New Fox section

had been considered to be the western extension of the Southern section because these two rock sequences are contiguous. The New Fox section constitutes a platform of pyroxene-phyric basaltic flows and autoclastic breccia, which were intruded by mafic to felsic plutons and subsequently overlain by tuff, greywacke, and a turbidite unit (Gilbert et al., 1980; Syme, 1985) (Fig. 3.2c). Minor iron formation and clastic sedimentary units occur in places throughout the Lynn Lake greenstone belt (Milligan, 1960; McRitchie, 1974; Gilbert et al., 1980).

The volcanic rocks of the Lynn Lake greenstone belt have been interpreted to be the products of numerous subaqueous volcanic environments including oceanic volcanic arcs (Milligan, 1960; Syme, 1985; Baldwin et al., 1987; Lewry et al., 1987; Van Schmus et al., 1987; Zwanzig et al., 1999; Jones et al., 2006), ocean islands (Fedikow, 1992), intra-arc rifts (Zwanzig et al., 1999), and mid-ocean ridges (Zwanzig et al., 1999). Peck and Smith (1989), however, proposed that the volcanic rocks in the Cartwright Lake area of the Southern section represent an active continental margin or continental volcanic arc. Furthermore, the geochemistry of Sickle Group rocks (Zwanzig, 1990), Pb-Pb isotope systematics of feldspars from rhyolitic and gabbroic rocks (Jurkowski, 1999), and Sm-Nd isotope systematics of rhyolites and diorites (Beaumont-Smith and Böhm, 2004) from the Lynn Lake region all support the presence of continental lithosphere in the Lynn Lake region during eruption of the volcanic rocks that ultimately formed the Lynn Lake greenstone belt.

The precise ages of Lynn Lake greenstone belt volcanic rocks have not been determined, however, they have been constrained by the ages of surrounding felsic volcanics (i.e., rhyolites), as well as mafic and felsic plutons. The volcanic rocks of the

Northern section have estimated U-Pb ages ranging from 1910 to 1886 Ma (Baldwin et al., 1987; Beaumont-Smith and Böhm, 2003), and the volcanic rocks from the Southern section have estimated U-Pb ages ranging from 1856 to 1842 Ma (Beaumont-Smith and Böhm, 2003). Furthermore, U-Pb dating of gabbroic plugs and dioritic, granitic, granodioritic, and tonalitic stocks from the Lynn Lake region suggests that at least five major magmatic events occurred between 1910 and 1831 Ma (Appendix A). Five regional tectonostructural events have also been identified in the Lynn Lake greenstone belt, and are summarized in Appendix B.

3.3. Sampling and Analytical Methods

3.3.1. Data Inclusion and Sampling Methods

Appendix D presents a summary of sampling methodologies and the individual study goals for all data included in this study. Data used in this synthesis includes original data (Chapter 2) as well as data previously reported in the studies of Gilbert (1980), Peck (1986), Peck and Smith (1989), Gilbert (1993), Zwanzig et al. (1999), Jones (2005), Jones et al. (2006), and Beaumont-Smith (2007). Inclusion of these datasets in this synthesis enables the most comprehensive evaluation of the lithogeochemistry of the Lynn Lake greenstone belt conducted to date.

All data collected and used in this study contain complete or near complete high-field strength element (HFSE) data sets so that the most up-to-date petrogenetic and geodynamic techniques can be employed. Included data were subsequently screened using the alteration criteria of Polat and Hofmann (2003) (i.e., all samples exhibited Ce/Ce* ~ 1.0 and loss on ignition values of < 3 wt.%). This ensured that only the most

robost lithogeochemical data and data-screening techniques were used when conducting tectonic and petrogenetic interpretations. Global positioning system (GPS) readings for sample locations and sample depths, where applicable, are provided in Appendix E.

3.3.2. Analytical Methods

All lithogeochemical analyses used in this study (i.e., Zwanzig et al., 1999; Jones, 2005; Jones et al., 2006; Beaumont-Smith, 2007; Chapter 2), with the exception of those of Peck (1986) and Peck and Smith (1989), were performed by Activation Laboratories Ltd. (ACTLabs), of Ancaster, Ontario, Canada. Major element contents of the rocks were determined using a Thermo Jarrell-Ash ENVIRO II inductively coupled plasma optical emission spectrometer (ICP-OES). The samples were mixed with a flux of lithium metaborate and lithium tetraborate, and fused at 1000 $^{\circ}$C in an induction furnace. Upon cooling, the beads were rapidly digested in a solution of 5% HNO_3 containing an internal standard, and mixed continuously until complete dissolution occurred. Minor and trace element contents of the samples were determined using a Perkin Elmer SCIEX ELAN 6000 inductively coupled plasma mass spectrometer (ICP-MS). Loss on ignition (LOI) was determined by measuring weight loss upon heating to 1100 $^{\circ}$C over a three-hour period. The analytical precision is estimated to be better than 6% for trace elements and 3% for major elements (Young, 2002).

Samples collected from the Cartwright Lake area (Peck, 1986; Peck and Smith, 1989), were physically stripped of any weathering rind and analyzed at the University of Windsor using a X-ray fluorescence (XRF) spectrometer following the techniques of Jenkins and DeVries (1982), Huang and Smith (1983), and Govindaruju, (1984). Select

representative samples were sent to X-ray Assay Laboratories (XRAL) of Don Mills, Ontario, Canada for REE analysis using instrumental neutron activation analysis (INAA). The accuracy and precision of these analyses are estimated using external calibration standards and duplicate samples, respectively. Precision is estimated to be better than 0.2 % for major elements and LOI (i.e., SiO_2, Al_2O_3, Fe_2O_3, MgO, CaO, Na_2O, K_2O, P_2O_5, MnO), better than 2 % for some transition and high-field strength elements (i.e., Rb, Sr, Y, Zr, Nb, Cr, Co, Cu, Zn, and Sc), better than 6 % for select transition elements (i.e., Ba, V, and Ni), and better than 20% for rare earth and select high-field strength elements (i.e., La, Ce, Nd, Sm, Eu, Tb, Yb, Lu, Hf, Ta, Th, and U).

3.4. Geochemical Results

The results of the major element oxide analyses were recalculated to a 100 wt. % anhydrous basis for comparison purposes. Chondrite and primitive mantle reservoir compositions used for normalization purposes are those of Sun and McDonough (1989) and Hofmann (1988), respectively. Europium (Eu/Eu*), Ce (Ce/Ce*), Nb (Nb/Nb*), Ti (Ti/Ti*), and Zr (Zr/Zr*) anomalies were calculated with respect to the neighbouring immobile elements, following the method of Taylor and McLennan (1985).

Rather than grouping samples based on locality, which was a common practice used in previous studies (cf., Zwanzig et al., 1999), all samples used in this study were grouped based on inter-element trends as they appear on chondrite- and primitive mantle-normalized diagrams. Accordingly, the samples are subdivided into three chemically distinct groups that are described individually below, and Figure 3.3 shows the occurrence of these groupings within the Lynn Lake greenstone belt.

Group 1 (G1) Volcanic Rocks

Two trends are apparent when the geochemical results are plotted on a Nb/Y vs. TiO_2 volcanic discrimination diagram and an Yb vs. La magma series diagram. Group 1 (G1) volcanic rocks trend between the subalkaline basalt and andesite fields on a Nb/Y vs. Zr/TiO_2 volcanic rock discrimination diagram (Fig. 3.4a) and between the transitional and calc-alkaline fields on an Yb vs. La magma series diagram (Fig. 3.4b), with the majority of samples plotting in the calc-alkaline field. The second group of samples (G1*) also trend between the subalkaline basalt and andesite fields on a Nb/Y vs. Zr/TiO_2 volcanic rock discrimination diagram (Fig. 3.4a), but plot primarily in the tholeiitic field on an Yb vs. La magma series diagram (Fig. 3.4b). This subgrouping is supported when the groups are compared by their respective Hf-Th-Ta* inter-element systematics (not shown). This subalkaline basalt to andesite suite of rocks has variable contents of SiO_2 (41.05 to 68.44 wt.%), MgO (1.42 to 8.95 wt.%), Al_2O_3 (9.61 to 23.64 wt.%), Ni (13 to 246 ppm), Cr (5 to 880 ppm), and Mg-numbers (13 to 65), and has large variations in Al_2O_3/TiO_2 (11 to 49), Zr/Y (1.8 to 8.9), Ti/Zr (21 to 139), and Zr/Nb (8 to 52).

Samples of G1 rocks display the following trends on chondrite- and primitive mantle-normalized diagrams (Figs. 3.4c and 3.4d): 1) variably fractionated REE patterns (La/Sm_{CN} = 1.39 to 3.21, La/Yb_{CN} = 2.34 to 19.13, Gd/Yb_{CN} = 0.94 to 4.03); 2) strong negative Nb anomalies (Nb/Th_{PM} = 0.09 to 0.66, Nb/La_{PM} = 0.22 to 0.72, Nb/Nb* = 0.16 to 0.60), and strong negative to weak positive Ti (Ti/Sm_{PM} = 0.14 to 1.04, Ti/Gd_{PM} = 0.42 to 2.24, Ti/Ti* = 0.23 to 1.15) and Zr (Zr/Nd_{PM} = 0.25 to 1.15, Zr/Sm_{PM} = 0.34 to 1.55; Zr/Zr* = 0.24 to 1.10) anomalies; 3) moderate negative to moderate positive Eu anomalies (Eu/Eu* = 0.66 to 1.56); and 4) negligible Ce anomalies (Ce/Ce* = 0.96 to

1.08). In contrast, samples of G1* rocks display the following trends on chondrite- and primitive mantle-normalized diagrams (Figs. 3.4e and 3.4f): 1) positively fractionated LREE patterns (La/Sm_{CN} = 1.12 to 2.11, La/Yb_{CN} = 1.09 to 1.89); 2) slightly negative to slightly positive HREE patterns (Gd/Yb_{CN} = 0.83 to 1.21); 3) strong to moderate negative Nb (Nb/Th_{PM} = 0.25 to 0.59, Nb/La_{PM} = 0.19 to 0.57, Nb/Nb* = 0.28 to 0.58) and Ti (Ti/Sm_{PM} = 0.52 to 0.90, Ti/Gd_{PM} = 0.55 to 1.34, Ti/Ti* = 0.55 to 0.93) anomalies, and moderate positive to moderate negative Zr (Zr/Nd_{PM} = 0.68 to 1.42, Zr/Sm_{PM} = 0.72 to 1.49, Zr/Zr* = 0.58 to 1.20) anomalies; 3) weak negative to weak positive Eu anomalies (Eu/Eu* = 0.78 to 1.20); and 4) negligible Ce anomalies (Ce/Ce* = 0.93 to 1.07).

Group 1 Ultramafic (G1U) Volcanic Rocks

Samples of G1U are differentiated by their elevated magnesium contents compared to samples of G1. High magnesium (> 10% MgO) samples plot within the komatiitic field on an [Al_2O_3] vs. [TiO_2] discrimination diagram (Fig. 3.5a) and in the transitional field on an Yb vs. La magma series diagram (Fig. 3.5b), however, these rocks have none of the primary characteristics (Chapter 2) that are required to conclusively identify a rock as a komatiite (cf., Kerr and Arndt, 2001). These samples display higher MgO (10.12 to 20.05 wt.%), Ni (33 to 536 ppm), and Cr (302 to 2120 ppm) contents and Mg-numbers (44 to 80) relative to 'normal' andesite and plot primarily between the basaltic andesite and andesite fields on a Nb/Y vs. Zr/TiO_2 discrimination diagram (Chapter 2). Therefore, these samples are classified as calc-alkaline high-Mg andesite (cf. McCarron and Smellie, 1998). Samples of high-Mg andesite have variable contents of SiO_2 (42.14 to 56.85 wt.%), and Al_2O_3 (4.57 to 14.94 wt.%), and large variations in Al_2O_3/TiO_2 (4 to 48), Zr/Y (1.0 to 8.7), Ti/Zr (31 to 164), and Zr/Nb (12 to 42).

Samples of G1U display the following trends on chondrite- and primitive mantle-normalized diagrams (Figs. 3.5c and 3.5d): 1) variably fractionated REE patterns (La/Sm_{CN} = 0.80 to 3.37, La/Yb_{CN} = 1.12 to 16.18, Gd/Yb_{CN} = 0.88 to 3.14); 2) strong negative Nb anomalies (Nb/Th_{PM} = 0.08 to 0.59, Nb/La_{PM} = 0.19 to 1.05, Nb/Nb* = 0.12 to 0.52), variably negative to moderate positive Ti anomalies (Ti/Sm_{PM} = 0.21 to 1.10, Ti/Gd_{PM} = 0.85 to 2.70, Ti/Ti* = 0.34 to 1.42), and variably negative Zr anomalies (Zr/Nd_{PM} = 0.22 to 1.12, Zr/Sm_{PM} = 0.26 to 1.18, Zr/Zr* = 0.20 to 0.85); 3) moderate negative to weak positive Eu anomalies (Eu/Eu* = 0.56 to 1.19); and 4) negligible Ce anomalies (Ce/Ce* = 0.97 to 1.07).

Group 2 (G2) Volcanic Rocks

Group 2 (G2) volcanic rocks trend between the subalkaline basalt and basaltic andesite fields on a Nb/Y vs. Zr/TiO_2 volcanic rock discrimination diagram (Fig. 3.6a) and plot primarily in the tholeiitic field on an Yb vs. La magma series diagram (Fig. 3.6b). The suite of tholeiitic subalkaline basalts and basaltic andesites has variable SiO_2 (47.27 to 63.57 wt.%), MgO (2.48 to 9.55 wt.%), Al_2O_3 (12.87 to 22.80 wt.%), Ni (17 to 850 ppm), Cr (10 to 668 ppm) contents, and Mg-numbers (27 to 58). These rocks also exhibit large variations in Al_2O_3/TiO_2 (7 to 56), Zr/Y (1.2 to 3.7), Ti/Zr (49 to 323), and Zr/Nb (10 to 39).

Samples of G2 display the following trends on chondrite- and primitive mantle-normalized diagrams (Figs. 3.6c and 3.6d): 1) relatively flat REE patterns (La/Sm_{CN} = 0.63 to 1.50, La/Yb_{CN} = 0.51 to 2.22, Gd/Yb_{CN} = 0.65 to 1.89); 2) variably negative to positive Nb (Nb/Th_{PM} = 0.54 to 2.47, Nb/La_{PM} = 0.37 to 1.57, Nb/Nb* = 0.50 to 1.71), Ti

(Ti/Sm_{PM} = 0.48 to 1.90, Ti/Gd_{PM} = 0.70 to 2.42, Ti/Ti* = 0.49 to 1.93), and Zr (Zr/Nd_{PM} = 0.52 to 1.43, Zr/Sm_{PM} = 0.52 to 1.34, Zr/Zr* = 0.43 to 1.10) anomalies; 3) variably negative to positive Eu anomalies (Eu/Eu* = 0.68 to 1.57); and 4) negligible Ce anomalies (Ce/Ce* = 0.95 to 1.09).

Group 3 (G3) Volcanic Rocks

Group 3 (G3) volcanic rocks trend between the subalkaline basalt and andesite fields on a Nb/Y vs. Zr/TiO_2 volcanic rock discrimination diagram (Fig. 3.7a) and plot primarily in the transitional field on an Yb vs. La magma series diagram (Fig. 3.7b). The suite of transitional subalkaline basalts and andesites have variable SiO_2 (39.24 to 65.48 wt.%), MgO (1.64 to 9.86 wt.%), Al_2O_3 (11.99 to 21.98 wt.%), Ni (17 to 1020 ppm), Cr (5 to 1350 ppm) contents, and Mg-numbers (29 to 65). These rocks exhibit large variations in Al_2O_3/TiO_2 (6 to 39), Zr/Y (1.7 to 6.5), Ti/Zr (39 to 232), and Zr/Nb (8 to 49).

Samples of G3 display the following trends on chondrite- and primitive mantle-normalized diagrams (Figs. 3.7c and 3.7d): 1) variably fractionated REE patterns (La/Sm_{CN} = 1.03 to 3.14, La/Yb_{CN} = 1.27 to 10.21, Gd/Yb_{CN} = 0.76 to 2.38); 2) variably negative to positive Nb (Nb/Th_{PM} = 0.51 to 3.04, Nb/La_{PM} = 0.20 to 1.31, Nb/Nb* = 0.32 to 1.95), Ti (Ti/Sm_{PM} = 0.38 to 1.38, Ti/Gd_{PM} = 0.61 to 3.15, Ti/Ti* = 0.46 to 1.55), and Zr (Zr/Nd_{PM} = 0.51 to 1.76, Zr/Sm_{PM} = 0.56 to 2.18, Zr/Zr* = 0.44 to 1.63) anomalies; 3) moderate negative to positive Eu anomalies (Eu/Eu* = 0.52 to 1.44); and 4) no Ce anomalies (Ce/Ce* = 0.96 to 1.10).

Group 3 Ultramafic (G3U) Volcanic Rocks

High-magnesium (> 10% MgO) samples plot primarily in the picritic field on an [Al_2O_3] vs. [TiO_2] mole proportion discrimination diagram (Fig. 3.8a) and in the transitional field on an Yb vs. La magma series diagram (Fig. 3.8b). Samples with picritic compositions have variable SiO_2 (44.93 to 61.42 wt.%), MgO (10.87 to 19.86 wt.%), Al_2O_3 (5.54 to 12.04 wt.%), Ni (172 to 2400 ppm), Cr (581 to 1710 ppm) contents, and Mg-numbers (60 to 74). These rocks also exhibit large variations in Al_2O_3/TiO_2 (6 to 14), Zr/Y (3.5 to 8.8), Ti/Zr (59 to 119), and Zr/Nb (9 to 26).

Samples of G3U display the following trends on chondrite- and primitive mantle-normalized diagrams (Figs. 3.8c and 3.8d): 1) variably fractionated REE patterns (La/Sm_{CN} = 1.33 to 1.82, La/Yb_{CN} =2.57 to 5.14, Gd/Yb_{CN} = 1.48 to 2.39); 2) variably negative to positive Nb (Nb/Th_{PM} = 0.66 to 1.42, Nb/La_{PM} = 0.56 to 1.07, Nb/Nb* = 0.32 to 1.95), Ti (Ti/Sm_{PM} = 0.67 to 1.13, Ti/Gd_{PM} = 1.54 to 3.53, Ti/Ti* = 0.46 to 1.55), and Zr (Zr/Nd_{PM} = 0.54 to 1.29, Zr/Sm_{PM} = 0.71 to 1.56, Zr/Zr* = 0.44 to 1.63); 3) moderate negative to weak positive Eu anomalies (Eu/Eu* = 0.66 to 1.14); and 4) no Ce anomalies (Ce/Ce* = 0.97 to 1.10).

3.5. Discussion

3.5.1. Effect of Metamorphism on Element Mobility

Element mobility can be significant, particularly in Precambrian rocks, which may have experienced multiple episodes of metamorphism, alteration, and deformation (e.g., Polat and Hofmann, 2003; Ordóñez-Calderón et al., 2008, and references therein). Patterns of deformation, alteration, and metamorphism in the Lynn Lake greenstone belt

can be locally complex; however, regional metamorphic grade typically ranges between upper greenschist and upper amphibolite facies, with the greatest proportion of rocks exhibiting middle amphibolite facies equilibrium mineral assemblages (Milligan, 1960; Gilbert et al., 1980). In addition, the compositions of these rocks may have been influenced by multiple episodes of felsic and mafic plutonism. It is therefore important to determine the effects of metamorphism, alteration, and deformation on the primary igneous geochemistry of the Lynn Lake volcanic rocks. All samples included in this study exhibit negligible Ce anomalies, suggesting that the LREE contents of the rocks have not been affected by secondary processes (cf., Polat and Hofmann, 2003) and, therefore, their compositions can be used to interpret the petrogenesis and geodynamic history of the region.

Research in Archean greenstone terranes (i.e., Dostal et al., 1980; Kerrich and Fyfe, 1981; Polat and Hofmann, 2003) has shown that, under amphibolites-facies metamorphic conditions, HFSE typically remain immobile, while large ion lithophile elements (LILE) are expected to be mobile. Concentrations of SiO_2 and CaO in G1 rocks exhibit relatively weak linear correlations with Zr (Fig. 3.9), reflecting the relative immobility of these elements with respect to Zr. In contrast, concentrations of LILE, SiO_2, and CaO in samples of G1*, G1U, G2, G3, and G3U are dispersed relative to Zr (Figs. 3.9 to 3.11), reflecting the relative mobility of these elements compared to Zr. The correlation between Zr, SiO_2, and CaO in G1 rocks suggests that these rocks are not as altered as the other assemblages, possibly due to timing of eruption. The majority of samples, however, display strong correlations between HFSE and Zr (Figs. 3.9 to 3.11) and coherent chondrite- and primitive mantle-normalized patterns, indicating that these

elements were relatively immobile during post-magmatic metamorphism, alteration and deformation. Consequently, the abundances of these elements accurately reflect the compositions of the volcanic rocks and can be used reliably for petrogenetic characterization.

3.5.2. Tectonic Setting of the Lynn Lake Volcanic Rocks

Studies of the rocks of the Lynn Lake greenstone belt after Bateman (1945) have considered the belt to be two separate and petrogenetically distinct volcanic sequences (i.e., the Northern and Southern sections). A more recent geochemical interpretation by Zwanzig et al. (1999), however, concluded that the Lynn Lake greenstone belt comprises at least three, compositionally and genetically distinct volcanic sequences (i.e., Northern, Southern and New Fox sections) that were interpreted to have been emplaced within intra-oceanic environments. In contrast, the grouping of the volcanic mafic to intermediate rocks based on Th-Nb-REE systematics (Figs. 3.3 to 3.7) resulted in the identification of at least three unique tectonic environments, which are not constrained by previously defined geologic boundaries (refer to Fig. 3.3). The REE patterns of G2, G3, and G3U rocks vary from flat (Fig. 3.6c and 3.6d) to LREE enriched (Figs. 3.7c, 3.7d, 3.8c, and 3.8d). Similar REE patterns have been reported from Phanerozoic plume-derived oceanic plateaus and ocean islands (Hards et al., 1995; Mahoney et al., 1995; Kerr et al., 1997; Hofmann, 2004; Kerr, 2004; Kerr and Mahoney, 2007). In contrast, REE patterns of G1, G1*, and G1U display depletions in Nb relative to Th and La, as well as Ti relative to MREE (Figs. 3.4c. 3.4d, 3.4e, and 3.4f), which are consistent with a subduction zone (forearc-arc-backarc) signature (Pearce and Peate, 1995; Woodhead et al., 1998; Pearce, 2008).

On continental rift basalt (CRB), ocean island basalt (OIB), mid-ocean ridge basalt (MORB), and island arc basalt (IAB) trace element ratio discrimination diagrams developed by Agrawal et al. (2008), G1 and G1U plot consistently in the IAB fields, near the MORB-CRB+OIB and OIB-CRB boundaries (Figs. 3.12a and 3.12b). The rocks comprising the G1* subgroup cluster tightly in the IAB field, and define a compositional trend in terms of HFSE ratios that projects from the MORB to IAB fields on the IAB-MORB-CRB+OIB diagram (Fig. 3.12a). Samples comprising G2 plot primarily in the MORB field and define a trend that projects toward the IAB field on an IAB-MORB-OIB+CRB diagram (Fig. 3.13a). These samples also define a trend between the OIB and CRB fields and the IAB field on an IAB-CRB-OIB diagram (Fig. 3.13b). Samples from G3 and G3U define trends similar to those from G2 (Figs. 3.14a), with the exception of the IAB-MORB-CRB+OIB diagram (Fig. 3.14b), where samples trend from CRB+OIB, through MORB, toward IAB. The compositional trends demonstrated by samples of G2, G2U, G3, and G3U rocks are interpreted to reflect enrichment of select HFSE (i.e., Th and La) and depletion (i.e., Nb) in a more primitive plume source by select HFSE (i.e., Th and La), which may indicate the contribution of continental crust or metasomatized lithospheric mantle to the source.

3.5.3. Crustal or Lithospheric Mantle Contamination

The Lynn Lake greenstone belt has been interpreted to represent a series of juxtaposed intra-oceanic environments (Zwanzig et al., 1999), however, the results of more recent geochemical (Peck and Smith, 1989; Zwanzig, 1990; Chapter 2) and isotopic (Jurkowski, 1999; Beaumont-Smith and Böhm, 2004) studies have shown that the plutonic and volcanic rocks that comprise the belt exhibit evidence of crustal

contamination. The compositional trends observed on Figures 3.12 to 3.14 indicate that the volcanic rocks of the Lynn Lake greenstone belt have been variably contaminated by either continental crust or metasomatized mantle.

In the absence of radiogenic isotope data, the most reliable indicator of crustal contamination by continental crust is the presence of a negative Nb anomaly, which is estimated by Nb/Nb*, Nb/Th_{PM} and Nb/La_{PM} (Nosova et al., 2010). These ratios in OIB, MORB, and continental tholeiites are close to 1, but decrease to between 0.2 and 0.6 in highly contaminated, within-plate continental rocks (Nosova et al., 2010). For example, Nb/La_{PM} ranges from 0.22 to 0.56 in komatiites of the Vetreny Belt of Karelia (Puchtel et al., 1997), and 0.15 to 0.25 in basic and ultrabasic rocks of the Bushveld province (Maier et al., 2000), whereas basalts of Etendeka are characterized by Nb/Nb* ratios ranging from 0.25 to 0.9 (Thompson et al., 2007). The type of contaminant (e.g., upper or lower continental crust) can be assessed from the degree of REE fractionation that is exhibited by rocks with varying degrees of contamination, which is reflected by Nb/Nb*. Samples of G1 and G1U show weak linear correlations of Nb/Nb* with La/Sm_{CN}, Nb/Th_{PM}, Nb/La_{PM} and La/Sm_{CN} with Nb/Th_{PM} and Nb/La_{PM} between the upper and lower continental crust values, reflecting a moderate to strong LREE fractionation in the contaminant (Fig. 3.15a). This trend may be interpreted to reflect varying degrees of contamination by upper continental crust, the average composition of which is characterized by Nb/Nb* = 0.22, La/Sm_{CN} = 3.40, Nb/Th_{PM} = 0.15, and Nb/La_{PM} = 0.38 (Rudnick and Gao, 2004). In contrast, the rocks comprising G1* do not show a correlation between Nb/Nb* with La/Sm_{CN}, Nb/Th_{PM}, Nb/La_{PM} or La/Sm_{CN} with Nb/Th_{PM} and Nb/La_{PM}, indicating that the observed Nb anomalies are most likely

representative of original magmatic chemistry and not the result of contamination by continental crust.

Samples from G2, G3, and G3U exhibit correlations of Nb/Nb* with La/Sm_{CN}, Nb/Th_{PM}, Nb/La_{PM} and La/Sm_{CN} with Nb/Th_{PM} and Nb/La_{PM}, and their compositions trend toward the lower continental crust value, reflecting moderate LREE fractionation in the contaminant (Figs. 3.15b and 3.15c). These results are consistent with contamination by lower continental crust, the average composition of which is characterized by Nb/Nb* = 0.55, La/Sm_{CN} =1.84, Nb/Th_{PM} = 0.55, and Nb/La_{PM} = 0.62 (Rudnick and Gao, 2004).

Though samples from G2, G3, and G3U exhibit Nb-Th-La relationships (Figs. 3.15b and 3.15c) that are consistent with contamination by lower continental crust, it is possible that the observed variations in Nb-Th-La systematics result from the interaction of the primary, mantle-derived melt with continental lithospheric mantle (CLM) because lower continental crust is almost chemically indistinguishable from CLM. Lassiter and DePaolo (1997) and Okamura et al. (2005), however, showed that relationships between La/Ta(Nb) and La/Sm_{CN} can be used to characterize the differences in contamination when asthenosphere plumes interact with CLM or continental crust. Samples of G2 plot near the primitive mantle value and the distribution of data points trend along the CLM vector, while data for samples of G3 and G3U trend toward the lower crust value, between the CLM and crustal assimilation vectors (Figs. 3.16a and 3.16b).

Although Th-Nb-LREE systematics suggest contamination by sub-continental lithospheric mantle, contamination by continental crust cannot be ruled out given that subduction-modified lithospheric mantle and continental crust share similar trace element

characteristics. Maxeiner and Rayner (2010) identified two periods of continental arc volcanism, circa 1920 to 1910 Ma and 1860 to 1850 Ma, along the southeast margin of the Hearne Craton. It is likely that this subducting slab modified the underlying lithospheric mantle, resulting in formation of a metasomatized mantle source that interacted with and modified the upwelling asthenospheric melt. Collectively, in the absence of radiogenic isotope data, contamination of Lynn Lake volcanic rocks by continental crust is more likely, although contamination by subduction-metasomatized sub-continental lithospheric mantle cannot be ruled out. Regardless, both scenarios indicate the presence of continental lithosphere in the region at the time of emplacement of the volcanic rocks included in this study.

3.5.4. Mantle Source Characteristics and Depth of Partial Melting

HFSE and REE distributions can be used to constrain the depth at which the magmas that produced the Lynn Lake volcanic rocks were produced, and when these magmas may have initially segregated from their mantle source. High pressure experimental studies show that high-Mg (i.e., komatiitic) melts can be produced by both low degrees of mantle melting at high pressure (i.e., greater depth) or high degrees of mantle melting at low pressure (i.e., shallow depth) (Wei et al., 1990; Herzberg, 1992; Arndt, 2003). Irving and Frey (1978) noted that HREE distributions were significantly higher in garnet megacrysts compared to their host volcanic liquids of kimberlitic to rhyolitic composition and proposed that rocks forming within the garnet stability field will have fractionated HREE values as a result. Volcanic rocks of G1, G1*, and G1U exhibit HREE that are, for the most part, strongly positively fractionated (Gd/Yb_{CN} = 0.83 to 4.03), suggesting that these rocks were primarily derived by low degrees of partial

melting that occurred at a depth within the garnet stability field (> 90 km). In contrast, volcanic rocks from G2, G3, and G3U exhibit HREE with slight negative to moderate positive fractionation (Gd/Yb_{CN} = 0.65 to 2.39), suggesting that these rocks were derived through a combination of low degrees of partial melting that occurred at a greater depth within the garnet stability field (> 90 km), and high degrees of partial melting at depths within the spinel stability field (< 90 km).

Pearce (1982, 2008) demonstrated that variations in Th/Yb vs. Nb(Ta)/Yb reflect a combination in degree of depletion or enrichment of the mantle source and fractional crystallization processes and can be employed to further discriminate basalts from one another according to tectonic environment (i.e., convergent margin magmas vs. within-plate and spreading center basalts). On this diagram (Fig. 3.17), G1 and G1U samples plot primarily in the calc-alkaline field, parallel to the mantle array, within the compositional subdivision commonly associated with continental volcanic arc rocks or alkaline oceanic volcanic arc rocks, and the data project along a trend that extends toward the upper crust value along the fractionation vector (Fig. 3.17a). Samples of G1* plot primarily in the tholeiitic field, and the data extend along the fractionation vector toward the calc-alkaline field. Volcanic rocks of G2 plot above the mantle array, between the E-MORB and N-MORB values, and the data extend along the fractionation vector toward the lower crust value (Fig. 3.17b). Samples from G3 and G3U plot closer to the E-MORB value, outside of the mantle array, and the data extend along the fractionation trend toward the OIB value (Fig. 3.17c).

The following geochemical characteristics suggest a petrogenetic link, through fractionation of a tholeiitic parental magma, between volcanic rock groups G2, G3, and

G3U: 1) compositional trends extend from the tholeiitic to transitional compositional fields on Figures 3.6a, 3.7b, and 3.8c; 2) samples plot along the same fractionation trends on Zr vs. incompatible trace element diagrams (Figs. 3.10 and 3.11); and 3) samples plot along the same fractionation trend on Nb/Y vs. Zr/Nb, Ti/Zr, Zr/Y, and Al_2O_3/TiO_2 diagrams (Fig. 3.18). Furthermore, the picritic rocks of G3U have relatively high Mg numbers (66 to 74; average of 68), and Ni (172 to 2400 ppm; average of 715 ppm), and Cr (273 to 1710 ppm; average of 1214 ppm) contents, suggesting that they have undergone limited, if any, magmatic differentiation; making it very likely that these rocks represent the primary mantle-derived melt composition according to the criteria of Frey et al. (1978) (i.e., Mg number > 68, Ni > 320). Samples of G1 and G1U plot from the transitional to calc-alkaline fields, while their subset (i.e., G1*) plot in the tholeiitic field (Figs. 3.4b and 3.5b).

3.5.5. Geodynamic Origin of the Lynn Lake Greenstone Belt

The three groups of volcanic rocks comprising the Lynn Lake greenstone belt exhibit three distinct compositional trends (Figs. 3.12 to 3.17), which reflect a variation in magma source composition, fractionation, and contamination processes. The trace element characteristics of G1, G1*, and G1U are consistent with a volcanic arc setting (Pearce and Peate, 1995; Woodhead et al., 1998; Pearce, 2008). Samples of G1 and G1U exhibit enrichments in Th and LREE compared to Nb, which support the contamination of the primary magma through the interaction with upper continental crust. This indicates that these rocks were likely erupted in a continental setting, which is consistent with the study of Peck and Smith (1989), which reported that rocks in the Cartwright Lake area (e.g., G1 and G1U) were produced by the eruption of calc-alkaline magma onto

exisiting crust, including the accreted tholeiitic and transitional rocks of G2, G3, and G3U. In contrast, G1* rocks show no evidence of crustal contamination and could represent primitive tholeiitic magmas that were erupted within an intra-oceanic setting. Field observations from the Cartwright Lake area (Peck and Smith, 1989) and the MacLellan Au-Ag deposit (Chapter 2) have identified variably contaminated rocks stratigraphically above uncontaminated, oceanic volcanic rocks. In light of these observations, it is likely that these intra-oceanic rocks represent the original oceanic platform.

Samples of G2 display flat REE patterns on chondrite- and primitive mantle-normalized diagrams (Figs. 3.7c and 3.7d), plot along compositional trends that extend toward the lower crust value on a Th/Yb vs. Nb(Ta)/Yb mantle array diagram (Fig. 3.17b), and plot in a combination of MORB and CRB-OIB fields on basalt discrimination diagrams (Figs. 3.13a and 3.13b). The flat REE patterns are comparable to those of Phanerozoic ocean plateau basalts (Kerr, 2003; Said and Kerrich, 2009, 2010), and Archean intra-oceanic counterparts erupted from mantle plume-sourced magmas (Polat et al., 1998; Kerrich et al., 1999a,b; Wyman and Kerrich, 2009).

Samples of G3 and G3U rocks display enriched, EMORB-style patterns on chondrite- and primitive mantle-normalized diagrams (Figs. 3.7c, 3.7d, 3.8c, and 3.8d), plot just above the mantle array, near the EMORB value, and define a compositional trend that extends toward the OIB value within the mantle array on a Th/Yb vs. Nb(Ta)/Yb mantle array diagram (Fig. 3.17c), and plot in a combination of the CRB-OIB and CRB+OIB fields of basalt discrimination diagrams (Fig. 3.14a and 3.14b). The REE patterns of G3 and G3U are comparable to those of the Neoarchean Pickle Crow

assemblage of the Uchi subprovince (Hollings and Kerrich, 2004; Young et al., 2006) and the Wawa greenstone belt of the Superior Province (Polat, 2009), which have been interpreted to be associated with ocean plateau settings. The compositions of volcanic rocks belonging to G2, G3, and G3U are consistent with emplacement in an intra-oceanic plateau setting; however, the Nb-Th-La-REE systematics (Figs. 3.15a and 3.15b) of these groups is consistent with the contamination of the primary melt through a combination of lower continental crust and metasomatized continental lithospheric mantle. Kerrich et al., (2005) proposed that this occurs because mantle plumes cannot induce melting beneath thick (over 200 km) continental lithosphere, but rather are 'steered' to thinner margins, where decompressional melting can occur at depths less than 150 km, resulting in plume-driven rifts at cratonic margins. Plume-craton interaction at a rifted, thinned craton margin has been proposed for the contaminated and uncontaminated komatiite-basalt sequence of Kambalda (Said and Kerrich, 2010; Said et al., 2010), the 3.51 Ga to 3.2 Ga basalt succession of the Pilbara craton (Arndt et al., 2001), the 3.0 Ga komatiite-basalt sequence of the North Caribou greenstone belt in the Superior Province (Hollings and Kerrich, 1999), and the volcanic rocks of the Taishan greenstone belt of the North China Craton (Polat et al., 2006).

Cox (1980) proposed that dense picritic magmas pond within deep sill complexes near the base of the crust (20 to 40 km depth). These sills provide an ideal environment for the fractionation of large volumes of magma within a comparatively restricted pressure range, and also one in which magmas are highly susceptible to crustal contamination (Patchett, 1980). Magmas from these lower sill complexes may feed directly to the surface via dykes, or they may pond again in shallower sill complexes,

where further fractional crystallization and crustal contamination may occur before eruption ultimately takes place. The presence of highly fractionated aluminous basalts in G2 and G3 (MgO < 4 wt. %; Al_2O_3 > 17 wt. %) suggests that the primary melt must have ponded for an extended period of time either within or under the attenuated lithosphere prior to eruption; similar to the model of Cox (1980).

In light of the above evidence, the following geodynamic model is proposed for the Lynn Lake greenstone belt (Figs. 3.3 and 3.19):

1. > 1900 Ma (Fig. 3.19a), an upwelling mantle plume impinges off the keel of the Hearne Craton and is redirected to a section of attenuated lithosphere near the Hearne margin. During redirection, plume material is variably contaminated by continental lithospheric mantle or a metasomatized mantle source.
2. ~ 1900 Ma (Fig. 3.19b), upwelling plume (picritic?) material causes rifting and assimilates continental lithosphere, resulting in the ponding of ultramafic and mafic magma within continental crust or sub-continental lithospheric mantle. Oceanic plateau formation begins at the periphery of the mantle plume head, represented by G2 rocks, erupting onto an oceanic platform (i.e., G1*). Upwelling mantle plume rifts continental lithosphere and deposits thick layers of G3 to G3U volcanic rocks.
3. 1900 to 1890 Ma (Fig. 3.19c), the package of G2, G3, and G3U rocks continue to rift from the continental lithosphere, resulting in the formation of a secondary plateau. Fractionation of plume material within the sub-continental lithospheric mantle generates rhyolitic melts, which erupt around

1900 Ma, potentially signifying the waning stages of extensional volcanism. Basal conglomerates, greywacke, and arkosic sandstone (i.e., Ralph Lake conglomerates, Zed Lake Greywacke) begin to accumulate (refer to Fig. 3).

4. 1890 to 1870 Ma (Fig. 3.19d), rifting ceases and subduction initiates at the cratonic margin as the Manikewan Ocean begins to close. The sedimentary rocks that comprise the Southern Indian Gneiss Belt, Zed Lake Greywacke, and Ralph Lake Conglomerate (Fig. 3), along with mantle-plume derived rocks, are obducted onto the continental margin with salvages of the original oceanic platform. Circa 1875 Ma, deep-seated gabbroic, tonalitic, and granitic plutons begin to intrude the accreted rocks. The Wathaman-Chipewyan-Baldock batholith begins to develop as well as formation of the accretionary wedge.
5. ~ 1870 Ma (Fig. 3.19e), the subducting slab generates calc-alkaline magmas, G1 and G1U, which overlay the previously accreted volcanic rocks. Sickle Group sediments begin to form to the South in the Kisseynew Basin (Fig. 3).
6. ~ 1830 Ma (Fig. 3.19f), terminal closure of the Manikewan Ocean occurs as the Superior and Hearne-Rae Cratons collide. Region approaches peak metamorphic conditions (e.g., amphibolite facies). This collision results in the formation of the Granville Lake Suture Zone, south of the Lynn Lake greenstone belt. Subsequent uplift, erosion, and glaciations result in the current level of exposure.

3.5.6. Implications for the Trans Hudson Orogen

Continental rift-related sequences have been identified along the margins of the Hearne and Superior Cratons, including the ca. 2075 Ma Courtenay Lake porphyry (Ansdell et al., 2000), ca. 2072 Ma Cauchon dykes (Heaman and Corkery, 1996), and sedimentary and volcanic rocks of the ca. 2040 Ma Povunknituk Group (Machado et al., 1993), ca. 2025 Ma Richmond Gulf Group (Chandler and Parrish, 1989), and the Ospwagan Group (Hamilton and Bleeker, 2002). Basaltic rocks from the ca. 1900 Ma Levesque Bay and Lawrence Point assemblages (Maxeiner and Demmans, 2000) of the southern Reindeer Lake area exhibit the same flat REE trends on chondrite- and primitive mantle-normalized diagrams and inter-element ratios as the G2 rocks of the Lynn Lake greenstone belt. These rocks are interpreted to represent tectonically dismembered remnants of oceanic crust that separated the La Ronge arc from the Flin Flon-Glennie Lake Complex (Lucas et al., 1997). Supracrustal rocks from the Courtenay Lake – Cairns Lake fold belt (Money, 1968; Coombe, 1994; Foseenier et al., 1995; MacNeil et al., 1997) and the Needle Falls Group (Ray, 1979; Coombe, 1994) of the Wollaston Domain are also interpreted to represent rift-derived volcanic and sedimentary sequences. Collectively, these assemblages could record a single or multiple rifting events, which resulted in the formation and subsequent growth of the Manikewan Ocean between ca. 2100 and 2000 Ma (Ansdell, 2005). Flowers et al., (2006) proposed that the emplacement of the Chipman mafic dyke swarm, and the Kramanitaur, Uvauk, and Daly Bay mafic granulite complexes along the northern Snowbird tectonic zone, were the result of an episode of continental-scale asthenospheric upwelling, which resulted in the formation of an ocean basin and the northward propagation of a continental rift system.

A similar system may account for the variation in mantle plume-derived rocks found in the Wollaston Domain and the Lynn Lake and La Ronge greenstone belts.

3.5.7. Implications for Regional Metallogeny

Previous geodynamic models for the Lynn Lake region have stressed the importance of exploration for volcanogenic massive sulphide (VMS) deposits (e.g., Syme, 1985; Zwanzig et al., 1999). These deposits, however, are not typically associated with greenstone belts that formed in near-continent or shallow-water environments (e.g., Shebandowan and Vermillion greenstone belts of the Wawa subprovince), which are akin to the environment proposed for the Lynn Lake greenstone belt (Fig. 19) (Lodge, 2012 and references therein). Lodge (2013) suggested that the affiliation of thicker crust with near-continent or shallow-water settings may inhibit VMS formation, making it highly unlikely that the Lynn Lake greenstone belt is a suitable host to VMS-style mineralization. At this point, it is important to reconsider the regional metallogeny of the Lynn Lake greenstone belt within the constraints of the revised geodynamic model (Fig. 19).

Sedimentary exhalative (i.e., Sedex) mineral deposits most commonly occur within rift-covered sequences, which consist of shallow-water sedimentary facies that are deposited during the thermal subsidence or rift sag stage, and cover both the buried site of the rift and its adjacent platform shoulders (Lydon, 1996). Sedex occurrences have been identified in the calc-silicate rocks of the Kasmere and Putahow Lakes area of northwest Manitoba (Weber et al., 1975) and within the sedimentary rocks of the Courtenay Lake-Cairns Lake fold belt (Delaney et al., 1997) of the Wollaston Domain in Saskatchewan.

In contrast, the Lynn Lake greenstone belt hosts a single significant Cu-Zn deposit (e.g., Fox Cu-Zn deposit). Lustig (1979) argued for both a volcanogenic and epigenetic origin for the Fox Cu-Zn deposit, but favoured a volcanogenic origin based on the assumption that the deposit was isoclinally folded, with the apex of the fold representing the western end of the ore zone, in order to explain the symmetry in the alteration zones situated concentrically about the ore zones. The same textural evidence used to classify the Fox Cu-Zn deposit as volcanogenic in origin has also been interpreted to represent the epigenetic replacement of pre-existing rocks by chalcopyrite and sphalerite through the action of hydrothermal solutions (Bateman, 1942; Boyle, 1970; Glass, 1972; Obinna, 1974; Boyle, 1976; Turek et al., 1976; Norman, 1977; Lustig, 1979). An epigenetic origin for the Fox Cu-Zn deposit is consistent with the proposed geodynamic model and the observations of Lodge (2012, 2013). Furthermore, the geologic similarities between the G2, G3, and G3U rocks of the Lynn Lake region to the rift-related volcanic rocks of the Wollaston Domain, and the presence of Sedex occurrences in the calc-silicate rocks of the Kasmere and Putahow Lakes area of northwest Manitoba (Weber et al., 1975) and the sedimentary rocks of the Courtenay Lake-Cairns Lake fold belt (Delaney et al., 1997) of the Wollaston Domain in Saskatchewan suggests that the relatively unexplored sedimentary belts that border the Lynn Lake greenstone belt could be suitable for the development of significant Sedex resources.

High-field strength element and trace-element systematics (i.e., Nb-Th-REE) of the G1 volcanic arc rocks in the Lynn Lake region show a continental volcanic arc affinity, which may represent a suitable environment for development of porphyry Cu, Au, Mo, W, and Sn deposits. These deposits occur in close association with epizonal and

mesozonal, felsic to intermediate intrusions, which exhibit a wide range of compositions and petrogenetic associations, and occur in a variety of tectonic settings (Kirkham, 1972). Although only one auriferous quartz-feldspar porphyritic dyke has been identified near the Burnt Timber deposit (Jones, 2005), the potential for this style of mineralization to occur within the greenston belt should be considered because of the large number of unexplored plutonic rocks that occur throughout the Lynn Lake region.

Regional volcanism in the Lynn Lake region ceased upon terminal closure of the Manikewan Ocean, which resulted in the development of sedimentary basins, thrust faulting, crustal thickening, and the generation of orogenic melts. This transition from a volcanic arc to a collisional orogenic setting can explain the number of significant gold deposits that are present throughout the belt (Richardson and Ostry, 1996). Recent identification of REE-rich carbonatites that are hosted by an anorogenic syenite complex near Eden Lake (Chakmouradian et al., 2008), however, demonstrates the regional potential for significant carbonatite-associated HFSE or, perhaps, Kiruna/Olympic Dam-type iron-copper-uranium-gold-silver deposits.

3.6. Conclusions

The following principal conclusions are drawn on the basis of field and geochemical characteristics of the ultramafic to intermediate volcanic rocks of the Paleoproterozoic (ca. 1900 Ma) Lynn Lake greenstone belt:

1. The Lynn Lake greenstone belt comprises mantle plume- and volcanic arc-derived volcanic rocks. Trace element systematics of the mantle plume-derived rocks are consistent with a rifted continental margin geodynamic setting. Volcanic arc-

derived rocks are subdivided based on their Th-La-Nb-REE systematics into primitive intra-oceanic- and contaminated continent-derived rocks, of which the latter is more common.

2. Major and trace element data indicate a petrogenetic link between the tholeiitic to transitional mantle plume-derived rocks; suggesting that a single plume generated the majority of the volcanic rocks. Continental volcanic arc rocks have a transitional to calc-alkaline affinity, however, intra-oceanic volcanic arc rocks are primarily tholeiitic.
3. Plume-derived rocks display two different REE patterns, stemming from different depths of partial melting within the spinel (< 90 km) and garnet (> 90 km) stability fields. Volcanic arc rocks display REE patterns that are consistent with partial melting in the garnet (> 90 km) stability field.
4. Porphyry Sn-W-Cu-Au-Ag-, and carbonatite-style mineralization have been either identified or considered as potential exploration targets based on the revised geodynamic model for the Lynn Lake region. The presence of Sedex-style deposits in the rift sedimentary and volcanic sequences of the Wollaston Domain suggest that the sedimentary belts bounding the Lynn Lake greenstone belt have the potential to host Sedex-style mineralization. Furthermore, the identification of an anorogenic syenite complex in the Lynn Lake region suggests that there is potential for Kiruna/Olympic Dam-type Fe-Cu-U-Au-Ag deposits.

3.7. References

Agrawal, S., Guevara, M., and Verma, S., 2008. Tectonic discrimination of basic and ultrabasic volcanic rocks through log-transformed ratios of immobile trace elements. International Geology Review 50, 1057-1079.

Ansdell, K.M., 2005. Tectonic evolution of the Manitoba-Saskatchewan segment of the Paleoproterozoic Trans-Hudson Orogen, Canada. Canadian Journal of Earth Sciences 42(4), 741-759.

Ansdell, K.M, MacNeil, A., Delaney, G.D., and Hamilton, M.A., 2000. Rifting and development of the Hearne passive margin: age constraint from the Cook Lake area, Saskatchewan. Geological Association of Canada – Mineralogical Association of Canada, GeoCanada 2000, Extended abstract 777.

Arndt, N.T., 2003. Komatiites, kimberlites, and boninites. Journal of Geophysical Research: Solid Earth 108(B6), 2293.

Arndt, N.T., Bruzak, G., and Reischmann, T., 2001. The oldest continental and oceanic plateaus: geochemistry of basalts and komatiites of the Pilbara Craton, Australia. Geological Society of America Special Papers 352, 359-387.

Augsten, B.E.K., Thorpe, R.I., Harris, D.C., and Fedikow, M.A.F, 1986. Ore Geology of the Agassiz (MacLellan) Gold Deposit in the Lynn Lake Region, Manitoba. Canadian Mineralogist 24, 369-377.

Baldwin, D.A., Syme, E.C., Zwanzig, H.V., Gordon, T.M., Hunt, P.A., and Stevens, R.D., 1987. U-Pb zircon ages from the Lynn Lake and Rusty Lake metavolcanic belts, Manitoba: two ages of Proterozoic Magmatism. Canadian Journal of Earth Sciences 24, 1053-1063.

Bateman, A.M., 1942. Economic mineral deposits. John Wiley and Sons, Inc., New York, 898 p.

Bateman, J.D., 1945. McVeigh Lake area, Manitoba; Geological Survey of Canada Paper 45-14, 34 p.

Beaumont-Smith, C.J., 2008. Geochemistry data for the Lynn Lake greenstone belt, Manitoba (NTS 64C11-16); Manitoba Science, Technology, Energy and Mines, Mantoba Geological Survey, Open File OF2007-1, 5 p. + Appendix.

Beaumont-Smith, C.J., and Böhm, C.O., 2002. Structural analysis and geochronological studies in the Lynn Lake greenstone belt and its gold-bearing shear zones (NTS 64C10, 11, 12, 14, 15 and 16), Manitoba; *in* Report of Activities 2002, Manitoba Industry, Trade and Mines, Manitoba Geological Survey, 159-170.

Beaumont-Smith, C.J., and Böhm, C.O., 2003. Tectonic evolution and gold metallogeny of the Lynn Lake greenstone belt, Manitoba (NTS 64C10, 11, 12, 14, 15 and 16), Manitoba; *in* Report of Activities 2003, Manitoba Industry, Economic Development and Mines, Manitoba Geological Survey, 39-49.

Beaumont-Smith, C.J., and Böhm, C.O., 2004. Structural analysis of the Lynn Lake greenstone belt, Manitoba (NTS 64C10, 11, 12, 14, 15 and 16); *in* Report of Activities 2004, Manitoba Industry, Economic Development and Mines, Manitoba Geological Survey, 55-68.

Beaumont-Smith, C.J., Machado, N., Peck, D.C., 2006. New uranium-lead geochronology results from the Lynn Lake greenstone belt, Manitoba (NTS 64C11-16); Manitoba Science, Technology, Energy and Mines, Manitoba Geological Survey, Geoscientific Paper GP2006-1, 11 p.

Bickford, M.E., and Van Schmus, W.R., 1985. Preliminary U-Pb age data for the Trans-Hudsonian Orogen in northern Saskwatchewan; new and revised results. Miscellaneous Report – Saskatchewan Mineral Resources 85-4, 63-66.

Boyle, R.W., 1970. The source of metals and gangue elements in hydrothermal deposits. *In* Pouba, Z., and Stemprok, M. (Eds.). Problems of hydrothermal ore deposition, International Union of Geological Sciences 2A, 3-6.

Boyle, R.W., 1976. Mineralization processes in Archean greenstone and sedimentary belts. Geological Survey of Canada Paper 75-15.

Chakmouradian, A.R., Mumin, A.H., Demeny, A., and Elliott, B., 2008. Postorogenic carbonatites at Eden Lake, Trans-Hudson Oroegn (northern Manitoba, Canada): Geological setting, mineralogy and geochemistry. Lithos 103, 503-526.

Chandler, F.W., and Parrish, R.R., 1989. Age of the Richmond Gulf Group and implications for rifting in the Trans-Hudson Orogen, Canada. Precambrian Research 44, 277-288.

Coombe, W., 1994. Sediment-hosted base metal deposits of the Wollaston Domain, northern Saskatchewan. Saskatchewan Geological Survey, Saskatchewan Energy and Mines, Report 213.

Cox, K.C., 1980. A Model for Flood Basalt Vulcanism. Journal of Petrology 21(4), 629-650.

Delaney, G.D., Janovic, Z., MacNeil, A., McGowan, J., and Tisdale, D., 1997. Geological investigations of the Courtenay Lake-Cairns Lake fold belt and the Hills Lake embayment, Johnson River inlier, Wollaston domain, northern Saskatchewan. *In* Summary of Investigations 1997, Saskatchewan Geological Survey, Saskatchewan Energy and Mines, Miscellaneous Report 97-4, 90-101.

Dostal, J., Strong, D.F., and Jamieson, R.A., 1980. Trace element mobility in the mylonite zone within the ophiolite aureole, St. Anthony Complex, Newfoundland. Earth and Planetary Science Letters 49, 188-192.

Fedikow, M.A.F., 1986. Geology of the Agassiz (MacLellan) Stratabound Au-Ag Deposit, Lynn Lake, Manitoba. Manitoba Energy and Mines, Geological Services Branch, Open File Report OF85-5, 80 p.

Fedikow, M.A.F., 1992. Rock geochemical alteration studies at the MacLellan Au-Ag deposit, Lynn Lake, Manitoba. Manitoba Energy and Mines, Geological Services, Economic geology Report ER92-1, 237 p.

Fedikow, M.A.F., and Gale, G.H., 1982. Mineral deposit studies in the Lynn Lake area. *In* Manitoba Mineral Resources Division, Report of Field Activities, 44-54.

Flowers, R.M., Bowring, S.A., and Williams, M.K., 2006. Timescales and significance of high-pressure, high-temperature metamorphism and mafic dike anatexis, Snowbird tectonic zone, Canada. Contributions to Mineralogy and Petrology 151(5), 558-581.

Fossenier, K., Delaney, G.D., and Watters, B.R., 1995. Lithogeochemistry of the volcanic rocks from the Lower Proterozoic Courtenay Lake Formation, Wollaston Domain. *In* Summary of Investigations 1995, Saskatchewan Geological Survey, Saskatchewan Energy and Mines, Miscellaneous Report 95-4, 49-60.

Gagnon, A., McKinnon, C., Tkaczuk, C., Burga, D., Puritch, E.J., McLaughlin, M., Bridson, P., Wenchang, N., and Yungang, W., 2013. Preliminary Economic Assessment for the MacLellan, Farley Lake, Burnt Timber, and Linkwood Properties, Lynn Lake Gold Camp, Manitoba. Effective December 2, 2013.

Gale, G.H., Koo, J., Solkoski, L., Southard, G.G., 1976. Evaluation of massive sulphide environments; *in* Non-renewable resource evaluation program (NREP): first annual report, 1975-1975, Canada Department of Energy, Mines and Resources, Manitoba Mines, Resources and Environmental Management, Mineral Resources Division, Open File Report 77-1, 34-46.

Gale, G.H., and Koo, J., 1977. Evaluation of massive sulphide environments; *in* Non-renewable resource evaluation program (NREP): second annual report, 1976-1977, Manitoba Mines, Resources and Environmental Management, Canada Department of Energy, Mines and Resources, Open File Report 77-7, 58-62.

Gale, G.H., Baldwin, D.A., and Koo, J., 1980. A geological evaluation of Precambrian massive sulfide deposit potential in Manitoba. Manitoba Department of Energy and Mines, Mineral Resources Division, Economic Geology Report ER79-1, 167 p.

Gilbert, H.P., Syme, E.C., and Zwanzig, H.V., 1980. Geology of the metavolcanic and volcaniclastic metasedimentary rocks in the Lynn Lake area; Manitoba Energy and Mines, Geological Services, Geological Paper GP80-1, 118 p.

Gilbert, H.P., 1993. Geology of the Barrington Lake-Melvin Lake-Fraser Lake area. Manitoba Energy and Mines, Geological Report GR87-3, 97 p.

Glass, D.J., 1972. Geology and mineral deposits of the Flin-Flon, Lynn Lake, and Thompson areas, Manitoba and Churchill-Siperior Front of the western Precambrian Shiel. 24th International Geological Congress Guidebook, Excursions A31 and C31.

Govindaraju, K., (Ed,), 1983. Special Issue: Geostandards Newsletter 8, 16 p.

Hamilton, M.A., and Bleeker, W., 2002. SHRIMP U-Pb geochronology of the Ospwagan Group: provenance and depositional age constraints of a Paleoproterozoic rift sequence, SE externides of the Tran-Hudson Orogen. Geological Asssociation of Canada – Mineralogical Association of Canada, Abstracts 27, 44.

Hanski, E., Huhma, H., Rastas, P., and Kamenetsky, V.S., 2001. The Palaeoproterozoic Komatiite-Picrite Association of Finnish Lapland. Journal of Petrology 42(5), 855-876.

Heaman, L.M., and Corkery, T., 1996. U-Pb geochronology of the Split Lake Block, Manitoba: preliminary results. *In*: Hajnal, Z., and Lewry, J. (Eds). Trans Hudson Lithoprobe Transect, Lithoprobe Report 55, 60-67.

Herzberg, C., 1992. Depth and degree of melting of komatiite. Journal of Geophysical Research 97, 4521-4540.

Hofmann, A.W., 1988. Chemical differentiation of the Earth: the relationship between mantle, continental crust, and oceanic crust. Earth and Planetary Science Letters 90, 297-314.

Hollings, P., and Kerrich, R., 2004. Geochemical systematic of tholeiites from the 2.86 Ga Pickle Crow assemblage, northwestern Ontario: arc basalts with positive and negative Nb-Hf anomalies. Precambrian Research 134, 1-20.

Huang, C.H., and Smith, T.E., 1983. Application of the linear relationship between the reciprocal of analyte-line intensity and reciprocal of concentration to the analysis of geologic materials. X-ray Spectrometry 12, 87-90.

Hunt, P.A., Zwanzig, H.V., Anonymous, 1990. Pre-Missi granitoid domes in the Puffy Lake area, Kisseynew gneiss belt, Manitoba. Geological Survey of Canada 89-02, 71-75.

Irving, A.J. and Frey, F.A., 1978. Distribution of trace elements between garnet megacrysts and host volcanic liquids of kimberlitic to rhyolitic composition. Geochimica et Cosmochimica Acta 42(6A), 771.

Jenkins, R., and DeVris, J. L., 1982. Practical x-ray spectrometry (fourth edition). Springer-Verlag, New York, 190 p.

Jones, L.R., 2005. Geology of the shear-hosted Burnt Timber deposit, Lynn Lake, northern Manitoba. Unpublished M.Sc. thesis, Laurentian University of Sudbury, 80 p.

Jones, L.R., Lafrance, B., and Beaumont-Smith, C.J., 2006. Structural controls on gold mineralization at the Burnt Timber mine in the Lynn Lake greenstone belt, Trans-Hudson Orogen, Manitoba. Exploration and Mining Geology, 15, 89-100.

Jurkowski, J.S., 1999. Uranium-lead geochronology study of Lynn Lake greenstone belt, Manitoba. Unpublished M.Sc. thesis, University of Windsor, p.

Kerr, A.C., and Arndt, N.T., 2001. A note on the IUGS reclassification of the high-Mg and picritic volcanic rocks. Journal of Petrology 42(11), 2169-2171.

Kerrich, R., and Fyfe, W.S., 1981. The gold-carbonate association: Sources of CO2 fixation reactions in Archean lode deposits. Chemical Geology 33, 265-294.

Kerrich, R., Polat, A., Wyman, D., and Hollings, P., 1999a. Trace element systematic of Mg-, to Fe- tholeiitic basalt suites of the Superior Province: Implications for Archean mantle reservrois and greenstone belt genesis. Lithos 46, 163-187.

Kerrich, R., Wyman, D., Hollings, P., and Polat, A., 1999b. Variability of Nb/U and Th/La in 3.0 to 2.7 Ga Superior Province ocean plateau basalts: implications for the timing of continental growth and lithosphere recycling. Earth and Planetary Science Letters 168, 101-115.

Kerrich, R., Goldfarb, R., and Richard, J.P., 2005. Metallogenic Provinces in an evolving geodynamic framework. Economic Geology 100, 1097-1136.

Kirkham, R.V., 1972. Porphyry deposits. *In* Report of Activities, Part B: November 1971 to March 1972. Geological Survey of Canada, Paper 72-1B, 62-64.

Lassiter, J.C., and DePaolo, J., 1997. Plume/Lithosphere interaction in the generation of continental and oceanic flood basalts: chemical and isotopic constraints. Geophysical Monograph 100, 335-355.

Lewry, J.F., Macdonald, R., Livesey, C., Meyer, M., Van Schmus, R., and Bickford, M.E., 1987. U-Pb geochronology of accreted terranes in the Trans-Hudson Orogen, Northern Saskatchewan, Canada. *In* Pharoah, T.C., Beckinsale, R.D., and Rickard, D. (Eds.). Geochemistry and mineralization of Proterozoic Volcanic Suites, Geological Society of London, Special Publication 33, 147-165.

Lodge, R.W.D., 2012. Winston Lake and Manitouwadge revisited: modern views of two volcanogenic massive sulphide (VMS)-endowed greenstone belts. A field trip guidebook; Ontario Geological Survey, Open File Report 6282, 34 p.

Lodge, R.W.D., 2013. Regional Volcanogenic Massive Sulphide Metallogeny of the NeoArchean Greenstone Belt Assemblages of the Northwest Margin of the Wawa Subprovince, Superior Province. Unpublished Ph.D. thsis, Laurentian University of Sudbury, 290 p.

Lucas, S.B., Stern, R.A., Syme, E.C., Zwanzig, H., Bailes, A.H., Ashton, K.E., Maxeiner, R.O., Ansdell, K.M., Lewry, J.F., Ryan, J.J., and Kraus, J., 1997. Tectonics of the southeastern Reindeer Zone, Trans-Hudson Orogen (Manitoba and Saskatchewan). Geological Association of Canada – Mineralogical Association of Canada Joint Annual Meeting, May 19-21, Ottawa, 93 p.

Lustig, G.N., 1979. Geology of the Fox orebody, northern Manitoba. Unpublished M.Sc. thesis, University of Manitoba, 87 p.

Lydon, J.W., 1996. Sedimentary exhalative sulphides (Sedex). *In* Eckstrand, O.R., Sinclair, W.D., and Thorpe, R.I. (Eds.). Geology of Canadian Mineral Deposit Types, Geological Survey of Canada, Geology of Canada 8, 130-152.

Machado, N., David, J., Scott, D.J., Lamothe, D., Philippe, S., and Gariepy, C., 1993. U-Pb geochronology of the western Cape Smith Belt, Canada: new insights on the age of initial rifting and arc magmatism. Precambrian Research 63, 211-224.

MacNeil, A., Delaney, G.D., and Ansdell, K., 1997. Geology of the Courtenay Lake Formation in the Cook Lake area, Wollaston Domain, northern Saskatchewan. *In* Summary of Investigations 1997, Saskatchewan Geological Survey, Saskatchewan Energy and Mines, Miscellaneous Report 97-4, 115-120.

Maier, W.D., Arndt, N.T., Curl, E.A., 2000. Progressive crustal contamination of the Bushveld Complex: evidence from Nd isotopic analyses of cumulate rocks. Contributions to Mineralogy and Petrology 140, 316-327.

Manikyamba, C., Kerrich, R., Polat, A., and Abhishek, S., 2013. Geochemistry to two stratigraphically-related ultramafic (komatiite) layers from the Neoarchean Sigegudda greenstone terrane, Western Dharwar Craton, India: Evidence for compositional diversity in Archean mantle plumes. Lithos 177, 120-135.

Maxeiner, R.O., and Demmans, C.J., 2000. The final pieces of the 'Bridge': Geology of the southern Reindeer Lake and Laurie Lake areas. *In* Summary of Investigations 2000, Vol. 2, Saskatchewan geological Survey, Saskatchewan Energy and Mines, Miscellaneous Report 2000-4.2, 30-50.

Maxeiner, R.O., and Rayner, N., 2010. Continental arc magmatism along the southeast Hearne Craton margin in Saskatchewan, Canada: Comparison of the 1.92-1.91 Ga Porter Bay Complex and the 1.86-1.85 Ga Wathaman Batholith.

McRitchie, W.D., 1974. The Sickle-Wasekwan debate: a review. Manitoba Mines Branch, Geological Paper 1/74, 23 p.

Milligan, G.C., 1960. Geology of the Lynn Lake District. Manitoba Mines Branch, Publication 57-1, 317 p.

Money, P.L., 1968. The Wollaston Lake fold-belt system, Saskatchewan-Manitoba. Canadian Journal of Earth Sciences 5, 1489-1504.

Norman, G.W.H., 1933. Graville Lake district, northern Manitoba. Geological Survey of Canada, Summary Report, Part C, 23-41.

Norman, G.W.H., 1977. Proterozoic massive sulfide replacements at Jerome, Arizona. Economic Geology 72, 642-656.

North American Geologic-Map Data Model Science Language Technical Team, 2004. Report on progress to develop a North American science-language standard for digital geologic-map databases; Appendix B – Classification of metamorphic and other composite-genesis rocks, including hydrothermally altered, impact-metamorphic, mylonitic, and cataclastic rocks, Version 1.0 (12/18/2004), *in* Soller, D.R., (Ed.). Digital Mapping Techniques `04—Workshop Proceedings: U.S. Geological Survey Open-File Report 2004-1451 56 p.

Nosova, A.A., Sazonova, L.V., Gorozhanin, V.M., Kuz'menkova, O.F., Dubinina, E.O., 2010. Mesoproterozoic olivine gabbronorites of the Bashkirian anticlinorium, the South Urals: Parental melts and specifics of magma evolution. Petrology 18(1), 50-83.

Obinna, F.C., 1974. The geology and some genetic aspects of Fox Mine Mineralization, Northern Manitoba. Unpublished M.Sc. Thesis, University of Manitoba, 96 p.

Okamura, S., Arculus, R.J., Martynov, Y.A., 2005. Cenozoic Magmatism of the North-Eastern Eurasian Margin: The Role of Lithosphere Versus Asthenosphere. Journal of Petrology 46(2), 221-253.

Ordóñez-Calderón, J.C., Polat, A., Fryer, B.J., Gagnon, J.E., Raith, J.G., and Appel, P.W.U., 2008. Evidence for HFSE and REE mobility during calc-silicate metasomatism, Mesoarchean (~3075 Ma) Ivisaartoq greenstone belt, southern West Greenland. Precambrian Research 161(3-4), 317-340.

Patchett, P.J., 1980. Thermal effects of basalt on continental crust and crustal contamination of magmas. Nature 283, 559-561.

Pearce, J.A., 1982. Trace element characteristics of lavas from destructive plate boundaries. In: Thorpe, R.S. (Ed.). Andesites: Orogenic Andesites and Related Rocks. John Wiley & Sons, Chichester, 525-548.

Pearce, J.A., 2008. Geochemical fingerprinting of oceanic basalts with applications to ophiolite classification and the search for Archean oceanic crust. Lithos 100, 14-48.

Pearce, J.A., and Peate, D.W., 1995. Tectonic implications of the composition of volcanic arc magmas. Annual Reviews of Earth and Planetary Sciences 23, 251-285.

Peck, D.C., 1986. The geology and geochemistry of the Cartwright Lake Area: Lynn Lake greenstone belt, Northwestern Manitoba. Unpublished M.Sc. Thesis, University of Windsor, 270 p.

Peck, D.C., and Smith, T.E., 1989. The geology and geochemistry of an early-Proterozoic volcanic arc association at Cartwright Lake Lynn Lake greenstone belt, Northwestern Manitoba. Canadian Journal of Earth Sciences 26, 716-736.

Polat, A., 2009. The geochemistry of Neoarchean (ca. 2700 Ma) tholeiitic basalts, transitional to alkaline basalts, and gabbros, Wawa Subprovince, Canada: Implications for petrogenetic and geodynamic processes. Precambrian Research 168, 83-105.

Polat, A., Kerrich, R., and Wyman, D., 1998. The late Archean Schreiber-Hemlo and White River-Dayohessarah greenstone belts, Superior Province: collages of oceanic plateaus, oceanic arcs, and subduction-accretion complexes. Tectonophysics 289, 295-326.

Polat, A., and Hofmann, A.W., 2003. Alteration and geochemical patterns in the 3.7-3.8 Ga Isua greenstone belt, West Greenland. Precambrian Research 126, 197-218.

Polat A., Li, J., Fryer, B., Kusky, T., Gagnon, J., and Zhang, S., 2006. Geochemical characteristics of the Neoarchean (2800-2700 Ma) Taishan Greenstone Belt, North China Craton: Evidence for plume-craton interaction. Chemical Geology 230, 60-87.

Puchtel, I.S., Haase, K.M., Hofmann, A.W., Chauvel, C., Kulikov, V.S., Garbe-Schönberg, C.-D., Nemchin, A.A., 1997. Petrology and geochemistry of crustally contaminated komatiitic basalts from the Vetreny Belt, southeastern Baltic Shield: evidence for an early Proterozoic mantle plume beneath rifted Archean continental lithosphere. Geochim Cosmochim Acta 61, 1205-1222.

Ray G.E., 1979. Reconnaissance bedrock geology: Wollaston East (part of NTS area 64L). *In* Summary of investigations 1979, Vol. 2, Saskatchewan geological Survey, Saskatchewan Minerals and Resources, Miscellaneous Report 49-10, 19-28.

Ray, G.E., and Wanless, R.K., 1980. The ages of the Wathaman Batholith, Johnson River Granite and Peter Lake Complex and their geological relationships to the Wollaston, Peter Lake and Rottenstone Domains of northern Saskatchewan. Canadian Journal of Earth Sciences 17, 333-347.

Richardson, D.J., and Ostry, G., 1996. Gold deposits of Manitoba. Energy and Mines, Economic Geology Report 86-1 (2nd Edition), 114 p.

Ross, P.-S., and Bédard, J.H., 2009. Magmatic affinity of modern and ancient subalkaline volcanic rocks determined from trace-element discriminant diagrams. Canadian Journal of Earth Sciences 46, 823-839.

Rudnick, R.L., and Gao, S., 2004. Composition of the Continental Crust. Treatise on Geochemistry 3, 1-64.

Said, N., and Kerrich, R., 2009. Geochemistry of coexisting depleted and enriched Paringa Basalts, in the 2.7 Ga Kalgoorlie Terrane, Yilgarn Craton, Western Australia: Evidence for a heterogeneous mantle plume event. Precambrian Research 174, 287-309.

Said, N., and Kerrich, R., 2010. Magnesian dyke suites of the 2.7 Ga Kambalda Sequence: Evidence for coeval melting of plume asthenosphere and metasomatised lithospheric mantle. Precambrian Research 180, 183-203.

Said, N., Kerrich, R., Groves, D.I., 2010. Geochemical systematics of Basalts of the Lower Basalt Unit, 2.7 Ga Kambalda Sequence: Plume Impingement at a Rifted Craton Margin. Lithos 115, 82-100.

Samson, I.M., and Gagnon, J.E., 1995. Episodic fluid infiltration and genesis of the Proterozoic MacLellan Au-Ag deposit, Lynn Lake greenstone belt, Manitoba. Exploration and Mining Geology 4-1, 33-50.

Samson, I.M., Blackburn, W.H., and Gagnon, J.E., 1999. Paragenesis and composition of amphibole and biotite in the MacLellan gold deposit, Lynn Lake greenstone belt, Manitoba, Canada. Canadian Mineralogist 37, 1405-1421.

Scholz, C.H., and Contreras, J.C., 1998. Mechanics of continental rift architecture. Geology (Boulder) 26(11), 967-970.

Strand, K., and Köykkä, J., 2012. Early Paleoproterozoic rift volcanism in the eastern Fennoscandian Shield related to the breakup of the Kenorland supercontinent. Precambrian Research 214-215, 95-105.

Sun, S.S., and McDonough, W.F., 1989. Chemical and isotopic systematic of oceanic basalts: implications for mantle composition and processes. Geological Society of London, Special Publications 42, 313-345.

Syme, E.C., 1985. Geochemistry of metavolcanic rocks in the Lynn lake belt; Manitoba Energy Mines, Geological Servies, Geological Report GR84-1.

Taylor, S.R., and McLennan, S.M., 1985. The continental crust: Its composition and evolution. Blackwell, Oxford, 312 pp.

Thompson, R.N., Riches, A.J.V., Antoshechkina, P.M., Pearson, D.G., Nowell, G.M., Ottley, C.J., Dickin, A.P., Hards, V.L., Nguno, A.K., and Niku-Paavola, V., 2007. Origin of CFB Magmatism: Multi-tiered Intracrustal Picrite-Rhyolite Magmatic Plumbing at Spitzkoppe, Western Namibia, during Early Cretaceous Etendeka Magmatism. Journal of Petrology 48(6), 1119-1154.

Turek, A., Tetley, N.W., and Jackson, T., 1976. A study of metal dispersion around the Fox ore body in Manitoba. Canadian Mineral and Metallurgical Bulletin 70, 104-110.

Turek, A., Woodhead, J., and Zwaznig, H.V., 2000. U-Pb age of the gabbro and other plutons at Lynn Lake (part of NTS 64C); *in* Report of Activities 2000, Manitoba Industry, trade and Mines, Manitoba Geological Survey, p. 97-104.

Van Schmus, W.R., Bickford, M.E., Lewry, J.F., and Macdonald, R., 1987. U-Pb geochronology in the Trans-Hudson orogen, northern Saskatchewan Canada. Canadian Journal of Earth Sciences 24, 407-424.

Weber, W., Schledewitz, D.C.P., Lamb, C.F., and Thomas, K.A., 1975. Geology of the Kasmere Lake-Whiskey Jack Lake (north half) area (Kasmere Project). Manitoba Department of Mines, Mineral Resources Division, Geological Services Branch 74-2, 163 p.

Wei, K., Tronnes, R.G., and Scrafe, C.M., 1990. Phase relations of aluminum-undepleted and aluminum-depleted komatiites at pressures of 4-12 GPa. Journal of Geophysical Research 95, 15,817-15,827.

West, H.B., Garcia, M.O., Gerlach, D.C., Romano, J., 1992. Geochemistry of tholeiites from Lanai, Hawaii. Contributions to Mineralogy and Petrology 112, 520-542.

Winchester, J.A., and Floyd, P.A., 1977. Geochemical discrimination of different magma series and their differentiation products using immobile elements. Chemical Geology 20, 325-343.

Woodhead, J.D., Eggins, S.M., and Johnson, R.W., 1998. Magma genesis in the New Britain island arc: further insights into the melting and mass transfer processes. Journal of Petrology 39, 1641-1668.

Wyman, D., and Kerrich, R., 2009. Plume and Arc magmatism in the Abitibi Subprovince: implications for the origin of Archean Continental Lithospheric Mantle. Precambrian Research 168, 4-22.

Young, G.M., 2002. Geochemical investigation of a Neoproterozoic glacial unit: The Mineral Fork Formation in the Wasatch Range, Utah. Geological Society of America Bulletin 114, 387.399.

Young, M.D., McNicoll, V., Helmstaedt, H., Skulski, T., and Percival, J.A., 2006. Pickle Lake revisited: New structural, geochronological and geochemical constraints on greenstone belt assembly, western Superior Province, Canada. Canadian Journal of Earth Sciences 46, 821-847.

Zwanzig, H.V., 1990. Kisseynew gneiss belt in Manitoba: stratigraphy, structure and tectonic evolution. In: Lewry, J.F., and Stauffer, M.R. (Eds.). The Early Proterozoic Trans-Hudson Orogen of North America. Geological Asssociation of Canada, Special Paper 37, 95-120.

Zwanzig, H.V., Syme, E.C., and Gilbert, H.P., 1999. Updated trace element geochemistry of ca. 1.9 Ga metavolcanic rocks in the Paleoproterozoic Lynn Lake Belt; Manitoba Industry, Trade and Mines, Geological Servies, Open File Report OF99-13, 48p. Plus map and diskette.

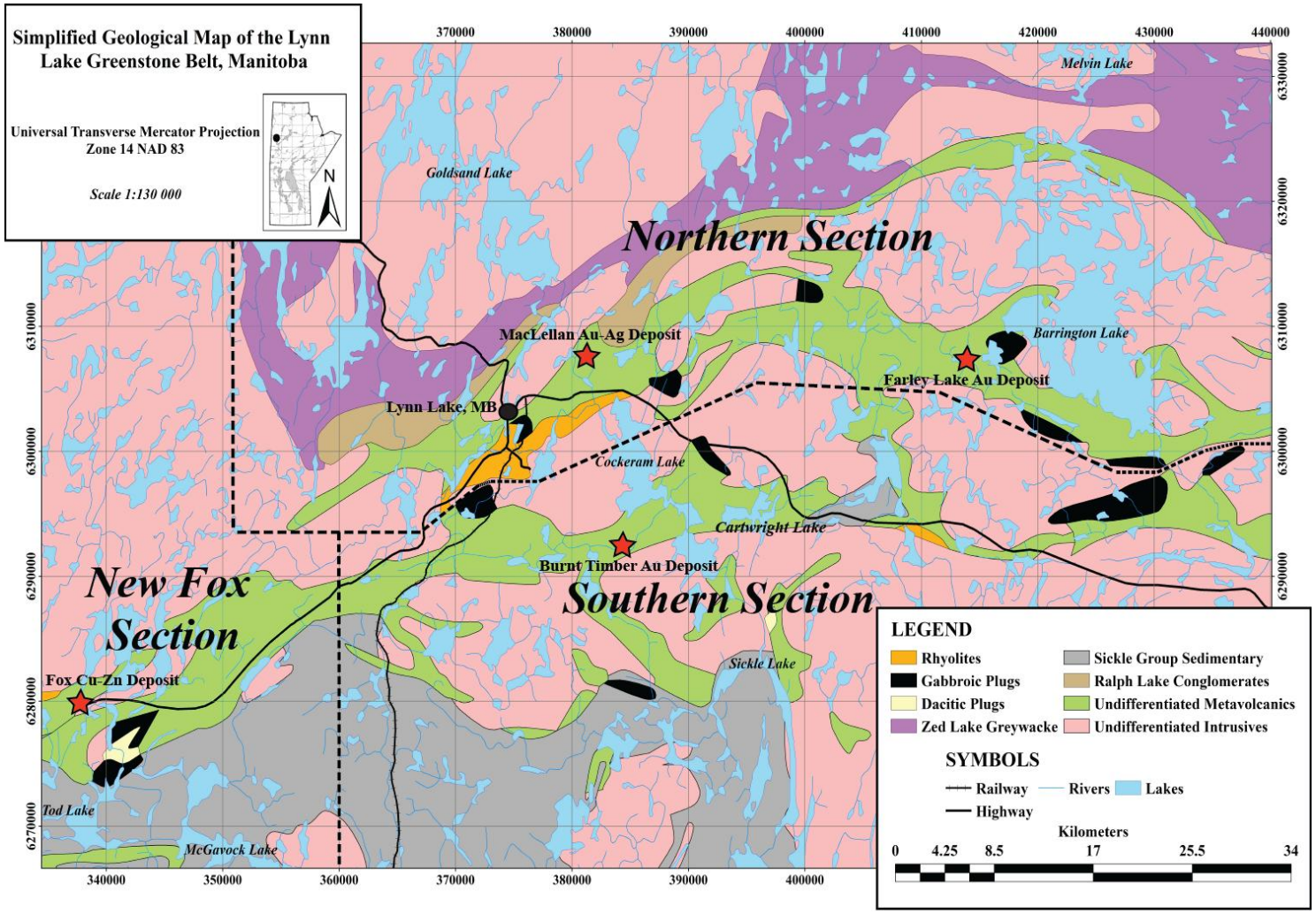

Figure 3.1 – Simplified regional geologic map of the Lynn Lake greenstone belt showing the greenstone belt subdivisions, and the MacLellan Au-Ag, Farley Lake Au, Burnt Timber Au, and Fox Cu-Zn deposits.

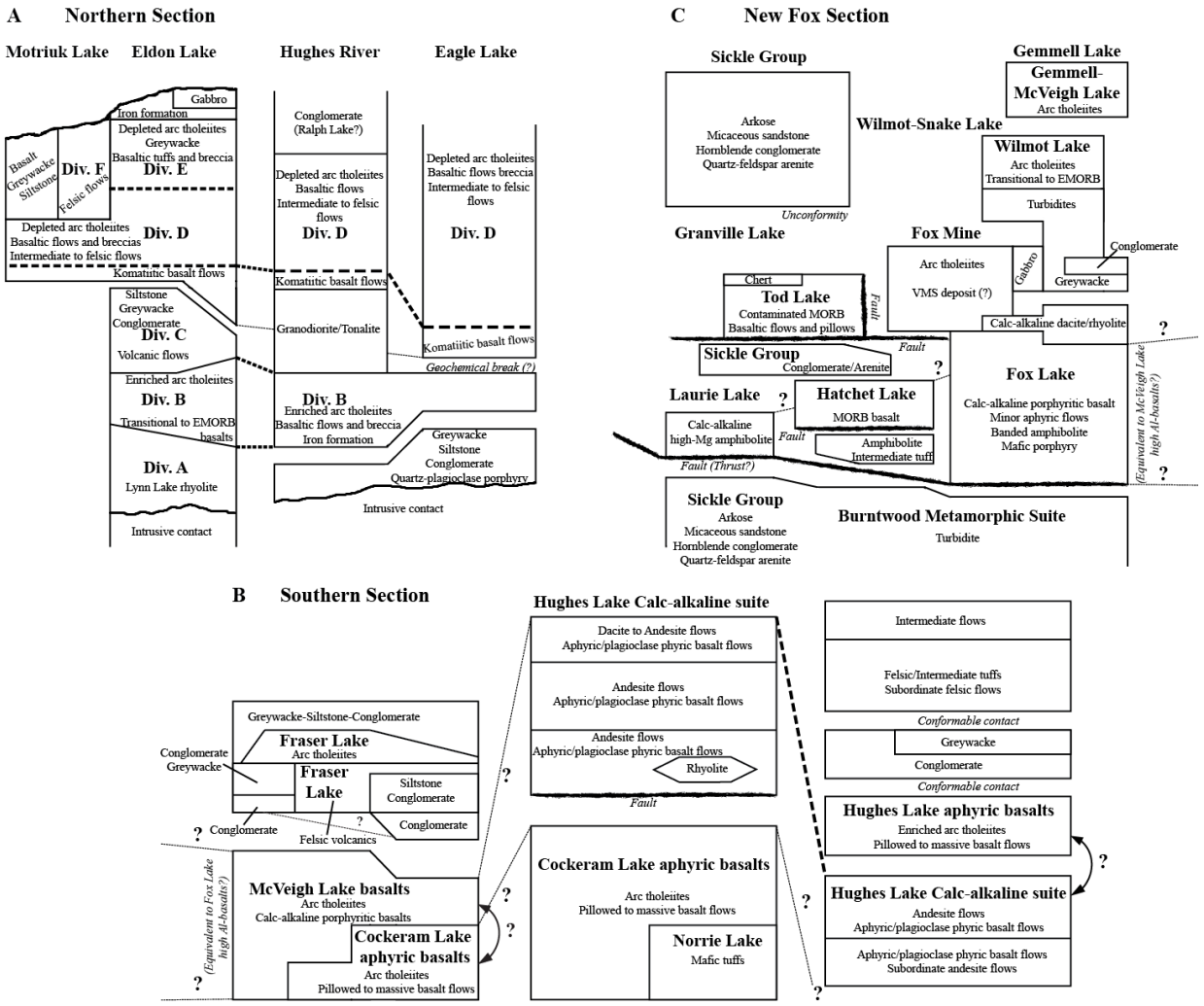

Figure 3.2 – Tectonostratigraphic sections of the Northern (A), Southern (B), and New Fox (C) sections of the Lynn Lake greenstone belt, showing inferred (dashed lines) and potential (dotted lines) geologic relationships (after Zwanzig et al., 1999).

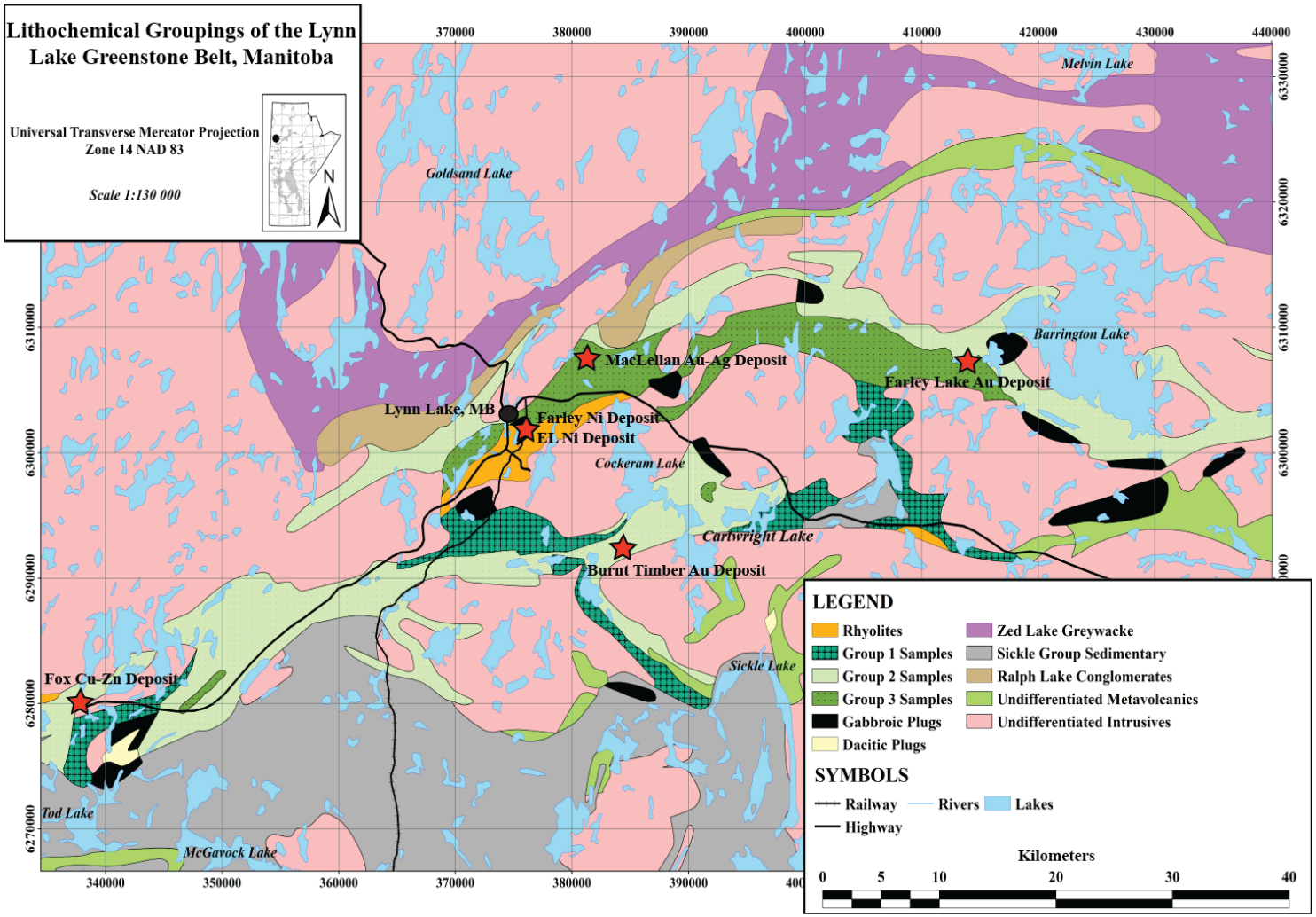

Figure 3.3 – Map of the Lynn Lake greenstone belt showing the distribution of the lithochemical groupings based on Th-Nb-LREE systematics.

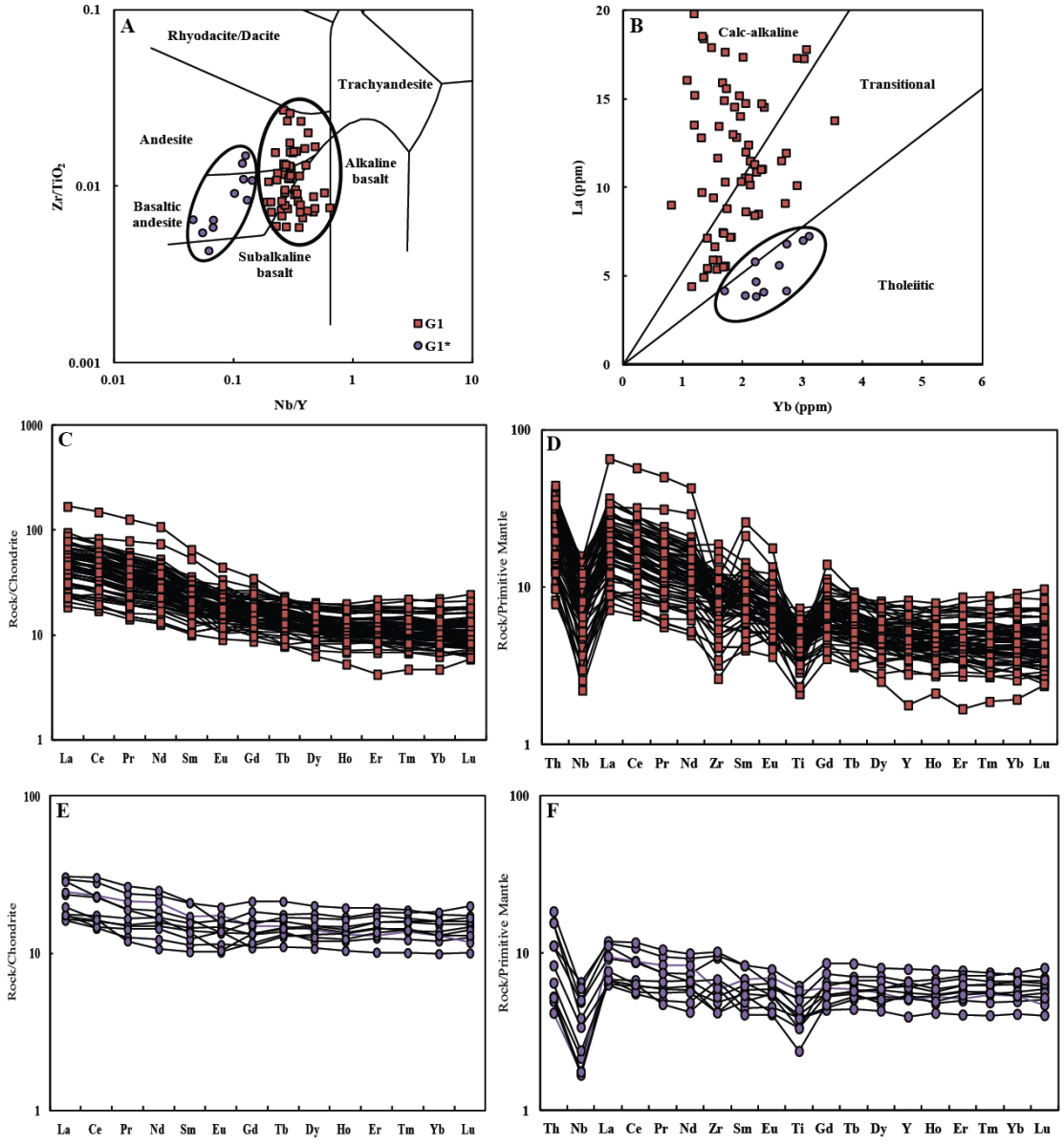
A
Rhyodacite/Dacite
Trachyandesite
Andesite
Alkaline basalt
Basaltic andesite
Subalkaline basalt
G1
G1*
Zr/TiO2
Nb/Y
B
Calc-alkaline
Transitional
Tholeiitic
La (ppm)
Yb (ppm)
C
Rock/Chondrite
La Ce Pr Nd Sm Eu Gd Tb Dy Ho Er Tm Yb Lu
D
Rock/Primitive Mantle
Th Nb La Ce Pr Nd Zr Sm Eu Ti Gd Tb Dy Y Ho Er Tm Yb Lu
E
Rock/Chondrite
La Ce Pr Nd Sm Eu Gd Tb Dy Ho Er Tm Yb Lu
F
Rock/Primitive Mantle
Th Nb La Ce Pr Nd Zr Sm Eu Ti Gd Tb Dy Y Ho Er Tm Yb Lu

Figure 3.4

Figure 3.4 – Nb/Y versus Zr/TiO_2 discrimination diagram (A) for volcanic rocks (see Winchester and Floyd, 1977), Yb versus La magma series diagram (B) (see Ross and Bedard, 2009), and paired chondrite-normalized REE (C) and primitive mantle-normalized multi-element (D) diagrams for G1 and G1*. Chondrite-normalizing values are from Sun and McDonough (1989) and primitive mantle-normalized values are from Hofmann (1988).

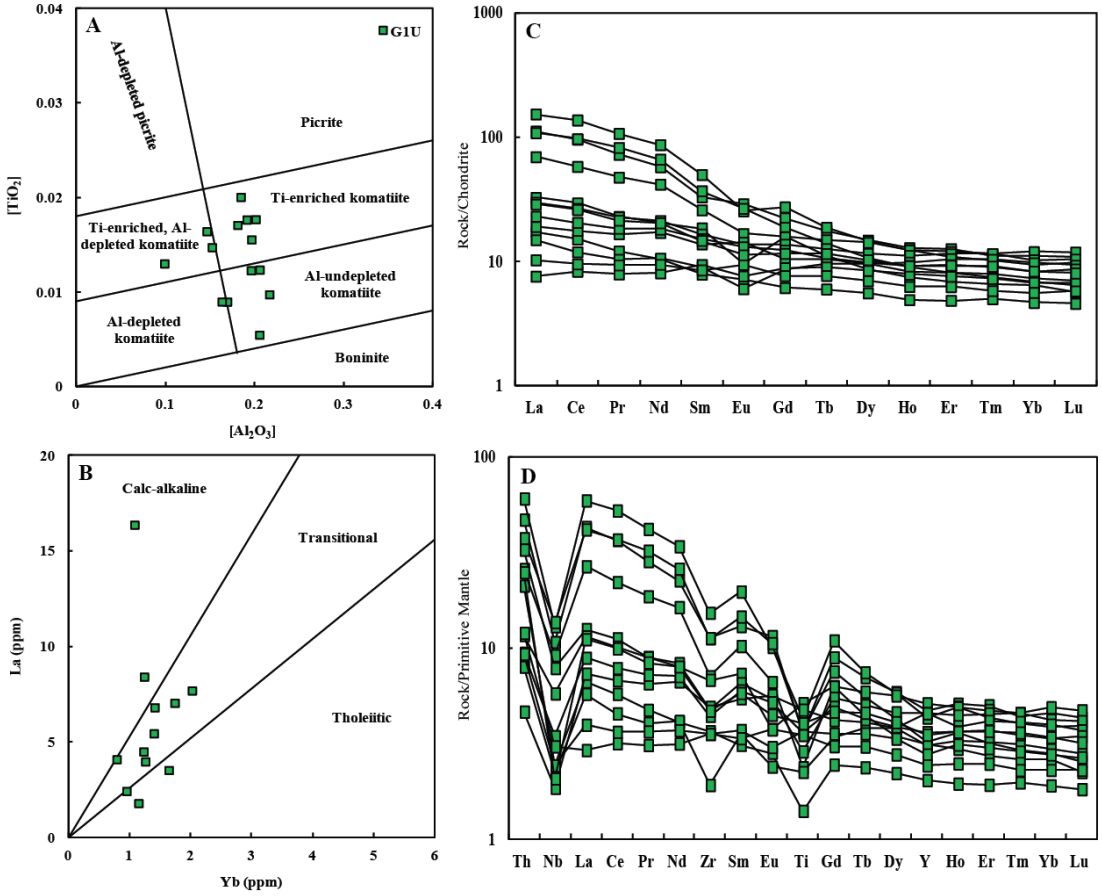

Figure 3.5 –[Al_2O_3] versus [TiO_2] mole proportion diagram (A) for ultramafic rocks (see Hanski et al., 2001), Yb versus La magma series diagram (B) (see Ross and Bedard, 2009), and paired chondrite-normalized REE (C) and primitive mantle-normalized multi-element (D) diagrams for G1U. [Al_2O_3] = Al_2O_3/(2/3-MgO-FeO) and [TiO_2] = TiO_2/(2/3-MgO-FeO). Chondrite-normalizing values are from Sun and McDonough (1989) and primitive mantle-normalized values are from Hofmann (1988).

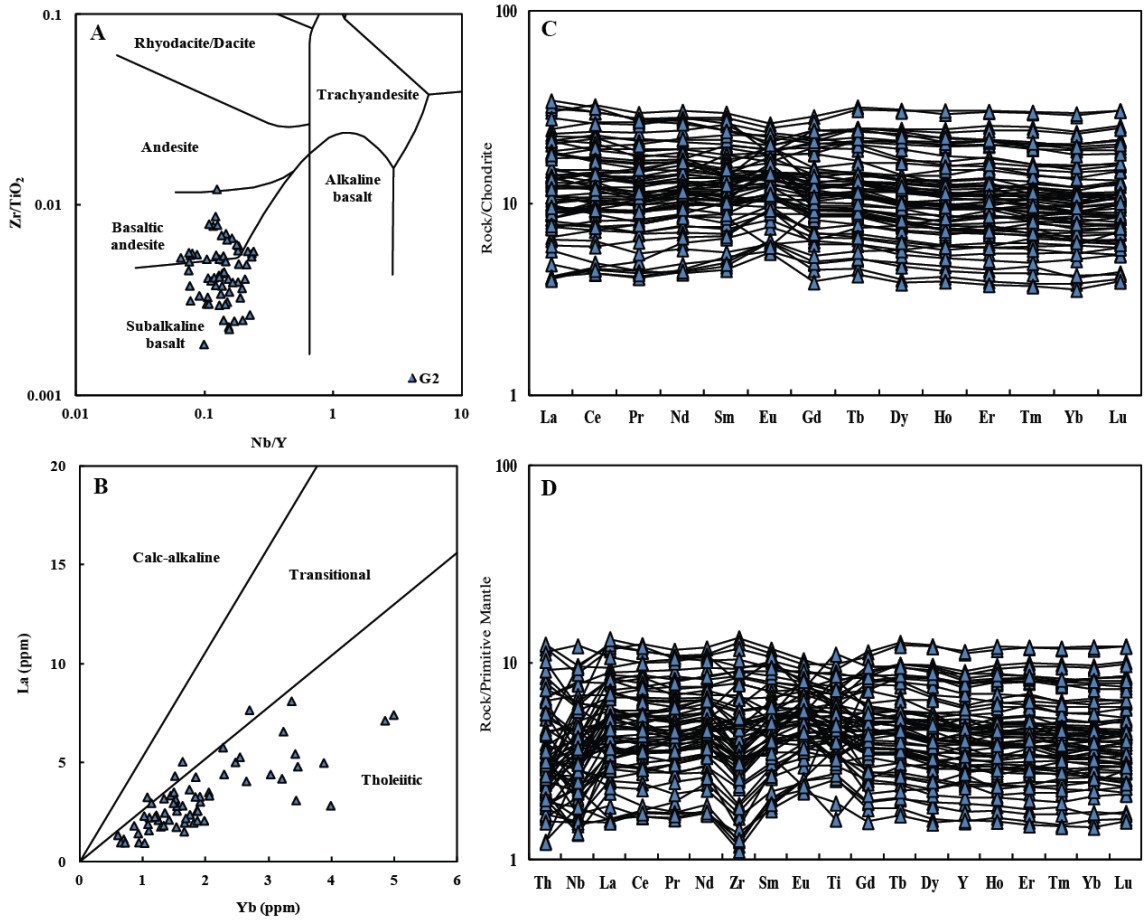

Figure 3.6 – Nb/Y versus Zr/TiO_2 discrimination diagram (A) for volcanic rocks (see Winchester and Floyd, 1977), Yb versus La magma series diagram (B) (see Ross and Bedard, 2009), and paired chondrite-normalized REE (C) and primitive mantle-normalized multi-element (D) diagrams for G2. Chondrite-normalizing values are from Sun and McDonough (1989) and primitive mantle-normalized values are from Hofmann (1988).

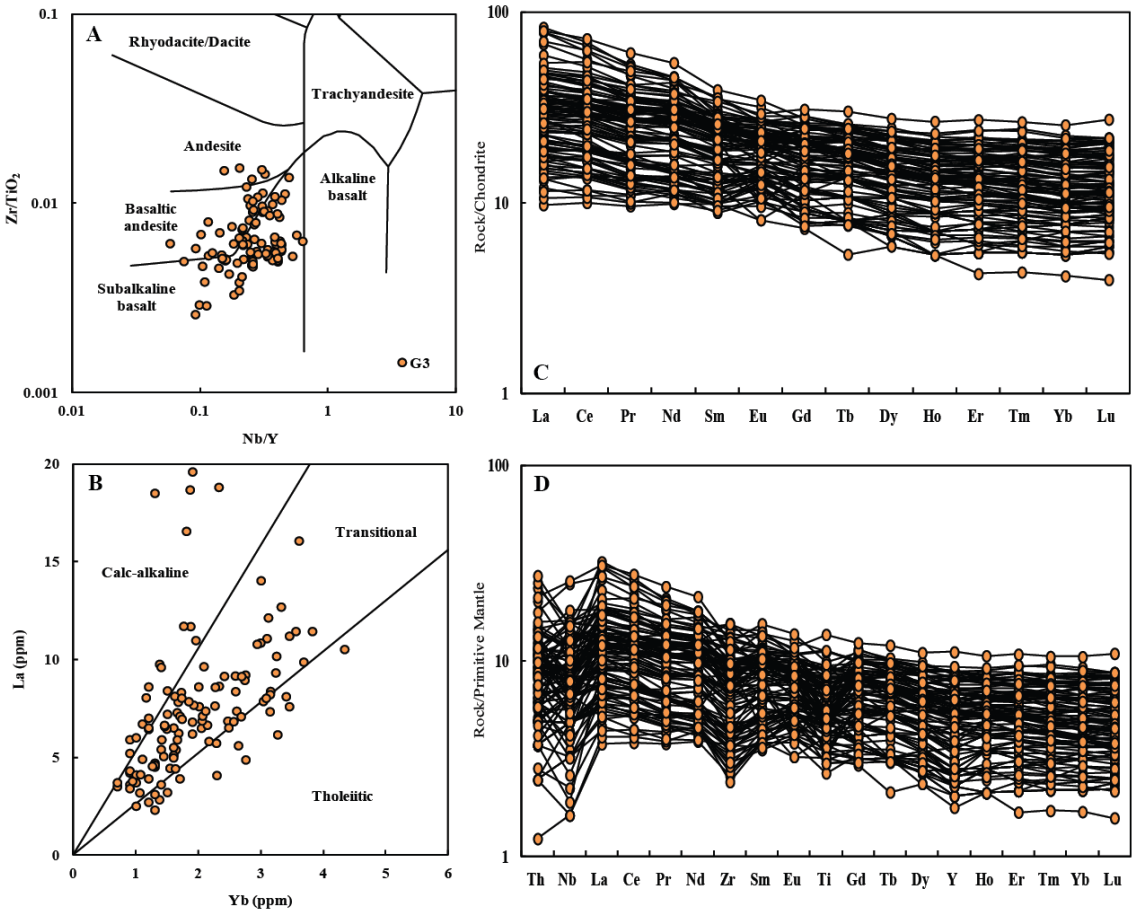

Figure 3.7 – Nb/Y versus Zr/TiO_2 discrimination diagram (A) for volcanic rocks (see Winchester and Floyd, 1977), Yb versus La magma series diagram (B) (see Ross and Bedard, 2009), and paired chondrite-normalized REE (C) and primitive mantle-normalized multi-element (D) diagrams for G3. Chondrite-normalizing values are from Sun and McDonough (1989) and primitive mantle-normalized values are from Hofmann (1988).

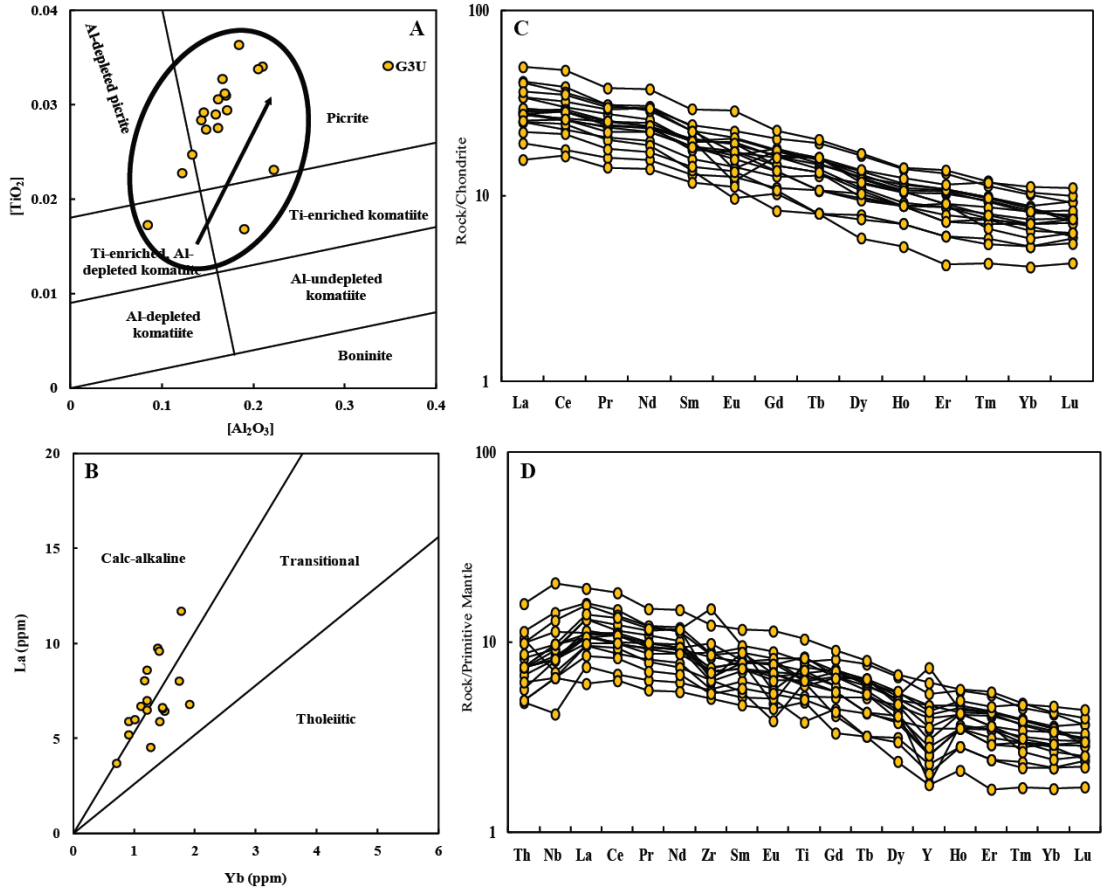

Figure 3.8 – $[Al_2O_3]$ versus $[TiO_2]$ mole proportion diagram (A) for ultramafic rocks (see Hanski et al., 2001), Yb versus La magma series diagram (B) (see Ross and Bedard, 2009), and paired chondrite-normalized REE (C) and primitive mantle-normalized multi-element (D) diagrams for G3U. $[Al_2O_3] = Al_2O_3/(2/3\text{-MgO-FeO})$ and $[TiO_2] = TiO_2/(2/3\text{-MgO-FeO})$. Chondrite-normalizing values are from Sun and McDonough (1989) and primitive mantle-normalized values are from Hofmann (1988).

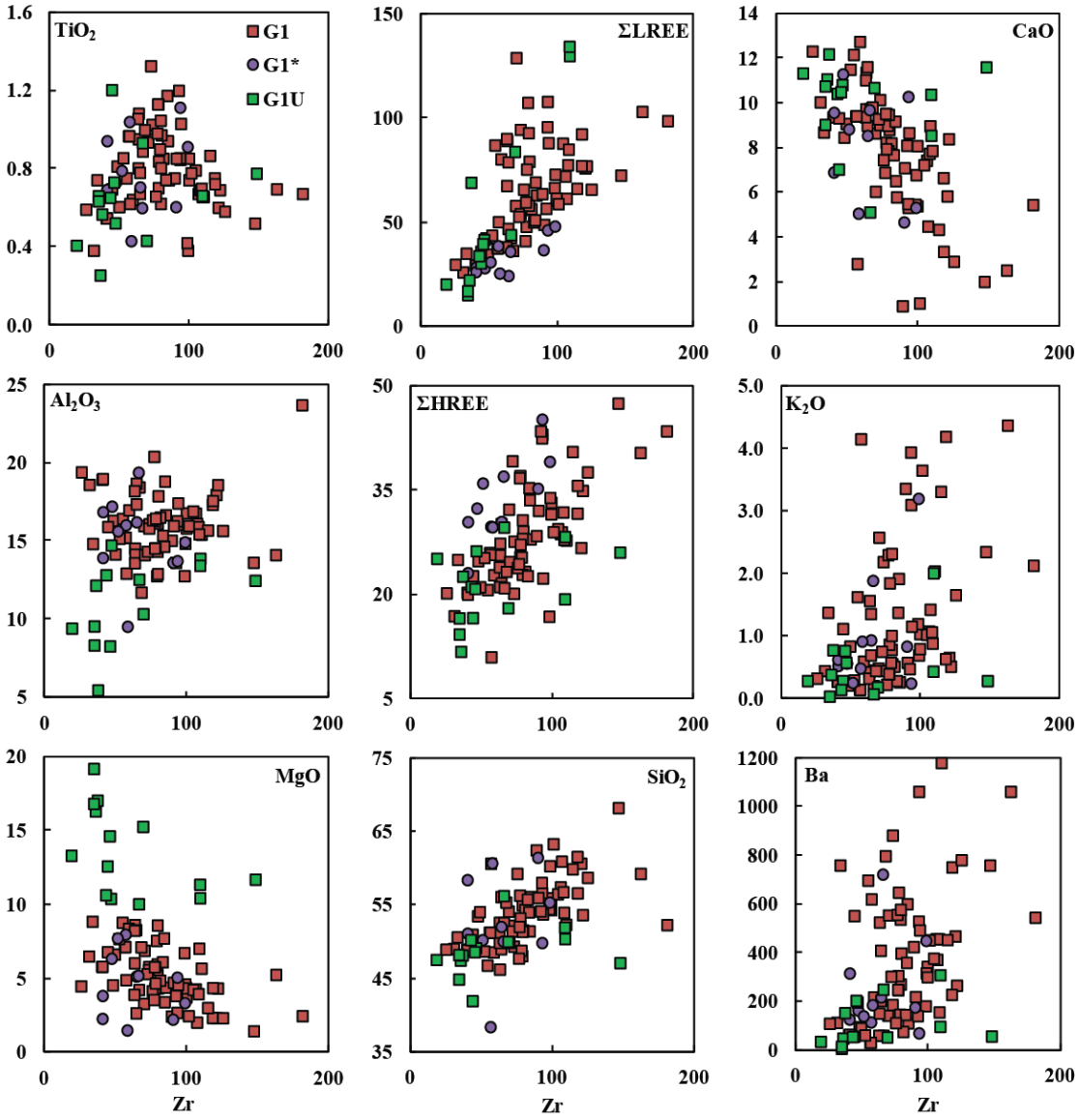

Figure 3.9 – Zr (ppm) versus TiO_2 (wt.%), Al_2O_3 (wt.%), MgO (wt.%), ΣLREE, ΣHREE, SiO_2 (wt.%), K_2O (wt.%), CaO (wt.%), Ba (ppm) variation diagrams for G1, G1*, and G1U. ΣLREE=La+Ce+Pr+Nd+Sm+Eu+Gd; ΣHREE=Y+Tb+Dy+Ho+Er+Tm+Yb+Lu.

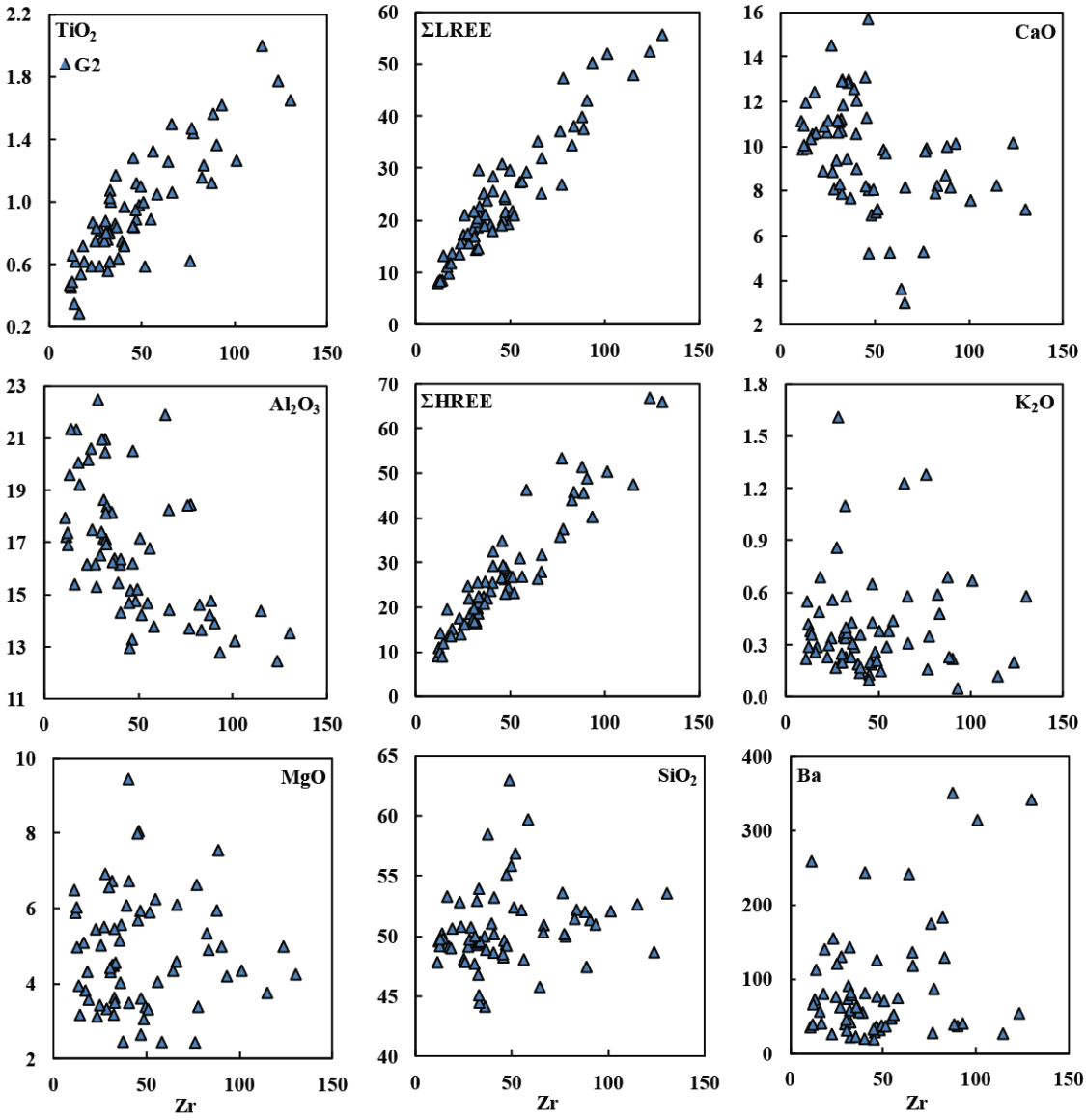

Figure 3.10 – Zr (ppm) versus TiO_2 (wt.%), Al_2O_3 (wt.%), MgO (wt.%), ΣLREE, ΣHREE, SiO_2 (wt.%), K_2O (wt.%), CaO (wt.%), Ba (ppm) variation diagrams for G2. ΣLREE=La+Ce+Pr+Nd+Sm+Eu+Gd; ΣHREE=Y+Tb+Dy+Ho+Er+Tm+Yb+Lu.

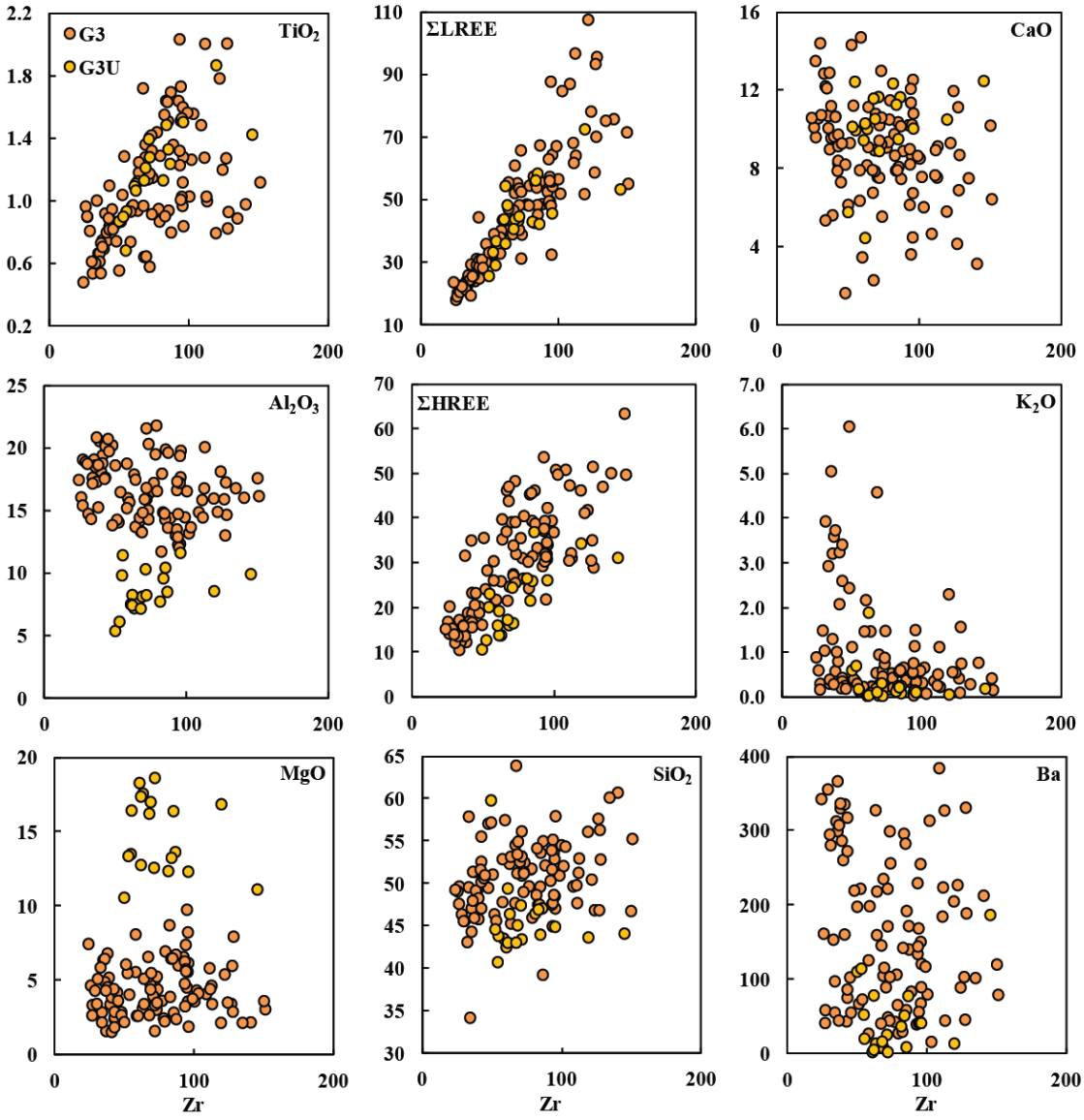

Figure 3.11 – Zr (ppm) versus TiO_2 (wt.%), Al_2O_3 (wt.%), MgO (wt.%), ΣLREE, ΣHREE, SiO_2 (wt.%), K_2O (wt.%), CaO (wt.%), Ba (ppm) variation diagrams for G3 and G3U. ΣLREE=La+Ce+Pr+Nd+Sm+Eu+Gd; ΣHREE=Y+Tb+Dy+Ho+Er+Tm+Yb+Lu.

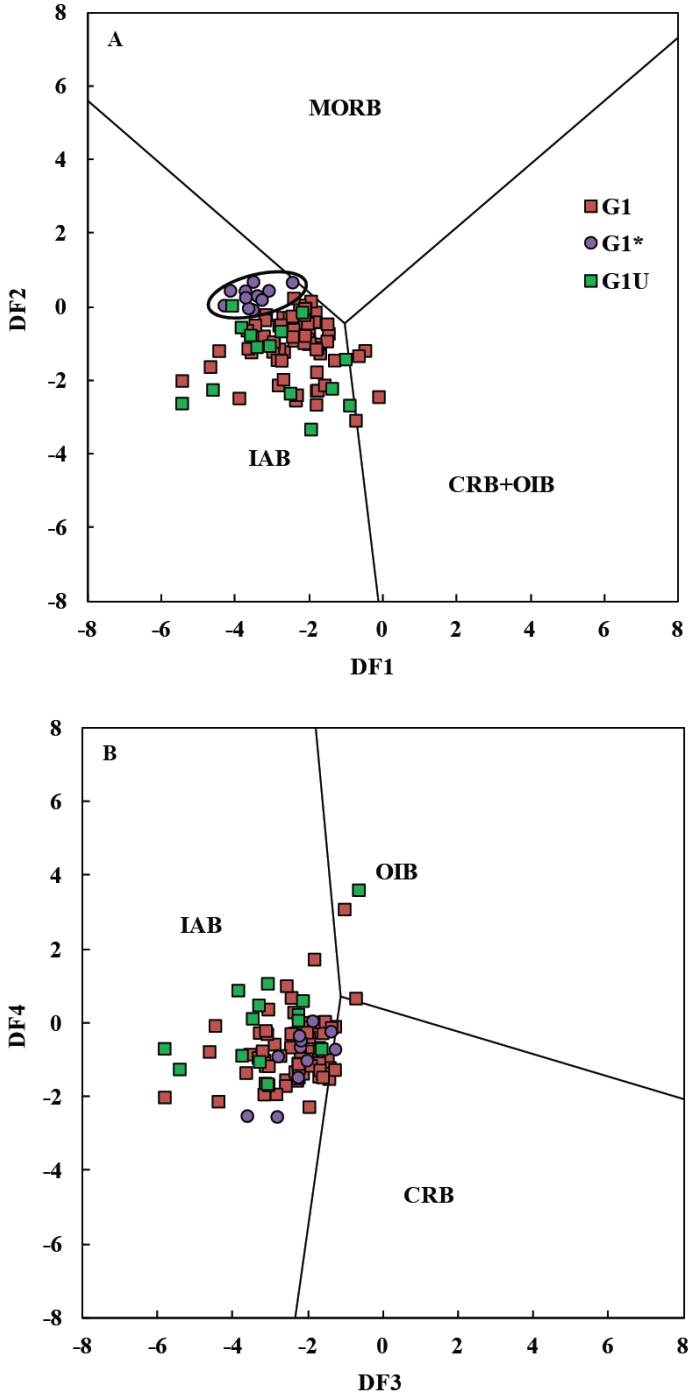

Figure 3.12

Figure 3.12 – Log-transformed immobile trace element tectonic discrimination diagrams (A and B) of G1, G1*, and G1U. Samples plot in the IAB field of the IAB-MORB-CRB+OIB and IAB-OIB-CRB diagrams (adopted from Agrawal et al., 2008), with the subset, G1*, plot closely to the MORB field on the IAB-MORB-CRB+OIB diagram. For diagram (a) DF1 = 0.3518 x ln(La/Th) + 0.6013 x ln(Sm/Th) - 1.345 x ln(Yb/Th) + 2.1056 x ln(Nb/Th) - 5.4763; DF2 = -0.305 x ln(La/Th) - 1.1801 x ln(Sm/Th) + 1.6189 x ln(Yb/Th) + 1.226 x ln(Nb/Th) - 0.9944. For diagram (b) DF3 = 0.5533 x ln(La/Th) + 0.2173 x ln(Sm/Th) - 0.0969 x ln(Yb/Th) + 2.0454 x ln(Nb/Th) - 5.6305; DF4 = -2.4498 x ln(La/Th) + 4.8562 x ln(Sm/Th) - 2.124 x ln(Yb/Th) - 0.1567 x ln(Nb/Th) + 0.94. MORB: Mid-ocean ridge basalts; IAB: Island-arc basalts; CRB: Continental rift basalts; and, OIB: Ocean island basalts.

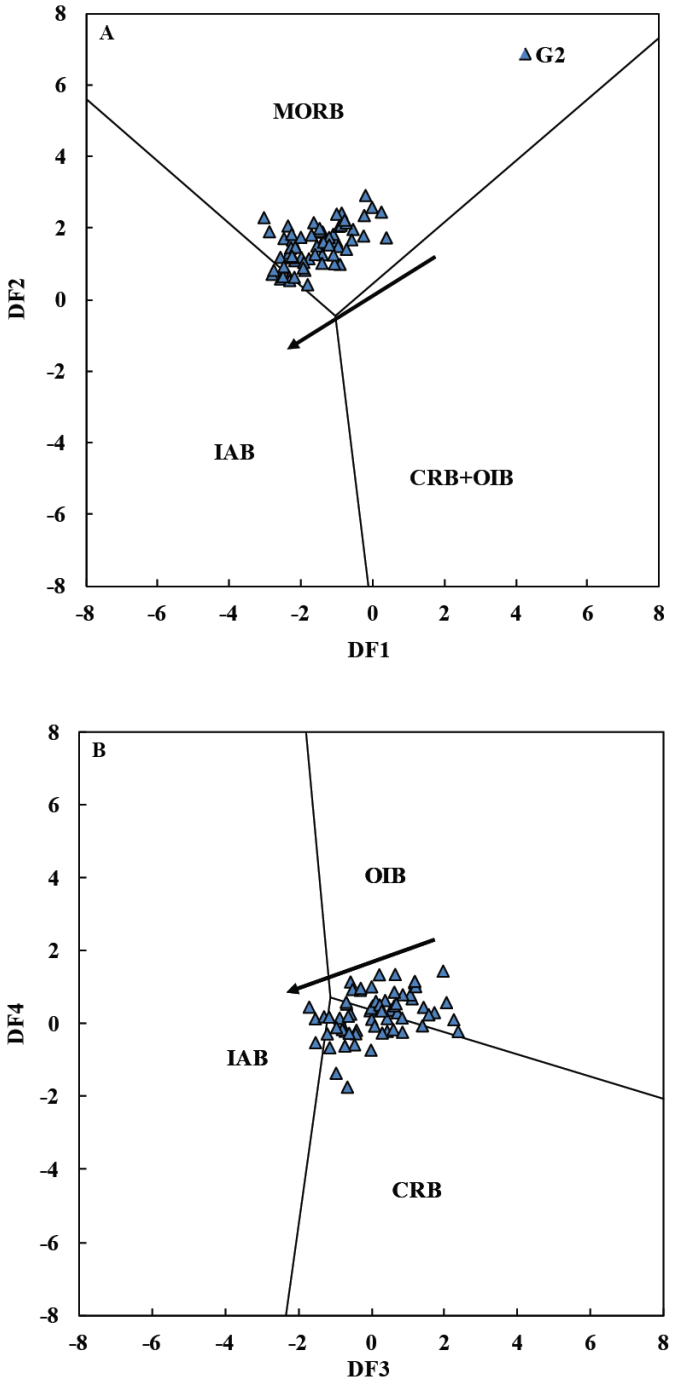

Figure 3.13

Figure 3.13 – Log-transformed immobile trace element tectonic discrimination diagrams (A and B) of G2. Samples plot in the MORB field of the IAB-MORB-CRB+OIB diagram (A) and trend between the OIB and CRB fields of the IAB-OIB-CRB diagram (B) (adopted from Agrawal et al., 2008). For diagram (a) DF1 = 0.3518 x ln(La/Th) + 0.6013 x ln(Sm/Th) - 1.345 x ln(Yb/Th) + 2.1056 x ln(Nb/Th) - 5.4763; DF2 = -0.305 x ln(La/Th) - 1.1801 x ln(Sm/Th) + 1.6189 x ln(Yb/Th) + 1.226 x ln(Nb/Th) - 0.9944. For diagram (b) DF3 = 0.5533 x ln(La/Th) + 0.2173 x ln(Sm/Th) - 0.0969 x ln(Yb/Th) + 2.0454 x ln(Nb/Th) - 5.6305; DF4 = -2.4498 x ln(La/Th) + 4.8562 x ln(Sm/Th) - 2.124 x ln(Yb/Th) - 0.1567 x ln(Nb/Th) + 0.94. MORB: Mid-ocean ridge basalts; IAB: Island-arc basalts; CRB: Continental rift basalts; and, OIB: Ocean island basalts.

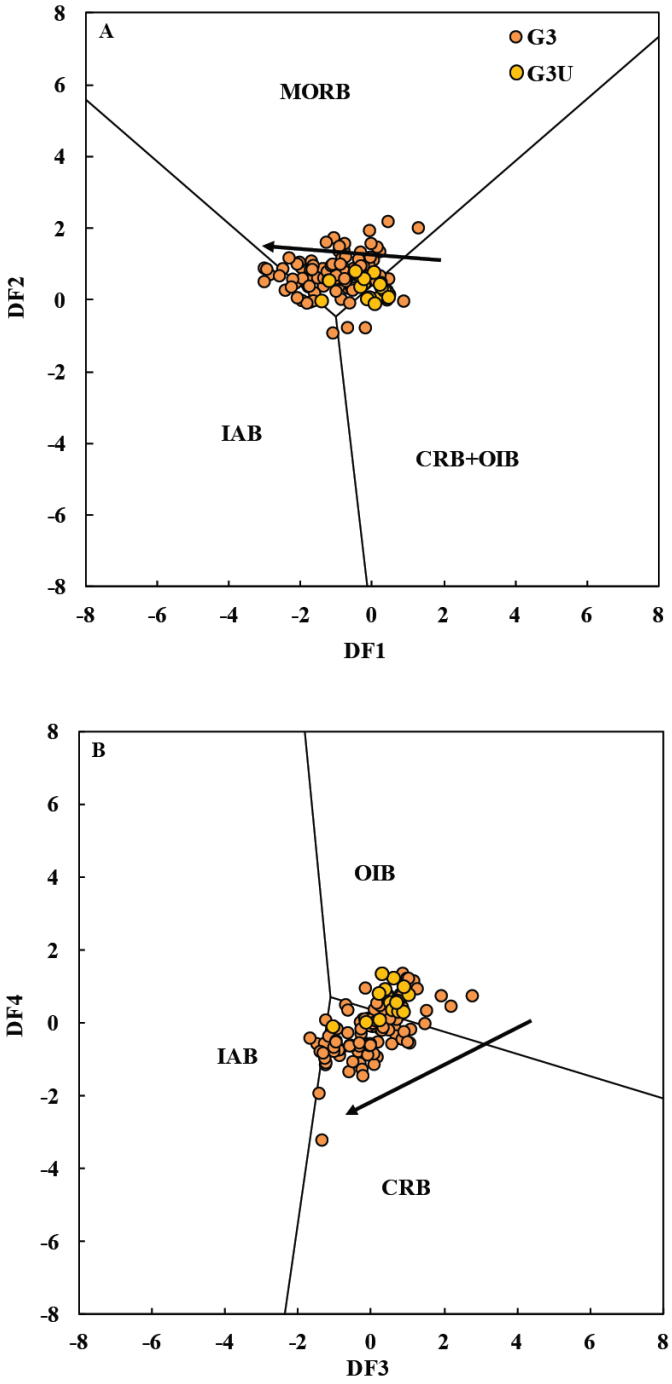

Figure 3.14

Figure 3.14 – Log-transformed immobile trace element tectonic discrimination diagrams (A and B) of Group 3 Lynn Lake volcanic rocks (G3) and ultramafic rocks (G3U). Samples plot in the MORB field of the IAB-MORB-CRB+OIB diagram (A) and trend between the OIB and CRB fields of the IAB-OIB-CRB diagram (B) (adopted from Agrawal et al., 2008). For diagram (a) DF1 = 0.3518 x ln(La/Th) + 0.6013 x ln(Sm/Th) - 1.345 x ln(Yb/Th) + 2.1056 x ln(Nb/Th) - 5.4763; DF2 = -0.305 x ln(La/Th) - 1.1801 x ln(Sm/Th) + 1.6189 x ln(Yb/Th) + 1.226 x ln(Nb/Th) - 0.9944. For diagram (b) DF3 = 0.5533 x ln(La/Th) + 0.2173 x ln(Sm/Th) - 0.0969 x ln(Yb/Th) + 2.0454 x ln(Nb/Th) - 5.6305; DF4 = -2.4498 x ln(La/Th) + 4.8562 x ln(Sm/Th) - 2.124 x ln(Yb/Th) - 0.1567 x ln(Nb/Th) + 0.94. MORB: Mid-ocean ridge basalts; IAB: Island-arc basalts; CRB: Continental rift basalts; and, OIB: Ocean island basalts.

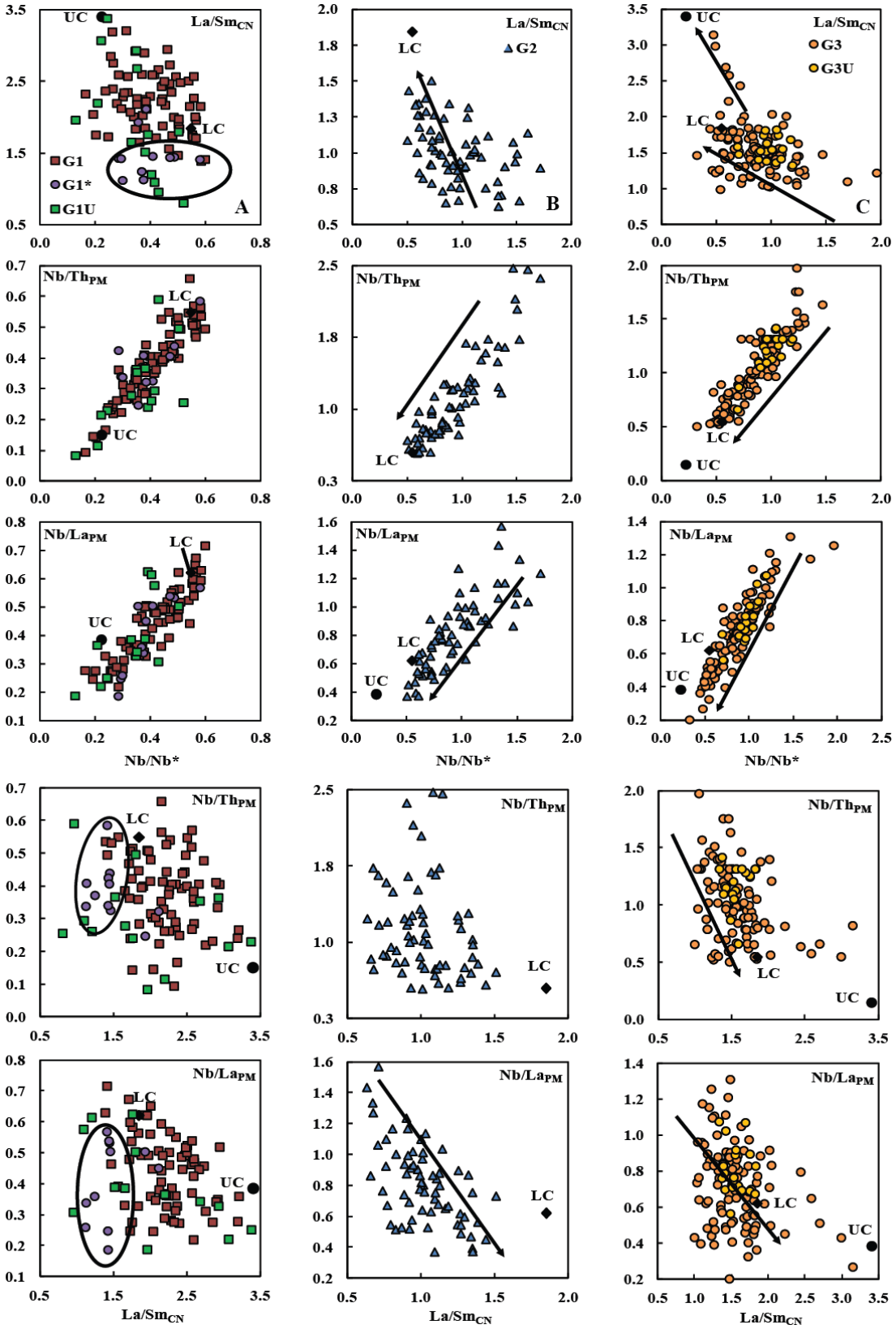

Figure 3.15

Figure 3.15 – Nb/Nb* versus La/Sm_{CN}, Nb/Th_{PM}, Nb/La_{PM}, and La/Sm_{CN} versus Nb/Th_{PM} and Nb/La_{PM} variation diagrams for G1, G1*, and G1U (A), G2 (B), and G3 and G3U (C). On these diagrams, G1 and G1U (A) trend between LC and UC values suggesting that these rocks were variably contaminated by continental crust during ascent. However, G1* (A) does not show the same positive correlation as G1 and G1U, suggesting a relatively uncontaminated source. Samples of G2 (B), G3, and G3U (C) trends towards LC and is indicative of LC or continental lithospheric mantle mixing. Upper crust (UC) and lower crust (LC) values are from Rudnick and Gao (2004). PM: primitive mantle-normalized after Hofmann (1988); and, CN: chondrite-normalied after Sun and McDonough (1989).

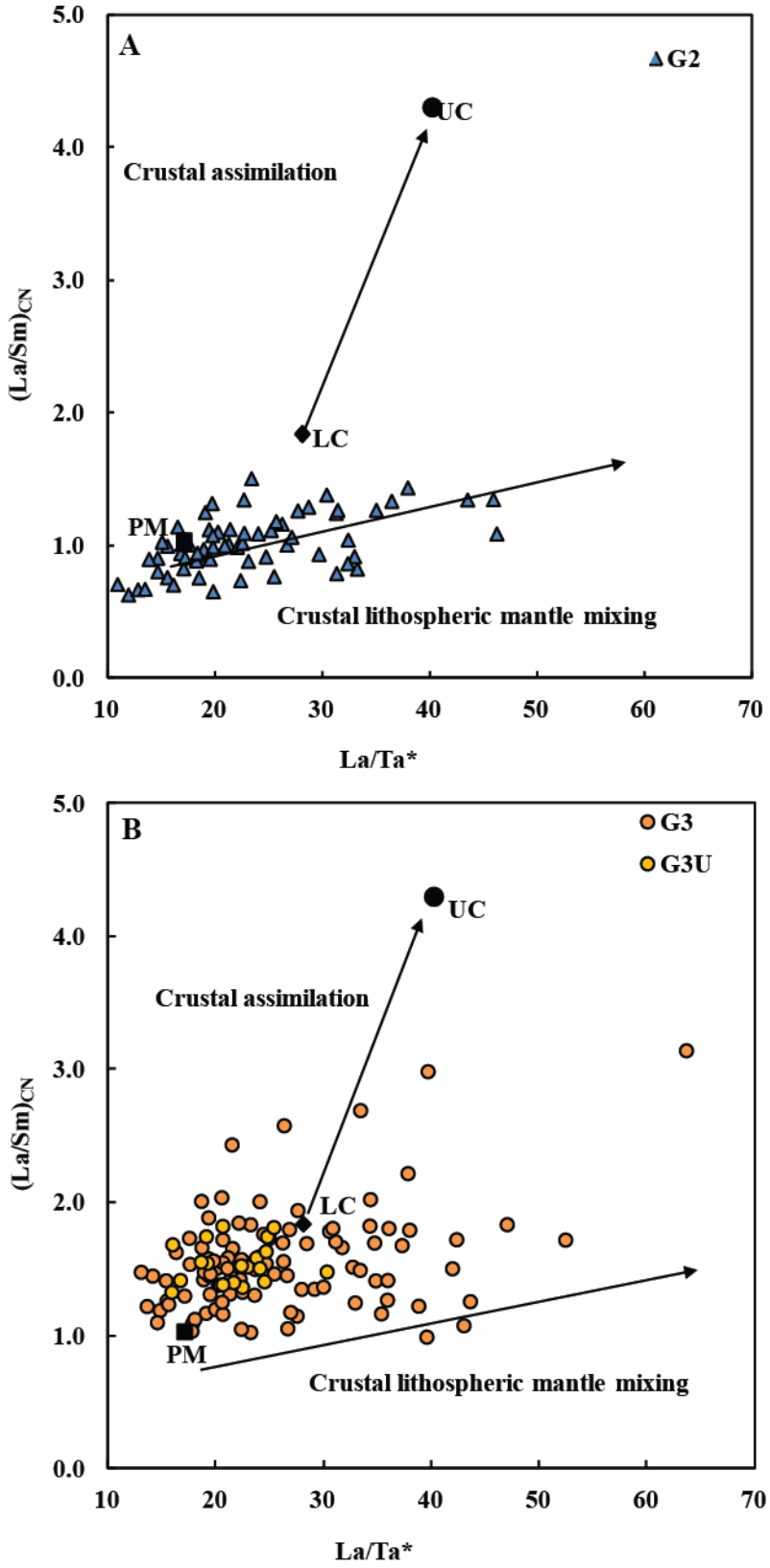
A
G2
UC
Crustal assimilation
LC
PM
Crustal lithospheric mantle mixing
(La/Sm)CN
La/Ta*
B
G3
G3U
UC
Crustal assimilation
LC
PM
Crustal lithospheric mantle mixing
(La/Sm)CN
La/Ta*

Figure 3.16

Figure 3.16 – La/Ta* versus La/Sm_{CN} illustrating the different trends (arrows) for contamination of plume-derived liquids by continental crust as against continental lithospheric mantle (CLM). Samples of G2 (A) plot from the PM value and along the CLM trend, which has been interpreted to be the result of an upwelling plume impinging along a Craton to a section of attenuated lithosphere. Samples of G3 and G3U (B) plot from the PM value towards the LC value suggesting a combination of CLM and crustal assimilation. Upper crust (UC) and lower crust (LC) values are from Rudnick and Gao (2004). Primitive mantle (PM) value is from Hofmann (1988). Vectors are from Lassiter and DePaolo (1997). Ta* = Nb/17.2.

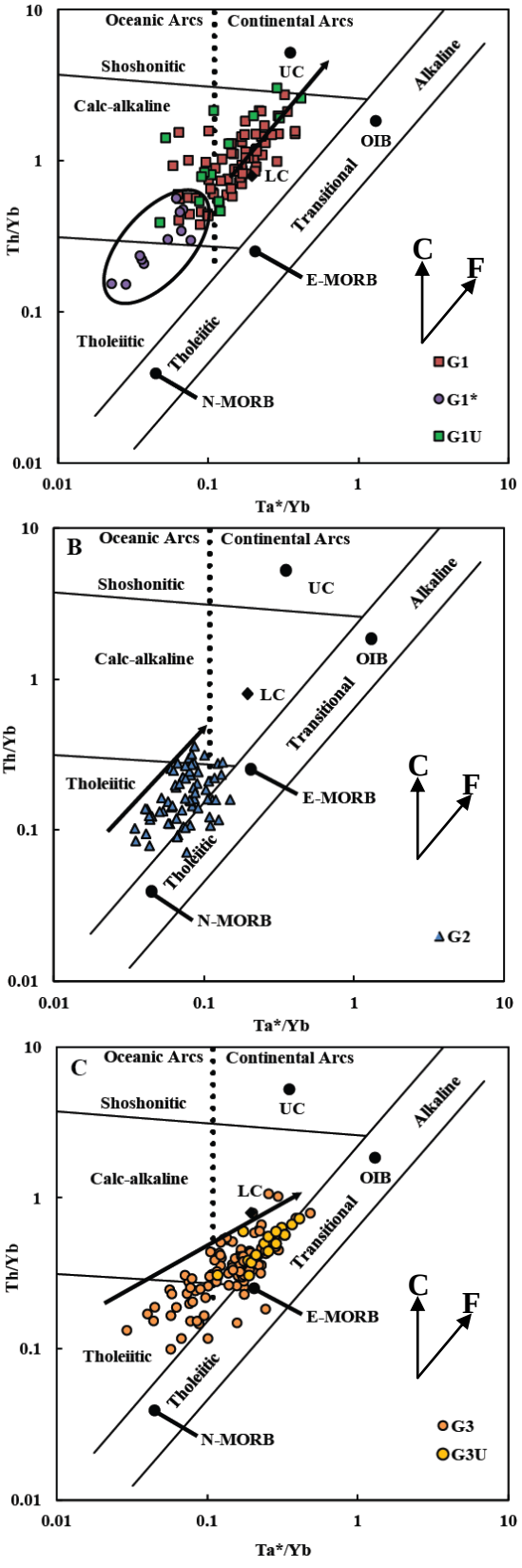
Oceanic Arcs
Continental Arcs
Shoshonitic
Calc-alkaline
Tholeiitic
Alkaline
Transitional
Tholeiitic
UC
OIB
LC
E-MORB
N-MORB
C
F
G1
G1*
G1U
Th/Yb
Ta*/Yb
10
1
0.1
0.01
B
G2
C
G3
G3U

Figure 3.17

Figure 3.17 – Ta*/Yb versus Th/Yb petrogenetic variation diagram for G1, G1*, and, G1U (A), G2 (B), and G3 and G3U (C). N-MORB, E-MORB, and OIB values are from Sun and McDonough, 1989. Lower crust (LC) and upper crust (UC) values are from Rudnick and Gao (2004). N-MORB: Normal Mid-ocean ridge basalt; E-MORB: Enriched Mid-ocean ridge basalts; OIB: Ocean island basalt. Adopted from Pearce (2008). Ta* = Nb/17.2. F: Within-plate fractionation vector; C: Crustal contamination vector.

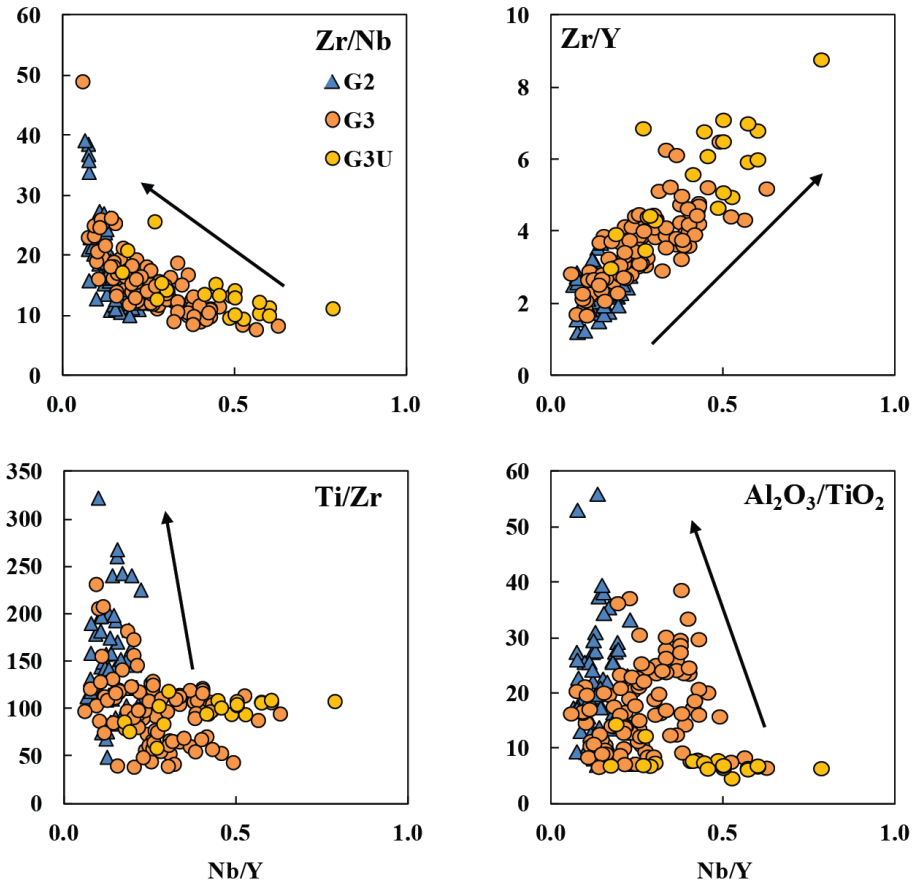

Figure 3.18 – Nb/Y versus Zr/Nb, Ti/Zr, Zr/Y, and Al_2O_3/TiO_2 variation diagrams for G2, G3, and G3U rocks. Trends (lines) support a petrogenetic link between the G2, G3, and G3U volcanic rocks.

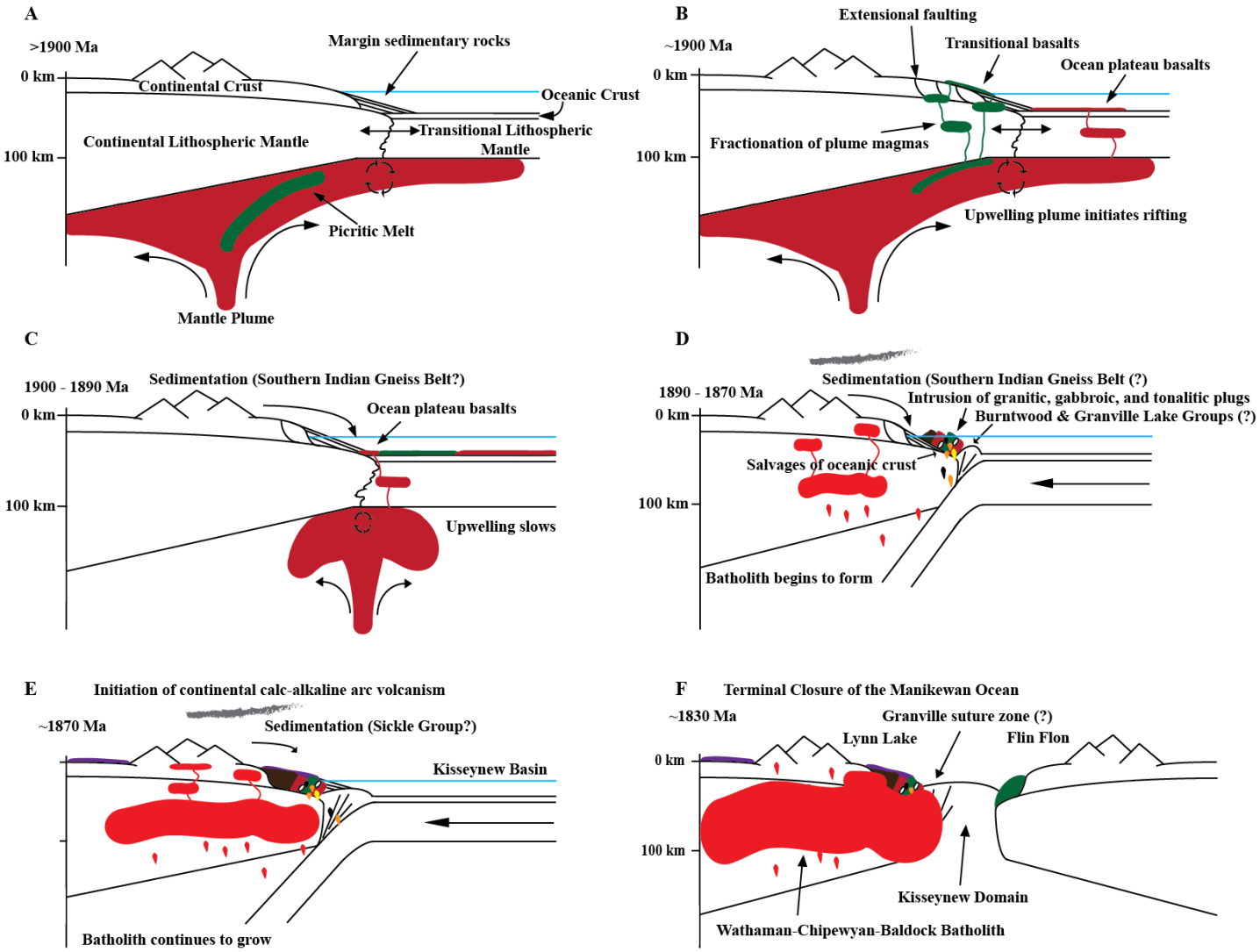

Figure 3.19 – Proposed geodynamic model for the formation of the Lynn Lake greenstone belt (see discussion for description).

CHAPTER 4

Conclusions, Implications, and Recommendations for Future Research

4.1. Conclusions

The following conclusions are drawn on the basis of field, petrographic, and geochemical characteristics of the Paleoproterozoic mafic to intermediate metavolcanic rocks of the Lynn Lake greenstone belt:

1. The host rock sequence to the MacLellan Au-Ag deposit is composed primarily of plagioclase-amphibole schist, quartz-plagioclase-biotite schist, and chlorite-amphibole schist. The igneous protoliths to the plagioclase-amphibole schist and chlorite-amphibole schist are transitional aluminous basalt and picrite, respectively. The quartz-plagioclase-biotite schist is interpreted, based on HFSE ratios, chondrite- and primitive mantle-normalized trends and the results of isocon analysis, to be the biotite-altered equivalent to transitional aluminous basalt.
2. Three volumetrically minor lithologies have been identified both within and in the vicinity of the MacLellan Au-Ag deposit. These rocks are amphibole schist, pods of amphibolite that occur within outcrops of amphibole schist, and quartz-amphibole schist. The igneous protoliths to the amphibole schist and amphibolites are calc-alkaline and high-magnesium andesites, respectively. The igneous protolith to the quartz-amphibole schist is alkaline basalt.
3. Major and trace element data suggest a petrogenetic link, via a transitional differentiation trend, between the aluminous basalt and picrite. Calc-alkaline and high-magnesium andesites have calc-alkaline affinity. In contrast, alkaline basalt

has distinct major and trace element characteristics, consistent with the existence of three distinct primary magma types.

4. The aluminous basalt and picrite display two different chondrite-normalized REE patterns that result from partial melting at depths within (> 90 km) and outside of (< 90 km) the garnet stability field, respectively. Alkaline basalt, calc-alkaline andesite, and high-magnesium andesite display chondrite-normalized REE patterns that are consistent with a depth of partial melting within the garnet stability field (> 90 km).
5. The trace element systematics of aluminous basalt and picrite are consistent with a rifted continental margin geodynamic setting. Calc-alkaline andesite and high-magnesium andesite have trace element systematics consistent with a subduction zone geodynamic setting. Alkaline basalt has trace element systematics consistent with an ocean island geodynamic setting. On the basis of these geochemical characteristics, the northern Lynn Lake greenstone belt is interpreted to be a rifted continental margin that erupted in a near-continent setting.
6. The Lynn Lake greenstone belt comprises mantle plume- and volcanic arc-derived volcanic rocks. Trace element systematics of the mantle plume-derived rocks are consistent with a rifted continental margin geodynamic setting. Volcanic arc-derived rocks are subdivided based on their Th-La-Nb-REE systematics into primitive intra-oceanic- and contaminated continent-derived rocks, of which the latter is more common.
7. Major and trace element data suggest a petrogenetic link between the tholeiitic to transitional mantle plume-derived rocks; suggesting that a single plume generated

the majority of the volcanic rocks. Continental volcanic arc rocks have a transitional to calc-alkaline affinity, however, intra-oceanic volcanic arc rocks are primarily tholeiitic.

8. Plume-derived rocks display two different REE patterns, resulting from different depths of partial melting within the spinel (< 90 km) and garnet (> 90 km) stability fields. Volcanic arc rocks display REE patterns that are consistent with partial melting in the garnet (> 90 km) stability field.

4.2. Implications

The following implications for the geology and mineral deposit potential of the Lynn Lake region can be derived from the conclusions of this study:

1. The host rock sequence to the MacLellan Au-Ag deposit is dominated by aluminous basalt and subordinate picrite. Based on Th-Nb-La-REE systematics, the host rock sequence is interpreted to have formed in a near-continent setting. Field relationships, petrography, and geochemical results are inconsistent with an exhalative origin for the MacLellan Au-Ag host rock sequence and for the Agassiz Metallotect.
2. Continental rift-related sequences and rift-derived volcanic and plutonic rocks have been identified along the margins of the Hearne and Superior Cratons, namely the ca. 2075 Ma Courtenay Lake porphyry (Ansdell et al., 2000), ca. 2072 Ma Cauchon dykes (Heaman and Corkery, 1996), and sedimentary and volcanic rocks of the ca. 2040 Ma Povunknituk Group (Machado et al., 1993), and ca. 2025 Ma Richmond Gulf Group (Chandler and Parrish, 1989), and the Ospwagan

Group (Hamilton and Bleeker, 2002). Supracrustal rocks from the Courtenay Lake – Cairns Lake fold belt (Money, 1968; Coombe, 1994; Foseenier et al., 1995; MacNeil et al., 1997) and the Needle Falls Group of the Wollaston Domain (Ray, 1979; Coombe, 1994) are also interpreted to represent rift-derived volcanic and sedimentary sequences. Basaltic rocks from the ca. 1900 Ma Levesque Bay and Lawrence Point assemblages (Maxeiner and Demmans, 2000) of the southern Reindeer Lake area exhibit the same flat REE trends on chondrite- and primitive mantle-normalized diagrams and inter-element ratios as the G2 rocks of the Lynn Lake greenstone belt. Collectively, these assemblages could record a single or multiple rifting events, which resulted in the formation and subsequent growth of the Manikewan Ocean between ca. 2100 and 2000 Ma.

3. The newly proposed geodynamic model for the Lynn Lake region suggests that the region could host a combination of sedimentary exhalative (i.e. Sedex), porphyry-style Sn-W-Cu-Au-Ag-, carbonatite-hosted HFSE, and Kiruna/Olympic Dam-type Fe-Cu-U-Au-Ag deposits. The presence of Sedex-style deposits in the rift sedimentary and volcanic sequences of the Wollaston Domain and the presence of an anorogenic syenite and carbonatite complex and the presence of porphyritic dykes and plutons in the Lynn Lake region are possible evidence supporting the regional mineral potential.

4.3. Suggestions for Future Research

The following recommendations for further study of the geology and mineral deposits of the Lynn Lake region can be derived from the conclusions of this study:

1. The 1910 Ma age of the Lynn Lake rhyolite (Baldwin et al., 1987) is inconsistent with the revised geodynamic model for the Lynn Lake greenstone belt. One plausible explanation is that this age represents an inherited age resulting from contamination by continental crust. Investigation of the Lynn Lake rhyolite including detailed field studies, petrography, and trace element and isotope lithogeochemistry is required to understand the potential petrogenetic link of these rocks with the mafic supracrustal rocks that comprise the remainder of the Lynn Lake greenstone belt.
2. A comprehensive and correlative project between the La Ronge and Lynn Lake greenstone belts that integrates field studies, petrography, and trace element and isotope lithogeochemistry is required to determine the potential relationships between the two belts and to further clarify the tectonic evolution of the Trans-Hudson Orogen.
3. An investigation, including field studies, petrography, and lithogeochemistry of the metamorphosed sedimentary, mafic, and felsic rocks that comprise the Southern Indian and Kisseynew Gneiss belts is required to determine the petrogenetic and geodynamic evolution of these belts, the relationship between these belts and the Lynn Lake greenstone belt, and to assess the mineral deposit potential of these belts.

4. Geologic investigations of the felsic to intermediate plutonic rocks that occur throughout the Lynn Lake greenstone belt is required to determine the geodynamic and petrogenetic evolution and to assess the mineral deposit potential of these rocks.

4.4. References

Ansdell, K.M, MacNeil, A., Delaney, G.D., and Hamilton, M.A., 2000. Rifting and development of the Hearne passive margin: age constraint from the Cook Lake area, Saskatchewan. Geological Association of Canada – Mineralogical Association of Canada, GeoCanada 2000, Extended abstract 777.

Baldwin, D.A., Syme, E.C., Zwanzig, H.V., Gordon, T.M., Hunt, P.A., and Stevens, R.D., 1987. U-Pb zircon ages from the Lynn Lake and Rusty Lake metavolcanic belts, Manitoba: two ages of Proterozoic Magmatism. Canadian Journal of Earth Sciences 24, 1053-1063.

Chandler, F.W., and Parrish, R.R., 1989. Age of the Richmond Gulf Group and implications for rifting in the Trans-Hudson Orogen, Canada. Precambrian Research 44, 277-288.

Coombe, W., 1994. Sediment-hosted base metal deposits of the Wollaston Domain, northern Saskatchewan. Saskatchewan Geological Survey, Saskatchewan Energy and Mines, Report 213.

Fossenier, K., Delaney, G.D., and Watters, B.R., 1995. Lithogeochemistry of the volcanic rocks from the Lower Proterozoic Courtenay Lake Formation, Wollaston Domain. *In* Summary of Investigations 1995, Saskatchewan Geological Survey, Saskatchewan Energy and Mines, Miscellaneous Report 95-4, 49-60.

Hamilton, M.A., and Bleeker, W., 2002. SHRIMP U-Pb geochronology of the Ospwagan Group: provenance and depositional age constraints of a Paleoproterozoic rift sequence, SE externides of the Tran-Hudson Orogen. Geological Asssociation of Canada – Mineralogical Association of Canada, Abstracts 27, 44.

Heaman, L.M., and Corkery, T., 1996. U-Pb geochronology of the Split Lake Block, Manitoba: preliminary results. *In*: Hajnal, Z., and Lewry, J. (Eds). Trans Hudson Lithoprobe Transect, Lithoprobe Report 55, 60-67.

Machado, N., David, J., Scott, D.J., Lamothe, D., Philippe, S., and Gariepy, C., 1993. U-Pb geochronology of the western Cape Smith Belt, Canada: new insights on the age of initial rifting and arc magmatism. Precambrian Research 63, 211-224.

MacNeil, A., Delaney, G.D., and Ansdell, K., 1997. Geology of the Courtenay Lake Formation in the Cook Lake area, Wollaston Domain, northern Saskatchewan. *In* Summary of Investigations 1997, Saskatchewan Geological Survey, Saskatchewan Energy and Mines, Miscellaneous Report 97-4, 115-120.

Maxeiner, R.O., and Demmans, C.J., 2000. The final pieces of the 'Bridge': Geology of the southern Reindeer Lake and Laurie Lake areas. *In* Summary of Investigations 2000, Vol. 2, Saskatchewan geological Survey, Saskatchewan Energy and Mines, Miscellaneous Report 2000-4.2, 30-50.

Money, P.L., 1968. The Wollaston Lake fold-belt system, Saskatchewan-Manitoba. Canadian Journal of Earth Sciences 5, 1489-1504.

Ray G.E., 1979. Reconnaissance bedrock geology: Wollaston East (part of NTS area 64L). *In* Summary of investigations 1979, Vol. 2, Saskatchewan geological Survey, Saskatchewan Minerals and Resources, Miscellaneous Report 49-10, 19-28.

APPENDIX A

Timing (Ma)	Associated Event	Reference
1910 to 1900	Regional rhyolite volcanism	Baldwin et al., 1987; Beaumont-Smith et al., 2006
1876	Tonilitic and granitic plutonism in the Southern section	Baldwin et al., 1987; Beaumont-Smith et al., 2006
1870	Cu-Ni rich gabbroic plugs (i.e., Farley and EL Mines) intrude the Northern section	Turek et al., 2000; Beaumont-Smith et al., 2006
1854	Granitic stocks associated with the emplacement of the Wathaman-Chipewyan-Baldock Batholith, were emplaced throughout the Lynn Lake region	Ray and Wanless, 1980; Bickford and Van Schmus, 1985; Hunt et al., 1990; Beaumont-Smith et al., 2006
1831	Tonalitic dykes intrude the New Fox section	Zwanzig et al., 1999; Beaumont-Smith et al., 2006

Summary of the relative timing for the major volcanic and plutonic occurrences within the Lynn Lake greenstone belt.

APPENDIX B

Deformation Event	Description
D1	Large-scale, isoclinal folds and minor faulting. Folds have steeply dipping, east-northeast striking axial plains, which are relatively consistently spaced at 2 km intervals.
D2	Large-scale folding and faulting associated with uplift of the supracrustal sequence followed be erosion and tilting of the previously faulted blocks.
D3	Thrust faulting with significant offsets occurring along the axes of major synclinal-anticlinal structures.
D4	Development of large-scale, east to northeast brittle and ductile shear zones.

Summary of the major structural events that affected the Lynn Lake greenstone belt (after Gilbert et al., 1980).

APPENDIX C

Lithology	Chlorite-amphibole Schist									
Sample	MG11-003	MG11-013 *	MG11-015	MG11-028 *	MG11-033 *	MG11-050 *	MG11-051 *	MG11-054 *	MG11-056 *	MG11-113 *
Easting (m)	383386	380934	380952	380302	380302	380048	380048	379973	380048	378578
Northing (m)	6306386	6307519	6307492	6307261	6307261	6307163	6307163	6307114	6307163	6306250
DDH	Outcrop	Outcrop	Outcrop	MG11-15	MG11-15	MG11-38	MG11-38	MG11-25	MG11-38	MG11-48
Depth (m)	-	-	-	257.57	305.86	84	83	118	89	314
SiO_2	46.50	47.28	48.14	61.40	45.77	52.39	48.76	46.19	46.37	46.62
Al_2O_3	12.04	8.53	9.83	5.54	8.69	8.76	6.70	8.17	8.01	7.78
TiO_2	1.56	1.27	1.52	0.89	1.35	1.18	0.98	1.19	1.15	1.23
Fe_2O_3	14.78	13.30	14.09	14.22	14.48	16.76	16.29	13.63	13.86	13.55
MnO	0.21	0.29	0.22	0.17	0.22	0.34	0.42	0.34	0.33	0.24
MgO	12.76	17.83	13.59	10.87	19.62	13.55	14.62	19.86	18.71	17.57
CaO	10.40	11.05	11.56	5.94	9.38	4.73	11.08	10.27	11.11	12.54
Na_2O	1.48	0.28	0.68	0.25	0.32	0.17	0.24	0.21	0.25	0.24
K_2O	0.12	0.05	0.24	0.63	0.04	2.01	0.78	0.04	0.05	0.13
P_2O_5	0.16	0.13	0.14	0.09	0.13	0.12	0.12	0.11	0.16	0.12
LOI	2.44	5.05	2.08	3.12	4.64	4.33	6.57	6.8	6.19	5.99
Total	100	100	100	100	100	100	100	100	100	100
Ni	530	930	530	380	770	340	390	890	820	730
Cr	1040	1480	990	1010	1460	920	1300	1500	1470	1330
Co	76	85	66	59	89	49	68	79	74	82
V	307	248	296	162	268	221	189	220	231	233
Sc	32	27	31	19	28	25	21	24	27	24
Cu	60	130	20	200	140	1110	1380	90	100	150
Zn	200	380	280	2080	200	920	670	500	310	240
Mo	*n.d.*	*n.d.*	*n.d.*	*n.d.*	*n.d.*	*n.d.*	*n.d.*	*n.d.*	*n.d.*	2.0
W	*n.d.*	1.0	*n.d.*	1.0	4.0	*n.d.*	*n.d.*	*n.d.*	*n.d.*	44
Sb	0.9	3.2	7.9	0.8	0.8	*n.d.*	*n.d.*	0.5	0.6	0.6
Sn	1.0	*n.d.*	*n.d.*	*n.d.*	*n.d.*	*n.d.*	*n.d.*	1.0	*n.d.*	1.0

** identifies an altered sample; DDH: diamond drill hole; n.d.: not detected*

Lithology	Chlorite-amphibole Schist									
Sample	MG11-003	MG11-013	MG11-015	MG11-028	MG11-033	MG11-050	MG11-051	MG11-054	MG11-056	MG11-113
Ba	42	8	52	111	3	79	115	3	6	17
Cs	*n.d.*	*n.d.*	*n.d.*	1.2	*n.d.*	4.6	1.3	*n.d.*	*n.d.*	*n.d.*
Rb	*n.d.*	*n.d.*	4	19	*n.d.*	40	18	*n.d.*	*n.d.*	*n.d.*
Sr	137	58	137	86	41	79	121	91	75	143
Pb	*n.d.*	*n.d.*	6	46	6	14	10	*n.d.*	*n.d.*	9
Ga	17	12	16	9	13	12	10	13	13	14
Zr	95	68	83	49	71	61	52	60	61	67
Hf	2.3	1.7	2.1	1.2	1.8	1.5	1.3	1.6	1.8	1.7
Nb	7.0	6.0	8.0	4.0	5.0	4.0	4.0	6.0	6.0	5.0
Ta	0.5	0.5	0.6	0.3	0.4	0.3	0.4	0.4	0.4	0.4
Th	0.8	0.7	0.8	0.4	0.6	0.4	0.5	0.6	0.6	0.6
U	0.4	0.2	0.2	n.d.	0.1	0.2	0.2	0.1	0.2	0.2
Y	17	10	14	7	10	9	8	10	12	11
La	6.8	6.7	9.6	3.7	7.0	5.9	5.2	6.5	8.6	6.0
Ce	17.8	17.3	22.1	10.0	17.4	14.8	13.2	17.3	21.5	15.8
Pr	2.40	2.28	2.93	1.35	2.29	1.89	1.69	2.39	2.83	2.09
Nd	11.1	10.7	13.4	6.5	10.9	8.7	8.0	11.1	13.8	10.3
Sm	3.1	2.8	3.4	1.8	3.0	2.1	2.2	2.7	3.4	2.8
Eu	1.10	1.01	1.19	0.65	1.11	0.56	0.78	1.00	1.00	0.91
Gd	3.4	3.0	3.6	1.7	3.0	2.1	2.2	2.8	3.3	2.8
Tb	0.6	0.5	0.6	0.3	0.5	0.3	0.3	0.4	0.6	0.4
Dy	3.5	2.5	3.1	1.5	2.7	2.0	1.9	2.4	3.0	2.6
Ho	0.7	0.5	0.6	0.3	0.5	0.4	0.4	0.5	0.6	0.5
Er	1.9	1.2	1.5	0.7	1.3	1.0	1.0	1.2	1.5	1.5
Tm	0.30	0.19	0.22	0.11	0.19	0.15	0.14	0.18	0.20	0.17
Yb	1.9	1.1	1.4	0.7	1.2	0.9	0.9	1.2	1.2	1.0
Lu	0.28	0.16	0.21	0.11	0.18	0.15	0.14	0.18	0.19	0.16

Lithology	Chlorite-amphibole Schist									
Sample	MG11-003	MG11-013	MG11-015	MG11-028	MG11-033	MG11-050	MG11-051	MG11-054	MG11-056	MG11-113
La/Sm_{CN}	1.42	1.54	1.82	1.33	1.51	1.81	1.53	1.55	1.63	1.38
Gd/Yb_{CN}	1.48	2.26	2.13	2.01	2.07	1.93	2.02	1.93	2.27	2.32
La/Yb_{CN}	2.57	4.37	4.92	3.79	4.18	4.70	4.14	3.89	5.14	4.30
Eu/Eu*	1.04	1.07	1.04	1.14	1.13	0.82	1.08	1.11	0.91	0.99
Ce/Ce*	1.08	1.09	1.02	1.10	1.07	1.09	1.09	1.08	1.07	1.09
Zr/Y	5.6	6.8	5.9	7.0	7.1	6.8	6.5	6.0	5.1	6.1
Ti/Zr	95	107	107	107	108	109	104	109	105	101
Al_2O_3/TiO_2	8	7	6	6	6	7	7	7	7	6
Zr/Hf	41	40	40	41	39	41	40	38	34	39
Zr/Zr*	1.12	0.86	0.85	0.99	0.86	0.99	0.86	0.76	0.62	0.86
Ti/Ti*	1.36	1.42	1.43	1.71	1.45	1.88	1.57	1.47	1.05	1.46
Nb/Nb*	1.01	0.93	0.97	1.11	0.82	0.88	0.84	1.02	0.89	0.89
Mg#	63	73	66	60	73	62	64	74	73	72
ΣLREE	77.70	70.79	87.22	44.70	72.70	61.05	54.27	67.79	81.43	64.7
ΣHREE	26.18	16.15	21.63	10.72	16.57	13.90	12.78	16.06	19.29	17.33

Lithology	**Plagioclase-amphibole Schist**									
Sample	MG11-006	MG11-007	MG11-037 *	MG11-038	MG11-039	MG11-040	MG11-055 *	MG11-057	MG11-074	MG11-094
Easting (m)	378686	378712	381336	381336	381336	381336	379973	380048	380727	380650
Northing (m)	6306608	6306571	6308189	6308189	6308189	6308189	6307114	6307163	6307854	6307099
DDH	Outcrop	Outcrop	MG11-41	MG11-41	MG11-41	MG11-41	MG11-25	MG11-38	MG11-14	MG11-18
Depth (m)	-	-	332	164	543.5	441	223	251	249	126.5
SiO_2	52.88	55.65	51.01	50.99	50.31	49.72	47.66	48.34	47.28	60.61
Al_2O_3	20.40	17.68	16.50	18.12	16.45	18.36	17.50	20.46	19.25	17.98
TiO_2	0.90	1.10	0.97	1.03	0.99	0.93	1.06	0.79	0.82	0.60
Fe_2O_3	10.24	11.09	11.43	11.94	12.89	13.47	9.63	10.29	13.45	8.04
MnO	0.15	0.20	0.20	0.17	0.23	0.20	0.21	0.19	0.15	0.08
MgO	2.45	2.55	2.87	2.96	4.79	3.46	2.90	4.10	4.42	2.31
CaO	8.31	8.42	14.46	12.56	10.36	9.76	16.10	11.25	10.78	5.62
Na_2O	4.15	2.87	2.30	1.86	3.30	3.23	3.41	2.41	2.31	4.26
K_2O	0.44	0.36	0.17	0.31	0.60	0.79	1.38	2.07	1.46	0.40
P_2O_5	0.09	0.08	0.09	0.05	0.07	0.08	0.15	0.09	0.06	0.09
LOI	0.56	0.72	4.77	1.23	1.94	1.74	7.57	2.95	2.08	2.58
Total	100	100	100	100	100	100	100	100	100	100
Ni	*n.d.*	*n.d.*	1020	*n.d.*	*n.d.*	*n.d.*	*n.d.*	20	*n.d.*	40
Cr	*n.d.*	*n.d.*	1350	*n.d.*	20	30	20	40	20	50
Co	24	19	103	29	40	35	21	36	39	37
V	179	132	240	303	327	309	219	233	319	173
Sc	25	29	23	33	37	36	31	29	37	22
Cu	60	30	1260	130	150	140	110	130	160	320
Zn	100	110	480	110	110	140	80	130	80	50
Mo	*n.d.*	*n.d.*	*n.d.*	*n.d.*	*n.d.*	*n.d.*	*n.d.*	*n.d.*	*n.d.*	*n.d.*
W	*n.d.*	*n.d.*	19	*n.d.*	*n.d.*	*n.d.*	15	4.0	*n.d.*	2.0
Sb	0.6	*n.d.*	*n.d.*	2.8	0.7	0.7	*n.d.*	*n.d.*	*n.d.*	4.5
Sn	*n.d.*	*n.d.*	*n.d.*	*n.d.*	*n.d.*	*n.d.*	*n.d.*	*n.d.*	*n.d.*	*n.d.*

Lithology	Plagioclase-amphibole Schist									
Sample	MG11-006	MG11-007	MG11-037	MG11-038	MG11-039	MG11-040	MG11-055	MG11-057	MG11-074	MG11-094
Ba	76	87	42	56	162	261	199	161	356	98
Cs	*n.d.*	*n.d.*	*n.d.*	*n.d.*	1.2	1.4	*n.d.*	*n.d.*	1.0	*n.d.*
Rb	4	3	*n.d.*	5	10	13	29	37	32	8
Sr	290	238	222	296	346	247	172	167	571	272
Pb	*n.d.*	*n.d.*	*n.d.*	6	*n.d.*	6	*n.d.*	26	6	9
Ga	18	19	15	19	17	17	17	17	18	17
Zr	42	42	26	33	25	39	58	40	28	33
Hf	1.1	1.2	0.8	1.0	0.7	1.1	1.4	1.1	0.7	0.9
Nb	3.0	3.0	1.0	2.0	1.0	2.0	3.0	4.0	2.0	3.0
Ta	0.2	0.2	0.1	0.1	*n.d.*	0.2	0.2	0.3	0.1	0.2
Th	0.5	0.2	0.1	0.2	0.2	0.3	0.5	0.5	0.2	0.3
U	0.4	0.1	n.d.	0.1	0.1	0.2	0.2	0.1	0.1	*n.d.*
Y	12	15	9	11	11	12	14	11	10	7
La	3.6	3.9	2.5	3.1	2.3	3.2	6.5	5.4	2.7	3.5
Ce	8.7	10.3	6.5	8.4	6.1	8.4	15.9	12.5	7.1	8.4
Pr	1.25	1.49	0.94	1.28	0.91	1.22	2.11	1.57	1.04	1.12
Nd	6.2	7.3	5.2	6.4	4.6	6.3	9.7	6.9	5.4	5.1
Sm	2.0	2.4	1.5	1.9	1.5	1.8	2.5	1.9	1.7	1.5
Eu	0.77	0.92	0.63	0.83	0.69	0.76	0.81	0.77	0.77	0.47
Gd	2.4	2.7	1.9	2.4	2.0	2.4	2.7	2.1	1.9	1.5
Tb	0.4	0.5	0.3	0.4	0.3	0.4	0.5	0.4	0.3	0.2
Dy	2.5	3.1	2.0	2.3	2.2	2.5	2.7	2.2	1.9	1.5
Ho	0.5	0.7	0.4	0.5	0.4	0.5	0.6	0.4	0.4	0.3
Er	1.5	1.8	1.2	1.4	1.3	1.5	1.6	1.2	1.2	0.7
Tm	0.22	0.28	0.17	0.20	0.20	0.23	0.24	0.20	0.18	0.11
Yb	1.4	1.7	1.0	1.3	1.3	1.5	1.6	1.4	1.2	0.7
Lu	0.22	0.27	0.16	0.20	0.21	0.23	0.23	0.22	0.17	0.10

Lithology	Plagioclase-amphibole Schist									
Sample	MG11-006	MG11-007	MG11-037	MG11-038	MG11-039	MG11-040	MG11-055	MG11-057	MG11-074	MG11-094
La/Sm_{CN}	1.16	1.05	1.08	1.05	0.99	1.15	1.68	1.83	1.03	1.51
Gd/Yb_{CN}	1.42	1.31	1.57	1.53	1.27	1.32	1.40	1.24	1.31	1.77
La/Yb_{CN}	1.84	1.65	1.79	1.71	1.27	1.53	2.91	2.77	1.61	3.59
Eu/Eu*	1.07	1.10	1.14	1.19	1.22	1.12	0.95	1.18	1.31	0.96
Ce/Ce*	1.01	1.05	1.04	1.03	1.03	1.04	1.05	1.05	1.04	1.04
Zr/Y	3.5	2.8	2.9	3.0	2.3	3.3	4.1	3.6	2.8	4.7
Ti/Zr	127	157	208	182	232	142	100	112	173	105
Al_2O_3/TiO_2	23	16	17	18	17	20	17	26	23	30
Zr/Hf	38	35	33	33	36	35	41	36	40	37
Zr/Zr*	0.82	0.69	0.64	0.65	0.66	0.80	0.81	0.76	0.64	0.82
Ti/Ti*	1.17	1.16	1.53	1.37	1.56	1.21	1.09	1.04	1.41	1.39
Nb/Nb*	0.75	1.14	0.67	0.86	0.50	0.69	0.56	0.82	0.92	0.99
Mg#	32	31	33	33	42	34	37	44.00	39	36
ΣLREE	49.92	58.01	42.17	57.31	55.10	60.08	71.22	60.14	57.61	43.59
ΣHREE	18.74	23.35	14.23	17.30	16.91	18.86	21.47	17.02	15.35	10.61

Lithology	Plagioclase-amphibole Schist								
Sample	MG11-095	MG11-098 *	MG11-099 *	MG11-105 *	MG11-106 *	MG11-108 *	MG11-110	MG11-111	MG11-116
Easting (m)	380650	380650	380650	380650	380650	380650	378578	378578	378578
Northing (m)	6307099	6307099	6307099	6307099	6307099	6307099	6306250	6306250	6306250
DDH	MG11-18	MG11-18	MG11-18	MG11-18	MG11-18	MG11-18	MG11-48	MG11-48	MG11-48
Depth (m)	194.5	292.7	293.7	257.8	188.5	223.4	96	302	349
SiO_2	50.78	55.42	52.48	39.24	48.43	48.13	53.78	59.97	65.48
Al_2O_3	21.21	18.65	20.41	21.87	19.03	20.19	16.99	16.35	13.68
TiO_2	0.72	0.79	0.87	0.76	0.63	0.72	1.19	1.02	0.66
Fe_2O_3	9.82	8.25	7.55	10.93	9.18	9.88	12.35	9.77	8.88
MnO	0.13	0.13	0.14	0.41	0.23	0.17	0.17	0.08	0.08
MgO	5.38	1.76	1.71	7.34	6.66	5.34	3.40	2.76	2.77
CaO	5.81	9.70	11.58	13.88	10.36	11.61	7.63	3.63	2.37
Na_2O	5.02	1.67	2.00	0.77	4.15	0.77	3.70	4.08	1.37
K_2O	1.02	3.54	3.19	4.71	1.25	3.11	0.59	2.21	4.57
P_2O_5	0.10	0.10	0.09	0.08	0.08	0.08	0.20	0.14	0.13
LOI	1.61	4.41	4.82	9.60	3.47	5.47	1.54	1.40	1.40
Total	100	100	100	100	100	100	100		
Ni	50	*n.d.*	*n.d.*	40	50	50	*n.d.*	*n.d.*	40
Cr	50	*n.d.*	20	70	80	120	30	30	*n.d.*
Co	27	27	31	36	35	43	30	22	29
V	154	168	187	166	168	196	238	189	75
Sc	23	23	25	27	28	30	35	29	19
Cu	120	130	150	*n.d.*	80	80	210	310	1380
Zn	100	80	70	70	100	90	160	450	210
Mo	*n.d.*	*n.d.*	*n.d.*	*n.d.*	*n.d.*	*n.d.*	*n.d.*	*n.d.*	*n.d.*
W	2.0	1.0	1.0	9.0	2.0	1.0	1.0	44	36
Sb	*n.d.*	6.4	5.8	33.6	1.1	0.6	*n.d.*	6.4	0.6
Sn	*n.d.*	*n.d.*	*n.d.*	*n.d.*	*n.d.*	*n.d.*	*n.d.*	*n.d.*	*n.d.*

Lithology	Plagioclase-amphibole Schist								
Sample	MG11-095	MG11-098	MG11-099	MG11-105	MG11-106	MG11-108	MG11-110	MG11-111	MG11-116
Ba	287	308	336	313	367	300	172	481	1007
Cs	*n.d.*	0.5	0.5	1.5	0.5	0.7	*n.d.*	1.3	1.5
Rb	20	59	54	109	26	48	12	36	77
Sr	290	159	186	134	224	109	423	189	157
Pb	6	7	8	6	5	*n.d.*	6	412	24
Ga	17	16	17	17	14	17	19	16	16
Zr	38	36	40	34	35	35	71	59	67
Hf	1.0	1.1	1.1	0.8	0.9	1.0	2.0	1.5	1.7
Nb	3.0	4.0	4.0	3.0	3.0	3.0	7.0	6.0	6.0
Ta	0.2	0.2	0.3	0.2	0.2	0.2	0.5	0.4	0.5
Th	0.4	0.3	0.3	0.4	0.3	0.4	0.8	0.7	1.0
U	0.1	*n.d.*	*n.d.*	0.1	0.1	0.1	0.3	0.6	0.3
Y	8	10	10	8	9	9	18	14	14
La	4.2	4.7	4.5	4.3	3.7	3.9	8.6	7.2	8.4
Ce	10.2	11.3	11.5	10.1	9.2	9.3	21.3	17.8	19.5
Pr	1.34	1.55	1.53	1.29	1.29	1.22	2.87	2.29	2.43
Nd	6.0	6.9	6.9	5.7	6.1	5.5	12.7	10.0	10.4
Sm	1.7	2.2	2.0	1.8	1.7	1.6	3.5	2.7	2.7
Eu	0.69	0.61	0.73	0.81	0.67	0.73	1.17	0.68	0.61
Gd	1.8	2.1	2.1	1.9	1.8	1.6	3.5	2.9	2.6
Tb	0.3	0.4	0.4	0.3	0.3	0.3	0.6	0.5	0.5
Dy	1.7	2.2	2.3	1.7	1.8	1.7	3.5	3.0	2.8
Ho	0.3	0.5	0.4	0.3	0.4	0.3	0.7	0.6	0.6
Er	0.9	1.3	1.2	0.9	1.0	0.9	2.1	1.7	1.7
Tm	0.14	0.20	0.19	0.14	0.15	0.16	0.31	0.25	0.26
Yb	0.9	1.3	1.3	0.9	1.0	1.2	2.0	1.5	1.5
Lu	0.14	0.21	0.21	0.15	0.15	0.18	0.31	0.24	0.24

Lithology	Plagioclase-amphibole Schist								
Sample	MG11-095	MG11-098	MG11-099	MG11-105	MG11-106	MG11-108	MG11-110	MG11-111	MG11-116
La/Sm_{CN}	1.59	1.38	1.45	1.54	1.41	1.57	1.59	1.72	2.01
Gd/Yb_{CN}	1.65	1.34	1.34	1.75	1.49	1.10	1.45	1.60	1.43
La/Yb_{CN}	3.35	2.59	2.48	3.43	2.65	2.33	3.08	3.44	4.02
Eu/Eu*	1.21	0.87	1.09	1.34	1.17	1.39	1.02	0.74	0.70
Ce/Ce*	1.05	1.03	1.07	1.05	1.03	1.05	1.05	1.07	1.06
Zr/Y	4.8	3.6	4.0	4.3	3.9	3.9	3.9	4.2	4.8
Ti/Zr	110	122	120	117	105	114	99	99	58
Al_2O_3/TiO_2	30	24	23	29	30	28	14	16	21
Zr/Hf	38	33	36	43	39	35	36	39	39
Zr/Zr*	0.82	0.64	0.74	0.73	0.75	0.81	0.74	0.78	0.87
Ti/Ti*	1.28	1.02	1.09	1.22	1.10	1.23	1.07	1.04	0.71
Nb/Nb*	0.78	1.14	1.16	0.77	0.96	0.81	0.90	0.90	0.70
Mg#	52	30	31	57	59	52	35	36	38
ΣLREE	48.93	52.36	54.26	52.90	52.46	53.85	88.64	72.57	65.64
ΣHREE	12.38	16.11	16.00	12.39	13.80	13.74	27.52	21.79	21.60

Lithology	**Quartz-plagioclase-biotite Schist**							
Sample	MG11-001	MG11-053	MG11-093 *	MG11-100	MG11-102 *	MG11-104 *	MG11-107 *	MG11-117 *
Easting (m)	383352	379973	380650	380650	380650	380650	380650	378578
Northing (m)	6306428	6307114	6307099	6307099	6307099	6307099	6307099	6306250
DDH	Outcrop	MG11-25	MG11-18	MG11-18	MG11-18	MG11-18	MG11-18	MG11-48
Depth (m)	-	328	291.7	294.7	264.8	256.8	224.4	362
SiO_2	55.19	51.73	52.36	49.29	48.74	51.77	48.70	60.46
Al_2O_3	18.29	21.11	21.14	21.07	16.20	16.73	19.75	14.67
TiO_2	0.92	0.89	0.88	0.86	0.68	0.61	0.75	0.79
Fe_2O_3	9.36	9.50	8.16	9.87	8.65	7.60	9.61	13.04
MnO	0.20	0.15	0.12	0.14	0.40	0.35	0.17	0.11
MgO	3.99	3.02	1.96	3.05	6.66	5.82	4.84	2.85
CaO	8.84	8.58	9.55	10.20	14.53	12.19	11.87	1.75
Na_2O	2.80	2.44	3.24	1.88	1.24	1.12	0.64	0.28
K_2O	0.26	2.44	2.49	3.52	2.79	3.72	3.57	5.96
P_2O_5	0.14	0.13	0.11	0.10	0.10	0.09	0.11	0.12
LOI	1.19	2.23	4.34	0.78	8.17	8.50	5.00	3.60
Total	100	100	100	100	100	100	100	100
Ni	*n.d.*	*n.d.*	*n.d.*	*n.d.*	50	20	60	*n.d.*
Cr	*n.d.*	30	*n.d.*	20	70	50	90	20
Co	44	27	28	23	26	15	37	24
V	174	182	190	187	148	114	189	126
Sc	27	29	26	26	22	18	29	26
Cu	50	140	150	210	70	*n.d.*	70	420
Zn	120	110	80	110	140	60	90	1230
Mo	*n.d.*	*n.d.*	*n.d.*	*n.d.*	*n.d.*	2.0	*n.d.*	*n.d.*
W	1.0	2.0	*n.d.*	2.0	13	11	*n.d.*	46.0
Sb	*n.d.*	*n.d.*	*n.d.*	n.d.	5.9	11	*n.d.*	*n.d.*
Sn	*n.d.*	1.0	*n.d.*	*n.d.*	*n.d.*	*n.d.*	*n.d.*	*n.d.*

Lithology	Quartz-plagioclase-biotite Schist							
Sample	MG11-001	MG11-053	MG11-093	MG11-100	MG11-102	MG11-104	MG11-107	MG11-117
Ba	143	220	273	318	154	281	337	776
Cs	*n.d.*	*n.d.*	0.6	0.7	1.2	1.1	0.8	0.7
Rb	2	41	51	65	61	82	56	94
Sr	447	255	282	156	110	91	122	125
Pb	10	*n.d.*	11	6	6	5	*n.d.*	61
Ga	18	18	16	19	13	14	17	18
Zr	82	47	42	42	32	30	37	47
Hf	2.0	1.2	1.0	1.2	0.9	0.8	1.0	1.5
Nb	5.0	5.0	4.0	4.0	3.0	3.0	3.0	5.0
Ta	0.3	0.3	0.3	0.3	0.2	0.2	0.2	0.4
Th	0.7	0.5	0.4	0.4	0.3	0.4	0.4	0.6
U	0.5	0.2	0.1	0.1	n.d.	0.2	0.1	0.2
Y	16	13	11	10	9	8	9	12
La	7.1	5.5	4.9	4.6	3.4	3.6	4.1	5.1
Ce	17.1	14.0	11.6	11.3	8.2	8.8	10.1	11.9
Pr	2.18	1.90	1.61	1.53	1.11	1.16	1.31	1.54
Nd	9.8	8.6	7.4	6.7	4.9	5.5	5.9	6.8
Sm	2.6	2.4	2.1	1.9	1.5	1.5	1.7	1.9
Eu	0.97	1.02	0.80	0.80	0.72	0.73	0.69	0.47
Gd	3.0	2.5	2.3	1.9	1.6	1.6	1.8	2.3
Tb	0.5	0.4	0.3	0.3	0.3	0.3	0.3	0.4
Dy	3.1	2.7	2.2	2.1	1.8	1.5	1.8	2.4
Ho	0.7	0.5	0.5	0.4	0.4	0.3	0.3	0.5
Er	1.8	1.6	1.3	1.2	1.0	0.9	1.0	1.5
Tm	0.27	0.24	0.18	0.19	0.14	0.14	0.16	0.24
Yb	1.7	1.6	1.1	1.3	0.9	0.9	1.0	1.6
Lu	0.30	0.23	0.17	0.21	0.14	0.15	0.16	0.24

Lithology	Quartz-plagioclase-biotite Schist							
Sample	MG11-001	MG11-053	MG11-093	MG11-100	MG11-102	MG11-104	MG11-107	MG11-117
La/Sm_{CN}	1.76	1.48	1.51	1.56	1.46	1.55	1.56	1.73
Gd/Yb_{CN}	1.46	1.29	1.73	1.21	1.47	1.47	1.49	1.19
La/Yb_{CN}	3.00	2.47	3.20	2.54	2.71	2.87	2.94	2.29
Eu/Eu*	1.06	1.27	1.11	1.29	1.42	1.44	1.21	0.69
Ce/Ce*	1.07	1.06	1.01	1.04	1.03	1.06	1.07	1.04
Zr/Y	5.1	3.6	3.8	4.2	3.6	3.8	4.1	3.9
Ti/Zr	66	109	120	117	113	108	115	95
Al_2O_3/TiO_2	20	24	24	25	24	27	26	19
Zr/Hf	41	39	42	35	36	38	37	31
Zr/Zr*	1.12	0.71	0.74	0.81	0.82	0.72	0.81	0.90
Ti/Ti*	0.95	1.08	1.36	1.35	1.08	1.05	1.26	1.00
Nb/Nb*	0.76	1.02	0.96	0.99	1.00	0.84	0.79	0.96
Mg#	46	39	32	38	60	60	50	30
ΣLREE	69.75	64.92	56.71	54.73	43.43	40.89	54.60	56.01
ΣHREE	24.37	20.27	16.75	15.70	13.68	12.19	13.72	18.88

Lithology	**Amphibole Schist**						
Sample	MG11-004	MG11-035	MG11-072	MG11-115	MG11-118	MG11-122	MG11-125
Easting (m)	383384	381336	380727	378578	378578	378810	378810
Northing (m)	6306404	6308189	6307854	6306250	6306250	6305494	6305494
DDH	Outcrop	MG11-41	MG11-14	MG11-48	MG11-48	MG11-53	MG11-53
Depth (m)	-	250	593	348	401	207	299
SiO_2	57.04	55.68	58.65	62.10	77.17	57.71	46.24
Al_2O_3	13.36	16.89	18.19	13.22	10.71	9.51	7.92
TiO_2	0.44	0.87	0.75	0.64	0.38	0.36	0.33
Fe_2O_3	13.57	9.74	8.07	11.45	4.25	24.93	32.55
MnO	0.21	0.16	0.09	0.13	0.04	0.15	0.24
MgO	7.03	4.95	4.49	4.98	1.57	1.97	2.40
CaO	5.70	8.38	3.45	2.86	1.37	4.22	9.22
Na_2O	1.32	2.65	1.82	0.41	0.25	0.69	0.35
K_2O	1.18	0.51	4.15	4.13	4.15	0.36	0.61
P_2O_5	0.15	0.16	0.34	0.08	0.10	0.11	0.14
LOI	2.50	0.98	2.12	1.36	1.52	-0.51	1.91
Total	100	100	100	100	100	100	100
Ni	170	90	*n.d.*	80	20	*n.d.*	*n.d.*
Cr	620	200	30	100	*n.d.*	30	30
Co	51	27	18	18	10	8	9
V	122	144	129	123	51	77	80
Sc	19	24	11	25	16	11	12
Cu	*n.d.*	*n.d.*	110	350	490	150	140
Zn	220	120	180	340	250	140	80
Mo	*n.d.*	*n.d.*	2.0	5.0	*n.d.*	3.0	3.0
W	*n.d.*	*n.d.*	1.0	24	13	2.0	*n.d.*
Sb	*n.d.*	*n.d.*	2.0	*n.d.*	0.9	*n.d.*	34
Sn	*n.d.*	*n.d.*	*n.d.*	*n.d.*	*n.d.*	*n.d.*	1.0

Lithology	Amphibole Schist						
Sample	MG11-004	MG11-035	MG11-072	MG11-115	MG11-118	MG11-122	MG11-125
Ba	179	74	749	618	1056	98	319
Cs	0.9	1.2	2.3	2.4	0.6	*n.d.*	1.4
Rb	24	7	66	85	43	6	14
Sr	86	270	139	127	124	21	104
Pb	*n.d.*	*n.d.*	65	31	303	*n.d.*	*n.d.*
Ga	15	17	20	18	10	12	8
Zr	98	81	118	57	81	70	57
Hf	2.3	2.1	3.0	1.4	2.2	1.8	1.3
Nb	4.0	4.0	9.0	4.0	3.0	3.0	3.0
Ta	0.4	0.3	0.6	0.3	0.2	0.1	0.1
Th	2.4	1.3	2.4	0.8	1.9	1.3	1.2
U	1.0	0.5	1.3	0.5	1.1	1.1	0.8
Y	11	15	23	7	18	18	21
La	12.8	10.3	17.3	9.0	10.8	10.1	11.0
Ce	29.9	23.7	39.8	21.3	24.1	23.0	24.1
Pr	3.49	2.92	4.73	2.56	3.03	2.84	3.08
Nd	14.1	12.1	19.9	11.5	13.5	12.5	13.1
Sm	3.0	2.9	4.5	2.7	3.6	3.0	3.2
Eu	0.69	1.08	1.35	0.64	0.61	0.76	0.71
Gd	2.4	3.2	4.5	2.3	3.5	3.2	3.2
Tb	0.4	0.5	0.8	0.3	0.6	0.5	0.6
Dy	2.1	3.1	4.4	1.6	3.5	3.1	3.6
Ho	0.4	0.6	0.9	0.3	0.8	0.7	0.8
Er	1.2	1.8	2.7	0.7	2.2	2.1	2.3
Tm	0.18	0.27	0.43	0.12	0.35	0.33	0.36
Yb	1.3	1.7	2.9	0.8	2.3	2.1	2.4
Lu	0.20	0.27	0.46	0.15	0.37	0.32	0.39

Lithology	Amphibole Schist						
Sample	MG11-004	MG11-035	MG11-072	MG11-115	MG11-118	MG11-122	MG11-125
La/Sm_{CN}	2.75	2.29	2.48	2.15	1.94	2.17	2.22
Gd/Yb_{CN}	1.53	1.56	1.28	2.38	1.26	1.26	1.10
La/Yb_{CN}	7.06	4.35	4.28	8.07	3.37	3.45	3.29
Eu/Eu*	0.79	1.08	0.92	0.79	0.53	0.75	0.68
Ce/Ce*	1.10	1.06	1.08	1.09	1.03	1.05	1.02
Zr/Y	8.9	5.4	5.1	8.1	4.5	3.9	2.7
Ti/Zr	26	63	37	65	27	31	34
Al_2O_3/TiO_2	30	19	24	21	28	26	24
Zr/Hf	43	39	39	41	37	39	44
Zr/Zr*	1.04	0.94	0.86	0.71	0.80	0.79	0.61
Ti/Ti*	0.60	0.90	0.50	1.17	0.33	0.38	0.29
Nb/Nb*	0.24	0.37	0.47	0.50	0.22	0.28	0.28
Mg#	51	50	52	46	42	14	13
ΣLREE	85.38	80.20	103.08	75.00	75.14	66.40	70.39
ΣHREE	16.78	23.24	35.59	10.97	28.12	27.15	31.45

Lithology	**Amphibolite**			**Quartz-amphibole Schist**			**G1. Amp. Dykes**		**G2 Amp.**
Sample	MG11-002	LL13-16	LL13-18	LL13-20	LL13-21	LL13-24	LL13-19	LL13-23	LL13-17
Easting (m)	383354	380431	382681	382677	382660	382389	382671	382342	382681
Northing (m)	6306437	6307384	6307261	6307268	6307254	6307106	6307226	6307107	6307261
DDH	Outcrop	Outcrop	Outcrop	Outcrop	Outcrop	Outcrop	Outcrop	Outcrop	Outcrop
Depth (m)	-	-	-	-	-	-	-	-	-
SiO_2	49.18	53.08	56.73	51.86	58.62	49.29	47.32	51.58	45.89
Al_2O_3	13.00	13.71	15.10	18.84	15.80	15.92	17.35	18.66	19.33
TiO_2	0.81	0.68	1.82	1.46	1.57	1.94	0.94	0.69	0.57
Fe_2O_3	10.55	8.68	12.58	11.35	11.16	13.03	14.39	12.64	13.02
MnO	0.24	0.15	0.11	0.11	0.08	0.21	0.22	0.17	0.17
MgO	12.19	11.58	2.14	2.86	0.91	6.72	7.08	4.43	7.94
CaO	12.10	10.60	6.02	9.25	5.06	9.25	8.80	7.90	8.86
Na_2O	1.20	0.68	4.03	2.10	3.73	3.22	2.69	3.63	2.21
K_2O	0.28	0.42	1.11	1.95	2.44	0.21	1.12	0.25	1.91
P_2O_5	0.45	0.43	0.36	0.22	0.64	0.21	0.09	0.05	0.09
LOI	2.27	2.49	1.30	1.00	0.95	1.12	1.69	1.85	1.98
Total	100	100	100	100	100	100	100	100	100
Ni	310	330	*n.d.*	30	*n.d.*	100	40	*n.d.*	70
Cr	730	960	*n.d.*	100	*n.d.*	70	60	*n.d.*	90
Co	31	45	24	26	14	63	52	34	49
V	132	161	207	215	45	314	315	317	176
Sc	21	26	29	23	23	30	38	44	34
Cu	n.d.	n.d.	10	n.d.	n.d.	n.d.	40	150	*n.d.*
Zn	190	220	100	90	60	190	340	90	250
Mo	*n.d.*	*n.d.*	*n.d.*	*n.d.*	*n.d.*	*n.d.*	*n.d.*	*n.d.*	*n.d.*
W	2.0	1.4	0.9	0.7	0.8	*n.d.*	*n.d.*	3.5	*n.d.*
Sb	0.6	4.3	*n.d.*	*n.d.*	*n.d.*	*n.d.*	*n.d.*	*n.d.*	*n.d.*
Sn	1.0	*n.d.*	*n.d.*	*n.d.*	*n.d.*	*n.d.*	*n.d.*	*n.d.*	*n.d.*

Lithology	Amphibolite		Quartz-amphibole Schist				G1. Amp. Dykes		G2 Amp.
Sample	MG11-002	LL13-16	LL13-18	LL13-20	LL13-21	LL13-24	LL13-19	LL13-23	LL13-17
Ba	55	95	224	507	662	96	261	151	385
Cs	*n.d.*	1.0	0.7	1.0	0.9	*n.d.*	0.5	*n.d.*	0.4
Rb	4	10	33	49	62	2	28	2	38
Sr	87	156	388	342	340	204	135	552	115
Pb	*n.d.*	36	6	7	5	*n.d.*	*n.d.*	8	*n.d.*
Ga	18	15	23	21	26	21	18	17	17
Zr	148	109	182	141	249	112	25	28	38
Hf	3.3	2.6	4.3	2.9	5.5	2.7	0.6	0.7	1.0
Nb	8.0	8.4	23.1	19.6	28.7	11.9	2.4	1.6	5.6
Ta	0.6	0.4	1.5	1.0	1.9	0.8	0.1	0.0	0.2
Th	4.9	3.0	3.0	1.9	3.2	1.1	0.2	0.3	0.5
U	1.7	1.5	0.9	0.5	0.9	0.3	0.1	0.2	0.2
Y	17	13	27	14	34	18	7	10	12
La	36.1	25.5	23.5	17.8	30.5	11.7	2.2	2.7	6.7
Ce	83.4	58.9	51.2	37.4	67.8	26.3	5.2	6.0	14.8
Pr	10.10	7.78	6.46	4.57	8.82	3.86	0.75	0.89	1.94
Nd	40.3	30.8	26.4	18.6	36.8	17.7	3.8	4.1	8.7
Sm	7.6	5.6	5.5	3.8	7.3	4.2	0.9	1.4	2.2
Eu	1.47	1.54	1.73	1.21	2.44	1.32	0.33	0.68	0.54
Gd	5.6	3.9	5.1	3.3	6.8	4.2	1.0	1.6	2.3
Tb	0.7	0.5	0.9	0.5	1.1	0.7	0.2	0.3	0.4
Dy	3.7	2.7	5.3	2.7	6.6	3.8	1.2	1.7	2.4
Ho	0.7	0.5	1.0	0.6	1.4	0.7	0.3	0.4	0.5
Er	1.8	1.3	2.9	1.6	4.0	1.9	0.7	1.1	1.4
Tm	0.26	0.19	0.40	0.22	0.63	0.26	0.12	0.17	0.19
Yb	1.6	1.2	2.6	1.4	4.0	1.6	0.8	1.1	1.1
Lu	0.25	0.16	0.40	0.20	0.54	0.23	0.12	0.15	0.15

Lithology	Amphibolite		Quartz-amphibole Schist				G1. Amp. Dykes		G2 Amp.
Sample	MG11-002	LL13-16	LL13-18	LL13-20	LL13-21	LL13-24	LL13-19	LL13-23	LL13-17
La/Sm_{CN}	3.07	2.93	2.75	3.06	2.69	1.81	1.57	1.19	1.99
Gd/Yb_{CN}	2.90	2.75	1.65	1.93	1.42	2.12	0.97	1.20	1.80
La/Yb_{CN}	16.18	15.77	6.58	8.99	5.51	5.15	1.91	1.77	4.58
Eu/Eu*	0.69	1.01	1.00	1.05	1.06	0.97	1.05	1.38	0.74
Ce/Ce*	1.07	1.03	1.02	1.02	1.01	0.96	0.97	0.95	1.01
Zr/Y	8.7	8.6	6.8	10.0	7.2	6.2	3.7	2.9	3.2
Ti/Zr	31	36	60	61	38	102	222	146	88
Al_2O_3/TiO_2	16	20	8	13	10	8	18	27	34
Zr/Hf	45	42	42	49	45	41	42	40	38
Zr/Zr*	0.58	0.57	1.04	1.17	1.05	0.90	0.92	0.79	0.60
Ti/Ti*	0.63	0.73	1.09	1.65	0.75	1.55	2.66	1.32	0.78
Nb/Nb*	0.20	0.32	0.93	1.13	0.98	1.14	1.21	0.58	0.99
Mg#	70	73	25	33	14	51	49	41	55
ΣLREE	205.57	159.99	148.92	109.65	183.48	99.24	52.18	61.35	71.12
ΣHREE	26.01	19.28	40.30	21.30	52.68	27.30	10.21	14.55	17.91

APPENDIX D

Study	Sampling Methodology and Study Goals
Gilbert et al., (1980)	A regional reconnaissance mapping and protolith study of the Lynn Lake region. Samples of least altered rocks were collected for major-element geochemical analysis to provide an initial framework for the Lynn Lake region.
Peck (1986); Peck and Smith (1989)	A study of the protoliths and tectonic setting of the Cartwright Lake area. Least-altered samples of local rock-types were selected for high-precision geochemical analysis and geochemical modelling.
Gilbert, (1993)	A local reconnaissance-style mapping and tectonics study of the Barrington Lake, Melvin Lake, and Fraser Lake areas. Samples of least altered rocks were collected for geochemical analysis and added to the Gilbert et al., (1980).
Jones (2005); Jones et al., (2006)	A study of the protoliths, tectonic setting, and gold mineralization of the Burnt Timber Au Deposit. Samples of least to most altered rocks were collected to construct a representative dataset of the area around the Burnt Timber Au Deposit, specifically the Johnson Shear Zone.
Beaumont-Smith, (2007)	An incomplete Ph.D. project on understanding the lithochemical relationships of the "Agassiz Metallotect" and surrounding area. Samples of least altered rocks were collected to provide a representative dataset for the area around the MacLellan Au-Ag Deposit.
Chapter 2	A study on the protoliths and petrogenesis of the host rock sequence to the MacLellan Au-Ag Deposit. Samples of least to most altered rocks were collected to construct a representative dataset for the host rock sequence to the MacLellan Au-Ag deposit and surrounding area.
This study	Representative samples were collected from drill cores outside of the main ore bodies of the Burnt Timber and Farley Lake Au Deposits. Samples provide additional infilling at these locations where sample density is low.

Summary of sampling methodologies and study goals for the data sets included in this study.

APPENDIX E

Group	**G1**								
Reference	**Zwanzig et al., 1999**								
Sample	32-76-229	32-80-996	32-76-975	32-76-459	32-76-460	12-78-147	12-78-147	12-78-146	12-78-146
Easting (m)	372752	423401	385892	373689	374031	337589	337589	337581	337581
Northing (m)	6301047	6314056	6305490	6301461	6301788	6278474	6278474	6278673	6278673
DDH	Outcrop	Outcrop	Outcrop	Outcrop	Outcrop	Outcrop	Outcrop	Outcrop	Outcrop
Depth (m)	-	-	-	-	-	-	-	-	-
SiO_2	52.20	58.02	51.43	61.50	54.94	60.82	54.80	49.87	54.04
Al_2O_3	23.64	16.93	18.80	16.25	15.98	14.95	16.15	18.90	16.45
TiO_2	0.67	0.68	0.94	0.70	0.75	0.38	0.96	0.39	0.82
Fe_2O_3	7.80	7.95	11.64	8.68	12.41	7.95	12.21	9.87	10.62
MnO	0.10	0.13	0.20	0.12	0.20	0.13	0.18	0.20	0.23
MgO	2.43	4.29	3.38	2.02	3.76	4.62	3.30	6.59	4.57
CaO	5.43	7.49	6.50	4.51	8.16	6.82	8.74	10.20	8.53
Na_2O	5.46	3.25	4.86	4.70	2.66	3.54	3.05	3.46	4.41
K_2O	2.11	1.06	1.89	1.40	1.01	0.69	0.48	0.44	0.21
P_2O_5	0.16	0.21	0.35	0.13	0.13	0.09	0.12	0.08	0.12
LOI	0.10	0.91	0.50	1.13	1.52	0.81	1.17	1.31	1.17
Total	100	100	100	100	100	100	100	100	100
Ni	*n.d.*	64	*n.d.*	33	*n.d.*	25	25	34	*n.d.*
Cr	*n.d.*	101	-20	33	*n.d.*	115	*n.d.*	107	40
Co	23	54	23	41	31	55	47	55	49
V	141	137	120	209	217	106	297	220	263
Sc	*n.d.*	*n.d.*	*n.d.*	*n.d.*	*n.d.*	*n.d.*	*n.d.*	*n.d.*	*n.d.*
Cu	64	34	27	41	77	50	101	59	28
Zn	96	96	109	89	120	66	91	68	75
Mo	3	*n.d.*	*n.d.*	*n.d.*	*n.d.*	*n.d.*	*n.d.*	*n.d.*	*n.d.*
W	42	251	32	83	66	199	134	86	137
Sb	*n.d.*	*n.d.*	*n.d.*	*n.d.*	*n.d.*	0.9	1.1	1.3	*n.d.*
Sn	1.7	*n.d.*	15	1.6	2.3	6.2	5.5	*n.d.*	*n.d.*

DDH: diamond drill hole; n.d.: not detected

Group	G1								
Reference	Zwanzig et al., 1999								
Sample	32-76-229	32-80-996	32-76-975	32-76-459	32-76-460	12-78-147	12-78-147	12-78-146	12-78-146
Ba	543	454	598	370	341	314	140	111	93
Cs	4.3	0.8	3.3	0.5	0.7	*n.d.*	*n.d.*	*n.d.*	*n.d.*
Rb	33	23	44	19	20	9	7	5	*n.d.*
Sr	345	371	297	241	255	279	403	188	145
Pb	7	*n.d.*	6	*n.d.*	*n.d.*	*n.d.*	8	*n.d.*	*n.d.*
Ga	24	19	20	17	19	14	19	12	16
Zr	181	106	84	107	99	99	70	31	48
Hf	5.0	2.8	2.4	3.0	2.9	2.8	2.1	0.9	1.4
Nb	7.8	6.7	7.5	6.0	5.9	6.9	5.5	2.2	4.7
Ta	0.6	1.5	0.5	0.7	0.6	1.3	1.0	0.6	0.9
Th	3.4	1.7	2.5	1.8	1.5	3.2	2.5	1.0	1.2
U	1.4	0.8	0.9	0.8	0.8	1.1	0.7	0.3	0.6
Y	30	20	23	19	23	23	22	12	17
La	17.3	14.5	12.0	10.5	10.1	14.5	10.9	4.4	7.5
Ce	42.0	30.0	27.1	24.9	23.4	30.1	23.5	10.5	16.9
Pr	5.23	3.59	3.64	3.22	3.18	3.80	2.86	1.35	2.15
Nd	21.9	15.8	16.5	14.2	14.8	16.1	12.7	5.9	9.7
Sm	5.5	3.7	4.1	3.7	3.7	3.6	3.3	1.5	2.5
Eu	1.47	1.06	1.23	1.01	1.09	0.84	1.06	0.52	0.87
Gd	5.1	3.3	4.5	3.7	4.1	3.9	3.4	1.8	2.7
Tb	0.8	0.5	0.7	0.6	0.7	0.6	0.6	0.3	0.5
Dy	4.8	3.2	3.8	3.5	3.8	3.7	3.6	1.8	2.9
Ho	1.0	0.6	0.8	0.7	0.8	0.8	0.7	0.4	0.6
Er	3.0	1.8	2.3	2.1	2.3	2.4	2.1	1.1	1.7
Tm	0.46	0.29	0.33	0.32	0.35	0.36	0.32	0.17	0.27
Yb	3.0	1.9	2.0	2.0	2.1	2.3	2.2	1.1	1.7
Lu	0.44	0.26	0.32	0.30	0.34	0.37	0.33	0.18	0.27

	G1								
Reference	**Zwanzig et al., 1999**								
Sample	32-76-229	32-80-996	32-76-975	32-76-459	32-76-460	12-78-147	12-78-147	12-78-146	12-78-146
La/Sm_{CN}	2.03	2.56	1.90	1.84	1.76	2.60	2.12	1.85	1.96
Gd/Yb_{CN}	1.40	1.47	1.82	1.50	1.59	1.37	1.28	1.30	1.34
La/Yb_{CN}	4.11	5.62	4.21	3.71	3.44	4.44	3.50	2.77	3.22
Eu/Eu*	0.85	0.93	0.88	0.84	0.86	0.69	0.96	0.97	1.03
Ce/Ce*	1.08	1.02	1.00	1.05	1.01	0.99	1.03	1.05	1.03
Zr/Y	6.0	5.3	3.6	5.5	4.4	4.2	3.1	2.6	2.8
Ti/Zr	22	38	67	39	45	23	82	74	102
Al_2O_3/TiO_2	35	25	20	23	21	39	17	49	20
Zr/Nb	23	16	11	18	17	14	13	14	10
Zr/Zr*	0.95	0.80	0.59	0.85	0.77	0.75	0.62	0.59	0.56
Zr/Sm_{PM}	1.31	1.15	0.82	1.15	1.06	1.09	0.84	0.80	0.77
Zr/Nd_{PM}	1.01	0.82	0.63	0.92	0.82	0.75	0.67	0.64	0.61
Ti/Ti*	0.37	0.54	0.60	0.54	0.53	0.32	0.75	0.59	0.80
Ti/Gd_{PM}	0.63	1.02	1.30	0.96	0.99	0.46	1.21	0.94	1.38
Ti/Sm_{PM}	0.26	0.39	0.49	0.40	0.42	0.22	0.61	0.53	0.70
Nb/Nb*	0.37	0.49	0.50	0.50	0.55	0.37	0.38	0.38	0.56
Nb/Th_{PM}	0.30	0.52	0.40	0.45	0.52	0.29	0.29	0.28	0.51
Nb/La_{PM}	0.45	0.46	0.62	0.56	0.58	0.47	0.51	0.50	0.62
Mg#	38	52	37	32	37	54	35	57	46
ΣLREE	98.41	71.88	68.96	61.20	60.38	72.81	57.78	25.97	42.20
ΣHREE	43.44	28.67	33.53	28.92	33.17	33.86	32.19	16.85	24.78

Group					**G1**				
Reference					**Zwanzig et al., 1999**				
Sample	52-76-876	52-76-126	52-76-877	32-78-5060	32-76-146	32-76-59	52-77-1309	52-77-1326	52-76-223
Easting (m)	376886	377075	377395	370263	370080	367400	409445	409237	399207
Northing (m)	6294213	6292326	6293913	6294284	6294053	6291595	6296367	6296198	6295459
DDH	Outcrop	Outcrop	Outcrop	Outcrop	Outcrop	Outcrop	Outcrop	Outcrop	Outcrop
Depth (m)	-	-	-	-	-	-	-	-	-
SiO_2	47.39	52.91	47.35	49.10	49.40	52.12	56.67	61.44	57.83
Al_2O_3	16.63	14.60	14.48	17.14	17.48	18.05	16.81	18.18	17.33
TiO_2	0.76	0.96	1.11	0.65	0.68	0.98	0.75	0.61	0.88
Fe_2O_3	10.05	10.03	12.95	9.03	9.13	11.30	8.24	6.35	9.21
MnO	0.14	0.20	0.23	0.16	0.15	0.18	0.10	0.08	0.13
MgO	8.87	6.05	8.82	8.44	8.32	4.36	4.41	2.33	4.47
CaO	12.31	9.77	11.63	12.87	11.69	8.88	5.83	5.89	5.56
Na_2O	2.05	4.77	1.63	1.85	2.28	3.30	6.74	4.27	3.62
K_2O	1.58	0.44	1.56	0.58	0.68	0.55	0.26	0.64	0.77
P_2O_5	0.22	0.27	0.25	0.17	0.19	0.28	0.18	0.20	0.20
LOI	1.83	1.19	1.21	1.57	1.30	0.80	0.81	1.33	2.92
Total	100	100	100	100	100	100	100	100	100
Ni	59	54	51	59	52	*n.d.*	44	27	*17*
Cr	290	200	274	229	214	22	39	26	37
Co	46	49	51	46	56	38	67	54	35
V	236	274	295	197	209	238	170	106	187
Sc	*n.d.*	*n.d.*	*n.d.*	*n.d.*	*n.d.*	*n.d.*	*n.d.*	*n.d.*	*n.d.*
Cu	70	139	93	88	103	36	23	*n.d.*	41
Zn	91	67	78	88	78	99	50	80	69
Mo	*n.d.*	*n.d.*	*n.d.*	*n.d.*	*n.d.*	*n.d.*	*n.d.*	*n.d.*	*n.d.*
W	98	172	109	84	90	118	273	303	115
Sb	1.9	*n.d.*	*n.d.*	0.7	*n.d.*	*n.d.*	0.7	*n.d.*	0.7
Sn	*n.d.*	1.0	1.2	*n.d.*	1.0	1.9	2.0	1.1	*n.d.*

Group	G1								
Reference	Zwanzig et al., 1999								
Sample	52-76-876	52-76-126	52-76-877	32-78-5060	32-76-146	32-76-59	52-77-1309	52-77-1326	52-76-223
Ba	695	211	523	215	407	396	109	466	298
Cs	0.7	*n.d.*	0.5	*n.d.*	*n.d.*	*n.d.*	*n.d.*	*n.d.*	*n.d.*
Rb	28	4	31	10	8	8	4	9	*13*
Sr	825	339	674	567	626	711	222	428	399
Pb	*n.d.*	*n.d.*	*n.d.*	5	*n.d.*	*n.d.*	*n.d.*	*n.d.*	*n.d.*
Ga	17	15	16	17	16	21	20	19	18
Zr	54	63	63	59	64	80	85	121	99
Hf	1.9	2.1	2.2	1.7	1.8	2.3	2.5	3.5	2.9
Nb	6.0	6.6	6.5	4.3	4.9	6.8	6.8	7.8	5.6
Ta	0.6	1.2	0.8	0.6	0.7	0.9	1.7	1.9	0.7
Th	2.9	2.1	2.4	1.8	2.0	2.0	1.6	2.5	1.9
U	0.9	0.9	1.0	0.7	0.7	0.6	1.1	1.5	0.7
Y	14	17	18	16	15	20	19	19	22
La	16.1	11.7	15.9	15.2	13.5	15.2	12.8	14.9	11.5
Ce	37.4	27.8	37.1	31.5	31.5	32.2	25.0	33.6	26.6
Pr	4.81	3.49	4.66	4.35	4.39	4.03	3.14	3.98	3.16
Nd	19.4	15.5	20.5	19.6	19.6	18.4	14.4	15.7	12.8
Sm	4.0	3.8	4.8	4.3	4.4	4.0	3.3	3.3	3.1
Eu	1.22	1.25	1.44	1.32	1.29	1.24	0.95	0.98	0.96
Gd	3.8	3.9	4.6	3.9	4.1	4.0	3.2	3.4	3.3
Tb	0.5	0.6	0.7	0.5	0.5	0.6	0.5	0.5	0.6
Dy	2.4	3.1	3.4	2.7	2.6	3.4	3.2	2.9	3.2
Ho	0.5	0.6	0.7	0.5	0.5	0.7	0.7	0.6	0.7
Er	1.4	1.8	1.9	1.4	1.4	2.0	1.9	1.8	2.2
Tm	0.18	0.25	0.26	0.19	0.20	0.29	0.30	0.26	0.32
Yb	1.1	1.6	1.7	1.2	1.2	1.9	1.9	1.7	2.1
Lu	0.18	0.23	0.24	0.16	0.17	0.28	0.28	0.28	0.36

Group	G1								
Reference	Zwanzig et al., 1999								
Sample	52-76-876	52-76-126	52-76-877	32-78-5060	32-76-146	32-76-59	52-77-1309	52-77-1326	52-76-223
La/Sm_{CN}	2.57	2.00	2.15	2.28	2.01	2.44	2.50	2.95	2.43
Gd/Yb_{CN}	2.94	2.07	2.30	2.69	2.83	1.69	1.39	1.66	1.29
La/Yb_{CN}	10.84	5.31	6.90	9.17	8.20	5.63	4.87	6.34	3.89
Eu/Eu*	0.96	1.00	0.94	0.99	0.94	0.95	0.90	0.90	0.92
Ce/Ce*	1.04	1.07	1.05	0.95	1.00	1.01	0.96	1.07	1.08
Zr/Y	3.8	3.6	3.4	3.6	4.3	4.0	4.4	6.5	4.5
Ti/Zr	83	90	102	65	63	73	52	30	51
Al_2O_3/TiO_2	22	15	13	26	26	18	22	30	20
Zr/Nb	9	10	10	14	13	12	13	15	18
Zr/Zr*	0.35	0.48	0.37	0.37	0.40	0.53	0.71	0.97	0.92
Zr/Sm_{PM}	0.54	0.67	0.53	0.54	0.59	0.79	1.02	1.47	1.29
Zr/Nd_{PM}	0.34	0.50	0.38	0.37	0.40	0.53	0.72	0.94	0.95
Ti/Ti*	0.53	0.65	0.63	0.43	0.44	0.66	0.64	0.50	0.72
Ti/Gd_{PM}	2.00	1.71	1.85	1.52	1.60	1.42	1.11	1.01	1.14
Ti/Sm_{PM}	0.40	0.54	0.48	0.32	0.33	0.52	0.48	0.39	0.59
Nb/Nb*	0.31	0.48	0.38	0.30	0.34	0.44	0.54	0.46	0.44
Nb/Th_{PM}	0.27	0.41	0.35	0.31	0.32	0.44	0.55	0.40	0.39
Nb/La_{PM}	0.37	0.56	0.41	0.28	0.36	0.45	0.52	0.52	0.49
Mg#	64	54	57	65	64	43	51	42	49
ΣLREE	86.76	67.32	88.92	80.14	78.71	78.99	62.75	75.74	61.36
ΣHREE	20.64	25.62	27.30	22.75	21.58	29.04	27.90	26.67	31.51

Group					**G1**				
Reference					**Zwanzig et al., 1999**				
Sample	52-76-684	52-76-650	52-76-668	52-76-838	52-77-1568	52-77-1790	32-78-5082	52-76-025	52-76-642
Easting (m)	376886	377075	377395	370263	370080	399003	357675	376309	399598
Northing (m)	6294213	6292326	6293913	6294284	6294053	6282542	6287567	6293626	6296733
DDH	Outcrop	Outcrop	Outcrop	Outcrop	Outcrop	Outcrop	Outcrop	Outcrop	Outcrop
Depth (m)	-	-	-	-	-	-	-	-	-
SiO_2	55.17	58.35	61.67	56.51	56.72	49.33	51.29	50.38	57.44
Al_2O_3	19.09	16.33	17.34	16.56	16.38	19.55	15.00	16.40	17.16
TiO_2	0.71	0.71	0.75	0.64	0.71	0.60	0.75	1.04	0.80
Fe_2O_3	5.74	7.92	5.15	7.94	8.93	10.40	10.54	11.11	8.43
MnO	0.07	0.15	0.07	0.12	0.13	0.19	0.17	0.17	0.15
MgO	4.43	4.04	2.32	5.31	4.35	4.49	8.95	5.88	4.28
CaO	8.61	7.94	6.65	8.24	8.28	12.40	8.79	10.34	7.34
Na_2O	5.47	3.25	5.17	3.70	3.52	2.59	2.96	2.19	3.08
K_2O	0.50	1.04	0.62	0.77	0.85	0.31	1.35	2.16	1.00
P_2O_5	0.21	0.27	0.26	0.20	0.14	0.13	0.19	0.34	0.31
LOI	1.92	2.30	0.71	1.94	1.16	1.62	1.27	1.55	1.79
Total	100	100	100	100	100	100	100	100	100
Ni	34	64	13	78	223	21	133	31	43
Cr	116	77	80	94	66	37	464	161	66
Co	38	42	28	43	51	41	58	45	37
V	133	123	147	146	187	267	286	263	131
Sc	*n.d.*	*n.d.*	*n.d.*	*n.d.*	*n.d.*	*n.d.*	*n.d.*	*n.d.*	*n.d.*
Cu	34	1000	56	19	59	68	107	98	51
Zn	67	121	38	65	100	104	88	89	136
Mo	*n.d.*	2	*n.d.*	*n.d.*	*n.d.*	*n.d.*	*n.d.*	*n.d.*	*n.d.*
W	173	114	132	191	197	120	136	123	119
Sb	*n.d.*	0.8	*n.d.*	0.6	*n.d.*	0.7	*n.d.*	2.0	0.7
Sn	1.3	4.4	1.4	*n.d.*	2.1	2.7	*n.d.*	1.2	*n.d.*

Group	G1								
Reference	Zwanzig et al., 1999								
Sample	52-76-684	52-76-650	52-76-668	52-76-838	52-77-1568	52-77-1790	32-78-5082	52-76-025	52-76-642
Ba	264	455	226	269	303	107	757	880	374
Cs	*n.d.*	*n.d.*	*n.d.*	*n.d.*	*n.d.*	*n.d.*	*n.d.*	0.9	*n.d.*
Rb	8	18	10	13	16	4	28	37	17
Sr	327	400	377	266	337	595	496	1040	521
Pb	*n.d.*	*n.d.*	*n.d.*	*n.d.*	*n.d.*	8	*n.d.*	6	5
Ga	13	17	18	14	18	19	15	19	20
Zr	122	108	118	79	77	25	33	73	104
Hf	3.8	3.3	3.6	2.5	2.3	0.8	1.0	2.3	3.1
Nb	7.1	6.6	7.1	5.7	5.0	1.4	2.6	8.7	8.0
Ta	1.6	0.9	1.0	1.1	1.2	0.6	0.7	1.0	0.9
Th	2.7	2.1	2.3	1.9	1.2	1.3	0.6	2.6	2.2
U	1.4	1.5	1.4	1.3	1.0	3.2	0.4	1.1	1.1
Y	24	22	22	19	18	14	17	19	20
La	14.7	14.7	14.0	10.3	8.8	4.9	5.5	17.6	17.4
Ce	32.5	34.0	33.9	23.8	19.7	11.1	12.9	39.6	38.4
Pr	3.98	4.13	4.15	2.82	2.46	1.52	1.79	4.87	4.37
Nd	17.0	16.1	16.3	11.9	10.8	7.3	8.9	21.6	18.6
Sm	3.7	3.6	3.6	2.8	2.5	1.8	2.4	4.6	4.1
Eu	1.02	1.07	1.13	0.89	0.83	0.78	0.83	1.41	1.20
Gd	3.9	3.7	3.8	3.4	2.8	2.1	2.6	4.5	3.6
Tb	0.6	0.6	0.6	0.5	0.5	0.4	0.4	0.6	0.6
Dy	3.8	3.2	3.3	3.1	2.7	2.1	2.8	3.3	3.5
Ho	0.8	0.7	0.7	0.7	0.6	0.5	0.6	0.7	0.7
Er	2.4	2.2	2.2	2.0	1.8	1.4	1.7	1.9	2.0
Tm	0.39	0.32	0.31	0.30	0.27	0.21	0.26	0.26	0.30
Yb	2.3	2.0	2.0	2.0	1.7	1.3	1.7	1.7	2.0
Lu	0.36	0.35	0.34	0.30	0.29	0.21	0.25	0.24	0.31

Group	G1								
Reference	Zwanzig et al., 1999								
Sample	52-76-684	52-76-650	52-76-668	52-76-838	52-77-1568	52-77-1790	32-78-5082	52-76-025	52-76-642
La/Sm_{CN}	2.59	2.66	2.50	2.35	2.27	1.75	1.47	2.47	2.73
Gd/Yb_{CN}	1.39	1.49	1.62	1.41	1.32	1.29	1.29	2.17	1.50
La/Yb_{CN}	4.57	5.18	5.15	3.77	3.65	2.63	2.37	7.45	6.24
Eu/Eu*	0.83	0.90	0.93	0.88	0.96	1.22	1.01	0.95	0.95
Ce/Ce*	1.04	1.07	1.09	1.08	1.04	1.00	1.00	1.05	1.08
Zr/Y	5.0	4.8	5.3	4.2	4.4	1.8	1.9	3.9	5.2
Ti/Zr	34	38	38	47	54	139	133	84	45
Al_2O_3/TiO_2	27	23	23	26	23	33	20	16	21
Zr/Nb	17	16	17	14	15	19	13	8	13
Zr/Zr*	0.89	0.82	0.88	0.78	0.86	0.40	0.42	0.42	0.69
Zr/Sm_{PM}	1.32	1.20	1.30	1.11	1.23	0.56	0.55	0.63	1.01
Zr/Nd_{PM}	0.88	0.82	0.88	0.81	0.88	0.42	0.46	0.41	0.69
Ti/Ti*	0.52	0.53	0.54	0.54	0.70	0.70	0.76	0.61	0.57
Ti/Gd_{PM}	0.85	0.96	1.09	0.89	1.15	1.24	1.26	1.70	1.12
Ti/Sm_{PM}	0.40	0.41	0.44	0.47	0.60	0.70	0.65	0.47	0.41
Nb/Nb*	0.41	0.43	0.45	0.47	0.55	0.20	0.50	0.47	0.47
Nb/Th_{PM}	0.35	0.41	0.40	0.41	0.54	0.14	0.53	0.44	0.48
Nb/La_{PM}	0.48	0.45	0.50	0.55	0.57	0.28	0.46	0.49	0.46
Mg#	60	50	47	57	49	46	63	51	50
ΣLREE	76.73	77.36	76.92	55.91	47.83	29.58	34.88	94.24	87.59
ΣHREE	34.86	31.79	31.61	27.97	25.40	20.14	24.97	27.57	29.39

Group					**G1**				
Reference				**Chapter 2**				**This study**	
Sample	MG11-004	MG11-035	MG11-072	MG11-115	MG11-118	MG11-122	MG11-125	LL13-01	LL13-02
Easting (m)	383384	381336	380727	378578	378578	378810	378810	383130	383734
Northing (m)	6306404	6308189	6307854	6306250	6306250	6305494	6305494	6291830	6291960
DDH	Outcrop	MG11-41	MG11-14	MG11-48	MG11-48	MG11-53	MG11-53	BT11-18	BT12-08
Depth (m)	-	250	593	348	401	207	299	89	125
SiO_2	57.04	55.68	58.65	62.10	77.17	57.71	46.24	50.48	52.15
Al_2O_3	13.36	16.89	18.19	13.22	10.71	9.51	7.92	13.75	15.53
TiO_2	0.44	0.87	0.75	0.64	0.38	0.36	0.33	0.81	1.13
Fe_2O_3	13.57	9.74	8.07	11.45	4.25	24.93	32.55	11.61	11.39
MnO	0.21	0.16	0.09	0.13	0.04	0.15	0.24	0.19	0.19
MgO	7.03	4.95	4.49	4.98	1.57	1.97	2.40	8.32	6.44
CaO	5.70	8.38	3.45	2.86	1.37	4.22	9.22	11.14	8.50
Na_2O	1.32	2.65	1.82	0.41	0.25	0.69	0.35	3.01	3.40
K_2O	1.18	0.51	4.15	4.13	4.15	0.36	0.61	0.41	0.93
P_2O_5	0.15	0.16	0.34	0.08	0.10	0.11	0.14	0.29	0.33
LOI	2.50	0.98	2.12	1.36	1.52	-0.51	1.91	2.00	7.42
Total	100	100	100	100	100	100	100	100	100
Ni	170	90	*n.d.*	80	20	*n.d.*	*n.d.*	90	40
Cr	620	200	30	100	*n.d.*	30	30	310	100
Co	51	27	18	18	10	8	9	43	32
V	122	144	129	123	51	77	80	270	259
Sc	19	24	11	25	16	11	12	37	24
Cu	*n.d.*	*n.d.*	110	350	490	150	140	*n.d.*	60
Zn	220	120	180	340	250	140	80	80	90
Mo	*n.d.*	*n.d.*	2.0	5.0	*n.d.*	3.0	3.0	*n.d.*	*n.d.*
W	*n.d.*	*n.d.*	1.0	24	13	2.0	*n.d.*	*n.d.*	0.5
Sb	*n.d.*	*n.d.*	2.0	*n.d.*	0.9	*n.d.*	34	*n.d.*	*n.d.*
Sn	*n.d.*	*n.d.*	*n.d.*	*n.d.*	*n.d.*	*n.d.*	1.0	*n.d.*	*n.d.*

Group					G1				
Reference				Chapter 2				This study	
Sample	MG11-004	MG11-035	MG11-072	MG11-115	MG11-118	MG11-122	MG11-125	LL13-01	LL13-02
Ba	179	74	749	618	1056	98	319	149	535
Cs	0.9	1.2	2.3	2.4	0.6	*n.d.*	1.4	*n.d.*	0.6
Rb	24	7	66	85	43	6	14	7	19
Sr	86	270	139	127	124	21	104	708	468
Pb	*n.d.*	*n.d.*	65	31	303	*n.d.*	*n.d.*	7	5
Ga	15	17	20	18	10	12	8	16	19
Zr	98	81	118	57	81	70	57	63	79
Hf	2.3	2.1	3.0	1.4	2.2	1.8	1.3	1.5	2.0
Nb	4.0	4.0	9.0	4.0	3.0	3.0	3.0	5.1	9.7
Ta	0.4	0.3	0.6	0.3	0.2	0.1	0.1	0.2	0.5
Th	2.4	1.3	2.4	0.8	1.9	1.3	1.2	2.9	2.2
U	1.0	0.5	1.3	0.5	1.1	1.1	0.8	1.1	0.9
Y	11	15	23	7	18	18	21	14	15
La	12.8	10.3	17.3	9.0	10.8	10.1	11.0	18.4	17.9
Ce	29.9	23.7	39.8	21.3	24.1	23.0	24.1	37.6	39.3
Pr	3.49	2.92	4.73	2.56	3.03	2.84	3.08	4.84	5.09
Nd	14.1	12.1	19.9	11.5	13.5	12.5	13.1	20.2	21.0
Sm	3.0	2.9	4.5	2.7	3.6	3.0	3.2	4.2	4.5
Eu	0.69	1.08	1.35	0.64	0.61	0.76	0.71	1.21	1.25
Gd	2.4	3.2	4.5	2.3	3.5	3.2	3.2	3.4	3.6
Tb	0.4	0.5	0.8	0.3	0.6	0.5	0.6	0.5	0.5
Dy	2.1	3.1	4.4	1.6	3.5	3.1	3.6	2.7	2.9
Ho	0.4	0.6	0.9	0.3	0.8	0.7	0.8	0.5	0.6
Er	1.2	1.8	2.7	0.7	2.2	2.1	2.3	1.4	1.6
Tm	0.18	0.27	0.43	0.12	0.35	0.33	0.36	0.21	0.23
Yb	1.3	1.7	2.9	0.8	2.3	2.1	2.4	1.3	1.5
Lu	0.20	0.27	0.46	0.15	0.37	0.32	0.39	0.19	0.22

Group	G1								
Reference	Chapter 2							This study	
Sample	MG11-004	MG11-035	MG11-072	MG11-115	MG11-118	MG11-122	MG11-125	LL13-01	LL13-02
La/Sm_{CN}	2.75	2.29	2.48	2.15	1.94	2.17	2.22	2.85	2.57
Gd/Yb_{CN}	1.53	1.56	1.28	2.38	1.26	1.26	1.10	2.12	2.04
La/Yb_{CN}	7.06	4.35	4.28	8.07	3.37	3.45	3.29	9.85	8.73
Eu/Eu*	0.79	1.08	0.92	0.79	0.53	0.75	0.68	0.98	0.95
Ce/Ce*	1.10	1.06	1.08	1.09	1.03	1.05	1.02	0.98	1.01
Zr/Y	8.9	5.4	5.1	8.1	4.5	3.9	2.7	4.4	5.2
Ti/Zr	26	63	37	65	27	31	34	76	79
Al_2O_3/TiO_2	30	19	24	21	28	26	24	17	14
Zr/Nb	25	20	13	14	27	23	19	12	8
Zr/Zr*	0.87	0.79	0.72	0.59	0.67	0.66	0.51	0.40	0.47
Zr/Sm_{PM}	1.30	1.11	1.04	0.84	0.90	0.93	0.71	0.60	0.70
Zr/Nd_{PM}	0.85	0.82	0.73	0.61	0.73	0.69	0.53	0.38	0.46
Ti/Ti*	0.49	0.69	0.44	0.77	0.38	0.35	0.33	0.59	0.74
Ti/Gd_{PM}	0.91	1.42	0.70	2.20	0.45	0.49	0.38	1.69	2.01
Ti/Sm_{PM}	0.30	0.63	0.34	0.49	0.22	0.26	0.22	0.41	0.50
Nb/Nb*	0.26	0.40	0.51	0.54	0.24	0.30	0.30	0.25	0.55
Nb/Th_{PM}	0.22	0.41	0.49	0.66	0.21	0.30	0.33	0.23	0.57
Nb/La_{PM}	0.31	0.39	0.52	0.44	0.28	0.30	0.27	0.28	0.54
Mg#	51	50	52	46	42	14	13	59	53
ΣLREE	66.38	56.20	92.08	50.00	59.14	55.40	58.39	89.86	92.67
ΣHREE	16.78	23.24	35.59	10.97	28.12	27.15	31.45	21.07	22.82

Group	G1								
Reference	**This study**					**Beaumont-Smith, 2007**			
Sample	LL13-03	LL13-04	LL13-06	LL13-10	LL13-25	103-99-1078	103-00-1213	103-00-1233	103-01-1606
Easting (m)	381180	412483	412137	412062	412389	376784	362235	359235	357791
Northing (m)	6292097	6307647	6307706	6307765	6307647	6291858	6290477	6289788	6288335
DDH	LW12-05	FL12-03	FL12-07	FL12-05	FL12-16	Outcrop	Outcrop	Outcrop	Outcrop
Depth (m)	85	38	75	86	28	-	-	-	-
SiO_2	52.59	54.45	66.70	66.09	53.26	58.34	51.22	58.53	56.40
Al_2O_3	15.91	16.03	16.03	16.65	15.06	16.51	13.39	16.39	16.06
TiO_2	1.03	0.68	0.80	0.81	1.00	0.87	0.94	0.86	0.86
Fe_2O_3	10.61	8.15	8.03	7.39	9.68	8.50	13.73	9.93	9.52
MnO	0.17	0.13	0.02	0.02	0.11	0.15	0.15	0.15	0.13
MgO	5.60	5.88	2.58	2.54	7.33	2.74	7.91	3.92	4.73
CaO	9.07	8.17	0.96	1.07	6.43	5.46	9.43	5.52	7.13
Na_2O	4.34	4.02	1.49	1.80	3.88	3.97	2.40	0.34	4.40
K_2O	0.43	2.00	3.25	3.52	2.52	3.01	0.54	3.87	0.57
P_2O_5	0.26	0.49	0.14	0.13	0.73	0.45	0.28	0.47	0.22
LOI	1.07	2.76	4.59	3.85	4.07	2.85	4.74	1.21	0.50
Total	100	100	100	100	100	100	100	100	100
Ni	40	60	80	100	130	*n.d.*	32	*n.d.*	32
Cr	130	120	230	280	180	13	275	125	90
Co	30	27	14	14	34	17	31	22	34
V	276	161	163	161	207	165	251	151	209
Sc	28	21	23	25	26	17	42	25	31
Cu	60	30	50	30	140	162	27	75	45
Zn	80	70	70	70	90	97	60	802	78
Mo	*n.d.*	*n.d.*	5.0	3.0	*n.d.*	*n.d.*	*n.d.*	*n.d.*	2.5
W	*n.d.*	0.6	1.0	1.3	*n.d.*	1.8	2.2	1.3	*n.d.*
Sb	*n.d.*	*n.d.*	*n.d.*	*n.d.*	*n.d.*	0.9	0.7	0.5	0.4
Sn	*n.d.*	*n.d.*	*n.d.*	*n.d.*	*n.d.*	1.2	*n.d.*	*n.d.*	1.6

Group					G1				
Reference	This study					Beaumont-Smith, 2007			
Sample	LL13-03	LL13-04	LL13-06	LL13-10	LL13-25	103-99-1078	103-00-1213	103-00-1233	103-01-1606
Ba	184	1178	422	450	552	1060	145	527	217
Cs	*n.d.*	6.6	2.6	3.7	33	0.8	*n.d.*	1.0	*n.d.*
Rb	5	32	84	99	51	*n.d.*	*n.d.*	*n.d.*	*n.d.*
Sr	335	1056	90	103	616	677	429	83	354
Pb	*n.d.*	9	*n.d.*	6	5	6	*n.d.*	12	*n.d.*
Ga	19	18	18	19	19	20	14	18	18
Zr	73	110	89	101	70	93	79	93	90
Hf	1.7	2.7	2.1	2.5	2.1	2.8	2.3	2.8	2.5
Nb	4.8	8.8	4.5	5.7	7.8	8.8	7.9	6.5	4.2
Ta	0.2	0.3	0.3	0.3	0.2	0.4	0.4	0.3	0.3
Th	1.5	3.2	2.2	1.9	1.9	3.0	3.1	2.3	1.4
U	0.5	2.3	3.8	3.1	1.3	1.3	1.0	0.9	0.6
Y	13	18	19	19	16	30	17	28	22
La	9.7	40.0	12.4	11.3	19.8	20.6	22.4	17.8	8.5
Ce	22.3	91.2	26.3	23.9	50.8	44.5	45.4	39.2	19.1
Pr	2.95	12.10	3.64	3.28	7.53	5.83	5.43	5.06	2.53
Nd	12.7	50.6	13.9	13.2	34.6	24.7	22.8	22.1	11.6
Sm	2.9	10.0	3.4	3.2	8.2	5.1	5.0	5.1	2.9
Eu	0.87	2.57	0.88	0.83	1.95	1.52	1.76	1.40	0.92
Gd	2.5	7.1	2.9	2.9	5.8	5.5	4.4	4.8	3.1
Tb	0.4	0.9	0.5	0.5	0.8	0.8	0.6	0.8	0.6
Dy	2.6	4.1	3.1	3.4	3.7	4.7	3.3	5.2	3.7
Ho	0.5	0.7	0.7	0.7	0.6	1.0	0.7	1.1	0.8
Er	1.4	1.7	2.0	2.1	1.6	2.9	1.7	3.1	2.4
Tm	0.21	0.24	0.32	0.34	0.20	0.43	0.24	0.45	0.37
Yb	1.3	1.5	2.1	2.2	1.2	2.8	1.5	3.1	2.3
Lu	0.20	0.21	0.33	0.32	0.15	0.46	0.22	0.47	0.34

Group					G1				
Reference	This study					Beaumont-Smith, 2007			
Sample	LL13-03	LL13-04	LL13-06	LL13-10	LL13-25	103-99-1078	103-00-1213	103-00-1233	103-01-1606
La/Sm_{CN}	2.17	2.59	2.35	2.26	1.56	2.59	2.92	2.25	1.88
Gd/Yb_{CN}	1.57	3.93	1.15	1.10	4.03	1.58	2.34	1.29	1.14
La/Yb_{CN}	5.32	19.13	4.26	3.70	12.04	5.18	10.39	4.18	2.70
Eu/Eu*	1.00	0.93	0.86	0.82	0.87	0.88	1.15	0.87	0.93
Ce/Ce*	1.02	1.02	0.96	0.96	1.02	1.00	1.01	1.01	1.01
Zr/Y	5.4	6.0	4.6	5.2	4.3	3.1	4.6	3.3	4.2
Ti/Zr	84	36	51	46	80	54	69	55	56
Al_2O_3/TiO_2	15	23	20	21	15	19	14	19	19
Zr/Nb	15	13	20	18	9	11	10	14	22
Zr/Zr*	0.69	0.28	0.75	0.89	0.24	0.48	0.43	0.50	0.90
Zr/Sm_{PM}	1.01	0.44	1.04	1.24	0.34	0.72	0.63	0.72	1.23
Zr/Nd_{PM}	0.70	0.27	0.78	0.94	0.25	0.46	0.42	0.51	0.95
Ti/Ti*	1.05	0.23	0.71	0.75	0.42	0.44	0.49	0.50	0.76
Ti/Gd_{PM}	2.21	1.24	1.02	1.00	2.24	0.84	1.64	0.79	1.07
Ti/Sm_{PM}	0.76	0.14	0.47	0.51	0.24	0.35	0.39	0.36	0.62
Nb/Nb*	0.45	0.28	0.31	0.44	0.46	0.40	0.34	0.37	0.44
Nb/Th_{PM}	0.41	0.36	0.27	0.39	0.55	0.38	0.33	0.37	0.39
Nb/La_{PM}	0.49	0.22	0.36	0.50	0.39	0.42	0.35	0.36	0.49
Mg#	51	59	39	41	60	39	53	44	50
ΣLREE	53.90	213.56	63.44	58.66	128.61	107.66	107.15	95.49	48.73
ΣHREE	20.08	27.74	28.37	28.95	24.64	42.96	25.30	42.41	32.02

Group	G1								
Reference	Beaumont-Smith, 2007								
Sample	103-01-1615	103-99-1127	103-99-1058	103-02-1801a	103-02-1801b	103-03-1862	94-00-61	95-00-14	95-01-46
Easting (m)	357059	411461	383728	373431	373431	370702	383274	380829	376500
Northing (m)	6289124	6293692	6291326	6302347	6302347	6300505	6291984	6307749	6303836
DDH	Outcrop	Outcrop	Outcrop	Outcrop	Outcrop	Outcrop	Outcrop	Outcrop	Outcrop
Depth (m)	-	-	-	-	-	-	-	-	-
SiO_2	56.01	59.43	60.42	61.34	54.42	55.07	54.05	54.46	53.12
Al_2O_3	15.39	16.36	14.38	16.05	14.23	14.91	17.51	15.57	18.61
TiO_2	0.75	0.66	0.71	0.89	0.61	1.19	1.03	0.70	0.90
Fe_2O_3	8.88	4.99	9.84	9.87	12.31	8.72	9.72	8.15	10.82
MnO	0.16	0.08	0.15	0.19	0.28	0.10	0.15	0.15	0.17
MgO	6.11	4.14	5.33	3.06	6.65	7.84	4.58	7.06	4.25
CaO	7.69	7.47	2.55	4.43	9.12	9.34	8.70	9.04	9.83
Na_2O	4.54	6.47	2.09	0.78	1.42	1.35	2.88	3.75	1.98
K_2O	0.28	0.22	4.31	3.23	0.82	1.36	1.13	0.87	0.20
P_2O_5	0.19	0.19	0.23	0.16	0.14	0.11	0.25	0.23	0.13
LOI	0.43	0.81	1.55	2.29	0.88	1.48	1.10	0.95	0.97
Total	100	100	100	100	100	100	100	100	100
Ni	84	60	48	37	98	72	34	81	*n.d.*
Cr	320	51	53	13	342	92	103	206	*n.d.*
Co	33	23	24	16	36	31	23	29	26
V	180	142	134	158	158	266	204	152	187
Sc	28	20	24	25	34	23	22	27	23
Cu	45	*n.d.*	42	123	*n.d.*	*n.d.*	11	74	16
Zn	84	*n.d.*	172	395	207	90	74	76	73
Mo	*n.d.*	*n.d.*	*n.d.*	6.6	7.5	*n.d.*	2.4	*n.d.*	*n.d.*
W	*n.d.*	*n.d.*	0.9	2.5	1.2	*n.d.*	*n.d.*	*n.d.*	*n.d.*
Sb	2.3	0.6	*n.d.*	*n.d.*	0.4	*n.d.*	0.6	*n.d.*	*n.d.*
Sn	*n.d.*	*n.d.*	1.5	1.6	*n.d.*	2.0	*n.d.*	1.0	*n.d.*

Group	G1								
Reference	Beaumont-Smith, 2007								
Sample	103-01-1615	103-99-1127	103-99-1058	103-02-1801a	103-02-1801b	103-03-1862	94-00-61	95-00-14	95-01-46
Ba	143	110	1060	451	88	358	491	154	57
Cs	*n.d.*	*n.d.*	3	0.7	*n.d.*	7.2	*n.d.*	0.6	*n.d.*
Rb	*n.d.*	*n.d.*	*n.d.*	*n.d.*	*n.d.*	*n.d.*	*n.d.*	*n.d.*	*n.d.*
Sr	392	266	110	72	146	419	719	486	297
Pb	7	*n.d.*	*n.d.*	*n.d.*	10	*n.d.*	13	*n.d.*	*n.d.*
Ga	18	13	18	19	15	18	17	20	17
Zr	83	76	162	115	49	84	94	108	66
Hf	2.4	2.2	4.0	3.2	1.5	2.7	2.2	2.8	1.9
Nb	4.4	4.9	7.1	7.5	2.8	5.1	5.2	4.3	3.9
Ta	0.3	0.3	0.4	0.5	0.1	0.5	0.3	0.3	0.3
Th	2.2	2.4	2.3	2.1	1.0	1.3	2.8	2.3	1.2
U	0.9	0.9	1.0	1.7	0.5	0.5	0.9	1.1	0.3
Y	15	16	25	28	14	25	15	19	14
La	9.4	13.4	20.7	11.5	5.9	8.4	18.5	15.6	7.1
Ce	20.3	28.9	45.6	26.8	13.5	20.1	38.0	34.8	16.5
Pr	2.59	3.39	5.20	3.59	1.87	2.54	4.38	4.62	2.22
Nd	11.4	13.4	20.5	15.1	8.1	11.3	18.5	20.2	10.0
Sm	2.7	2.7	4.6	3.7	2.2	3.1	3.8	4.2	2.6
Eu	0.94	0.77	1.14	1.24	0.60	1.73	1.08	1.32	0.97
Gd	2.6	2.9	5.1	4.1	2.2	3.7	3.5	4.0	3.0
Tb	0.5	0.5	0.8	0.7	0.4	0.6	0.5	0.6	0.5
Dy	2.7	2.8	4.9	4.6	2.4	3.9	2.7	3.3	2.8
Ho	0.6	0.6	1.0	1.0	0.5	0.8	0.5	0.7	0.5
Er	1.7	1.6	3.3	2.9	1.6	2.4	1.5	1.9	1.6
Tm	0.24	0.24	0.53	0.44	0.25	0.35	0.21	0.25	0.22
Yb	1.5	1.6	3.8	2.6	1.6	2.2	1.3	1.7	1.4
Lu	0.23	0.24	0.62	0.41	0.25	0.33	0.19	0.24	0.20

Group	G1								
Reference	Beaumont-Smith, 2007								
Sample	103-01-1615	103-99-1127	103-99-1058	103-02-1801a	103-02-1801b	103-03-1862	94-00-61	95-00-14	95-01-46
La/Sm_{CN}	2.26	3.21	2.90	2.01	1.71	1.73	3.19	2.40	1.75
Gd/Yb_{CN}	1.45	1.51	1.12	1.28	1.16	1.38	2.22	1.94	1.77
La/Yb_{CN}	4.50	6.05	3.96	3.12	2.69	2.75	10.09	6.50	3.66
Eu/Eu*	1.08	0.84	0.72	0.97	0.83	1.56	0.91	0.98	1.05
Ce/Ce*	1.01	1.05	1.08	1.02	1.00	1.07	1.03	1.01	1.02
Zr/Y	5.4	4.6	6.4	4.1	3.5	3.4	6.1	5.6	4.8
Ti/Zr	54	52	26	45	73	84	66	39	80
Al_2O_3/TiO_2	21	25	20	18	23	12	17	22	21
Zr/Nb	19	16	23	15	17	17	18	25	17
Zr/Zr*	0.86	0.72	0.96	0.88	0.67	0.81	0.65	0.68	0.74
Zr/Sm_{PM}	1.22	1.11	1.40	1.23	0.88	1.06	0.99	1.03	1.00
Zr/Nd_{PM}	0.89	0.69	0.97	0.93	0.74	0.90	0.62	0.66	0.81
Ti/Ti*	0.71	0.66	0.43	0.58	0.79	0.70	0.79	0.46	0.79
Ti/Gd_{PM}	1.40	1.17	0.52	0.93	1.09	1.51	2.21	1.15	1.80
Ti/Sm_{PM}	0.59	0.52	0.32	0.50	0.58	0.80	0.59	0.35	0.72
Nb/Nb*	0.35	0.31	0.37	0.56	0.42	0.55	0.26	0.26	0.48
Nb/Th_{PM}	0.26	0.27	0.41	0.48	0.36	0.51	0.24	0.25	0.42
Nb/La_{PM}	0.46	0.36	0.34	0.65	0.48	0.60	0.28	0.27	0.54
Mg#	58	62	52	38	52	64	48	63	44
ΣLREE	49.94	65.57	102.82	65.96	34.46	50.90	87.83	84.79	42.52
ΣHREE	22.61	23.79	40.34	40.45	21.01	35.26	22.28	27.85	20.90

Group	**G1**								
Reference	**Beaumont-Smith, 2007**								
Sample	95-01-82	95-01-103	95-01-268	95-01-337	95-01-247	95-01-201	94-00-64	95-01-22	94-00-62
Easting (m)	375730	374235	372225	370063	370648	372662	383006	377355	383275
Northing (m)	6303565	6302525	6300754	6299988	6300403	6301522	6292443	6304777	6292002
DDH	Outcrop	Outcrop	Outcrop	Outcrop	Outcrop	Outcrop	Outcrop	Outcrop	Outcrop
Depth (m)	-	-	-	-	-	-	-	-	-
SiO_2	48.59	57.49	51.45	55.94	68.44	59.05	52.52	61.30	52.10
Al_2O_3	20.74	19.13	18.25	11.82	13.66	15.72	14.65	9.61	15.47
TiO_2	1.00	0.80	1.06	1.01	0.52	0.58	1.14	0.43	0.98
Fe_2O_3	13.25	7.65	12.68	10.35	8.06	15.22	12.23	19.99	11.82
MnO	0.16	0.14	0.18	0.16	0.07	0.11	0.19	0.30	0.20
MgO	3.61	2.70	3.90	7.17	1.42	2.30	5.80	1.49	7.23
CaO	7.00	9.20	9.39	9.90	2.00	2.91	9.59	5.09	9.55
Na_2O	3.25	1.47	2.64	3.05	3.37	2.29	3.23	0.73	2.37
K_2O	2.26	1.32	0.32	0.43	2.32	1.65	0.39	0.90	0.14
P_2O_5	0.14	0.11	0.14	0.16	0.14	0.16	0.25	0.15	0.13
LOI	1.50	2.53	0.72	1.22	0.61	0.36	0.80	1.03	1.74
Total	100	100	100	100	100	100	100	100	100
Ni	22	22	*n.d.*	246	*n.d.*	*n.d.*	40	*n.d.*	32
Cr	28	43	14	880	13	15	119	16	40
Co	38	28	30	54	11	9	34	9	40
V	174	160	273	256	85	75	268	71	255
Sc	26	30	39	39	17	16	40	14	43
Cu	362	156	140	110	49	28	95	96	233
Zn	129	61	102	72	87	97	104	84	93
Mo	*n.d.*	*n.d.*	*n.d.*	*n.d.*	2.3	2.5	3.1	3.3	*n.d.*
W	16	1.7	*n.d.*	*n.d.*	*n.d.*	0.5	*n.d.*	0.7	*n.d.*
Sb	*n.d.*	*n.d.*	*n.d.*	*n.d.*	*n.d.*	*n.d.*	0.8	0.3	0.6
Sn	*n.d.*	*n.d.*	*n.d.*	*n.d.*	1.1	1.2	*n.d.*	*n.d.*	*n.d.*

Group	G1								
Reference	Beaumont-Smith, 2007								
Sample	95-01-82	95-01-103	95-01-268	95-01-337	95-01-247	95-01-201	94-00-64	95-01-22	94-00-62
Ba	554	201	58	795	757	779	246	184	29
Cs	1.2	0.3	*n.d.*	1.2	1.6	1.2	*n.d.*	0.9	*n.d.*
Rb	*n.d.*	*n.d.*	*n.d.*	*n.d.*	*n.d.*	*n.d.*	*n.d.*	*n.d.*	*n.d.*
Sr	205	158	312	154	207	205	379	10	272
Pb	21	*n.d.*	*n.d.*	*n.d.*	10	9	*n.d.*	*n.d.*	8
Ga	20	17	21	13	16	16	15	10	14
Zr	77	64	63	68	147	125	77	58	56
Hf	2.2	2.1	1.8	1.8	4.2	3.7	1.9	1.7	1.3
Nb	4.5	5.1	3.5	3.9	4.5	4.6	3.6	2.4	2.3
Ta	0.3	0.4	0.2	0.2	0.3	0.2	0.2	0.1	0.2
Th	1.3	1.2	0.9	1.0	3.6	2.7	1.1	1.3	1.0
U	0.4	0.4	0.3	0.2	1.7	1.5	0.5	0.7	0.3
Y	17	20	16	15	32	25	26	20	18
La	6.7	8.6	5.6	5.4	13.8	11.9	11.0	4.7	7.2
Ce	16.4	19.1	14.9	14.1	30.5	27.1	24.3	10.1	15.3
Pr	2.14	2.36	2.06	1.94	3.78	3.39	2.96	1.14	1.82
Nd	9.8	10.3	9.2	8.8	15.6	14.5	13.1	5.0	7.9
Sm	2.5	2.6	2.6	2.5	3.8	3.6	3.2	1.6	2.0
Eu	0.59	0.85	1.03	0.92	0.84	1.06	1.04	0.59	0.75
Gd	2.8	2.9	2.7	2.6	4.0	4.0	3.8	2.4	2.5
Tb	0.5	0.5	0.5	0.5	0.8	0.7	0.6	0.5	0.4
Dy	2.8	3.5	3.1	3.0	5.0	4.5	3.9	3.2	2.8
Ho	0.6	0.7	0.6	0.6	1.1	0.9	0.8	0.7	0.6
Er	1.6	2.2	1.8	1.8	3.6	2.8	2.4	2.3	1.8
Tm	0.25	0.34	0.28	0.25	0.56	0.43	0.36	0.36	0.27
Yb	1.5	2.0	1.7	1.6	3.5	2.7	2.3	2.2	1.8
Lu	0.23	0.30	0.26	0.23	0.53	0.41	0.34	0.33	0.27

Group	**G1**								
Reference	**Beaumont-Smith, 2007**								
Sample	95-01-82	95-01-103	95-01-268	95-01-337	95-01-247	95-01-201	94-00-64	95-01-22	94-00-62
La/Sm_{CN}	1.71	2.15	1.39	1.41	2.37	2.12	2.22	1.93	2.34
Gd/Yb_{CN}	1.53	1.18	1.31	1.38	0.94	1.21	1.34	0.89	1.15
La/Yb_{CN}	3.13	3.03	2.34	2.47	2.80	3.15	3.41	1.51	2.89
Eu/Eu*	0.68	0.95	1.19	1.12	0.66	0.86	0.91	0.93	1.03
Ce/Ce*	1.06	1.04	1.08	1.07	1.04	1.04	1.04	1.07	1.04
Zr/Y	4.6	3.1	4.0	4.4	4.5	5.0	3.0	2.9	3.2
Ti/Zr	77	73	101	88	21	28	87	44	102
Al_2O_3/TiO_2	21	24	17	12	26	27	13	22	16
Zr/Nb	17	12	18	17	32	27	21	24	25
Zr/Zr*	0.89	0.72	0.74	0.84	1.10	0.99	0.69	1.20	0.82
Zr/Sm_{PM}	1.21	0.99	0.97	1.10	1.55	1.37	0.96	1.47	1.13
Zr/Nd_{PM}	0.95	0.76	0.84	0.94	1.15	1.06	0.72	1.42	0.88
Ti/Ti*	1.15	0.75	0.96	0.97	0.43	0.43	0.86	0.55	1.07
Ti/Gd_{PM}	1.82	1.08	1.75	1.81	0.42	0.60	1.38	0.55	1.53
Ti/Sm_{PM}	0.83	0.64	0.87	0.87	0.29	0.34	0.75	0.59	1.04
Nb/Nb*	0.56	0.58	0.58	0.60	0.23	0.29	0.38	0.35	0.30
Nb/Th_{PM}	0.47	0.56	0.54	0.49	0.17	0.22	0.44	0.25	0.29
Nb/La_{PM}	0.67	0.59	0.63	0.72	0.33	0.38	0.33	0.50	0.31
Mg#	35	41	38	58	26	23	48	13	55
ΣLREE	40.91	46.76	38.00	36.21	72.32	65.58	59.44	25.41	37.42
ΣHREE	24.36	30.10	23.89	23.24	47.43	37.54	37.00	29.65	25.70

Group				**G1**					
Reference				**Beaumont-Smith, 2007**					**L.J., 2005**
Sample	94-00-69	103-00-1263	103-00-1412	103-99-1023	95-00-12	94-00-67	94-00-69	94-00-62	94-00-28
Easting (m)	383321	357503	372326	379959	380988	382800	383321	383275	386473
Northing (m)	6291989	6287203	6293572	6293155	6307704	6292019	6291989	6292002	6292612
DDH	Outcrop	Outcrop	Outcrop	Outcrop	Outcrop	Outcrop	Outcrop	Outcrop	Outcrop
Depth (m)	-	-	-	-	-	-	-	-	-
SiO_2	50.73	51.09	49.34	53.69	52.69	51.96	50.79	52.11	55.42
Al_2O_3	19.67	19.76	15.34	16.57	13.21	14.45	19.63	15.47	13.93
TiO_2	0.57	0.61	0.86	0.84	0.82	1.34	0.57	0.98	1.23
Fe_2O_3	8.54	9.02	11.81	10.84	10.49	13.34	8.52	11.81	13.21
MnO	0.14	0.17	0.21	0.16	0.18	0.22	0.14	0.20	0.19
MgO	6.00	5.27	7.77	4.70	8.79	5.34	6.00	7.24	3.89
CaO	9.71	9.88	11.64	8.00	9.71	9.36	9.71	9.56	8.28
Na_2O	4.28	2.22	2.52	3.09	1.67	2.92	4.28	2.37	3.13
K_2O	0.26	1.86	0.29	1.83	2.22	0.76	0.26	0.14	0.47
P_2O_5	0.10	0.12	0.21	0.28	0.21	0.31	0.10	0.13	0.25
LOI	3.17	1.49	0.80	0.89	3.29	0.15	3.17	1.74	1.67
Total	100	100	100	100	100	100	100	100	100
Ni	38	55	90	63	100	34	38	32	22
Cr	40	159	351	85	609	49	40	40	20
Co	32	31	37	34	38	*n.d.*	*n.d.*	*n.d.*	*n.d.*
V	156	144	263	257	222	341	164	278	326
Sc	29	33	39	33	36	40	29	43	38
Cu	58	52	*n.d.*	85	76	82	58	233	79
Zn	62	80	96	73	116	94	62	93	94
Mo	2.6	*n.d.*	2.5	*n.d.*	*n.d.*	*n.d.*	3.0	*n.d.*	*n.d.*
W	*n.d.*	1.3	1.2	*n.d.*	*n.d.*	*n.d.*	*n.d.*	*n.d.*	*n.d.*
Sb	0.4	1.0	0.4	1.1	0.2	1.1	0.4	0.6	0.4
Sn	*n.d.*	*n.d.*	1.1	*n.d.*	*n.d.*	*n.d.*	*n.d.*	*n.d.*	*n.d.*

L.J., 2005 - Jones, 2005

Group				**G1**					
Reference				**Beaumont-Smith, 2007**					**L.J., 2005**
Sample	94-00-69	103-00-1263	103-00-1412	103-99-1023	95-00-12	94-00-67	94-00-69	94-00-62	94-00-28
Ba	61	720	59	646	576	300	61	29	139
Cs	*n.d.*	1.1	*n.d.*	0.6	2.1	*n.d.*	*n.d.*	*n.d.*	*n.d.*
Rb	*n.d.*	*n.d.*	*n.d.*	*n.d.*	*n.d.*	12	2	*n.d.*	10
Sr	414	175	266	712	266	422	414	272	416
Pb	19	22	*n.d.*	27	*n.d.*	*n.d.*	7	13	*n.d.*
Ga	12	19	17	20	17	16	12	14	16
Zr	40	66	52	78	79	72	40	56	92
Hf	1.0	1.8	1.4	2.6	2.2	1.8	1.0	1.3	2.2
Nb	1.6	3.1	1.8	3.2	3.7	3.0	2.0	2.0	5.0
Ta	0.1	0.2	0.2	0.3	0.3	0.2	0.1	0.2	0.2
Th	0.8	1.3	1.0	2.9	1.6	1.1	0.8	2.8	1.3
U	0.3	0.7	0.3	1.3	0.6	0.5	0.3	0.9	0.6
Y	14	26	17	18	21	27	14	18	30
La	5.4	6.8	7.4	13.0	10.5	9.1	5.4	7.2	10.1
Ce	11.9	14.0	16.6	31.1	22.7	20.6	11.9	15.3	22.4
Pr	1.43	1.80	2.28	4.00	3.02	2.66	1.43	1.82	2.79
Nd	6.2	7.8	10.8	17.9	13.9	12.0	6.2	7.9	12.8
Sm	1.6	2.1	2.8	4.1	3.3	3.2	1.6	2.0	3.3
Eu	0.69	0.61	0.92	1.19	1.09	1.11	0.69	0.75	1.07
Gd	2.0	2.7	2.8	3.9	3.4	3.9	2.0	2.5	4.0
Tb	0.3	0.5	0.5	0.6	0.6	0.7	0.3	0.4	0.8
Dy	2.2	3.8	3.0	3.4	3.5	4.3	2.2	2.8	4.7
Ho	0.5	0.8	0.6	0.7	0.7	0.9	0.5	0.6	1.0
Er	1.4	2.6	1.9	2.0	2.2	2.7	1.4	1.8	3.1
Tm	0.21	0.41	0.27	0.28	0.32	0.41	0.21	0.27	0.47
Yb	1.4	2.7	1.7	1.8	2.1	2.7	1.4	1.8	2.9
Lu	0.21	0.43	0.25	0.28	0.31	0.41	0.21	0.27	0.46

Group				G1					
Reference				Beaumont-Smith, 2007					L.J., 2005
Sample	94-00-69	103-00-1263	103-00-1412	103-99-1023	95-00-12	94-00-67	94-00-69	94-00-62	94-00-28
La/Sm_{CN}	2.19	2.11	1.73	2.04	2.07	1.84	2.18	2.32	1.98
Gd/Yb_{CN}	1.18	0.83	1.41	1.78	1.35	1.19	1.18	1.15	1.14
La/Yb_{CN}	2.78	1.79	3.17	5.09	3.60	2.42	2.77	2.87	2.50
Eu/Eu*	1.18	0.78	1.00	0.91	0.99	0.96	1.18	1.03	0.90
Ce/Ce*	1.05	0.98	0.99	1.06	0.99	1.03	1.05	1.04	1.03
Zr/Y	3.0	2.6	3.1	4.3	3.8	2.7	2.9	3.1	3.1
Ti/Zr	81	55	98	65	61	110	82	103	78
Al_2O_3/TiO_2	35	32	18	20	16	11	35	16	11
Zr/Nb	26	21	28	24	22	24	20	28	18
Zr/Zr*	0.74	0.94	0.55	0.52	0.68	0.67	0.73	0.81	0.82
Zr/Sm_{PM}	1.01	1.26	0.75	0.75	0.96	0.90	0.99	1.11	1.11
Zr/Nd_{PM}	0.80	1.03	0.59	0.53	0.70	0.73	0.79	0.87	0.88
Ti/Ti*	0.70	0.70	0.80	0.58	0.63	0.96	0.70	1.06	0.87
Ti/Gd_{PM}	1.10	0.62	1.44	1.29	1.09	1.39	1.10	1.52	1.17
Ti/Sm_{PM}	0.73	0.62	0.66	0.43	0.52	0.88	0.73	1.03	0.77
Nb/Nb*	0.27	0.38	0.24	0.19	0.32	0.34	0.35	0.16	0.50
Nb/Th_{PM}	0.26	0.32	0.24	0.15	0.30	0.36	0.33	0.09	0.51
Nb/La_{PM}	0.29	0.45	0.25	0.25	0.35	0.33	0.37	0.28	0.49
Mg#	58	54	57	46	62	44	58	55	47
ΣLREE	29.29	35.85	43.55	75.23	57.86	52.57	29.22	37.47	56.46
ΣHREE	19.95	36.94	25.23	27.14	30.65	39.12	20.22	25.94	43.43

Group	G1				G1U				
Reference	**L.J., 2005**	**D.P., 1986**	**Chapter 2**		**This study**		**Zwanzig et al., 1999**		
Sample	94-00-64	141	MG11-002	LL13-16	LL13-07	LL13-08	32-78-5138	12-77-632	32-76-193
Easting (m)	383006	-	383354	380431	412452	412483	383155	337740	371701
Northing (m)	6292443	-	6306437	6307384	6307733	6307647	6308648	6274827	6293685
DDH	Outcrop	Outcrop	Outcrop	Outcrop	FL12-02	FL12-03	Outcrop	Outcrop	Outcrop
Depth (m)	-	-	-	-	289	273	-	-	-
SiO_2	52.53	56.69	49.18	53.08	50.91	42.14	51.32	56.85	49.89
Al_2O_3	14.65	16.1	13.00	13.71	5.76	4.57	10.59	12.67	14.94
TiO_2	1.14	0.52	0.81	0.68	0.60	1.21	0.44	0.94	0.53
Fe_2O_3	12.22	7.44	10.55	8.68	10.49	31.45	9.33	10.50	10.31
MnO	0.19	0.12	0.24	0.15	0.19	0.24	0.20	0.18	0.17
MgO	5.80	6.37	12.19	11.58	18.00	12.63	15.65	10.12	10.53
CaO	9.60	7.71	12.10	10.60	12.87	7.05	10.95	5.16	10.97
Na_2O	3.23	4.27	1.20	0.68	0.37	0.27	1.12	3.32	1.98
K_2O	0.39	0.64	0.28	0.42	0.74	0.27	0.18	0.07	0.56
P_2O_5	0.25	0.14	0.45	0.43	0.08	0.18	0.23	0.19	0.11
LOI	0.80	1.68	2.27	2.49	4.87	1.51	2.56	0.77	1.33
Total	100	100	100	100	100	100	100	100	100
Ni	40	94	310	330	260	*n.d.*	402	33	112
Cr	119	150	730	960	570	*n.d.*	1670	302	327
Co	*n.d.*	38	31	45	62	12	62	52	70
V	279	116	132	161	135	334	154	247	209
Sc	40	-	21	26	47	27	*n.d.*	*n.d.*	*n.d.*
Cu	95	13	*n.d.*	*n.d.*	*n.d.*	*n.d.*	10.3	167	45
Zn	104	48	190	220	110	110	114	84	91
Mo	3.0	-	*n.d.*	*n.d.*	*n.d.*	*n.d.*	*n.d.*	*n.d.*	*n.d.*
W	*n.d.*	-	2.0	1.4	3.2	9.3	87	105	139
Sb	0.8	-	0.6	4.3	*n.d.*	*n.d.*	0.6	0.3	*n.d.*
Sn	*n.d.*	-	1.0	*n.d.*	*n.d.*	*n.d.*	*n.d.*	*n.d.*	1.9

D.P., 1986 - Peck, 1986

Group	G1				G1U				
Reference	**L.J., 2005**	**D.P., 1986**	**Chapter 2**		**This study**		**Zwanzig et al., 1999**		
Sample	94-00-64	141	MG11-002	LL13-16	LL13-07	LL13-08	32-78-5138	12-77-632	32-76-193
Ba	246	116	55	95	151	54	51	247	195
Cs	*n.d.*	*n.d.*	*n.d.*	1.0	22	4.0	0.9	*n.d.*	*n.d.*
Rb	6	12	4	10	17	6	5	*n.d.*	13
Sr	379	316	87	156	126	24	66	657	176
Pb	8	-	*n.d.*	36	*n.d.*	*n.d.*	*n.d.*	16	*n.d.*
Ga	15	-	18	15	9	15	12	11	13
Zr	77	73	148	109	37	44	69	66	46
Hf	1.9	1.7	3.3	2.6	1.1	1.1	1.9	1.9	1.5
Nb	4.0	6.0	8.0	8.4	2.6	2.3	5.6	4.8	3.6
Ta	0.2	0.8	0.6	0.4	0.04	0.04	0.6	0.8	0.9
Th	1.0	1.2	4.9	3.0	0.6	1.0	2.1	2.6	0.9
U	0.3	0.8	1.7	1.5	0.4	0.7	0.8	0.7	0.3
Y	26	18	17	13	15	11	12	20	18
La	11.0	9.4	36.1	25.5	8.4	4.0	16.4	7.7	7.0
Ce	24.3	20.0	83.4	58.9	24.3	10.9	35.3	17.9	16.2
Pr	2.96	-	10.10	7.78	4.09	1.64	4.49	2.17	2.15
Nd	13.1	9.0	40.3	30.8	20.4	8.3	19.4	9.4	9.9
Sm	3.2	2.1	7.6	5.6	5.7	2.3	3.9	2.8	2.5
Eu	1.04	0.73	1.47	1.54	1.32	0.65	0.96	0.55	0.78
Gd	3.8	-	5.6	3.9	4.7	2.5	3.2	3.2	2.8
Tb	0.6	0.4	0.7	0.5	0.7	0.4	0.4	0.6	0.5
Dy	3.9	-	3.7	2.7	3.4	2.2	2.2	3.6	2.9
Ho	0.8	-	0.7	0.5	0.6	0.4	0.4	0.7	0.6
Er	2.4	-	1.8	1.3	1.5	1.2	1.1	2.0	1.9
Tm	0.36	-	0.26	0.19	0.21	0.19	0.17	0.29	0.29
Yb	2.3	1.7	1.6	1.2	1.2	1.3	1.1	2.0	1.7
Lu	0.34	0.26	0.25	0.16	0.15	0.18	0.14	0.30	0.26

Group	**G1**				**G1U**				
Reference	**L.J., 2005**	**D.P., 1986**	**Chapter 2**		**This study**		**Zwanzig et al., 1999**		
Sample	94-00-64	141	MG11-002	LL13-16	LL13-07	LL13-08	32-78-5138	12-77-632	32-76-193
La/Sm_{CN}	2.22	2.90	3.07	2.93	0.96	1.10	2.68	1.76	1.80
Gd/Yb_{CN}	1.37	-	2.90	2.75	3.14	1.65	2.47	1.31	1.34
La/Yb_{CN}	3.43	4.01	16.18	15.77	4.86	2.26	10.85	2.73	2.90
Eu/Eu*	0.91	-	0.69	1.01	0.78	0.82	0.83	0.56	0.90
Ce/Ce*	1.04	-	1.07	1.03	1.02	1.05	1.01	1.08	1.02
Zr/Y	3.0	4.1	8.7	8.6	2.5	4.1	5.5	3.3	2.6
Ti/Zr	88	43	31	36	92	164	37	84	67
Al_2O_3/TiO_2	13	31	16	20	10	4	24	13	28
Zr/Nb	19	12	19	13	14	19	12	14	13
Zr/Zr*	0.69	0.97	0.49	0.48	0.20	0.58	0.45	0.74	0.54
Zr/Sm_{PM}	0.96	1.39	0.77	0.77	0.26	0.75	0.70	0.93	0.73
Zr/Nd_{PM}	0.72	0.99	0.45	0.43	0.22	0.65	0.44	0.86	0.58
Ti/Ti*	0.86	-	0.41	0.41	0.34	1.42	0.37	1.06	0.53
Ti/Gd_{PM}	1.39	0.88	1.37	1.61	1.29	2.70	1.13	1.30	0.85
Ti/Sm_{PM}	0.75	0.53	0.22	0.25	0.21	1.10	0.23	0.70	0.44
Nb/Nb*	0.44	0.65	0.22	0.35	0.43	0.41	0.35	0.39	0.50
Nb/Th_{PM}	0.53	0.66	0.21	0.36	0.59	0.29	0.35	0.24	0.50
Nb/La_{PM}	0.36	0.63	0.22	0.33	0.31	0.58	0.34	0.62	0.50
Mg#	48	63	70	73	77	44	77	66	67
ΣLREE	59.40	-	184.57	133.99	68.88	30.29	83.69	43.82	41.43
ΣHREE	36.70	-	26.01	19.28	22.55	16.59	18.01	29.60	26.20

Group	G1U							G1*	
Reference	**Zwanzig et al., 1999**		**Beaumont-Smith, 2007**					**H.Z., 1999**	**D.P., 1986**
Sample	95-01-72	95-01-182	32-76-117	103-03-1861	95-01-198	103-01-1673	103-01-1687	32-80-1137	157
Easting (m)	375868	372032	373410	370744	372604	347028	343166	416331	-
Northing (m)	6303283	6300240	6291249	6300622	6301610	6279577	6280022	6309747	-
DDH	Outcrop	Outcrop	Outcrop	Outcrop	Outcrop	Outcrop	Outcrop	Outcrop	Outcrop
Depth (m)	-	-	-	-	-	-	-	-	-
SiO_2	48.97	52.17	51.19	49.10	46.94	49.41	49.70	51.18	52.04
Al_2O_3	12.53	14.35	13.06	9.71	9.98	8.52	8.45	16.86	12.67
TiO_2	0.26	0.68	0.66	0.42	0.69	0.65	0.75	0.94	0.93
Fe_2O_3	8.46	9.15	11.07	13.96	12.20	12.13	13.68	14.42	14.20
MnO	0.15	0.15	0.19	0.29	0.20	0.30	0.22	0.21	0.23
MgO	16.81	10.79	10.82	13.73	20.05	17.22	14.95	3.81	6.18
CaO	11.40	8.83	10.61	11.69	9.43	11.01	10.72	9.57	10.66
Na_2O	1.00	1.63	2.11	0.66	0.40	0.61	0.67	2.38	2.68
K_2O	0.37	1.95	0.14	0.27	-0.01	0.03	0.75	0.52	0.24
P_2O_5	0.05	0.30	0.15	0.18	0.12	0.12	0.13	0.10	0.17
LOI	3.04	2.93	1.86	3.30	3.99	1.51	1.53	0.47	3.76
Total	100	100	100	100	100	100	100	100	100
Ni	482	259	124	472	536	464	216	*n.d*	32
Cr	895	771	646	1360	2120	1880	1380	26	50
Co	64	46	52	38	39	73	68	54	57
V	88	167	223	213	232	207	263	373	261
Sc	26	34	*n.d.*	24	35	34	46	*n.d*	47
Cu	77	*n.d.*	137	12	*n.d.*	26	28	207	82
Zn	59	83	81	118	123	44	78	95	97
Mo	*n.d.*	*n.d.*	16	*n.d.*	*n.d.*	*n.d.*	*n.d.*	*n.d*	-
W	*n.d.*	1.6	74	*n.d.*	0.7	*n.d.*	*n.d.*	127	-
Sb	0.4	*n.d.*	1.0	0.5	0.2	1.2	4.3	*n.d*	-
Sn	*n.d.*	1.0	8.4	4.7	*n.d.*	*n.d.*	*n.d.*	1.1	-

H.Z., 1999 - Zwanzig et al., 1999

Group	G1U							G1*	
Reference	Zwanzig et al., 1999		Beaumont-Smith, 2007					H.Z., 1999	D.P., 1986
Sample	95-01-72	95-01-182	32-76-117	103-03-1861	95-01-198	103-01-1673	103-01-1687	32-80-1137	157
Ba	46	307	53	33	5	13	202	314	54
Cs	0.3	2.4	*n.d.*	1.0	*n.d.*	*n.d.*	2.4	*n.d.*	0.9
Rb	*n.d.*	*n.d.*	*n.d.*	*n.d.*	*n.d.*	*n.d.*	*n.d.*	6	1
Sr	224	252	384	16	21	156	210	223	282
Pb	*n.d.*	*n.d.*	12	*n.d.*	*n.d.*	*n.d.*	*n.d.*	*n.d.*	-
Ga	9	15	13	14	11	9	11	16	-
Zr	36	109	43	19	34	34	46	41	47
Hf	1.0	2.8	1.3	0.6	1.0	1.0	1.4	1.2	1.5
Nb	1.5	6.6	2.1	1.4	1.9	1.5	1.3	1.3	2.0
Ta	0.1	0.4	0.4	*n.d.*	0.1	0.1	0.2	0.7	*n.d.*
Th	1.7	3.8	0.8	0.6	1.0	0.8	2.0	0.4	0.6
U	0.5	1.1	0.3	0.2	0.3	0.1	0.5	0.4	0.2
Y	8	19	14	18	11	10	14	21	26
La	4.1	26.2	5.4	3.5	1.8	2.4	6.8	3.9	6.70
Ce	9.2	58.5	12.5	7.3	5.1	5.8	15.9	9.8	14.00
Pr	1.15	6.85	1.75	0.98	0.75	0.88	2.03	1.44	-
Nd	4.9	26.7	8.4	4.9	3.8	4.4	9.5	7.3	8.0
Sm	1.2	5.0	2.3	1.4	1.4	1.3	2.2	2.2	2.3
Eu	0.41	1.68	0.76	0.35	0.44	0.54	0.65	0.85	0.92
Gd	1.3	4.6	2.5	1.8	1.8	1.6	2.4	2.7	-
Tb	0.2	0.7	0.4	0.4	0.3	0.3	0.4	0.5	0.5
Dy	1.4	3.7	2.5	2.4	2.1	1.8	2.6	3.0	-
Ho	0.3	0.7	0.5	0.6	0.4	0.4	0.5	0.7	-
Er	0.8	2.1	1.5	1.7	1.2	1.0	1.5	2.1	-
Tm	0.13	0.28	0.23	0.26	0.18	0.15	0.23	0.31	-
Yb	0.8	1.9	1.4	1.6	1.1	1.0	1.4	2.0	2.7
Lu	0.12	0.27	0.22	0.24	0.17	0.15	0.20	0.32	0.40

Group	G1U							G1*	
Reference	**Zwanzig et al., 1999**		**Beaumont-Smith, 2007**					**H.Z., 1999**	**D.P., 1986**
Sample	95-01-72	95-01-182	32-76-117	103-03-1861	95-01-198	103-01-1673	103-01-1687	32-80-1137	157
La/Sm_{CN}	2.20	3.37	1.52	1.66	0.80	1.21	1.96	1.13	1.88
Gd/Yb_{CN}	1.32	1.99	1.49	0.88	1.31	1.36	1.39	1.10	-
La/Yb_{CN}	3.70	9.92	2.79	1.54	1.12	1.83	3.46	1.37	1.81
Eu/Eu*	1.02	1.07	0.96	0.69	0.83	1.16	0.86	1.06	-
Ce/Ce*	1.04	1.07	1.00	0.96	1.07	0.97	1.05	1.02	-
Zr/Y	4.4	5.9	3.0	1.0	3.2	3.6	3.3	1.9	1.8
Ti/Zr	43	36	91	131	115	110	96	139	119
Al_2O_3/TiO_2	48	21	20	23	14	13	11	18	14
Zr/Nb	24	16	20	14	18	23	36	31	24
Zr/Zr*	0.85	0.54	0.56	0.41	0.85	0.83	0.57	0.58	0.63
Zr/Sm_{PM}	1.18	0.86	0.74	0.54	0.95	1.05	0.81	0.72	0.81
Zr/Nd_{PM}	0.90	0.50	0.62	0.46	1.12	0.96	0.59	0.68	0.72
Ti/Ti*	0.53	0.36	0.71	0.78	1.11	1.03	0.89	0.93	-
Ti/Gd_{PM}	0.91	0.98	1.32	0.70	1.63	1.88	1.46	1.31	0.99
Ti/Sm_{PM}	0.45	0.28	0.60	0.63	0.98	1.04	0.69	0.90	0.86
Nb/Nb*	0.20	0.24	0.38	0.33	0.52	0.40	0.12	0.37	0.36
Nb/Th_{PM}	0.12	0.23	0.37	0.28	0.26	0.26	0.08	0.41	0.44
Nb/La_{PM}	0.37	0.25	0.39	0.39	1.05	0.61	0.19	0.34	0.30
Mg#	80	70	66	66	77	74	68	34	46
ΣLREE	22.15	129.62	33.75	20.17	15.07	16.94	39.47	28.28	-
ΣHREE	11.75	28.24	21.08	25.13	16.56	14.24	20.77	30.39	-

Group	G1*								
Reference	**Jones, 2005**		**Beaumont-Smith, 2007**						
Sample	94-00-16	94-00-46	103-01-2004	103-99-1039	103-99-1078	103-00-1249	103-01-1616	103-01-1654	103-01-1624
Easting (m)	385764	384561	361847	384732	376784	344865	357149	367111	357015
Northing (m)	6292076	6291824	6290050	6292030	6291858	6280558	6289263	6285392	6289439
DDH	Outcrop	Outcrop	Outcrop	Outcrop	Outcrop	Outcrop	Outcrop	Outcrop	Outcrop
Depth (m)	-	-	-	-	-	-	-	-	-
SiO_2	64.90	52.17	41.05	57.10	52.51	50.26	53.04	59.19	50.84
Al_2O_3	14.38	14.35	17.11	15.38	16.38	17.39	16.50	14.10	15.80
TiO_2	0.64	1.16	1.11	0.94	0.72	0.74	0.72	0.70	0.80
Fe_2O_3	8.46	13.41	12.38	11.15	10.55	10.41	12.02	13.03	11.56
MnO	0.12	0.22	0.17	0.16	0.19	0.17	0.17	0.22	0.16
MgO	2.33	5.28	8.51	3.43	6.97	6.40	5.21	2.28	7.79
CaO	4.92	10.75	17.41	5.47	9.59	11.41	8.69	6.98	8.92
Na_2O	3.36	2.28	1.55	3.06	1.84	2.53	2.63	2.75	3.73
K_2O	0.80	0.23	0.46	3.15	1.12	0.56	0.92	0.62	0.25
P_2O_5	0.12	0.14	0.24	0.17	0.13	0.14	0.10	0.13	0.15
LOI	4.60	4.81	5.09	2.16	1.24	0.91	1.77	0.45	0.48
Total	100	100	100	100	100	100	100	100	100
Ni	*n.d*	23	103	47	32	40	36	-20	61
Cr	7	81	275	33	188	280	127	5	213
Co	*n.d*	*n.d*	47	27	36	36	47	29	47
V	109	264	261	201	226	226	239	98	272
Sc	24	47	37	35	36	42	43	41	52
Cu	86	70	47	57	175	107	80	40	91
Zn	69	81	90	101	39	76	92	107	78
Mo	n.d	3.0	*n.d.*	*n.d.*	*n.d.*	*n.d.*	2.2	2.3	*n.d.*
W	1.0	*n.d*	*n.d.*	18	*n.d.*	*n.d.*	*n.d.*	*n.d.*	*n.d.*
Sb	0.6	1.3	0.9	*n.d.*	0.4	1.6	0.7	0.5	1.0
Sn	*n.d*	*n.d*	*n.d.*	*n.d.*	*n.d.*	*n.d.*	*n.d.*	*n.d.*	*n.d.*

Group	G1*								
Reference	**Jones, 2005**		**Beaumont-Smith, 2007**						
Sample	94-00-16	94-00-46	103-01-2004	103-99-1039	103-99-1078	103-00-1249	103-01-1616	103-01-1654	103-01-1624
Ba	174	68	113	448	549	162	215	125	138
Cs	*n.d.*	*n.d.*	*n.d.*	0.9	2.7	0.6	*n.d.*	*n.d.*	*n.d.*
Rb	13.0	*n.d.*	*n.d.*	*n.d.*	*n.d.*	*n.d.*	*n.d.*	*n.d.*	*n.d.*
Sr	120	243	308	164	413	241	298	180	364
Pb	5	*n.d.*	*n.d.*	8	*n.d.*	8	7	*n.d.*	*n.d.*
Ga	11	15	16	19	16	17	17	14	16
Zr	90	93	57	98	44	47	64	40	51
Hf	2.2	2.2	1.5	3.2	1.4	1.4	1.8	1.1	1.5
Nb	3.0	4.0	1.1	3.7	2.0	1.5	2.1	1.0	1.1
Ta	0.2	0.3	0.2	0.3	0.1	0	0.2	0.1	*n.d.*
Th	0.9	0.9	0.3	1.5	0.7	0.5	0.7	0.4	0.4
U	0.4	0.3	0.2	1.3	0.4	0.2	0.3	0.3	0.3
Y	24	31	20	26	15	22	21	15	24
La	5.6	7.0	5.8	7.2	5.9	4.1	3.8	4.2	4.2
Ce	13.9	17.2	14.2	18.5	13.7	9.9	8.8	9.0	10.7
Pr	1.81	2.27	2.02	2.53	1.85	1.42	1.20	1.35	1.58
Nd	8.7	10.9	9.9	11.7	8.7	6.9	5.7	6.7	7.9
Sm	2.5	3.2	2.6	3.2	2.3	2.1	1.7	1.9	2.4
Eu	0.78	1.14	1.01	0.90	0.83	0.78	0.66	0.80	0.94
Gd	3.3	4.4	3.1	3.8	2.5	2.8	2.3	2.2	3.1
Tb	0.6	0.8	0.6	0.7	0.4	0.5	0.5	0.4	0.6
Dy	3.8	5.1	3.6	4.5	2.6	3.7	3.3	2.7	4.2
Ho	0.8	1.1	0.7	1.0	0.6	0.8	0.8	0.6	0.9
Er	2.6	3.2	2.1	3.0	1.6	2.4	2.3	1.7	2.9
Tm	0.40	0.48	0.35	0.46	0.24	0.35	0.36	0.26	0.42
Yb	2.6	3.0	2.2	3.1	1.5	2.3	2.2	1.7	2.7
Lu	0.39	0.44	0.30	0.51	0.24	0.38	0.36	0.25	0.41

Group	G1*								
Reference	**Jones, 2005**		**Beaumont-Smith, 2007**						
Sample	94-00-16	94-00-46	103-01-2004	103-99-1039	103-99-1078	103-00-1249	103-01-1616	103-01-1654	103-01-1624
La/Sm_{CN}	1.45	1.41	1.43	1.46	1.65	1.25	1.44	1.42	1.12
Gd/Yb_{CN}	1.05	1.21	1.15	1.01	1.38	0.97	0.85	1.09	0.96
La/Yb_{CN}	1.54	1.67	1.89	1.68	2.83	1.25	1.24	1.77	1.09
Eu/Eu*	0.83	0.93	1.09	0.79	1.05	0.99	1.01	1.20	1.04
Ce/Ce*	1.07	1.06	1.01	1.06	1.01	1.01	1.01	0.93	1.02
Zr/Y	3.8	3.0	2.9	3.8	2.9	2.1	3.1	2.6	2.1
Ti/Zr	40	72	110	55	94	93	66	102	92
Al_2O_3/TiO_2	23	12	15	16	23	24	23	20	20
Zr/Nb	30	23	52	27	22	32	31	39	47
Zr/Zr*	1.11	0.91	0.64	0.92	0.57	0.71	1.18	0.66	0.68
Zr/Sm_{PM}	1.43	1.16	0.86	1.22	0.76	0.88	1.49	0.85	0.85
Zr/Nd_{PM}	1.27	1.04	0.70	1.03	0.62	0.83	1.38	0.74	0.79
Ti/Ti*	0.57	0.75	0.89	0.74	0.73	0.75	0.87	0.78	0.69
Ti/Gd_{PM}	0.66	1.05	1.34	0.83	1.31	0.88	0.90	1.16	0.82
Ti/Sm_{PM}	0.52	0.74	0.84	0.61	0.64	0.73	0.87	0.78	0.70
Nb/Nb*	0.48	0.58	0.28	0.40	0.36	0.36	0.47	0.29	0.30
Nb/Th_{PM}	0.44	0.59	0.42	0.33	0.39	0.37	0.41	0.34	0.34
Nb/La_{PM}	0.53	0.57	0.19	0.50	0.33	0.36	0.54	0.25	0.26
Mg#	35	44	58	38	57	55	46	26	57
ΣLREE	36.59	46.11	38.53	47.94	35.80	27.97	24.24	26.12	30.78
ΣHREE	35.19	45.12	29.72	39.05	22.61	32.34	30.42	23.06	35.94

Group	**G1***			**G2**				
Reference	**C.B.-S., 2007**			**Zwanzig et al., 1999**				
Sample	95-00-16	32-76-505	32-76-497	32-78-5198	32-76-139	32-76-690	32-76-511	32-76-528
Easting (m)	380845	394508	374866	401209	369886	366764	393567	390006
Northing (m)	6307840	6315505	6302926	6317867	6302354	6300096	6314697	6312298
DDH	Outcrop	Outcrop	Outcrop	Outcrop	Outcrop	Outcrop	Outcrop	Outcrop
Depth (m)	-	-	-	-	-	-	-	-
SiO_2	47.60	47.27	51.04	50.13	48.58	49.50	51.60	52.53
Al_2O_3	20.55	21.17	22.62	17.41	20.81	17.25	15.62	14.78
TiO_2	1.06	0.82	0.77	0.46	0.76	0.76	0.76	0.90
Fe_2O_3	12.74	11.26	8.67	13.02	11.68	12.00	11.04	13.64
MnO	0.17	0.19	0.13	0.22	0.15	0.18	0.18	0.22
MgO	4.15	4.52	3.35	5.95	3.46	6.76	6.14	6.29
CaO	10.18	11.34	8.14	9.98	10.73	11.15	12.70	9.92
Na_2O	2.74	2.26	3.62	2.25	3.42	2.01	1.70	1.34
K_2O	0.74	1.09	1.59	0.54	0.34	0.34	0.19	0.29
P_2O_5	0.06	0.08	0.08	0.02	0.06	0.05	0.07	0.10
LOI	1.29	1.13	0.93	1.06	0.73	1.00	0.85	0.38
Total	100	100	100	100	100	100	100	100
Ni	*n.d.*	*n.d.*	*n.d.*	35	*n.d.*	132	45	35
Cr	15	22	*n.d.*	79	*n.d.*	284	201	115
Co	40	31	32	56	42	76	51	58
V	289	296	236	318	285	305	314	337
Sc	36	*n.d.*	*n.d.*	*n.d.*	*n.d.*	*n.d.*	*n.d.*	*n.d.*
Cu	172	91	87	20	121	41	46	63
Zn	95	77	94	103	86	109	78	99
Mo	*n.d.*	*n.d.*	*n.d.*	*n.d.*	*n.d.*	*n.d.*	*n.d.*	*n.d.*
W	*n.d.*	63	64	110	78	112	83	75
Sb	0.3	*n.d.*	*n.d.*	*n.d.*	*n.d.*	1.1	*n.d.*	*n.d.*
Sn	*n.d.*	*n.d.*	*n.d.*	*n.d.*	*n.d.*	*n.d.*	*n.d.*	*n.d.*

C.B.-S., 2007– Beaumont-Smith, 2007

Group	G1*	G2						
Reference	C.B.-S., 2007	Zwanzig et al., 1999						
Sample	95-00-16	32-76-505	32-76-497	32-78-5198	32-76-139	32-76-690	32-76-511	32-76-528
Ba	92	143	639	258	76	73	55	47
Cs	0.2	2.6	*n.d.*	*n.d.*	*n.d.*	*n.d.*	*n.d.*	*n.d.*
Rb	*n.d.*	18	22	12	3	3	*n.d.*	*n.d.*
Sr	293	303	272	188	223	195	170	119
Pb	8	*n.d.*	*n.d.*	*n.d.*	*n.d.*	*n.d.*	*n.d.*	*n.d.*
Ga	16	19	21	16	18	16	16	16
Zr	27	32	28	11	25	31	39	54
Hf	2.4	1.0	0.9	0.4	0.8	1.0	1.2	1.6
Nb	2.1	2.4	2.5	1.0	2.0	1.7	2.2	3.9
Ta	0.2	0.4	0.4	0.5	0.5	0.6	0.5	0.5
Th	0.9	0.2	0.2	0.3	0.2	0.3	0.2	0.3
U	0.2	*n.d.*	0.4	0.1	0.2	0.3	0.3	0.2
Y	13	14	13	8	11	12	16	22
La	3.1	2.5	2.1	1.1	2.2	1.6	2.6	3.5
Ce	7.6	6.2	5.5	2.6	5.7	4.4	6.1	9.1
Pr	1.16	0.91	0.85	0.39	0.86	0.74	0.94	1.37
Nd	6.1	4.9	4.6	2.1	4.6	4.0	5.1	7.3
Sm	1.9	1.6	1.5	0.8	1.5	1.3	1.7	2.3
Eu	0.77	0.71	0.65	0.33	0.62	0.51	0.59	0.84
Gd	2.2	1.9	1.8	1.0	1.7	1.8	2.2	2.9
Tb	0.4	0.3	0.3	0.2	0.3	0.3	0.4	0.5
Dy	2.4	2.2	2.0	1.2	2.0	1.9	2.6	3.3
Ho	0.5	0.5	0.4	0.3	0.4	0.4	0.6	0.7
Er	1.5	1.4	1.3	0.7	1.2	1.2	1.7	2.2
Tm	0.21	0.22	0.20	0.12	0.17	0.19	0.25	0.33
Yb	1.3	1.3	1.2	0.7	1.1	1.1	1.5	2.0
Lu	0.20	0.21	0.19	0.11	0.16	0.16	0.23	0.31

Group	**G1***			**G2**				
Reference	**C.B.-S., 2007**			**Zwanzig et al., 1999**				
Sample	95-00-16	32-76-505	32-76-497	32-78-5198	32-76-139	32-76-690	32-76-511	32-76-528
La/Sm_{CN}	1.06	1.00	0.90	0.92	0.97	0.76	0.99	0.99
Gd/Yb_{CN}	1.44	1.16	1.17	1.18	1.31	1.35	1.17	1.18
La/Yb_{CN}	1.78	1.32	1.21	1.18	1.46	1.04	1.20	1.23
Eu/Eu*	1.15	1.24	1.23	1.12	1.18	1.00	0.94	0.99
Ce/Ce*	0.98	1.01	1.02	0.96	1.01	1.00	0.95	1.02
Zr/Y	2.0	2.4	2.2	1.5	2.2	2.7	2.4	2.5
Ti/Zr	232	152	164	241	183	146	116	98
Al_2O_3/TiO_2	19	26	29	37	27	23	21	16
Zr/Nb	13	13	11	11	12	18	17	14
Zr/Zr*	0.46	0.66	0.62	0.51	0.54	0.77	0.76	0.77
Zr/Sm_{PM}	0.56	0.80	0.75	0.57	0.66	0.92	0.92	0.95
Zr/Nd_{PM}	0.55	0.79	0.76	0.67	0.65	0.95	0.93	0.91
Ti/Ti*	1.22	1.06	1.08	1.22	1.09	1.20	1.00	0.86
Ti/Gd_{PM}	2.35	1.70	1.75	1.87	1.93	1.96	1.38	1.23
Ti/Sm_{PM}	1.17	1.09	1.09	1.23	1.08	1.21	0.95	0.83
Nb/Nb*	0.47	1.11	1.39	0.71	1.17	0.98	1.07	1.50
Nb/Th_{PM}	0.33	1.28	1.65	0.55	1.52	0.87	1.33	2.04
Nb/La_{PM}	0.68	0.97	1.17	0.91	0.90	1.10	0.86	1.10
Mg#	39	44	43	48	37	53	52	48
ΣLREE	22.87	18.74	16.96	8.38	17.27	14.39	19.16	27.37
ΣHREE	19.88	19.79	18.61	10.97	16.26	16.96	23.72	31.04

Group					**G2**				
Reference					**Zwanzig et al., 1999**				
Sample	12-74-55	12-74-65	32-80-964	32-79-526	32-79-515	32-80-1057	32-79-595	32-76-436	12-74-71
Easting (m)	428848	419612	417211	430103	428454	337437	429905	376853	427496
Northing (m)	6303792	6304804	6309526	6302776	6301524	6274593	6306420	6310230	6300508
DDH	Outcrop	Outcrop	Outcrop	Outcrop	Outcrop	Outcrop	Outcrop	Outcrop	Outcrop
Depth (m)	-	-	-	-	-	-	-	-	-
SiO_2	49.03	50.44	53.10	55.15	63.57	51.08	53.30	50.79	54.71
Al_2O_3	18.40	16.81	14.29	16.21	14.90	19.40	16.31	19.82	15.81
TiO_2	0.48	0.76	0.97	0.89	0.99	0.63	0.60	0.35	0.30
Fe_2O_3	12.27	12.15	15.86	12.35	7.25	11.47	13.26	10.55	10.80
MnO	0.16	0.18	0.24	0.19	0.14	0.27	0.24	0.18	0.18
MgO	6.65	6.69	3.48	2.65	3.09	3.61	5.50	3.99	5.22
CaO	11.41	9.54	8.98	8.06	7.00	10.69	8.98	12.09	10.61
Na_2O	1.33	3.16	2.58	3.76	2.67	2.11	1.53	1.81	2.05
K_2O	0.22	0.20	0.36	0.64	0.26	0.68	0.23	0.38	0.26
P_2O_5	0.05	0.07	0.14	0.08	0.14	0.06	0.05	0.03	0.05
LOI	1.34	1.09	0.29	0.51	0.76	1.03	0.86	1.11	1.16
Total	100	100	100	100	100	100	100	100	100
Ni	49	73	*n.d.*	*n.d.*	*n.d.*	17	*n.d.*	41	41
Cr	84	214	*n.d.*	*n.d.*	*n.d.*	32	*n.d.*	33	*n.d.*
Co	54	54	57	50	47	51	65	42	46
V	307	322	524	364	336	303	340	257	223
Sc	*n.d.*	*n.d.*	*n.d.*	*n.d.*	*n.d.*	*n.d.*	*n.d.*	*n.d.*	*n.d.*
Cu	78	84	37	135	21	231	35	229	106
Zn	65	71	88	112	53	152	59	112	72
Mo	*n.d.*	*n.d.*	*n.d.*	*n.d.*	*n.d.*	*n.d.*	*n.d.*	*n.d.*	*n.d.*
W	141	76	171	184	260	158	208	68	111
Sb	*n.d.*	*n.d.*	*n.d.*	*n.d.*	1.5	*n.d.*	*n.d.*	*n.d.*	*n.d.*
Sn	*n.d.*	*n.d.*	*n.d.*	3.1	1.9	*n.d.*	1.0	*n.d.*	*n.d.*

Group	G2								
Reference	Zwanzig et al., 1999								
Sample	12-74-55	12-74-65	32-80-964	32-79-526	32-79-515	32-80-1057	32-79-595	32-76-436	12-74-71
Ba	35	39	243	126	32	140	26	72	56
Cs	*n.d.*	*n.d.*	*n.d.*	*n.d.*	*n.d.*	*n.d.*	*n.d.*	*n.d.*	*n.d.*
Rb	*n.d.*	*n.d.*	3	3	*n.d.*	7	*n.d.*	4	3
Sr	173	156	196	156	157	222	88	261	65
Pb	*n.d.*	*n.d.*	*n.d.*	*n.d.*	*n.d.*	*n.d.*	*n.d.*	*n.d.*	*n.d.*
Ga	14	14	17	16	18	18	17	15	11
Zr	11	29	40	47	48	18	22	13	16
Hf	0.4	1.0	1.3	1.5	1.4	0.6	0.7	0.4	0.6
Nb	0.9	1.9	2.2	2.8	3.1	1.4	1.5	0.8	1.0
Ta	0.7	0.4	0.9	0.9	1.3	0.8	1.0	0.3	0.5
Th	0.2	0.2	0.5	0.4	0.4	0.2	0.2	0.2	0.2
U	0.2	0.2	0.4	0.2	0.5	0.2	0.1	0.1	0.2
Y	6	12	21	20	17	11	12	6	13
La	1.0	2.4	3.3	3.0	2.0	1.9	1.8	1.3	1.5
Ce	2.6	6.4	8.5	7.9	5.9	4.6	4.4	3.0	3.9
Pr	0.39	0.94	1.30	1.30	0.98	0.66	0.66	0.42	0.52
Nd	2.0	4.7	7.1	6.6	5.5	3.6	3.5	2.0	2.7
Sm	0.7	1.5	2.2	2.1	1.8	1.1	1.1	0.7	0.9
Eu	0.36	0.56	0.76	0.77	0.93	0.47	0.52	0.32	0.36
Gd	0.9	1.9	2.5	2.6	2.2	1.4	1.5	0.8	1.3
Tb	0.2	0.3	0.4	0.5	0.4	0.2	0.3	0.2	0.3
Dy	1.0	2.0	2.9	3.0	2.5	1.6	1.8	1.0	1.9
Ho	0.2	0.4	0.6	0.6	0.5	0.3	0.4	0.2	0.5
Er	0.7	1.2	1.9	1.9	1.6	1.0	1.2	0.6	1.5
Tm	0.10	0.19	0.32	0.30	0.27	0.17	0.20	0.09	0.24
Yb	0.7	1.2	2.1	1.9	1.7	1.1	1.3	0.6	1.7
Lu	0.10	0.19	0.33	0.29	0.27	0.16	0.20	0.10	0.28

Group					**G2**				
Reference					**Zwanzig et al., 1999**				
Sample	12-74-55	12-74-65	32-80-964	32-79-526	32-79-515	32-80-1057	32-79-595	32-76-436	12-74-71
La/Sm_{CN}	0.88	1.01	1.00	0.94	0.71	1.09	1.00	1.26	1.16
Gd/Yb_{CN}	1.18	1.29	1.02	1.11	1.12	1.05	0.96	1.09	0.65
La/Yb_{CN}	1.08	1.39	1.17	1.14	0.85	1.26	0.99	1.60	0.66
Eu/Eu*	1.37	1.01	1.00	1.01	1.41	1.17	1.21	1.32	1.03
Ce/Ce*	1.05	1.06	1.00	0.97	1.04	1.02	1.00	0.98	1.08
Zr/Y	1.8	2.5	1.9	2.3	2.8	1.7	1.8	2.1	1.2
Ti/Zr	261	152	145	114	122	201	158	159	109
Al_2O_3/TiO_2	38	22	15	18	15	31	27	56	53
Zr/Nb	12	15	19	16	15	14	15	16	16
Zr/Zr*	0.51	0.64	0.59	0.73	0.88	0.53	0.64	0.65	0.60
Zr/Sm_{PM}	0.60	0.78	0.74	0.89	1.06	0.65	0.78	0.76	0.74
Zr/Nd_{PM}	0.65	0.77	0.70	0.87	1.07	0.64	0.78	0.80	0.72
Ti/Ti*	1.22	1.10	1.06	0.96	1.02	1.16	1.01	1.04	0.64
Ti/Gd_{PM}	2.05	1.75	1.34	1.32	1.67	1.63	1.30	1.64	0.50
Ti/Sm_{PM}	1.40	1.06	0.96	0.92	1.16	1.17	1.10	1.08	0.73
Nb/Nb*	0.87	0.90	0.59	0.98	1.35	0.73	0.80	0.61	0.71
Nb/Th_{PM}	0.81	1.01	0.54	1.03	1.17	0.74	0.78	0.61	0.77
Nb/La_{PM}	0.94	0.80	0.64	0.93	1.57	0.71	0.82	0.62	0.65
Mg#	52	52	30	30	46	38	45	43	49
ΣLREE	8.06	18.39	25.68	24.19	19.35	13.74	13.54	8.58	11.18
ΣHREE	9.03	17.39	29.30	28.88	24.51	15.16	17.58	9.00	19.56

Group	G2								
Reference	**Zwanzig et al., 1999**								
Sample	12-74-55	32-78-5126	12-74-76	32-79-227	32-79-230	32-76-301	32-76-368	32-76-511	12-74-75
Easting (m)	428848	382410	429168	429016	428748	370890	400162	393567	428529
Northing (m)	6303792	6309729	6301773	6301687	6301735	6301615	6312023	6314697	6301687
DDH	Outcrop	Outcrop	Outcrop	Outcrop	Outcrop	Outcrop	Outcrop	Outcrop	Outcrop
Depth (m)	-	-	-	-	-	-	-	-	-
SiO_2	50.47	50.82	49.60	49.63	50.12	53.26	50.43	59.07	50.26
Al_2O_3	21.63	20.19	17.53	21.55	18.22	18.75	13.59	16.55	18.56
TiO_2	0.63	0.87	0.49	0.55	0.86	0.56	0.97	0.65	1.45
Fe_2O_3	10.66	11.78	12.90	10.33	12.23	10.35	11.53	9.97	13.07
MnO	0.16	0.16	0.30	0.17	0.21	0.19	0.19	0.13	0.19
MgO	3.21	3.13	6.08	3.86	5.16	4.53	6.07	2.48	3.41
CaO	10.04	10.89	11.03	10.64	9.47	8.36	16.05	7.77	9.96
Na_2O	2.77	1.78	1.61	2.94	3.40	3.55	0.88	3.01	2.54
K_2O	0.36	0.30	0.41	0.29	0.23	0.36	0.18	0.29	0.35
P_2O_5	0.07	0.08	0.04	0.05	0.09	0.08	0.10	0.08	0.20
LOI	0.90	0.58	1.29	0.81	0.57	0.77	1.06	2.51	0.32
Total	100	100	100	100	100	100	100	100	100
Ni	17	*n.d.*	41	20	*n.d.*	25	19	119	*n.d.*
Cr	*n.d.*	17	46	25	*n.d.*	30	21	668	*n.d.*
Co	38	56	60	50	40	43	40	57	41
V	227	384	293	231	258	283	166	328	196
Sc	*n.d.*	*n.d.*	*n.d.*	*n.d.*	*n.d.*	*n.d.*	*n.d.*	*n.d.*	*n.d.*
Cu	79	232	12	15	-10	206	86	17	17
Zn	66	71	127	60	46	95	109	89	40
Mo	*n.d.*	*n.d.*	*n.d.*	*n.d.*	*n.d.*	*n.d.*	*n.d.*	*n.d.*	*n.d.*
W	137	238	185	169	122	68	85	94	157
Sb	*n.d.*	*n.d.*	*n.d.*	21	1.1	*n.d.*	*n.d.*	0.7	*n.d.*
Sn	*n.d.*	1.2	*n.d.*	*n.d.*	1.0	*n.d.*	*n.d.*	1.2	*n.d.*

Group	G2								
Reference	Zwanzig et al., 1999								
Sample	12-74-55	32-78-5126	12-74-76	32-79-227	32-79-230	32-76-301	32-76-368	32-76-511	12-74-75
Ba	113	155	39	40	22	23	91	36	56
Cs	*n.d.*	*n.d.*	*n.d.*	*n.d.*	*n.d.*	*n.d.*	*n.d.*	*n.d.*	*n.d.*
Rb	4	3	3	*n.d.*	*n.d.*	*n.d.*	5	*n.d.*	*n.d.*
Sr	347	215	137	189	160	235	202	152	175
Pb	*n.d.*	*n.d.*	*n.d.*	*n.d.*	*n.d.*	*n.d.*	*n.d.*	*n.d.*	*n.d.*
Ga	18	17	14	17	17	18	17	14	16
Zr	14	23	12	17	32	35	31	46	37
Hf	0.5	0.7	0.4	0.5	1.0	1.2	1.0	1.4	1.2
Nb	1.2	2.1	1.1	1.4	1.9	3.1	2.6	3.8	2.7
Ta	0.6	1.2	0.9	0.9	0.7	0.5	0.5	0.6	0.8
Th	0.3	0.2	0.1	0.2	0.3	0.2	0.3	0.2	0.5
U	0.2	0	0.2	*n.d.*	0.2	0.2	0.1	0.1	0.3
Y	8	9	7	10	15	15	11	18	15
La	1.8	2.3	1.0	1.0	3.4	3.5	3.0	3.6	3.1
Ce	4.7	5.3	2.8	2.8	7.9	8.5	7.2	8.3	8.7
Pr	0.66	0.76	0.42	0.47	1.02	1.26	0.99	1.20	1.19
Nd	3.3	4.1	2.2	2.9	4.9	6.7	4.9	6.3	6.0
Sm	1.1	1.2	0.8	1.0	1.6	2.0	1.5	2.1	1.8
Eu	0.54	0.56	0.36	0.43	0.89	0.88	0.63	0.78	0.74
Gd	1.3	1.4	1.0	1.3	2.0	2.3	1.7	2.4	2.3
Tb	0.2	0.3	0.2	0.2	0.4	0.4	0.3	0.5	0.4
Dy	1.4	1.6	1.2	1.4	2.1	2.6	1.8	2.9	2.5
Ho	0.3	0.3	0.3	0.3	0.5	0.5	0.4	0.6	0.5
Er	0.8	1.0	0.7	0.9	1.4	1.5	1.1	1.8	1.6
Tm	0.13	0.15	0.11	0.14	0.21	0.25	0.17	0.27	0.23
Yb	0.9	1.0	0.7	0.9	1.4	1.5	1.1	1.7	1.5
Lu	0.14	0.15	0.11	0.14	0.21	0.22	0.18	0.27	0.25

Group	G2								
Reference	Zwanzig et al., 1999								
Sample	12-74-55	32-78-5126	12-74-76	32-79-227	32-79-230	32-76-301	32-76-368	32-76-511	12-74-75
La/Sm_{CN}	1.11	1.25	0.80	0.63	1.38	1.12	1.32	1.14	1.10
Gd/Yb_{CN}	1.20	1.15	1.17	1.15	1.13	1.26	1.23	1.15	1.23
La/Yb_{CN}	1.52	1.63	0.97	0.75	1.67	1.69	1.87	1.50	1.49
Eu/Eu*	1.43	1.32	1.25	1.16	1.55	1.25	1.22	1.07	1.11
Ce/Ce*	1.05	0.99	1.07	1.01	1.05	1.00	1.02	0.97	1.10
Zr/Y	1.7	2.4	1.8	1.7	2.2	2.3	2.8	2.5	2.5
Ti/Zr	268	226	243	193	115	146	107	123	104
Al_2O_3/TiO_2	34	23	35	40	28	21	33	14	26
Zr/Nb	11	11	11	12	17	11	12	12	14
Zr/Zr*	0.43	0.60	0.53	0.57	0.67	0.55	0.68	0.74	0.64
Zr/Sm_{PM}	0.52	0.77	0.61	0.66	0.82	0.69	0.86	0.89	0.80
Zr/Nd_{PM}	0.52	0.70	0.66	0.71	0.80	0.64	0.79	0.90	0.75
Ti/Ti*	1.14	1.47	1.22	1.09	0.71	0.92	0.82	1.04	0.74
Ti/Gd_{PM}	2.04	2.42	1.94	1.63	1.22	1.63	1.40	1.55	1.19
Ti/Sm_{PM}	1.25	1.55	1.34	1.15	0.85	0.90	0.82	0.98	0.74
Nb/Nb*	0.64	1.05	1.32	1.33	0.67	1.23	1.06	1.60	0.79
Nb/Th_{PM}	0.60	1.22	1.50	1.23	0.79	1.73	1.28	2.46	0.74
Nb/La_{PM}	0.68	0.90	1.17	1.43	0.56	0.88	0.87	1.04	0.84
Mg#	37	34	48	43	36	46	46	51	33
ΣLREE	13.26	15.63	8.57	9.89	21.61	25.21	19.75	24.65	23.91
ΣHREE	11.99	14.00	10.11	13.68	21.09	22.40	16.45	26.37	22.00

Group				**G2**					
Reference				**Zwanzig et al., 1999**					
Sample	12-78-160	12-77-639	12-77-641	52-77-1524	52-76-346	52-77-1710	32-76-112	32-76-110	32-76-110
Easting (m)	348652	337622	337479	389869	386834	382488	371978	372134	372134
Northing (m)	6281050	6279532	6279674	6283101	6297098	6288564	6290511	6290325	6290325
DDH	Outcrop	Outcrop	Outcrop	Outcrop	Outcrop	Outcrop	Outcrop	Outcrop	Outcrop
Depth (m)	-	-	-	-	-	-	-	-	-
SiO_2	49.96	49.19	49.62	49.62	50.90	50.82	49.93	50.22	60.34
Al_2O_3	15.27	16.35	16.51	16.51	16.76	17.27	20.67	15.46	13.93
TiO_2	0.85	0.74	0.85	0.85	0.61	0.67	0.81	0.83	1.06
Fe_2O_3	11.71	10.92	11.96	11.96	8.41	12.00	11.71	14.17	13.13
MnO	0.16	0.17	0.16	0.16	0.15	0.20	0.18	0.21	0.27
MgO	8.11	9.55	5.65	5.65	5.71	5.07	3.21	6.99	2.48
CaO	11.36	10.68	13.17	13.17	15.04	10.27	10.80	8.96	5.31
Na_2O	2.28	2.18	1.69	1.69	2.16	3.36	2.26	2.25	2.95
K_2O	0.20	0.14	0.31	0.31	0.17	0.29	0.34	0.85	0.44
P_2O_5	0.10	0.08	0.08	0.08	0.09	0.04	0.09	0.07	0.10
LOI	0.76	0.74	1.35	1.41	2.91	0.84	0.8	1.26	0.89
Total	100	100	100	100	100	100	100	100	100
Ni	*n.d.*	152	165	27	143	*n.d.*	25	27	*n.d.*
Cr	*n.d.*	322	397	166	232	30	*n.d.*	56	*n.d.*
Co	39	50	52	52	52	47	65	63	53
V	286	287	249	292	208	337	284	340	31
Sc	*n.d.*	*n.d.*	*n.d.*	*n.d.*	*n.d.*	*n.d.*	*n.d.*	*n.d.*	*n.d.*
Cu	151	139	94	78	80	86	792	76	82
Zn	99	85	58	95	63	84	143	103	150
Mo	*n.d.*	*n.d.*	*n.d.*	*n.d.*	*n.d.*	*n.d.*	*n.d.*	*n.d.*	*n.d.*
W	93	31	31	107	123	111	184	121	302
Sb	*n.d.*	1.1	1.1	*n.d.*	*n.d.*	*n.d.*	*n.d.*	*n.d.*	*n.d.*
Sn	*n.d.*	*n.d.*	*n.d.*	*n.d.*	*n.d.*	*n.d.*	20	*n.d.*	6.2

Group	G2								
Reference	Zwanzig et al., 1999								
Sample	12-78-160	12-77-639	12-77-641	52-77-1524	52-76-346	52-77-1710	32-76-112	32-76-110	32-76-110
Ba	87	28	20	63	62	66	58	130	74
Cs	*n.d.*	*n.d.*	1.0	*n.d.*	*n.d.*	*n.d.*	*n.d.*	*n.d.*	*n.d.*
Rb	*n.d.*	*n.d.*	*n.d.*	3	*n.d.*	*n.d.*	3	17	4
Sr	346	113	140	201	399	165	185	129	120
Pb	*n.d.*	*n.d.*	*n.d.*	*n.d.*	*n.d.*	*n.d.*	*n.d.*	*n.d.*	8
Ga	20	15	14	18	15	15	19	15	19
Zr	77	45	40	36	27	12	32	27	58
Hf	2.4	1.4	1.2	1.3	1.0	0.5	1.0	0.9	1.9
Nb	5.9	2.8	2.1	2.2	1.3	1.0	1.9	1.4	2.7
Ta	0.8	0.3	0.2	0.6	0.7	0.6	1.0	0.6	1.4
Th	0.4	0.2	0.2	0.2	0.1	0.1	0.2	0.2	0.4
U	0.2	0.3	0.5	*n.d.*	0.4	0.2	0.2	0.1	0.3
Y	26	20	17	17	17	10	17	15	31
La	5.8	2.1	2.0	2.4	2.2	0.9	2.6	1.8	3.1
Ce	16.0	6.2	5.6	6.6	5.7	2.8	6.5	4.9	8.8
Pr	2.52	1.01	0.87	1.03	0.85	0.41	0.99	0.78	1.38
Nd	13.1	5.4	4.8	5.8	4.5	2.1	5.5	4.1	7.9
Sm	4.0	2.0	1.8	2.0	1.5	0.7	1.9	1.5	3.1
Eu	1.36	0.80	0.70	0.76	0.61	0.37	0.73	0.59	1.11
Gd	4.5	2.7	2.2	2.5	2.1	1.1	2.3	2.0	4.0
Tb	0.8	0.5	0.4	0.5	0.4	0.2	0.4	0.4	0.8
Dy	4.4	3.3	2.9	3.0	2.6	1.4	2.9	2.4	5.2
Ho	0.9	0.7	0.6	0.6	0.6	0.3	0.6	0.5	1.1
Er	2.6	2.1	1.7	1.8	1.7	1.0	1.8	1.6	3.3
Tm	0.36	0.31	0.27	0.28	0.27	0.16	0.29	0.24	0.52
Yb	2.3	2.0	1.8	1.7	1.7	1.0	1.9	1.5	3.4
Lu	0.33	0.32	0.28	0.29	0.27	0.18	0.28	0.25	0.53

Group	G2								
Reference	Zwanzig et al., 1999								
Sample	12-78-160	12-77-639	12-77-641	52-77-1524	52-76-346	52-77-1710	32-76-112	32-76-110	32-76-110
La/Sm_{CN}	0.94	0.67	0.70	0.76	0.93	0.83	0.88	0.73	0.65
Gd/Yb_{CN}	1.65	1.12	1.02	1.17	1.03	0.88	1.03	1.08	0.97
La/Yb_{CN}	1.82	0.75	0.78	0.98	0.94	0.66	0.99	0.82	0.65
Eu/Eu*	0.98	1.05	1.06	1.04	1.05	1.26	1.07	1.03	0.97
Ce/Ce*	1.03	1.05	1.05	1.04	1.02	1.09	1.01	1.03	1.04
Zr/Y	3.0	2.2	2.3	2.1	1.6	1.2	1.8	1.8	1.8
Ti/Zr	112	111	110	140	132	323	150	179	109
Al_2O_3/TiO_2	13	18	22	19	27	26	26	19	13
Zr/Nb	13	16	19	11	12	17	11	12	12
Zr/Zr*	0.62	0.80	0.78	0.60	0.59	0.57	0.58	0.63	0.68
Zr/Sm_{PM}	0.77	0.90	0.87	0.70	0.70	0.66	0.68	0.71	0.75
Zr/Nd_{PM}	0.72	1.03	1.02	0.76	0.73	0.73	0.72	0.82	0.90
Ti/Ti*	0.88	0.87	0.88	0.93	0.79	1.56	0.93	1.14	0.75
Ti/Gd_{PM}	1.79	1.20	1.14	1.36	0.99	1.82	1.22	1.52	0.87
Ti/Sm_{PM}	0.77	0.89	0.86	0.88	0.83	1.90	0.91	1.13	0.73
Nb/Nb*	1.48	1.52	1.33	1.21	0.85	0.96	0.96	0.82	0.85
Nb/Th_{PM}	2.15	1.73	1.66	1.59	1.26	0.92	1.23	0.88	0.84
Nb/La_{PM}	1.02	1.33	1.06	0.92	0.58	1.00	0.74	0.76	0.86
Mg#	34	58	63	48	57	46	35	49	27
ΣLREE	47.30	20.16	18.04	21.15	17.49	8.39	20.49	15.66	29.31
ΣHREE	37.53	29.41	25.53	25.73	24.76	14.24	25.58	22.00	46.28

Group	G2								
Reference	This Study				Beaumont-Smith, 2007				
Sample	LL13-09	LL13-11	LL13-12	LL13-05	103-99-1016	103-99-1021	103-99-1022	103-99-1041	103-99-1042
Easting (m)	383730	381180	381180	412418	377838	380219	380034	382507	382540
Northing (m)	6292040	6292097	6292097	6307756	6291961	6293169	6293133	6291545	6291564
DDH	BT12-01	LW12-05	LW12-05	FL12-01	Outcrop	Outcrop	Outcrop	Outcrop	Outcrop
Depth (m)	153	23	86	278	-	-	-	-	-
SiO_2	52.83	54.03	52.22	52.50	50.52	52.49	53.57	50.96	52.10
Al_2O_3	14.97	14.13	14.14	14.91	13.80	14.36	13.53	21.24	18.90
TiO_2	1.10	1.28	1.39	1.18	1.48	1.13	1.65	1.16	1.55
Fe_2O_3	11.72	12.97	15.12	13.70	14.58	13.61	16.13	12.49	16.36
MnO	0.18	0.21	0.23	0.20	0.22	0.22	0.24	0.12	0.16
MgO	6.33	5.07	5.07	5.45	6.67	6.00	4.25	3.74	4.75
CaO	8.47	8.53	8.31	8.07	9.85	8.79	7.18	5.40	3.11
Na_2O	3.85	3.12	3.16	3.27	2.61	2.58	2.66	4.35	2.37
K_2O	0.30	0.48	0.22	0.59	0.16	0.69	0.58	0.42	0.56
P_2O_5	0.26	0.19	0.14	0.12	0.11	0.13	0.20	0.12	0.14
LOI	3.25	1.8	0.58	1.08	0.67	0.33	0.03	3.1	3.14
Total	100	100	100	100	100	100	100	100	100
Ni	60	*n.d.*	*n.d.*	*n.d.*	86	71	87	34	54
Cr	70	20	*n.d.*	*n.d.*	114	51	21	-5	10
Co	39	41	44	39	45	50	49	38	39
V	298	282	340	299	404	293	388	307	381
Sc	36	44	48	47	51	49	44	40	50
Cu	70	20	*n.d.*	10	68	45	79	141	85
Zn	80	100	110	100	69	89	120	93	114
Mo	*n.d.*	*n.d.*	*n.d.*	*n.d.*	*n.d.*	*n.d.*	*n.d.*	*n.d.*	*n.d.*
W	1.1	0.5	*n.d.*	*n.d.*	2.7	*n.d.*	0.6	0.5	*n.d.*
Sb	*n.d.*	*n.d.*	*n.d.*	*n.d.*	2.4	1.3	1.2	*n.d.*	*n.d.*
Sn	*n.d.*	*n.d.*	*n.d.*	*n.d.*	*n.d.*	*n.d.*	*n.d.*	*n.d.*	*n.d.*

Group	G2								
Reference	This Study				Beaumont-Smith, 2007				
Sample	LL13-09	LL13-11	LL13-12	LL13-05	103-99-1016	103-99-1021	103-99-1022	103-99-1041	103-99-1042
Ba	118	129	37	183	27	350	341	77	136
Cs	0.1	0.4	*n.d.*	0.5	*n.d.*	*n.d.*	*n.d.*	*n.d.*	*n.d.*
Rb	5	9	*n.d.*	11	*n.d.*	*n.d.*	*n.d.*	*n.d.*	*n.d.*
Sr	474	254	296	265	159	222	368	197	204
Pb	8	23	*n.d.*	*n.d.*	7	*n.d.*	10	*n.d.*	9
Ga	18	20	20	18	18	19	23	19	20
Zr	66	83	90	82	77	87	130	47	66
Hf	1.7	2.4	2.3	2.2	2.8	3.1	4.2	1.0	1.6
Nb	3.7	4.9	4.8	4.2	3.6	3.9	5.4	1.8	2.5
Ta	0.1	0.2	0.3	0.2	0.3	0.3	0.5	*n.d.*	0.1
Th	0.7	0.5	0.5	0.5	0.7	0.6	1.0	0.1	0.2
U	0.4	0.3	0.3	0.3	0.3	0.4	0.6	0.1	0.1
Y	21	31	33	29	35	34	44	15	19
La	5.0	4.8	5.5	4.2	2.8	5.0	7.1	2.8	3.3
Ce	11.5	13.2	14.5	11.7	8.2	13.9	19.8	7.4	8.9
Pr	1.69	2.05	2.21	1.81	1.23	1.99	2.79	1.03	1.22
Nd	8.1	9.7	11.2	9.0	6.5	10.1	14.1	5.3	6.1
Sm	2.2	3.1	3.9	3.0	2.7	3.3	4.5	1.7	1.9
Eu	0.86	1.10	1.16	1.04	1.06	1.17	1.51	0.84	0.79
Gd	2.6	4.2	4.6	3.7	4.3	4.5	5.8	2.5	3.0
Tb	0.5	0.8	0.9	0.8	0.9	0.9	1.2	0.5	0.5
Dy	3.5	5.3	6.0	5.4	6.2	6.1	7.8	2.9	3.4
Ho	0.8	1.2	1.2	1.1	1.4	1.3	1.7	0.6	0.7
Er	2.5	3.5	3.6	3.3	4.2	4.0	5.0	1.8	2.2
Tm	0.38	0.51	0.52	0.49	0.63	0.61	0.75	0.24	0.30
Yb	2.5	3.5	3.4	3.2	4.0	3.9	4.8	1.5	1.9
Lu	0.38	0.55	0.55	0.48	0.65	0.62	0.77	0.24	0.28

Group	G2								
Reference	This Study				Beaumont-Smith, 2007				
Sample	LL13-09	LL13-11	LL13-12	LL13-05	103-99-1016	103-99-1021	103-99-1022	103-99-1041	103-99-1042
La/Sm_{CN}	1.50	1.01	0.90	0.91	0.67	0.99	1.02	1.06	1.09
Gd/Yb_{CN}	0.87	0.99	1.12	0.96	0.89	0.96	0.99	1.37	1.29
La/Yb_{CN}	1.46	1.00	1.14	0.94	0.51	0.93	1.06	1.31	1.24
Eu/Eu*	1.11	0.94	0.83	0.95	0.95	0.93	0.90	1.23	1.00
Ce/Ce*	0.97	1.03	1.02	1.04	1.08	1.08	1.08	1.06	1.09
Zr/Y	3.1	2.7	2.8	2.8	2.2	2.6	2.9	3.0	3.5
Ti/Zr	96	89	91	85	115	77	76	144	137
Al_2O_3/TiO_2	14	11	10	13	9	13	8	18	12
Zr/Nb	14	13	16	19	21	22	24	26	26
Zr/Zr*	0.91	0.88	0.78	0.91	1.04	0.88	0.94	0.89	1.10
Zr/Sm_{PM}	1.22	1.07	0.91	1.09	1.12	1.06	1.14	1.09	1.34
Zr/Nd_{PM}	1.00	1.05	0.98	1.12	1.43	1.06	1.13	1.07	1.32
Ti/Ti*	1.07	0.87	0.89	0.89	1.04	0.74	0.84	1.16	1.47
Ti/Gd_{PM}	1.22	1.01	1.13	1.02	1.05	0.82	0.97	2.06	2.23
Ti/Sm_{PM}	1.05	0.86	0.74	0.83	1.15	0.73	0.78	1.40	1.64
Nb/Nb*	0.72	1.10	1.01	1.03	0.97	0.82	0.75	1.03	1.12
Nb/Th_{PM}	0.71	1.19	1.17	1.06	0.73	0.86	0.74	1.69	1.66
Nb/La_{PM}	0.73	1.01	0.88	0.99	1.27	0.78	0.76	0.63	0.75
Mg#	52	44	40	44	48	47	34	37	37
ΣLREE	31.96	38.10	43.05	34.45	26.91	39.89	55.65	21.62	25.22
ΣHREE	31.78	45.79	48.90	44.00	53.36	51.44	65.98	23.09	27.95

Group	G2								
Reference	Beaumont-Smith, 2007								
Sample	103-99-1043	103-99-1046	103-99-1069	103-99-1075	103-00-1268	103-00-1270	103-00-1270	103-00-1408	103-01-1621
Easting (m)	384401	383895	377561	376798	352910	353453	353453	366041	340342
Northing (m)	6291702	6291547	6292030	6292262	6285022	6285720	6285720	6288040	6280628
DDH	Outcrop	Outcrop	Outcrop	Outcrop	Outcrop	Outcrop	Outcrop	Outcrop	Outcrop
Depth (m)	-	-	-	-	-	-	-	-	-
SiO_2	56.21	47.67	50.26	50.58	53.12	53.44	48.66	48.24	48.89
Al_2O_3	19.32	22.80	12.87	16.50	13.33	14.60	13.08	15.01	14.80
TiO_2	0.65	1.31	1.83	0.72	1.69	2.03	1.29	1.59	0.85
Fe_2O_3	9.76	15.67	16.46	11.26	12.54	13.73	19.93	14.44	12.05
MnO	0.12	0.15	0.24	0.16	0.20	0.16	0.17	0.16	0.18
MgO	2.56	4.53	5.15	6.78	4.38	3.82	5.74	7.67	8.06
CaO	5.54	3.77	10.49	12.15	10.55	8.37	8.29	10.16	13.19
Na_2O	4.23	2.74	2.31	1.56	3.91	3.48	2.57	2.36	1.80
K_2O	1.23	1.18	0.20	0.17	0.05	0.12	0.13	0.23	0.10
P_2O_5	0.38	0.18	0.20	0.11	0.24	0.24	0.14	0.13	0.07
LOI	4.17	3.97	2.61	1.04	3.58	0.76	1.02	1.15	0.56
Total	100	100	100	100	100	100	100	100	100
Ni	25	43	*n.d.*	103	56	*n.d.*	*n.d.*	73	118
Cr	*n.d.*	58	26	182	86	14	13	179	312
Co	22	44	48	55	43	30	44	52	52
V	163	345	417	235	378	423	392	403	303
Sc	35	54	50	42	41	39	55	50	47
Cu	28	13	28	182	482	*n.d.*	31	128	95
Zn	76	105	139	-30	104	55	78	112	69
Mo	*n.d.*	*n.d.*	*n.d.*	*n.d.*	*n.d.*	*n.d.*	*n.d.*	*n.d.*	*n.d.*
W	1.4	1.9	*n.d.*	*n.d.*	*n.d.*	*n.d.*	*n.d.*	*n.d.*	2.5
Sb	1.5	0.6	0.5	0.5	0.5	1.7	0.7	0.4	1.5
Sn	*n.d.*	*n.d.*	*n.d.*	*n.d.*	*n.d.*	*n.d.*	*n.d.*	1.2	1.3

Group	G2								
Reference	Beaumont-Smith, 2007								
Sample	103-99-1043	103-99-1046	103-99-1069	103-99-1075	103-00-1268	103-00-1270	103-00-1270	103-00-1408	103-01-1621
Ba	175	242	54	81	40	27	19	39	33
Cs	*n.d.*	*n.d.*	*n.d.*	*n.d.*	*n.d.*	*n.d.*	*n.d.*	*n.d.*	*n.d.*
Rb	*n.d.*	*n.d.*	*n.d.*	*n.d.*	*n.d.*	*n.d.*	*n.d.*	*n.d.*	*n.d.*
Sr	209	154	114	297	206	362	160	116	103
Pb	*n.d.*	9	6	*n.d.*	6	*n.d.*	6	*n.d.*	*n.d.*
Ga	18	21	21	16	18	21	18	21	15
Zr	76	64	123	40	93	115	45	88	45
Hf	1.9	1.5	3.6	1.3	2.6	3.2	1.2	2.6	1.3
Nb	2.9	2.5	6.0	1.7	5.8	7.5	3.5	2.3	1.1
Ta	0.2	0.1	0.4	*n.d.*	0.4	0.5	0.2	0.2	0
Th	0.3	0.3	1.0	0.3	0.7	0.9	0.2	0.4	0.2
U	0.3	0.2	0.4	0.2	0.6	0.3	-0.1	0.2	*n.d.*
Y	24	17	45	22	27	32	23	31	18
La	5.3	5.1	7.4	4.4	7.7	6.6	4.1	4.4	2.1
Ce	13.5	12.6	18.2	10.1	18.3	16.0	10.6	12.0	6.0
Pr	1.76	1.65	2.60	1.44	2.60	2.44	1.57	1.92	0.95
Nd	8.9	8.5	13.0	6.8	12.5	12.8	7.9	10.1	5.2
Sm	2.7	2.6	4.3	2.1	3.7	4.1	2.4	3.5	1.7
Eu	0.95	1.04	1.43	0.82	1.28	1.05	1.14	1.32	0.72
Gd	4.0	3.7	5.5	2.8	4.2	4.9	3.2	4.4	2.4
Tb	0.7	0.6	1.1	0.5	0.8	0.9	0.6	0.8	0.5
Dy	4.2	3.6	7.7	3.5	4.9	5.8	4.1	5.4	3.2
Ho	0.9	0.7	1.7	0.8	1.0	1.2	0.9	1.2	0.7
Er	2.9	2.0	5.0	2.5	2.8	3.5	2.7	3.5	2.0
Tm	0.40	0.26	0.76	0.35	0.41	0.51	0.40	0.49	0.30
Yb	2.5	1.6	5.0	2.3	2.7	3.2	2.6	3.0	1.9
Lu	0.40	0.25	0.77	0.37	0.41	0.50	0.41	0.46	0.28

Group	G2								
Reference	Beaumont-Smith, 2007								
Sample	103-99-1043	103-99-1046	103-99-1069	103-99-1075	103-00-1268	103-00-1270	103-00-1270	103-00-1408	103-01-1621
La/Sm_{CN}	1.24	1.26	1.12	1.34	1.34	1.03	1.07	0.82	0.79
Gd/Yb_{CN}	1.29	1.89	0.91	1.01	1.29	1.26	0.99	1.19	1.08
La/Yb_{CN}	1.49	2.22	1.07	1.38	2.04	1.46	1.10	1.05	0.80
Eu/Eu*	0.88	1.02	0.91	1.03	0.99	0.71	1.26	1.04	1.09
Ce/Ce*	1.08	1.07	1.02	0.98	1.00	0.98	1.02	1.01	1.04
Zr/Y	3.2	3.7	2.7	1.8	3.4	3.6	1.9	2.9	2.5
Ti/Zr	49	118	86	107	105	105	171	106	113
Al_2O_3/TiO_2	30	17	7	23	8	7	10	9	17
Zr/Nb	26	26	21	23	16	15	13	39	39
Zr/Zr*	0.88	0.78	0.95	0.61	0.79	0.91	0.59	0.86	0.86
Zr/Sm_{PM}	1.10	0.98	1.15	0.75	1.00	1.10	0.73	1.01	1.05
Zr/Nd_{PM}	1.04	0.91	1.16	0.72	0.91	1.10	0.70	1.06	1.04
Ti/Ti*	0.49	0.97	0.96	0.72	1.05	1.33	1.02	0.98	0.96
Ti/Gd_{PM}	0.70	2.18	1.01	0.89	1.70	1.75	1.37	1.46	1.28
Ti/Sm_{PM}	0.48	1.04	0.89	0.72	0.94	1.03	1.12	0.96	1.06
Nb/Nb*	0.83	0.74	0.79	0.58	0.88	1.11	1.46	0.64	0.72
Nb/Th_{PM}	1.26	1.14	0.78	0.85	1.03	1.09	2.47	0.80	0.95
Nb/La_{PM}	0.55	0.49	0.80	0.39	0.75	1.14	0.86	0.51	0.55
Mg#	34	36	38	54	41	36	36	51	57
ΣLREE	37.17	35.21	52.43	28.50	50.26	47.90	30.85	37.60	19.12
ΣHREE	35.85	26.43	66.91	32.57	40.26	47.50	34.90	45.62	26.66

Group				**G2**					
Reference				**Beaumont-Smith, 2007**					
Sample	94-00-53	95-00-09	95-00-10	95-00-11	95-00-17	95-00-18	95-00-30	95-00-32	95-00-45
Easting (m)	384519	381315	381239	381201	380881	380954	380441	380508	380664
Northing (m)	6291811	6307872	6307806	6307730	6307914	6307998	6307604	6307661	6307705
DDH	Outcrop	Outcrop	Outcrop	Outcrop	Outcrop	Outcrop	Outcrop	Outcrop	Outcrop
Depth (m)	-	-	-	-	-	-	-	-	-
SiO_2	54.23	49.75	44.85	46.35	55.73	48.60	45.49	53.25	50.40
Al_2O_3	13.78	18.47	18.44	17.65	15.18	16.97	18.30	17.45	21.13
TiO_2	1.32	1.01	1.19	1.12	1.10	1.34	1.04	1.02	0.81
Fe_2O_3	14.21	11.80	15.82	15.19	13.98	15.82	15.00	12.91	10.16
MnO	0.21	0.19	0.25	0.26	0.20	0.23	0.23	0.23	0.15
MgO	4.53	4.58	4.09	3.65	3.38	4.09	5.51	3.37	4.34
CaO	7.90	11.90	13.05	13.52	8.05	9.80	13.03	7.16	10.71
Na_2O	3.02	1.85	1.81	1.61	2.09	2.68	0.92	4.15	2.04
K_2O	0.64	0.37	0.42	0.57	0.21	0.38	0.40	0.38	0.20
P_2O_5	0.15	0.09	0.09	0.07	0.09	0.09	0.08	0.08	0.05
LOI	3.97	0.73	1.57	2.57	0.27	0.38	0.90	0.50	1.24
Total	100	100	100	100	100	100	100	100	100
Ni	*n.d.*	*n.d.*	*n.d.*	*n.d.*	*n.d.*	*n.d.*	*n.d.*	*n.d.*	*n.d.*
Cr	23	15	22	86	*n.d.*	*n.d.*	63	*n.d.*	57
Co	35	30	30	35	28	38	37	25	23
V	278	316	346	286	248	418	341	137	266
Sc	48	39	39	38	38	46	46	41	35
Cu	124	37	78	95	220	103	74	*n.d.*	85
Zn	70	126	145	151	101	129	149	149	131
Mo	*n.d.*	*n.d.*	*n.d.*	*n.d.*	*n.d.*	*n.d.*	*n.d.*	*n.d.*	*n.d.*
W	*n.d.*	*n.d.*	*n.d.*	0.5	*n.d.*	*n.d.*	*n.d.*	*n.d.*	*n.d.*
Sb	0.9	0.4	0.9	0.7	*n.d.*	*n.d.*	0.9	0.6	0.3
Sn	1.1	*n.d.*	*n.d.*	*n.d.*	*n.d.*	*n.d.*	*n.d.*	*n.d.*	*n.d.*

Group	G2								
Reference	Beaumont-Smith, 2007								
Sample	94-00-53	95-00-09	95-00-10	95-00-11	95-00-17	95-00-18	*95-00-30*	*95-00-32*	*95-00-45*
Ba	314	78	63	82	37	52	42	71	31
Cs	*n.d.*	0.1	*n.d.*	0.2	*n.d.*	*n.d.*	0.3	0.2	*n.d.*
Rb	*n.d.*	*n.d.*	*n.d.*	*n.d.*	*n.d.*	*n.d.*	*n.d.*	*n.d.*	*n.d.*
Sr	231	230	202	232	225	201	150	209	228
Pb	*n.d.*	*n.d.*	*n.d.*	*n.d.*	*n.d.*	*n.d.*	*n.d.*	*n.d.*	9
Ga	15	20	21	20	21	23	13	18	16
Zr	101	33	36	33	49	56	32	50	30
Hf	2.4	1.1	1.0	1.1	1.6	1.5	0.8	1.3	0.8
Nb	3.7	1.6	1.4	1.6	2.6	2.3	1.0	1.4	0.8
Ta	0.3	0.1	0.1	0.1	0	0.2	0.1	0.1	0.1
Th	0.8	0.2	0.2	0.2	0.4	0.2	0.1	0.3	0.2
U	0.4	0.1	0.1	0.2	1.3	0.1	0.1	0.2	0.2
Y	35	15	14	15	18	18	13	18	11
La	8.1	3.0	2.1	4.3	4.3	3.3	1.8	2.6	2.3
Ce	19.3	7.4	5.7	10.3	10.1	8.7	4.6	6.9	5.7
Pr	2.56	1.15	0.96	1.55	1.52	1.44	0.74	1.05	0.86
Nd	12.2	6.1	5.4	7.7	7.7	7.7	4.0	5.7	4.4
Sm	3.7	1.8	1.8	2.1	2.1	2.3	1.3	1.9	1.3
Eu	1.21	0.85	0.72	1.18	1.00	0.94	0.35	0.82	0.64
Gd	4.9	2.4	2.4	2.6	2.9	3.1	1.9	2.8	1.8
Tb	0.9	0.4	0.4	0.4	0.5	0.5	0.3	0.5	0.3
Dy	5.7	2.6	2.5	2.6	3.0	3.3	2.2	3.1	2.0
Ho	1.2	0.6	0.5	0.6	0.7	0.7	0.4	0.6	0.4
Er	3.6	1.6	1.5	1.6	2.0	2.1	1.4	1.8	1.3
Tm	0.53	0.23	0.21	0.22	0.27	0.28	0.21	0.29	0.18
Yb	3.4	1.5	1.4	1.5	1.8	1.8	1.3	1.9	1.2
Lu	0.52	0.22	0.20	0.22	0.28	0.27	0.20	0.28	0.18

Group	G2								
Reference	Beaumont-Smith, 2007								
Sample	94-00-53	95-00-09	95-00-10	95-00-11	95-00-17	95-00-18	95-00-30	95-00-32	95-00-45
La/Sm_{CN}	1.43	1.04	0.77	1.35	1.29	0.91	0.92	0.86	1.09
Gd/Yb_{CN}	1.21	1.31	1.40	1.40	1.29	1.40	1.17	1.26	1.24
La/Yb_{CN}	1.73	1.43	1.07	2.06	1.67	1.28	0.99	0.99	1.37
Eu/Eu*	0.87	1.25	1.06	1.57	1.23	1.07	0.68	1.08	1.26
Ce/Ce*	1.04	0.99	0.97	0.98	0.97	0.98	0.97	1.03	1.00
Zr/Y	2.9	2.2	2.5	2.1	2.7	3.1	2.6	2.8	2.7
Ti/Zr	75	182	198	198	134	143	190	119	159
Al_2O_3/TiO_2	10	18	15	16	14	13	18	17	26
Zr/Nb	27	21	25	20	19	24	34	37	36
Zr/Zr*	0.87	0.57	0.66	0.47	0.70	0.76	0.83	0.88	0.72
Zr/Sm_{PM}	1.10	0.71	0.79	0.62	0.91	0.96	1.00	1.04	0.89
Zr/Nd_{PM}	1.01	0.66	0.81	0.52	0.78	0.88	1.00	1.08	0.85
Ti/Ti*	0.78	1.07	1.35	0.93	0.98	1.17	1.93	0.98	1.13
Ti/Gd_{PM}	1.07	1.91	2.34	2.02	1.69	2.05	2.19	1.51	1.91
Ti/Sm_{PM}	0.74	1.17	1.40	1.10	1.09	1.22	1.70	1.11	1.27
Nb/Nb*	0.51	0.72	0.90	0.60	0.67	0.91	0.72	0.61	0.50
Nb/Th_{PM}	0.58	0.98	1.20	0.98	0.75	1.21	1.00	0.70	0.67
Nb/La_{PM}	0.45	0.53	0.67	0.37	0.60	0.69	0.52	0.53	0.37
Mg#	39	43	34	32	32	34	42	34	46
ΣLREE	51.99	22.69	19.00	29.72	29.68	27.52	14.66	21.85	16.99
ΣHREE	50.36	22.21	20.80	22.46	27.00	26.89	18.63	26.84	16.80

Group	G2				G3			
Reference	Beaumont-Smith, 2007				Zwanzig et al., 1999			
Sample	95-00-50	95-01-61	95-01-137	103-99-1106	32-80-802	32-76-779	32-76-251	32-78-5180
Easting (m)	379104	375784	372184	360719	414016	395347	369493	398919
Northing (m)	6306536	6304158	6303848	6288651	6306719	6310374	6297745	6311156
DDH	Outcrop	Outcrop	Outcrop	Outcrop	Outcrop	Outcrop	Outcrop	Outcrop
Depth (m)	-	-	-	-	-	-	-	-
SiO_2	49.35	48.69	48.20	57.32	50.55	50.99	52.57	48.87
Al_2O_3	20.20	17.80	17.59	14.34	17.51	13.19	14.52	12.42
TiO_2	0.72	0.85	0.89	0.59	1.46	1.66	1.37	1.61
Fe_2O_3	10.47	12.86	15.09	10.82	14.29	12.84	11.34	13.35
MnO	0.17	0.22	0.22	0.17	0.19	0.19	0.16	0.19
MgO	4.35	5.11	4.46	5.95	3.72	6.68	6.08	8.31
CaO	12.51	11.35	11.29	7.25	9.24	10.35	8.98	12.63
Na_2O	1.70	2.50	1.94	3.32	2.63	3.63	4.35	2.22
K_2O	0.49	0.56	0.25	0.15	0.19	0.33	0.39	0.26
P_2O_5	0.04	0.06	0.06	0.09	0.21	0.14	0.24	0.14
LOI	0.49	0.98	0.79	0.64	1.51	1.04	0.43	1.08
Total	100	100	100	100	100	100	100	100
Ni	850	*n.d.*	*n.d.*	21	*n.d.*	101	185	188
Cr	30	21	10	198	*n.d.*	257	394	486
Co	31	44	44	30	57	51	43	76
V	271	322	364	230	313	326	296	330
Sc	37	44	44	46	*n.d.*	*n.d.*	*n.d.*	*n.d.*
Cu	46	175	90	94	77	144	95	158
Zn	64	84	51	113	109	121	89	90
Mo	*n.d.*	*n.d.*	*n.d.*	*n.d.*	*n.d.*	*n.d.*	6	*n.d.*
W	*n.d.*	*n.d.*	0.5	*n.d.*	171	50	69	145
Sb	*n.d.*	0.8	*n.d.*	0.6	*n.d.*	*n.d.*	*n.d.*	*n.d.*
Sn	*n.d.*	*n.d.*	1.2	*n.d.*	*n.d.*	4.2	1.3	1.1

Group	G2				G3			
Reference	Beaumont-Smith, 2007				Zwanzig et al., 1999			
Sample	95-00-50	95-01-61	95-01-137	103-99-1106	32-80-802	32-76-779	32-76-251	32-78-5180
Ba	80	121	45	37	44	40	84	68
Cs	0.1	*n.d.*	*n.d.*	*n.d.*	*n.d.*	*n.d.*	*n.d.*	*n.d.*
Rb	*n.d.*	*n.d.*	*n.d.*	*n.d.*	*n.d.*	3	2.7	*n.d.*
Sr	176	189	171	127	322	178	242	217
Pb	*n.d.*	5	*n.d.*	*n.d.*	*n.d.*	*n.d.*	*n.d.*	*n.d.*
Ga	17	16	18	14	22	16	17	19
Zr	18	25	30	51	76	92	88	95
Hf	0.6	0.9	1.0	1.5	2.4	2.7	2.7	2.7
Nb	1.8	1.5	1.7	1.9	6.3	8.5	6.0	8.7
Ta	0.1	0.1	0.1	0.1	1.2	0.7	0.6	1.2
Th	0.1	0.3	0.4	0.5	0.5	0.8	0.7	0.8
U	0	0.1	0.1	0.2	0.2	0.3	0.3	0.2
Y	9	11	13	16	25	20	23	21
La	1.4	3.3	3.2	2.8	6.5	7.3	6.6	7.8
Ce	3.7	7.4	7.5	7.3	16.6	18.8	17.5	20.0
Pr	0.60	1.03	1.09	1.09	2.56	2.81	2.53	2.89
Nd	3.1	5.3	5.5	5.4	13.4	14.1	12.9	14.2
Sm	1.0	1.6	1.6	1.6	3.8	3.9	3.7	4.0
Eu	0.54	0.63	0.83	0.65	1.30	1.32	1.25	1.45
Gd	1.4	1.9	2.1	2.2	4.4	4.3	4.2	4.1
Tb	0.2	0.3	0.4	0.4	0.7	0.7	0.7	0.7
Dy	1.6	2.1	2.4	2.5	4.1	3.8	3.9	3.9
Ho	0.3	0.4	0.5	0.5	0.8	0.7	0.8	0.8
Er	1.0	1.2	1.4	1.7	2.3	2.0	2.4	1.9
Tm	0.15	0.18	0.21	0.25	0.35	0.28	0.34	0.27
Yb	0.9	1.1	1.3	1.6	2.0	1.7	2.1	1.7
Lu	0.15	0.16	0.19	0.26	0.29	0.22	0.31	0.23

Group	G2				G3			
Reference	Beaumont-Smith, 2007				Zwanzig et al., 1999			
Sample	95-00-50	95-01-61	95-01-137	103-99-1106	32-80-802	32-76-779	32-76-251	32-78-5180
La/Sm_{CN}	0.90	1.33	1.26	1.18	1.09	1.19	1.17	1.26
Gd/Yb_{CN}	1.28	1.45	1.28	1.13	1.76	2.17	1.64	2.05
La/Yb_{CN}	1.11	2.19	1.72	1.25	2.28	3.15	2.23	3.35
Eu/Eu*	1.35	1.12	1.38	1.07	0.97	0.97	0.97	1.09
Ce/Ce*	0.97	0.99	0.98	1.02	1.00	1.02	1.04	1.03
Zr/Y	1.9	2.3	2.3	3.2	3.0	4.6	3.9	4.4
Ti/Zr	241	199	175	69	113	107	93	101
Al_2O_3/TiO_2	28	21	20	24	12	8	11	8
Zr/Nb	10	16	17	27	12	11	15	11
Zr/Zr*	0.57	0.50	0.58	1.02	0.62	0.71	0.74	0.73
Zr/Sm_{PM}	0.69	0.63	0.73	1.32	0.79	0.92	0.95	0.94
Zr/Nd_{PM}	0.70	0.59	0.67	1.16	0.70	0.79	0.84	0.81
Ti/Ti*	1.23	1.16	1.01	0.74	0.91	1.04	0.89	0.98
Ti/Gd_{PM}	2.20	2.21	1.86	1.02	2.00	2.81	1.80	2.71
Ti/Sm_{PM}	1.48	1.13	1.15	0.81	0.80	0.89	0.79	0.85
Nb/Nb*	1.71	0.57	0.59	0.61	1.23	1.30	1.04	1.29
Nb/Th_{PM}	2.37	0.70	0.65	0.55	1.57	1.46	1.21	1.51
Nb/La_{PM}	1.24	0.47	0.54	0.67	0.96	1.15	0.90	1.11
Mg#	45	44	37	52	34	51	52	55
ΣLREE	11.81	21.07	21.79	21.05	48.51	52.60	48.66	54.54
ΣHREE	13.56	16.25	19.73	23.25	35.61	29.34	33.41	30.90

Group				**G3**					
Reference				**Zwanzig et al., 1999**					
Sample	32-76-604	32-76-498	32-80-89	52-77-1803	32-78-5130	32-80-801	32-76-286	32-76-651	32-76-254
Easting (m)	377034	375533	411414	408015	382287	413682	370724	382828	371966
Northing (m)	6303627	6302937	6308632	6307177	6309334	6306681	6299621	6305931	6299930
DDH	Outcrop	Outcrop	Outcrop	Outcrop	Outcrop	Outcrop	Outcrop	Outcrop	Outcrop
Depth (m)	-	-	-	-	-	-	-	-	-
SiO_2	53.35	58.26	49.82	53.65	55.74	61.31	52.05	52.22	52.80
Al_2O_3	20.21	19.89	14.33	19.97	16.30	16.19	19.64	21.98	18.03
TiO_2	1.01	0.84	1.51	1.15	1.13	0.99	0.96	0.88	0.95
Fe_2O_3	8.74	6.55	13.39	10.57	12.59	9.58	12.01	8.84	13.03
MnO	0.18	0.12	0.17	0.16	0.21	0.12	0.24	0.17	0.19
MgO	3.46	1.93	6.67	3.72	3.11	2.23	2.49	2.30	3.20
CaO	9.21	8.72	10.41	6.96	6.50	3.18	9.43	10.61	8.25
Na_2O	3.35	3.19	3.30	3.31	4.02	5.41	2.48	2.40	1.92
K_2O	0.24	0.31	0.26	0.31	0.17	0.77	0.54	0.44	1.47
P_2O_5	0.24	0.19	0.15	0.20	0.23	0.23	0.17	0.17	0.16
LOI	0.38	0.45	0.87	3.41	0.38	1.41	0.37	0.83	0.76
Total	100	100	100	100	100	100	100	100	100
Ni	*n.d.*	*n.d.*	80	*n.d.*	*n.d.*	*n.d.*	*n.d.*	*n.d.*	185
Cr	26	*n.d.*	146	*n.d.*	*n.d.*	*n.d.*	*n.d.*	*n.d.*	394
Co	53	34	67	36	52	40	32	21	43
V	154	104	343	115	171	65	225	110	296
Sc	*n.d.*	*n.d.*	*n.d.*	*n.d.*	*n.d.*	*n.d.*	*n.d.*	*n.d.*	*n.d.*
Cu	19	101	98	93	79	17	97	33	95
Zn	81	77	88	130	110	86	92	77	89
Mo	2.3	*n.d.*	*n.d.*	*n.d.*	*n.d.*	*n.d.*	*n.d.*	*n.d.*	5.5
W	214	174	157	131	186	203	83	96	69
Sb	*n.d.*	*n.d.*	0.6	1.1	*n.d.*	*n.d.*	1.2	*n.d.*	*n.d.*
Sn	1.2	1.5	1.7	1.4	*n.d.*	1.3	1.1	2.0	1.3

Group	G3								
Reference	Zwanzig et al., 1999								
Sample	32-76-604	32-76-498	32-80-89	52-77-1803	32-78-5130	32-80-801	32-76-286	32-76-651	32-76-254
Ba	45	121	59	151	80	213	107	66	328
Cs	*n.d.*	*n.d.*	*n.d.*	*n.d.*	*n.d.*	*n.d.*	*n.d.*	*n.d.*	1.6
Rb	*n.d.*	4.5	*n.d.*	3.4	*n.d.*	12.6	6.4	3.9	30.6
Sr	381	406	195	388	211	295	346	377	289
Pb	*n.d.*	*n.d.*	*n.d.*	*n.d.*	*n.d.*	*n.d.*	6	*n.d.*	13
Ga	19	21	18	23	21	20	20	20	20
Zr	112	95	84	95	150	140	77	78	62
Hf	2.9	2.8	2.6	2.9	3.9	4.1	2.2	2.1	1.8
Nb	9.8	6.9	7.5	9.6	8.7	11.1	5.1	5.5	4.0
Ta	1.3	1.2	1.3	1.0	1.3	1.5	0.7	0.7	0.5
Th	0.9	0.7	0.7	0.4	0.5	1.0	0.7	0.8	0.9
U	1.1	0	0.2	0.6	0.3	0.7	0.5	0.5	0.2
Y	21	23	28	23	35	35	21	18	18
La	11.0	8.6	6.8	7.6	7.3	11.1	7.6	8.3	6.2
Ce	25.7	19.7	17.5	21.3	19.2	28.1	18.2	18.3	14.8
Pr	3.36	2.74	2.50	2.94	2.90	3.93	2.52	2.43	2.05
Nd	15.0	13.9	12.5	14.6	14.7	19.8	12.0	11.5	10.3
Sm	3.8	3.9	3.6	4.0	4.3	5.5	3.3	3.2	2.8
Eu	1.30	1.35	1.29	1.22	1.60	1.54	1.13	1.13	0.95
Gd	4.1	4.1	4.2	4.2	5.1	5.9	3.7	3.3	3.1
Tb	0.6	0.7	0.7	0.7	0.9	0.9	0.6	0.6	0.5
Dy	3.6	4.3	4.4	4.3	5.6	5.8	3.5	3.3	3.0
Ho	0.8	0.9	0.9	0.8	1.2	1.1	0.8	0.7	0.6
Er	2.2	2.5	2.6	2.5	3.4	3.1	2.2	1.8	1.9
Tm	0.31	0.39	0.41	0.35	0.51	0.50	0.33	0.29	0.28
Yb	2.0	2.3	2.5	2.3	3.1	3.1	2.0	1.7	1.7
Lu	0.29	0.35	0.37	0.33	0.50	0.43	0.32	0.25	0.26

Group				**G3**					
Reference				**Zwanzig et al., 1999**					
Sample	32-76-604	32-76-498	32-80-89	52-77-1803	32-78-5130	32-80-801	32-76-286	32-76-651	32-76-251
La/Sm_{CN}	1.89	1.44	1.24	1.22	1.10	1.30	1.46	1.70	1.45
Gd/Yb_{CN}	1.72	1.45	1.42	1.53	1.35	1.57	1.52	1.60	1.55
La/Yb_{CN}	4.03	2.66	1.99	2.42	1.67	2.57	2.71	3.46	2.66
Eu/Eu*	1.02	1.03	1.01	0.91	1.04	0.83	0.98	1.06	0.99
Ce/Ce*	1.04	0.99	1.04	1.10	1.02	1.04	1.02	1.00	1.01
Zr/Y	5.2	4.2	3.1	4.1	4.4	4.0	3.6	4.4	3.5
Ti/Zr	53	53	107	71	45	42	74	67	90
Al_2O_3/TiO_2	20	24	9	17	14	16	21	25	19
Zr/Nb	11	14	11	10	17	13	15	14	15
Zr/Zr*	0.87	0.75	0.73	0.72	1.10	0.78	0.71	0.75	0.68
Zr/Sm_{PM}	1.19	0.98	0.94	0.93	1.39	1.01	0.92	0.98	0.90
Zr/Nd_{PM}	0.92	0.84	0.83	0.80	1.25	0.87	0.79	0.83	0.74
Ti/Ti*	0.66	0.54	0.98	0.75	0.59	0.49	0.70	0.68	0.82
Ti/Gd_{PM}	1.45	1.02	1.73	1.40	1.01	0.90	1.34	1.43	1.59
Ti/Sm_{PM}	0.57	0.46	0.90	0.59	0.56	0.38	0.61	0.59	0.73
Nb/Nb*	1.11	1.00	1.25	1.95	1.69	1.18	0.79	0.79	0.62
Nb/Th_{PM}	1.38	1.26	1.43	3.04	2.43	1.40	0.93	0.95	0.60
Nb/La_{PM}	0.88	0.79	1.10	1.26	1.17	1.00	0.67	0.65	0.64
Mg#	44	37	50	41	33	32	29	34	33
ΣLREE	64.12	54.27	48.37	55.90	55.14	75.80	48.42	48.20	40.20
ΣHREE	31.14	34.13	39.45	34.63	49.77	50.11	31.14	26.55	25.94

Group					**G3**				
Reference					**Zwanzig et al., 1999**				
Sample	32-76-257	32-76-650	32-76-288	32-76-475	12-78-159	12-78-160	12-78-161	12-78-161	52-76-416
Easting (m)	372345	383364	370993	373645	348652	348845	348845	348845	391593
Northing (m)	6300470	6306129	6300426	6303025	6281050	6281188	6281188	6281188	6296239
DDH	Outcrop	Outcrop	Outcrop	Outcrop	Outcrop	Outcrop	Outcrop	Outcrop	Outcrop
Depth (m)	-	-	-	-	-	-	-	-	-
SiO_2	53.05	53.92	55.28	54.21	51.00	47.27	54.94	60.55	53.19
Al_2O_3	16.58	19.98	19.73	19.22	15.93	14.33	16.68	16.91	16.10
TiO_2	1.16	0.94	0.80	0.76	1.41	1.06	1.04	0.90	1.15
Fe_2O_3	14.13	9.80	9.28	10.18	13.58	15.00	12.12	8.03	11.83
MnO	0.20	0.17	0.17	0.17	0.19	0.23	0.19	0.16	0.18
MgO	4.46	2.87	2.44	5.73	5.08	5.62	3.65	2.19	4.03
CaO	5.62	8.14	7.52	6.53	10.23	14.59	8.59	7.57	7.67
Na_2O	3.11	3.38	3.98	2.99	2.16	1.43	2.30	3.15	5.30
K_2O	1.48	0.63	0.62	0.13	0.25	0.36	0.33	0.30	0.28
P_2O_5	0.20	0.16	0.17	0.09	0.16	0.11	0.17	0.24	0.26
LOI	0.73	0.93	0.99	2.19	0.43	1.9	0.64	0.48	0.35
Total	100	100	100	100	100	100	100	100	100
Ni	188	*n.d.*	*n.d.*	80	*n.d.*	*n.d.*	*n.d.*	*n.d.*	*n.d.*
Cr	486	26	*n.d.*	146	*n.d.*	*n.d.*	*n.d.*	*n.d.*	*n.d.*
Co	76	53	34	67	36	52	40	32	21
V	330	154	104	343	115	171	65	225	110
Sc	*n.d.*	*n.d.*	*n.d.*	*n.d.*	*n.d.*	*n.d.*	*n.d.*	*n.d.*	*n.d.*
Cu	158	19	101	98	93	79	17	97	33
Zn	90	81	77	88	130	110	86	92	77
Mo	*n.d.*	2.3	*n.d.*	*n.d.*	*n.d.*	*n.d.*	*n.d.*	*n.d.*	*n.d.*
W	145	214	174	157	131	186	203	83	96
Sb	*n.d.*	*n.d.*	*n.d.*	0.6	1.1	*n.d.*	*n.d.*	1.2	*n.d.*
Sn	1.1	1.2	1.5	1.7	1.4	*n.d.*	1.3	1.1	2.0

Group	G3								
Reference	Zwanzig et al., 1999								
Sample	32-76-257	32-76-650	32-76-288	32-76-475	12-78-159	12-78-160	12-78-161	12-78-161	52-76-416
Ba	257	193	141	28	50	222	81	102	90
Cs	0.9	*n.d.*	*n.d.*	*n.d.*	*n.d.*	*n.d.*	*n.d.*	*n.d.*	*n.d.*
Rb	21	9.6	11	*n.d.*	*n.d.*	3.6	2.9	*n.d.*	*n.d.*
Sr	221	354	172	184	305	123	262	286	178
Pb	*n.d.*	6	*n.d.*	*n.d.*	*n.d.*	*n.d.*	*n.d.*	*n.d.*	*n.d.*
Ga	20	21	19	19	19	15	18	20	16
Zr	73	85	86	57	71	51	100	134	70
Hf	2.1	2.5	2.6	1.7	2.1	1.6	2.6	3.7	2.3
Nb	4.7	5.6	7.4	4.8	5.9	4.2	7.8	9.8	4.8
Ta	0.5	1.1	0.8	0.5	0.7	0.5	1.0	1.3	0.7
Th	0.9	0.8	1.1	0.7	0.7	0.4	0.9	1.2	0.7
U	0.4	0.3	0	0.2	0.4	0.3	0.5	0.6	0.5
Y	22	22	26	18	23	17	26	33	27
La	5.8	7.7	9.2	5.4	6.9	4.4	8.6	12.1	8.9
Ce	14.5	17.6	21.0	12.0	17.3	11.4	21.5	29.4	21.8
Pr	1.95	2.51	2.87	1.66	2.62	1.72	3.02	3.93	2.83
Nd	9.4	12.0	13.9	8.2	12.3	8.7	14.1	18.0	13.1
Sm	2.9	3.3	3.6	2.2	3.7	2.5	3.9	5.0	3.5
Eu	1.10	1.19	0.93	0.78	1.38	0.93	1.25	1.58	1.15
Gd	3.3	3.6	4.2	2.7	4.1	2.9	4.3	5.2	4.0
Tb	0.6	0.6	0.7	0.5	0.7	0.5	0.7	0.9	0.7
Dy	3.7	3.6	4.4	2.8	4.0	2.8	4.0	5.3	4.3
Ho	0.7	0.7	0.9	0.6	0.8	0.6	0.8	1.1	0.9
Er	2.1	2.2	2.8	1.8	2.3	1.6	2.5	3.1	2.8
Tm	0.33	0.33	0.46	0.28	0.33	0.24	0.36	0.47	0.43
Yb	2.2	1.9	2.7	1.6	2.1	1.5	2.3	3.1	2.7
Lu	0.33	0.28	0.41	0.26	0.32	0.23	0.36	0.48	0.43

Group	G3								
Reference	Zwanzig et al., 1999								
Sample	32-78-5180	32-76-604	32-76-498	32-80-89	52-77-1803	32-78-5130	32-80-801	32-76-286	32-76-651
La/Sm_{CN}	1.31	1.50	1.66	1.58	1.20	1.12	1.42	1.56	1.66
Gd/Yb_{CN}	1.25	1.53	1.26	1.34	1.67	1.53	1.55	1.39	1.21
La/Yb_{CN}	1.92	2.86	2.40	2.36	2.39	2.07	2.72	2.79	2.34
Eu/Eu*	1.10	1.07	0.73	0.99	1.08	1.05	0.94	0.94	0.94
Ce/Ce*	1.06	0.99	1.00	0.98	1.00	1.01	1.03	1.04	1.06
Zr/Y	3.3	3.9	3.3	3.1	3.0	3.1	3.8	4.1	2.6
Ti/Zr	94	67	56	78	119	121	62	40	98
Al_2O_3/TiO_2	14	21	25	25	11	14	16	19	14
Zr/Nb	16	15	12	12	12	12	13	14	14
Zr/Zr*	0.82	0.78	0.71	0.78	0.61	0.63	0.78	0.82	0.60
Zr/Sm_{PM}	1.02	1.02	0.96	1.03	0.77	0.80	1.02	1.07	0.80
Zr/Nd_{PM}	0.95	0.87	0.76	0.85	0.71	0.72	0.86	0.91	0.65
Ti/Ti*	0.92	0.69	0.61	0.77	0.89	0.97	0.67	0.47	0.80
Ti/Gd_{PM}	1.50	1.39	0.82	1.28	1.94	1.91	1.29	0.81	1.18
Ti/Sm_{PM}	0.86	0.61	0.48	0.72	0.82	0.87	0.56	0.38	0.70
Nb/Nb*	0.75	0.80	0.84	0.86	0.99	1.14	1.03	0.94	0.69
Nb/Th_{PM}	0.71	0.89	0.88	0.84	1.13	1.38	1.17	1.09	0.89
Nb/La_{PM}	0.80	0.72	0.79	0.89	0.86	0.95	0.91	0.80	0.54
Mg#	38	37	34	53	43	43	37	35	40
ΣLREE	38.92	47.81	55.75	32.88	48.30	32.64	56.61	75.28	55.30
ΣHREE	32.06	31.53	38.84	26.13	33.93	24.16	36.91	47.06	39.16

Group				**G3**					
Reference				**Zwanzig et al., 1999**					
Sample	52-76-391	52-76-421	32-76-90	32-78-5019	52-76-315	52-76-373	32-76-83	94-00-61	94-00-53
Easting (m)	391358	392058	372890	366369	387269	390835	373948	383274	384519
Northing (m)	6296688	6297056	6291697	6290311	6294256	6297644	6291896	6291984	6291811
DDH	Outcrop	Outcrop	Outcrop	Outcrop	Outcrop	Outcrop	Outcrop	Outcrop	Outcrop
Depth (m)	-	-	-	-	-	-	-	-	-
SiO_2	51.81	49.97	46.61	50.39	51.82	55.15	51.92	54.02	54.23
Al_2O_3	14.63	15.33	16.78	19.35	15.39	14.34	14.51	17.50	13.74
TiO_2	1.29	1.45	1.31	0.91	0.76	0.98	0.88	1.03	1.32
Fe_2O_3	13.96	13.15	14.09	12.58	11.61	12.49	12.85	9.76	14.26
MnO	0.18	0.22	0.21	0.22	0.16	0.21	0.19	0.15	0.22
MgO	4.86	3.12	7.07	3.42	6.89	5.33	6.20	4.58	4.53
CaO	9.05	13.25	11.64	9.76	9.66	6.85	9.47	8.69	7.90
Na_2O	3.69	2.98	1.95	2.98	3.00	3.92	3.40	2.88	3.02
K_2O	0.27	0.23	0.22	0.31	0.59	0.55	0.41	1.13	0.64
P_2O_5	0.26	0.31	0.12	0.08	0.12	0.18	0.17	0.25	0.15
LOI	0.54	1.81	0.91	1.40	0.64	0.92	1.23	1.10	3.97
Total	100	100	100	100	100	100	100	100	100
Ni	35	31	48	*n.d.*	55	23	37	34	*n.d.*
Cr	32	*n.d.*	93	*n.d.*	111	86	50	103	23
Co	55	48	66	49	49	59	50	*n.d.*	*n.d.*
V	358	431	340	370	258	287	297	216	296
Sc	*n.d.*	*n.d.*	*n.d.*	*n.d.*	*n.d.*	*n.d.*	*n.d.*	22	48
Cu	65	40	45	240	139	160	142	11	124
Zn	116	139	115	64	84	133	98	74	70
Mo	*n.d.*	*n.d.*	*n.d.*	*n.d.*	*n.d.*	*n.d.*	*n.d.*	2.0	2.0
W	110	116	129	126	76	143	92	*n.d.*	*n.d.*
Sb	*n.d.*	0.9	1.1	1.0	*n.d.*	0.8	1.2	0.6	0.9
Sn	*n.d.*	1.1	3.0	1.5	*n.d.*	1.1	*n.d.*	*n.d.*	1.0

Group	G3								
Reference	Zwanzig et al., 1999								
Sample	52-76-391	52-76-421	32-76-90	32-78-5019	52-76-315	52-76-373	32-76-83	94-00-61	94-00-53
Ba	106	45	28	59	331	146	68	491	314
Cs	*n.d.*	*n.d.*	*n.d.*	*n.d.*	*n.d.*	*n.d.*	*n.d.*	*n.d.*	*n.d.*
Rb	*n.d.*	*n.d.*	*n.d.*	4	13	8	5	21	11
Sr	194	239	170	269	286	127	257	719	231
Pb	*n.d.*	*n.d.*	*n.d.*	7	*n.d.*	*n.d.*	*n.d.*	*n.d.*	*n.d.*
Ga	20	23	20	19	15	14	16	17	15
Zr	68	72	79	26	37	66	50	94	101
Hf	2.3	2.5	2.3	0.8	1.3	2.3	1.6	2.2	2.4
Nb	3.4	5.2	6.5	1.4	1.6	3.2	2.2	5.0	4.0
Ta	0.6	0.8	1.0	0.6	0.3	0.8	0.5	0.3	0.3
Th	0.6	0.9	0.8	0.2	0.4	0.8	0.5	0.8	0.4
U	0.4	0.5	0.3	0.3	0.2	0.5	0.3	0.4	0.1
Y	30	33	28	14	22	32	24	15	35
La	8.4	11.4	8.4	2.8	4.1	6.2	4.9	18.5	8.1
Ce	19.5	26.4	19.7	6.7	10.6	16.1	11.5	38.0	19.3
Pr	2.61	3.21	2.84	1.04	1.43	2.23	1.64	4.38	2.56
Nd	12.7	14.7	14.1	5.5	6.8	10.6	8.2	18.5	12.2
Sm	3.6	4.1	3.8	1.6	2.1	3.2	2.6	3.8	3.7
Eu	1.28	1.43	1.28	0.76	0.80	1.00	0.93	1.08	1.21
Gd	4.1	4.5	4.5	1.9	2.8	4.1	3.4	3.5	4.9
Tb	0.8	0.8	0.8	0.4	0.5	0.8	0.6	0.5	0.9
Dy	4.9	5.3	4.7	2.2	3.4	4.8	4.0	2.7	5.7
Ho	1.1	1.1	1.0	0.5	0.8	1.1	0.9	0.5	1.2
Er	3.1	3.3	2.8	1.4	2.2	3.3	2.8	1.5	3.6
Tm	0.49	0.54	0.42	0.22	0.34	0.50	0.44	0.21	0.53
Yb	3.1	3.6	2.6	1.4	2.3	3.3	2.8	1.3	3.4
Lu	0.50	0.53	0.38	0.20	0.37	0.54	0.45	0.19	0.52

Group	G3								
Reference	Zwanzig et al., 1999								
Sample	52-76-391	52-76-421	32-76-90	32-78-5019	52-76-315	52-76-373	32-76-83-1	94-00-61	94-00-53
La/Sm_{CN}	1.45	1.31	1.50	1.66	1.58	1.20	1.12	1.42	1.56
Gd/Yb_{CN}	1.55	1.25	1.53	1.26	1.34	1.67	1.53	1.55	1.39
La/Yb_{CN}	2.66	1.92	2.86	2.40	2.36	2.39	2.07	2.72	2.79
Eu/Eu*	0.99	1.10	1.07	0.73	0.99	1.08	1.05	0.94	0.94
Ce/Ce*	1.01	1.06	0.99	1.00	0.98	1.00	1.01	1.03	1.04
Zr/Y	3.5	3.3	3.9	3.3	3.1	3.0	3.1	3.8	4.1
Ti/Zr	90	94	67	56	78	119	121	62	40
Al_2O_3/TiO_2	19	14	21	25	25	11	14	16	19
Zr/Nb	15	16	15	12	12	12	12	13	14
Zr/Zr*	0.68	0.82	0.78	0.71	0.78	0.61	0.63	0.78	0.82
Zr/Sm_{PM}	0.90	1.02	1.02	0.96	1.03	0.77	0.80	1.02	1.07
Zr/Nd_{PM}	0.74	0.95	0.87	0.76	0.85	0.71	0.72	0.86	0.91
Ti/Ti*	0.82	0.92	0.69	0.61	0.77	0.89	0.97	0.67	0.47
Ti/Gd_{PM}	1.59	1.50	1.39	0.82	1.28	1.94	1.91	1.29	0.81
Ti/Sm_{PM}	0.73	0.86	0.61	0.48	0.72	0.82	0.87	0.56	0.38
Nb/Nb*	0.62	0.75	0.80	0.84	0.86	0.99	1.14	1.03	0.94
Nb/Th_{PM}	0.60	0.71	0.89	0.88	0.84	1.13	1.38	1.17	1.09
Nb/La_{PM}	0.64	0.80	0.72	0.79	0.89	0.86	0.95	0.91	0.80
Mg#	33	38	37	34	53	43	43	37	35
ΣLREE	40.20	38.92	47.81	55.75	32.88	48.30	32.64	56.61	75.28
ΣHREE	25.94	32.06	31.53	38.84	26.13	33.93	24.16	36.91	47.06

Group					**G3**				
Reference					**Chapter 2**				
Sample	MG11-039	MG11-055	MG11-037	MG11-040	MG11-116	MG11-001	MG11-006	MG11-038	MG11-057
Easting (m)	381336	379973	381336	381336	378578	383352	378686	381336	380048
Northing (m)	6308189	6307114	6308189	6308189	6306250	6306428	6306608	6308189	6307163
DDH	MG11-41	MG11-25	MG11-41	MG11-41	MG11-48	Outcrop	Outcrop	MG11-41	MG11-38
Depth (m)	543.5	223	332	441	349	-	-	164	251
SiO_2	55.19	52.88	55.65	51.01	50.99	50.31	49.72	51.73	47.66
Al_2O_3	18.29	20.40	17.68	16.50	18.12	16.45	18.36	21.11	17.50
TiO_2	0.92	0.90	1.10	0.97	1.03	0.99	0.93	0.89	1.06
Fe_2O_3	9.36	10.24	11.09	11.43	11.94	12.89	13.47	9.50	9.63
MnO	0.20	0.15	0.20	0.20	0.17	0.23	0.20	0.15	0.21
MgO	3.99	2.45	2.55	2.87	2.96	4.79	3.46	3.02	2.90
CaO	8.84	8.31	8.42	14.46	12.56	10.36	9.76	8.58	16.10
Na_2O	2.80	4.15	2.87	2.30	1.86	3.30	3.23	2.44	3.41
K_2O	0.26	0.44	0.36	0.17	0.31	0.60	0.79	2.44	1.38
P_2O_5	0.14	0.09	0.08	0.09	0.05	0.07	0.08	0.13	0.15
LOI	1.94	7.57	4.77	1.74	1.40	1.19	0.56	1.23	2.95
Total	100	100	100	100	100	100	100	100	100
Ni	*n.d.*	*n.d.*	1020	*n.d.*	40	*n.d.*	*n.d.*	*n.d.*	20
Cr	20	20	1350	30	*n.d.*	*n.d.*	*n.d.*	*n.d.*	40
Co	40	21	103	35	29	44	24	29	36
V	327	219	240	309	75	174	179	303	233
Sc	37	31	23	36	19	27	25	33	29
Cu	150	110	1260	140	1380	50	60	130	130
Zn	110	80	480	140	210	120	100	110	130
Mo	*n.d.*	*n.d.*	*n.d.*	*n.d.*	*n.d.*	*n.d.*	*n.d.*	*n.d.*	*n.d.*
W	*n.d.*	15	19	*n.d.*	36	1.0	*n.d.*	*n.d.*	4.0
Sb	0.7	*n.d.*	*n.d.*	0.7	0.6	*n.d.*	0.6	2.8	*n.d.*
Sn	*n.d.*	*n.d.*	*n.d.*	*n.d.*	*n.d.*	*n.d.*	*n.d.*	*n.d.*	*n.d.*

Group					G3				
Reference					Chapter 2				
Sample	MG11-039	MG11-055	MG11-037	MG11-040	MG11-116	MG11-001	MG11-006	MG11-038	MG11-057
Ba	162	199	42	261	1007	143	76	56	161
Cs	1.2	*n.d.*	*n.d.*	1.4	1.5	*n.d.*	*n.d.*	*n.d.*	*n.d.*
Rb	10	29	*n.d.*	13	77	2.0	4.0	5.0	37
Sr	346	172	222	247	157	447	290	296	167
Pb	*n.d.*	*n.d.*	*n.d.*	6	24	10	*n.d.*	6	26
Ga	17	17	15	17	16	18	18	19	17
Zr	25	58	26	39	67	82	42	33	40
Hf	0.7	1.4	0.8	1.1	1.7	2.0	1.1	1.0	1.1
Nb	1.0	3.0	1.0	2.0	6.0	5.0	3.0	2.0	4.0
Ta	*n.d.*	0.2	0.1	0.2	0.5	0.3	0.2	0.1	0.3
Th	0.2	0.5	0.1	0.3	1.0	0.7	0.5	0.2	0.5
U	0.1	0.2	*n.d.*	0.2	0	0.5	0.4	0.1	0.1
Y	11	14	9	12	14	16	12	11	11
La	2.3	6.5	2.5	3.2	8.4	7.1	3.6	3.1	5.4
Ce	6.1	15.9	6.5	8.4	19.5	17.1	8.7	8.4	12.5
Pr	0.91	2.11	0.94	1.22	2.43	2.18	1.25	1.28	1.57
Nd	4.6	9.7	5.2	6.3	10.4	9.8	6.2	6.4	6.9
Sm	1.5	2.5	1.5	1.8	2.7	2.6	2.0	1.9	1.9
Eu	0.69	0.81	0.63	0.76	0.61	0.97	0.77	0.83	0.77
Gd	2.0	2.7	1.9	2.4	2.6	3.0	2.4	2.4	2.1
Tb	0.3	0.5	0.3	0.4	0.5	0.5	0.4	0.4	0.4
Dy	2.2	2.7	2.0	2.5	2.8	3.1	2.5	2.3	2.2
Ho	0.4	0.6	0.4	0.5	0.6	0.7	0.5	0.5	0.4
Er	1.3	1.6	1.2	1.5	1.7	1.8	1.5	1.4	1.2
Tm	0.20	0.24	0.17	0.23	0.26	0.27	0.22	0.20	0.20
Yb	1.3	1.6	1.0	1.5	1.5	1.7	1.4	1.3	1.4
Lu	0.21	0.23	0.16	0.23	0.24	0.30	0.22	0.20	0.22

Group					G3				
Reference					Chapter 2				
Sample	MG11-039	MG11-055	MG11-037	MG11-040	MG11-116	MG11-001	MG11-006	MG11-038	MG11-057
La/Sm_{CN}	1.66	1.68	1.08	1.15	2.01	1.76	1.16	1.05	1.83
Gd/Yb_{CN}	1.21	1.40	1.57	1.32	1.43	1.46	1.42	1.53	1.24
La/Yb_{CN}	2.34	2.91	1.79	1.53	4.02	3.00	1.84	1.71	2.77
Eu/Eu*	0.94	0.95	1.14	1.12	0.70	1.06	1.07	1.19	1.18
Ce/Ce*	1.06	1.05	1.04	1.04	1.06	1.07	1.01	1.03	1.05
Zr/Y	2.6	4.1	2.9	3.3	4.8	5.1	3.5	3.0	3.6
Ti/Zr	98	100	208	142	58	66	127	182	112
Al_2O_3/TiO_2	14	17	17	20	21	20	23	18	26
Zr/Nb	14	15	16	15	12	12	12	12	13
Zr/Zr*	0.60	0.68	0.54	0.67	0.73	0.94	0.69	0.55	0.64
Zr/Sm_{PM}	0.80	0.92	0.69	0.86	0.99	1.25	0.84	0.69	0.84
Zr/Nd_{PM}	0.65	0.73	0.61	0.76	0.79	1.02	0.83	0.63	0.71
Ti/Ti*	0.80	0.99	1.25	1.03	0.77	0.80	0.99	1.07	0.89
Ti/Gd_{PM}	1.18	1.71	2.56	1.74	1.22	1.51	1.80	2.19	1.51
Ti/Sm_{PM}	0.70	0.82	1.29	1.09	0.51	0.74	0.95	1.13	0.84
Nb/Nb*	0.69	0.60	0.72	0.74	0.75	0.81	0.81	0.92	0.88
Nb/Th_{PM}	0.89	0.79	1.32	0.88	0.79	0.94	0.79	1.32	1.05
Nb/La_{PM}	0.54	0.46	0.40	0.62	0.71	0.70	0.83	0.64	0.74
Mg#	40	37	33	34	38	46	32	33	44
ΣLREE	55.30	40.22	19.17	24.08	46.64	42.75	24.92	24.31	31.14
ΣHREE	39.16	21.47	14.23	18.86	21.60	24.37	18.74	17.30	17.02

Group					**G3**				
Reference					**Chapter 2**				
Sample	MG11-074	MG11-095	MG11-105	MG11-108	MG11-110	MG11-111	MG11-007	MG11-098	MG11-099
Easting (m)	380727	380650	380650	380650	378578	378578	378712	380650	380650
Northing (m)	6307854	6307099	6307099	6307099	6306250	6306250	6306571	6307099	6307099
DDH	MG11-14	MG11-18	MG11-18	MG11-18	MG11-48	MG11-48	Outcrop	MG11-18	MG11-18
Depth (m)	249	194.5	257.8	223.4	96	302	-	292.7	293.7
SiO_2	48.34	47.28	52.36	60.61	50.78	55.42	52.48	49.29	48.74
Al_2O_3	20.46	19.25	21.14	17.98	21.21	18.65	20.41	21.07	16.20
TiO_2	0.79	0.82	0.88	0.60	0.72	0.79	0.87	0.86	0.68
Fe_2O_3	10.29	13.45	8.16	8.04	9.82	8.25	7.55	9.87	8.65
MnO	0.19	0.15	0.12	0.08	0.13	0.13	0.14	0.14	0.40
MgO	4.10	4.42	1.96	2.31	5.38	1.76	1.71	3.05	6.66
CaO	11.25	10.78	9.55	5.62	5.81	9.70	11.58	10.20	14.53
Na_2O	2.41	2.31	3.24	4.26	5.02	1.67	2.00	1.88	1.24
K_2O	2.07	1.46	2.49	0.40	1.02	3.54	3.19	3.52	2.79
P_2O_5	0.09	0.06	0.11	0.09	0.10	0.10	0.09	0.10	0.10
LOI	2.08	1.61	9.60	5.47	1.54	1.40	0.72	4.41	4.82
Total	100	100	100	100	100	100	100	100	100
Ni	*n.d.*	50	40	50	*n.d.*	*n.d.*	*n.d.*	*n.d.*	*n.d.*
Cr	20	50	70	120	30	30	*n.d.*	*n.d.*	20
Co	39	27	36	43	30	22	19	27	31
V	319	154	166	196	238	189	132	168	187
Sc	37	23	27	30	35	29	29	23	25
Cu	160	120	*n.d.*	80	210	310	30	130	150
Zn	80	100	70	90	160	450	110	80	70
Mo	*n.d.*	*n.d.*	*n.d.*	*n.d.*	*n.d.*	*n.d.*	*n.d.*	*n.d.*	*n.d.*
W	*n.d.*	2.0	9.0	1.0	1.0	44	*n.d.*	1.0	1.0
Sb	*n.d.*	*n.d.*	34	0.6	*n.d.*	6.4	*n.d.*	6.4	5.8
Sn	*n.d.*	*n.d.*	*n.d.*	*n.d.*	*n.d.*	*n.d.*	*n.d.*	*n.d.*	*n.d.*

Group					G3				
Reference					Chapter 2				
Sample	MG11-074	MG11-095	MG11-105	MG11-108	MG11-110	MG11-111	MG11-007	MG11-098	MG11-099
Ba	356	287	313	300	172	481	87	308	336
Cs	1.0	*n.d.*	1.5	0.7	*n.d.*	1.3	*n.d.*	0.5	0.5
Rb	32	20	109	48	12	36	3.0	59	54
Sr	571	290	134	109	423	189	238	159	186
Pb	6	6	6	*n.d.*	6	412	*n.d.*	7	8
Ga	18	17	17	17	19	16	19	16	17
Zr	28	38	34	35	71	59	42	36	40
Hf	0.7	1.0	0.8	1.0	2.0	1.5	1.2	1.1	1.1
Nb	2.0	3.0	3.0	3.0	7.0	6.0	3.0	4.0	4.0
Ta	0.1	0.2	0.2	0.2	0.5	0.4	0.2	0.2	0.3
Th	0.2	0.4	0.4	0.4	0.8	0.7	0.2	0.3	0.3
U	0.1	0.1	0.1	0.1	0.3	0.6	0.1	*n.d.*	*n.d.*
Y	10	8	8	9	18	14	15	10	10
La	2.7	4.2	4.3	3.9	8.6	7.2	3.9	4.7	4.5
Ce	7.1	10.2	10.1	9.3	21.3	17.8	10.3	11.3	11.5
Pr	1.04	1.34	1.29	1.22	2.87	2.29	1.49	1.55	1.53
Nd	5.4	6.0	5.7	5.5	12.7	10.0	7.3	6.9	6.9
Sm	1.7	1.7	1.8	1.6	3.5	2.7	2.4	2.2	2.0
Eu	0.77	0.69	0.81	0.73	1.17	0.68	0.92	0.61	0.73
Gd	1.9	1.8	1.9	1.6	3.5	2.9	2.7	2.1	2.1
Tb	0.3	0.3	0.3	0.3	0.6	0.5	0.5	0.4	0.4
Dy	1.9	1.7	1.7	1.7	3.5	3.0	3.1	2.2	2.3
Ho	0.4	0.3	0.3	0.3	0.7	0.6	0.7	0.5	0.4
Er	1.2	0.9	0.9	0.9	2.1	1.7	1.8	1.3	1.2
Tm	0.18	0.14	0.14	0.16	0.31	0.25	0.28	0.20	0.19
Yb	1.2	0.9	0.9	1.2	2.0	1.5	1.7	1.3	1.3
Lu	0.17	0.14	0.15	0.18	0.31	0.24	0.27	0.21	0.21

Group					G3				
Reference					Chapter 2				
Sample	MG11-074	MG11-095	MG11-055	MG11-037	MG11-040	MG11-116	MG11-001	MG11-006	MG11-038
La/Sm_{CN}	1.03	1.59	1.54	1.57	1.59	1.72	1.05	1.38	1.45
Gd/Yb_{CN}	1.31	1.65	1.75	1.10	1.45	1.60	1.31	1.34	1.34
La/Yb_{CN}	1.61	3.35	3.43	2.33	3.08	3.44	1.65	2.59	2.48
Eu/Eu*	1.31	1.21	1.34	1.39	1.02	0.74	1.10	0.87	1.09
Ce/Ce*	1.04	1.05	1.05	1.05	1.05	1.07	1.05	1.03	1.07
Zr/Y	2.8	4.8	4.3	3.9	3.9	4.2	2.8	3.6	4.0
Ti/Zr	173	110	117	114	99	99	157	122	120
Al_2O_3/TiO_2	23	30	29	28	14	16	16	24	23
Zr/Nb	14	14	11	12	10	10	14	9	10
Zr/Zr*	0.54	0.69	0.62	0.69	0.62	0.66	0.58	0.54	0.63
Zr/Sm_{PM}	0.66	0.89	0.75	0.87	0.81	0.87	0.70	0.65	0.80
Zr/Nd_{PM}	0.63	0.78	0.73	0.78	0.68	0.72	0.70	0.64	0.71
Ti/Ti*	1.01	0.94	0.81	0.93	0.88	1.05	1.05	0.98	0.98
Ti/Gd_{PM}	1.91	2.19	2.10	1.58	1.67	1.84	1.83	1.60	1.74
Ti/Sm_{PM}	1.02	0.87	0.79	0.89	0.72	0.77	0.98	0.71	0.85
Nb/Nb*	0.98	0.84	0.83	0.87	0.97	0.97	1.23	1.22	1.25
Nb/Th_{PM}	1.32	0.99	0.99	0.99	1.15	1.13	1.97	1.76	1.76
Nb/La_{PM}	0.74	0.71	0.69	0.76	0.81	0.83	0.76	0.85	0.88
Mg#	39	52	57	32	35	36	31	30	31
ΣLREE	20.61	25.93	25.90	23.85	53.64	43.57	29.01	29.36	29.26
ΣHREE	15.35	12.38	12.39	13.74	27.52	21.79	23.35	16.11	16.00

Group					**G3**				
Reference					**Chapter 2**				
Sample	MG11-094	MG11-106	MG11-104	MG11-107	MG11-053	MG11-093	MG11-100	MG11-102	MG11-117
Easting (m)	380650	380650	380650	380650	379973	380650	380650	380650	378578
Northing (m)	6307099	6307099	6307099	6307099	6307114	6307099	6307099	6307099	6306250
DDH	MG11-18	MG11-18	MG11-18	MG11-18	MG11-25	MG11-18	MG11-18	MG11-18	MG11-48
Depth (m)	126.5	188.5	256.8	224.4	328	291.7	294.7	264.8	362
SiO_2	51.77	39.24	48.43	48.70	48.13	53.78	59.97	65.48	60.46
Al_2O_3	16.73	21.87	19.03	19.75	20.19	16.99	16.35	13.68	14.67
TiO_2	0.61	0.76	0.63	0.75	0.72	1.19	1.02	0.66	0.79
Fe_2O_3	7.60	10.93	9.18	9.61	9.88	12.35	9.77	8.88	13.04
MnO	0.35	0.41	0.23	0.17	0.17	0.17	0.08	0.08	0.11
MgO	5.82	7.34	6.66	4.84	5.34	3.40	2.76	2.77	2.85
CaO	12.19	13.88	10.36	11.87	11.61	7.63	3.63	2.37	1.75
Na_2O	1.12	0.77	4.15	0.64	0.77	3.70	4.08	1.37	0.28
K_2O	3.72	4.71	1.25	3.57	3.11	0.59	2.21	4.57	5.96
P_2O_5	0.09	0.08	0.08	0.11	0.08	0.20	0.14	0.13	0.12
LOI	2.58	3.47	8.5	5.00	2.23	4.34	0.78	8.17	3.6
Total	100	100	100	100	100	100	100	100	100
Ni	40	50	20	60	*n.d.*	*n.d.*	*n.d.*	50	*n.d.*
Cr	50	80	50	90	30	*n.d.*	20	70	20
Co	37	35	15	37	27	28	23	26	24
V	173	168	114	189	182	190	187	148	126
Sc	22	28	18	29	29	26	26	22	26
Cu	320	80	*n.d.*	70	140	150	210	70	420
Zn	50	100	60	90	110	80	110	140	1230
Mo	*n.d.*	*n.d.*	2.0	*n.d.*	*n.d.*	*n.d.*	*n.d.*	*n.d.*	*n.d.*
W	2.0	2.0	11	*n.d.*	2.0	*n.d.*	2.0	13	46
Sb	4.5	1.1	11	*n.d.*	*n.d.*	*n.d.*	*n.d.*	5.9	*n.d.*
Sn	*n.d.*	*n.d.*	*n.d.*	*n.d.*	1.0	*n.d.*	*n.d.*	*n.d.*	*n.d.*

Group					G3				
Reference					Chapter 2				
Sample	MG11-094	MG11-106	MG11-104	MG11-107	MG11-053	MG11-093	MG11-100	MG11-102	MG11-117
Ba	98	367	281	337	220	273	318	154	776
Cs	*n.d.*	0.5	1.1	0.8	*n.d.*	0.6	0.7	1.2	0.7
Rb	8.0	26	82	56	41	51	65	61	94
Sr	272	224	91	122	255	282	156	110	125
Pb	9	5	5	*n.d.*	*n.d.*	11	6	6	61
Ga	17	14	14	17	18	16	19	13	18
Zr	33	35	30	37	47	42	42	32	47
Hf	0.9	0.9	0.8	1.0	1.2	1.0	1.2	0.9	1.5
Nb	3.0	3.0	3.0	3.0	5.0	4.0	4.0	3.0	5.0
Ta	0.2	0.2	0.2	0.2	0.3	0.3	0.3	0.2	0.4
Th	0.3	0.3	0.4	0.4	0.5	0.4	0.4	0.3	0.6
U	*n.d.*	0.1	0.2	0.1	0.2	0.1	0.1	*n.d.*	0.2
Y	7	9	8	9	13	11	10	9	12
La	3.5	3.7	3.6	4.1	5.5	4.9	4.6	3.4	5.1
Ce	8.4	9.2	8.8	10.1	14.0	11.6	11.3	8.2	11.9
Pr	1.12	1.29	1.16	1.31	1.90	1.61	1.53	1.11	1.54
Nd	5.1	6.1	5.5	5.9	8.6	7.4	6.7	4.9	6.8
Sm	1.5	1.7	1.5	1.7	2.4	2.1	1.9	1.5	1.9
Eu	0.47	0.67	0.73	0.69	1.02	0.80	0.80	0.72	0.47
Gd	1.5	1.8	1.6	1.8	2.5	2.3	1.9	1.6	2.3
Tb	0.2	0.3	0.3	0.3	0.4	0.3	0.3	0.3	0.4
Dy	1.5	1.8	1.5	1.8	2.7	2.2	2.1	1.8	2.4
Ho	0.3	0.4	0.3	0.3	0.5	0.5	0.4	0.4	0.5
Er	0.7	1.0	0.9	1.0	1.6	1.3	1.2	1.0	1.5
Tm	0.11	0.15	0.14	0.16	0.24	0.18	0.19	0.14	0.24
Yb	0.7	1.0	0.9	1.0	1.6	1.1	1.3	0.9	1.6
Lu	0.10	0.15	0.15	0.16	0.23	0.17	0.21	0.14	0.24

Group					G3				
Reference					Chapter 2				
Sample	MG11-094	MG11-106	MG11-104	MG11-107	MG11-053	MG11-093	MG11-100	MG11-102	MG11-117
La/Sm_{CN}	1.51	1.41	1.55	1.56	1.48	1.51	1.56	1.46	1.73
Gd/Yb_{CN}	1.77	1.49	1.47	1.49	1.29	1.73	1.21	1.47	1.19
La/Yb_{CN}	3.59	2.65	2.87	2.94	2.47	3.20	2.54	2.71	2.29
Eu/Eu*	0.96	1.17	1.44	1.21	1.27	1.11	1.29	1.42	0.69
Ce/Ce*	1.04	1.03	1.06	1.07	1.06	1.01	1.04	1.03	1.04
Zr/Y	4.7	3.9	3.8	4.1	3.6	3.8	4.2	3.6	3.9
Ti/Zr	105	105	108	115	109	120	117	113	95
Al_2O_3/TiO_2	30	30	27	26	24	24	25	24	19
Zr/Nb	11	12	10	12	9	11	11	11	9
Zr/Zr*	0.69	0.63	0.61	0.68	0.60	0.62	0.68	0.69	0.76
Zr/Sm_{PM}	0.88	0.82	0.80	0.87	0.78	0.80	0.88	0.85	0.98
Zr/Nd_{PM}	0.79	0.70	0.67	0.77	0.67	0.69	0.77	0.80	0.85
Ti/Ti*	1.04	0.84	0.75	0.96	0.81	0.93	1.00	0.85	1.08
Ti/Gd_{PM}	2.34	1.74	1.70	2.01	1.52	2.16	1.78	1.90	1.32
Ti/Sm_{PM}	0.82	0.77	0.77	0.89	0.76	0.85	0.92	0.86	0.84
Nb/Nb*	1.06	1.03	0.90	0.85	1.09	1.03	1.07	1.07	1.03
Nb/Th_{PM}	1.32	1.32	0.99	0.99	1.32	1.32	1.32	1.32	1.10
Nb/La_{PM}	0.85	0.81	0.83	0.73	0.90	0.81	0.86	0.88	0.97
Mg#	36	59	60	50	39	32	38	60	30
ΣLREE	21.59	24.46	22.89	25.60	35.92	30.71	28.73	21.43	30.01
ΣHREE	10.61	13.80	12.19	13.72	20.27	16.75	15.70	13.68	18.88

)

Group	G3								
Reference	Beaumont-Smith, 2007								
Sample	103-99-1112	103-99-1116	103-99-1118	103-99-1139	103-00-1214	95-01-159	95-01-147	103-99-1053	103-00-1246
Easting (m)	360448	357879	358150	404443	362158	371860	373333	382911	358966
Northing (m)	6289196	6288021	6288182	6294849	6290644	6302152	6301739	6291433	6288695
DDH	Outcrop	Outcrop	Outcrop	Outcrop	Outcrop	Outcrop	Outcrop	Outcrop	Outcrop
Depth (m)	-	-	-	-	-	-	-	-	-
SiO_2	40.42	53.34	54.11	52.28	54.04	51.23	46.55	57.74	47.15
Al_2O_3	14.04	13.76	13.44	15.65	15.00	20.96	17.94	16.44	17.68
TiO_2	1.74	1.19	1.38	1.56	0.95	0.96	1.28	0.82	1.28
Fe_2O_3	23.16	14.38	14.81	14.78	8.80	10.01	15.92	10.70	13.19
MnO	0.21	0.19	0.20	0.22	0.18	0.12	0.23	0.17	0.17
MgO	6.95	5.15	4.47	4.33	8.15	4.28	3.53	2.24	6.20
CaO	10.47	9.13	7.97	4.92	8.90	7.40	11.46	5.99	10.84
Na_2O	1.98	2.34	3.00	5.46	2.80	4.70	2.63	3.56	2.81
K_2O	0.65	0.25	0.26	0.35	0.75	0.26	0.24	2.24	0.35
P_2O_5	0.37	0.28	0.35	0.44	0.43	0.09	0.22	0.11	0.32
LOI	2.52	0.49	0.85	5.2	1.98	1.20	1.80	2.93	0.42
Total	100	100	100	100	100	100	100	100	100
Ni	*n.d.*	*n.d.*	*n.d.*	*n.d.*	162	*n.d.*	*n.d.*	28	81
Cr	95	30	13	9	497	14	*n.d.*	*n.d.*	73
Co	47	44	36	32	37	26	39	21	45
V	377	331	352	327	178	286	317	151	261
Sc	46	43	36	35	25	35	38	30	38
Cu	102	92	90	22	29	128	296	29	64
Zn	149	120	45	156	227	72	106	115	81
Mo	*n.d.*	*n.d.*	*n.d.*	*n.d.*	*n.d.*	*n.d.*	*n.d.*	*n.d.*	*n.d.*
W	3.4	*n.d.*	*n.d.*	*n.d.*	2.6	*n.d.*	*n.d.*	25	*n.d.*
Sb	0.5	1.0	0.5	2.9	0.9	*n.d.*	*n.d.*	0.7	0.4
Sn	*n.d.*	*n.d.*	*n.d.*	1.1	*n.d.*	*n.d.*	*n.d.*	1.1	*n.d.*

Group	G3								
Reference	Beaumont-Smith, 2007								
Sample	103-99-1112	103-99-1116	103-99-1118	103-99-1139	103-00-1214	95-01-159	95-01-147	103-99-1053	103-00-1246
Ba	172	160	236	385	189	103	219	206	90
Cs	*n.d.*	*n.d.*	*n.d.*	*n.d.*	*n.d.*	0.1	*n.d.*	1.3	*n.d.*
Rb	*n.d.*	*n.d.*	*n.d.*	*n.d.*	*n.d.*	*n.d.*	*n.d.*	*n.d.*	*n.d.*
Sr	151	368	319	203	213	256	208	230	488
Pb	9	7	*n.d.*	8	9	*n.d.*	*n.d.*	*n.d.*	*n.d.*
Ga	22	19	19	23	18	21	18	17	22
Zr	86	63	68	108	128	44	63	119	95
Hf	2.4	1.8	2.0	3.0	3.3	1.3	2.0	3.0	2.6
Nb	4.5	3.9	5.1	7.3	9.6	3.5	5.1	4.7	6.1
Ta	0.3	0.3	0.3	0.4	0.6	0.2	0.4	0.3	0.3
Th	1.0	0.7	0.8	1.2	1.9	0.5	1.0	0.5	0.9
U	0.6	0.3	0.4	0.6	0.9	0.1	0.3	0.3	0.4
Y	31	27	33	35	20	14	23	31	29
La	11.2	7.9	10.2	16.1	18.7	5.0	9.2	7.6	10.8
Ce	26.2	17.4	23.3	34.6	40.6	12.3	21.5	19.5	25.2
Pr	3.43	2.35	3.19	4.47	5.03	1.59	2.95	2.65	3.37
Nd	15.9	11.6	14.8	20.3	21.2	6.9	13.5	12.4	15.3
Sm	4.2	3.0	3.6	4.7	4.5	1.9	3.5	3.6	3.9
Eu	1.51	1.20	1.35	1.56	1.36	0.90	1.20	1.15	1.41
Gd	5.0	3.8	4.6	5.4	4.3	2.3	3.8	4.9	4.5
Tb	0.9	0.7	0.8	1.0	0.6	0.4	0.7	0.9	0.8
Dy	5.4	4.6	4.8	5.7	3.6	2.7	4.3	5.4	5.0
Ho	1.2	0.9	1.1	1.2	0.7	0.5	0.9	1.2	1.0
Er	3.6	2.9	3.4	3.6	2.0	1.6	2.6	3.6	3.0
Tm	0.53	0.44	0.50	0.55	0.29	0.23	0.41	0.54	0.44
Yb	3.5	3.0	3.2	3.6	1.9	1.4	2.6	3.5	3.0
Lu	0.53	0.46	0.52	0.55	0.28	0.21	0.39	0.54	0.46

Group	G3								
Reference	Beaumont-Smith, 2007								
Sample	103-99-1112	103-99-1116	103-99-1118	103-99-1139	103-00-1214	95-01-159	95-01-147	103-99-1053	103-00-1246
La/Sm_{CN}	1.72	1.70	1.83	2.22	2.69	1.73	1.71	1.35	1.79
Gd/Yb_{CN}	1.20	1.04	1.17	1.24	1.90	1.35	1.22	1.18	1.23
La/Yb_{CN}	2.33	1.86	2.25	3.20	7.19	2.51	2.54	1.58	2.60
Eu/Eu*	1.01	1.08	1.02	0.95	0.95	1.32	1.01	0.83	1.03
Ce/Ce*	1.04	0.99	1.00	1.00	1.03	1.07	1.01	1.06	1.02
Zr/Y	2.8	2.4	2.1	3.1	6.5	3.2	2.7	3.9	3.3
Ti/Zr	118	112	120	83	44	129	118	40	81
Al_2O_3/TiO_2	8	12	10	10	16	22	14	20	14
Zr/Nb	19	16	13	15	13	13	12	25	16
Zr/Zr*	0.61	0.62	0.54	0.64	0.76	0.71	0.54	1.02	0.71
Zr/Sm_{PM}	0.82	0.84	0.75	0.92	1.13	0.93	0.73	1.30	0.96
Zr/Nd_{PM}	0.66	0.67	0.56	0.65	0.74	0.78	0.57	1.17	0.76
Ti/Ti*	0.93	0.83	0.83	0.77	0.58	0.98	0.88	0.50	0.77
Ti/Gd_{PM}	1.39	1.10	1.19	1.17	1.42	1.87	1.37	0.65	1.21
Ti/Sm_{PM}	0.86	0.85	0.81	0.68	0.44	1.08	0.77	0.47	0.70
Nb/Nb*	0.50	0.60	0.64	0.61	0.58	0.83	0.60	0.84	0.71
Nb/Th_{PM}	0.62	0.72	0.83	0.82	0.66	1.00	0.66	1.16	0.90
Nb/La_{PM}	0.40	0.49	0.50	0.45	0.51	0.69	0.55	0.61	0.56
Mg#	37	42	37	37	65	46	31	29	48
ΣLREE	67.39	47.21	60.97	87.04	95.63	30.92	55.59	51.86	64.41
ΣHREE	46.23	39.80	47.10	50.87	29.04	20.66	35.32	46.27	42.34

Group	G3								
Reference	Beaumont-Smith, 2007								
Sample	103-00-1268	103-01-1604	103-01-2001	103-01-2016	94-00-26	94-00-67	95-01-3	95-01-15	95-01-16
Easting (m)	352910	357892	361836	401016	386139	382800	378180	377683	377685
Northing (m)	6285022	6288138	6289448	6295510	6291320	6292019	6305413	6304840	6304906
DDH	Outcrop	Outcrop	Outcrop	Outcrop	Outcrop	Outcrop	Outcrop	Outcrop	Outcrop
Depth (m)	-	-	-	-	-	-	-	-	-
SiO_2	57.79	47.96	48.49	49.21	52.09	51.98	47.84	56.11	54.65
Al_2O_3	15.96	14.51	16.98	15.63	17.04	14.47	19.66	15.16	17.78
TiO_2	1.28	1.73	1.35	0.96	1.04	1.34	0.64	0.66	1.00
Fe_2O_3	10.96	16.53	12.96	14.09	12.60	13.33	10.30	9.27	12.00
MnO	0.07	0.22	0.20	0.20	0.16	0.22	0.16	0.24	0.20
MgO	3.46	6.64	6.42	8.35	4.74	5.34	3.62	5.63	5.79
CaO	4.18	7.97	9.19	8.15	7.67	9.36	15.12	11.03	4.65
Na_2O	5.65	3.83	3.55	2.94	3.27	2.92	1.55	0.84	2.26
K_2O	0.43	0.20	0.53	0.23	1.11	0.73	1.01	0.94	1.47
P_2O_5	0.23	0.41	0.33	0.24	0.26	0.31	0.10	0.11	0.21
LOI	0.45	0.15	1.49	2.61	1.42	1.54	4.20	2.06	2.84
Total	100	100	100	100	100	100	100	100	100
Ni	*n.d.*	67	104	68	50	34	72	*n.d.*	*n.d.*
Cr	5	168	200	338	31	49	116	6	16
Co	24	56	52	43	41	35	37	18	18
V	186	346	278	265	145	337	149	90	130
Sc	25	42	38	41	21	40	29	19	27
Cu	51	58	46	12	36	82	82	65	20
Zn	38	150	103	89	106	94	55	101	118
Mo	*n.d.*	*n.d.*	*n.d.*	*n.d.*	3.2	*n.d.*	*n.d.*	*n.d.*	*n.d.*
W	*n.d.*	*n.d.*	*n.d.*	*n.d.*	*n.d.*	*n.d.*	*n.d.*	2.0	*n.d.*
Sb	0.3	0.4	1.0	1.1	*n.d.*	1.1	0.4	0.1	*n.d.*
Sn	*n.d.*	*n.d.*	*n.d.*	*n.d.*	*n.d.*	*n.d.*	*n.d.*	*n.d.*	*n.d.*

Group	G3								
Reference	Beaumont-Smith, 2007								
Sample	103-00-1268	103-01-1604	103-01-2001	103-01-2016	94-00-26	94-00-67	95-01-3	95-01-15	95-01-16
Ba	104	41	135	126	328	300	295	116	256
Cs	0.7	*n.d.*	*n.d.*	*n.d.*	0.7	*n.d.*	0.7	0.3	0.9
Rb	*n.d.*	*n.d.*	*n.d.*	*n.d.*	*n.d.*	*n.d.*	*n.d.*	*n.d.*	*n.d.*
Sr	84	272	260	210	385	422	172	124	119
Pb	6	9	*n.d.*	*n.d.*	*n.d.*	7	*n.d.*	*n.d.*	*n.d.*
Ga	15	19	20	16	15	16	15	16	19
Zr	126	66	93	57	112	72	29	68	95
Hf	3.5	1.9	2.3	1.4	2.4	1.8	0.9	2.0	2.8
Nb	7.5	2.7	3.5	1.2	8.5	3.3	2.4	3.9	5.2
Ta	0.6	0.2	0.3	0.2	0.4	0.2	0.2	0.3	0.3
Th	1.2	0.6	0.7	0.3	2.0	0.8	0.5	0.9	1.1
U	0.7	0.3	0.3	0.2	0.9	0.3	0.1	0.5	0.5
Y	21	25	25	20	22	27	9	17	21
La	9.6	5.6	7.4	5.7	19.6	9.1	3.8	6.9	6.5
Ce	23.8	13.9	18.1	14.1	42.1	20.6	8.6	15.9	13.0
Pr	3.27	2.01	2.54	1.97	4.91	2.66	1.14	2.07	1.53
Nd	14.9	10.1	12.5	10.0	20.5	12.0	5.3	9.7	6.6
Sm	3.4	2.8	3.4	2.5	4.2	3.2	1.4	2.5	1.7
Eu	0.56	1.19	1.31	0.92	1.20	1.11	0.59	0.83	0.87
Gd	3.2	3.4	3.8	2.8	4.3	3.9	1.6	2.9	2.3
Tb	0.6	0.7	0.7	0.5	0.7	0.7	0.3	0.5	0.5
Dy	3.7	4.3	4.4	3.6	3.8	4.3	1.7	3.0	3.6
Ho	0.8	0.9	0.9	0.8	0.8	0.9	0.3	0.6	0.8
Er	2.2	2.8	2.7	2.3	2.1	2.7	1.0	1.8	2.5
Tm	0.32	0.43	0.42	0.37	0.30	0.41	0.15	0.27	0.40
Yb	2.1	2.6	2.6	2.3	1.9	2.7	0.9	1.7	2.5
Lu	0.32	0.39	0.40	0.35	0.28	0.41	0.14	0.25	0.37

Group	G3								
Reference	Beaumont-Smith, 2007								
Sample	103-00-1268	103-01-1604	103-01-2001	103-01-2016	94-00-26	94-00-67	95-01-3	95-01-15	95-01-16
La/Sm_{CN}	1.85	1.27	1.42	1.47	2.99	1.84	1.80	1.81	2.43
Gd/Yb_{CN}	1.28	1.08	1.19	1.02	1.86	1.19	1.43	1.39	0.76
La/Yb_{CN}	3.32	1.52	2.02	1.80	7.39	2.44	2.87	2.87	1.88
Eu/Eu*	0.52	1.17	1.12	1.05	0.86	0.97	1.21	0.94	1.33
Ce/Ce*	1.04	1.02	1.03	1.03	1.05	1.02	1.01	1.03	1.01
Zr/Y	6.1	2.7	3.7	2.8	5.0	10.8	30.5	23.0	17.8
Ti/Zr	61	156	86	98	55	109	125	57	61
Al_2O_3/TiO_2	12	8	13	16	16	16	22	14	20
Zr/Nb	17	25	26	49	13	22	12	18	18
Zr/Zr*	1.03	0.72	0.83	0.66	0.70	0.68	0.64	0.81	1.63
Zr/Sm_{PM}	1.49	0.93	1.10	0.90	1.05	0.90	0.86	1.10	2.18
Zr/Nd_{PM}	1.04	0.81	0.91	0.70	0.67	0.74	0.68	0.86	1.76
Ti/Ti*	1.43	1.28	0.90	0.88	0.69	0.96	0.95	0.63	1.04
Ti/Gd_{PM}	1.73	1.85	1.44	1.16	1.53	1.39	1.85	1.06	1.11
Ti/Sm_{PM}	0.81	1.29	0.84	0.79	0.52	0.88	0.97	0.56	1.20
Nb/Nb*	0.79	0.52	0.58	0.32	0.49	0.44	0.65	0.55	0.71
Nb/Th_{PM}	0.80	0.58	0.70	0.51	0.55	0.53	0.66	0.55	0.64
Nb/La_{PM}	0.77	0.48	0.48	0.20	0.43	0.36	0.64	0.55	0.80
Mg#	38	44	50	54	43	44	41	55	49
ΣLREE	58.77	39.02	48.97	38.00	96.77	52.60	22.35	40.87	32.52
ΣHREE	30.60	37.07	37.21	30.44	32.21	39.19	14.07	24.76	32.01

Group	**G3**								
Reference	**Beaumont-Smith, 2007**								
Sample	95-01-17	95-01-32	95-01-51	103-03-1901	103-00-1270	103-00-1270	95-00-21	103-04-2100	95-00-75
Easting (m)	377680	381597	376420	381139	353453	353453	380931	348241	378239
Northing (m)	6304924	6309256	6304285	6307554	6285720	6285720	6308282	6281322	6305905
DDH	Outcrop	Outcrop	Outcrop	Outcrop	Outcrop	Outcrop	Outcrop	Outcrop	Outcrop
Depth (m)	-	-	-	-	-	-	-	-	-
SiO_2	56.72	58.60	47.56	48.53	51.59	54.89	52.34	50.69	49.77
Al_2O_3	17.37	19.07	18.38	13.48	15.23	13.81	14.86	16.13	11.99
TiO_2	0.83	0.57	1.22	2.08	1.82	1.57	1.61	1.30	1.59
Fe_2O_3	10.05	7.90	12.51	14.77	13.15	14.82	14.78	13.06	14.06
MnO	0.15	0.09	0.21	0.18	0.21	0.13	0.19	0.19	0.17
MgO	2.95	2.28	3.59	6.22	5.55	4.20	3.90	5.95	8.93
CaO	6.96	6.31	12.15	11.53	9.52	6.10	8.89	7.80	9.98
Na_2O	3.15	3.93	3.59	2.86	2.09	4.04	2.51	4.41	3.18
K_2O	1.58	1.12	0.55	0.11	0.56	0.09	0.60	0.27	0.19
P_2O_5	0.24	0.12	0.24	0.25	0.28	0.36	0.31	0.20	0.14
LOI	0.46	1.49	1.46	3.07	1.6	0.69	1.45	1.38	0.79
Total	100	100	100	100	100	100	100	100	100
Ni	*n.d.*	22	*n.d.*	100	81	*n.d.*	*n.d.*	104	272
Cr	5	6	24	209	403	14	*n.d.*	267	689
Co	18	13	24	44	44	34	31	47	62
V	100	67	238	325	330	224	306	278	328
Sc	24	19	34	30	40	35	31	36	50
Cu	*n.d.*	194	*n.d.*	27	103	23	*n.d.*	95	159
Zn	110	300	116	88	110	77	221	83	76
Mo	*n.d.*	*n.d.*	*n.d.*	*n.d.*	*n.d.*	*n.d.*	*n.d.*	*n.d.*	*n.d.*
W	*n.d.*	*n.d.*	0.7	*n.d.*	*n.d.*	3.3	0.6	*n.d.*	*n.d.*
Sb	*n.d.*	0.4	*n.d.*	1.2	*n.d.*	0.6	*n.d.*	*n.d.*	0.4
Sn	1.4	*n.d.*	*n.d.*	1.9	*n.d.*	*n.d.*	1.2	*n.d.*	*n.d.*

Group	G3								
Reference	Beaumont-Smith, 2007								
Sample	95-01-17	95-01-32	95-01-51	103-03-1901	103-00-1270	103-00-1270	95-00-21	103-04-2100	95-00-75
Ba	332	198	90	46	227	17	118	185	30
Cs	0.8	0.8	*n.d.*	*n.d.*	*n.d.*	*n.d.*	0.4	*n.d.*	*n.d.*
Rb	*n.d.*	*n.d.*	*n.d.*	*n.d.*	*n.d.*	*n.d.*	*n.d.*	*n.d.*	*n.d.*
Sr	253	135	290	200	214	246	143	249	293
Pb	5	7	6	33	6	6	9	*n.d.*	*n.d.*
Ga	19	12	23	21	23	23	22	21	15
Zr	127	49	123	127	121	102	98	110	82
Hf	3.7	1.4	3.4	3.6	3.2	2.8	2.8	3.2	2.5
Nb	6.9	4.2	7.0	15.3	15.7	6.7	9.9	7.3	9.6
Ta	2.5	0.3	0.4	1.0	0.9	0.4	0.7	0.5	0.6
Th	1.2	1.0	1.6	1.4	1.7	0.9	1.3	1.1	0.9
U	0.5	0.8	0.6	0.4	0.9	0.6	0.5	0.4	0.2
Y	34	11	28	24	28	33	26	21	18
La	11.4	6.4	14.0	16.6	18.8	12.7	10.8	11.7	9.1
Ce	27.6	14.0	31.5	38.4	44.1	33.4	25.0	28.2	21.7
Pr	3.63	1.71	3.94	4.84	5.77	4.66	3.60	3.43	3.03
Nd	16.7	7.0	17.6	21.3	25.2	21.2	17.0	15.7	14.3
Sm	4.4	1.6	4.5	5.3	6.0	5.4	4.2	3.9	3.6
Eu	1.26	0.59	1.59	1.84	1.99	1.64	1.54	1.41	1.30
Gd	5.2	1.8	5.1	5.2	5.7	5.8	5.0	3.9	4.4
Tb	0.9	0.3	0.9	0.8	0.9	1.0	0.9	0.6	0.8
Dy	6.0	2.0	5.3	4.4	5.4	6.2	4.9	3.5	4.4
Ho	1.3	0.4	1.0	0.8	1.0	1.3	1.0	0.7	0.9
Er	3.9	1.3	3.2	2.3	2.8	3.6	2.9	2.2	2.7
Tm	0.62	0.19	0.48	0.31	0.38	0.52	0.45	0.31	0.37
Yb	3.8	1.2	3.0	1.8	2.3	3.3	2.9	1.9	2.4
Lu	0.55	0.18	0.43	0.26	0.33	0.51	0.45	0.28	0.34

Group	G3								
Reference	Beaumont-Smith, 2007								
Sample	95-01-17	95-01-32	95-01-51	103-03-1901	103-00-1270	103-00-1270	95-00-21	103-04-2100	95-00-75
La/Sm_{CN}	1.69	2.58	2.02	2.01	2.04	1.52	1.66	1.94	1.63
Gd/Yb_{CN}	1.12	1.26	1.41	2.38	2.01	1.44	1.42	1.74	1.50
La/Yb_{CN}	2.15	3.84	3.36	6.58	5.80	2.74	2.63	4.48	2.72
Eu/Eu*	0.81	1.05	1.02	1.07	1.05	0.90	1.03	1.10	1.00
Ce/Ce*	1.05	1.04	1.04	1.05	1.04	1.07	0.99	1.09	1.01
Zr/Y	20.9	33.4	15.1	6.5	8.4	8.8	3.8	5.2	4.4
Ti/Zr	39	68	58	95	88	91	96	69	114
Al_2O_3/TiO_2	14	12	8	13	16	16	9	12	8
Zr/Nb	18	12	18	8	8	15	10	15	8
Zr/Zr*	0.86	0.85	0.81	0.69	0.57	0.55	0.67	0.81	0.65
Zr/Sm_{PM}	1.16	1.21	1.10	0.95	0.81	0.75	0.93	1.13	0.89
Zr/Nd_{PM}	0.93	0.86	0.86	0.73	0.59	0.59	0.71	0.86	0.70
Ti/Ti*	0.49	0.81	0.63	0.98	0.80	0.76	0.85	0.82	0.98
Ti/Gd_{PM}	0.61	1.31	1.13	3.15	2.18	1.33	1.51	1.93	1.82
Ti/Sm_{PM}	0.40	0.74	0.57	0.81	0.64	0.62	0.80	0.70	0.91
Nb/Nb*	0.69	0.61	0.53	1.13	1.00	0.70	0.97	0.72	1.24
Nb/Th_{PM}	0.79	0.58	0.57	1.40	1.21	0.95	1.02	0.85	1.46
Nb/La_{PM}	0.60	0.65	0.50	0.92	0.83	0.52	0.91	0.62	1.05
Mg#	37	36	36	45	46	36	34	47	56
ΣLREE	70.16	33.18	78.21	93.41	107.54	84.76	67.16	68.20	57.47
ΣHREE	51.53	16.21	41.85	35.13	41.24	49.80	39.49	30.58	30.32

Group	G3								
Reference	Beaumont-Smith, 2007								
Sample	103-00-1270	103-00-1244	103-00-1267	103-00-1267	103-00-1268	103-01-1612	103-01-1680	103-03-1852	103-03-1883
Easting (m)	353453	358975	353140	353140	352910	357203	350639	372176	365784
Northing (m)	6285720	6288612	6285339	6285339	6285022	6288794	6280568	6301194	6300652
DDH	Outcrop	Outcrop	Outcrop	Outcrop	Outcrop	Outcrop	Outcrop	Outcrop	Outcrop
Depth (m)	-	-	-	-	-	-	-	-	-
SiO_2	50.21	47.94	48.30	47.99	55.71	54.33	52.95	46.20	52.10
Al_2O_3	12.91	14.99	14.64	14.90	14.88	13.61	17.75	13.24	17.69
TiO_2	1.06	1.65	2.03	1.65	1.75	2.05	1.26	1.55	0.90
Fe_2O_3	14.42	16.20	17.21	16.23	12.81	14.19	12.00	17.04	12.66
MnO	0.22	0.24	0.22	0.24	0.13	0.18	0.24	0.35	0.19
MgO	6.08	6.55	4.50	6.57	5.70	4.84	3.37	7.61	4.49
CaO	11.97	7.98	9.06	8.00	3.66	6.20	8.43	12.41	7.96
Na_2O	2.88	3.48	3.30	3.44	5.10	3.42	3.24	0.68	3.71
K_2O	0.12	0.58	0.51	0.61	0.05	0.54	0.57	0.75	0.21
P_2O_5	0.15	0.38	0.24	0.37	0.21	0.63	0.20	0.17	0.08
LOI	3.81	0.66	1.51	0.69	0.53	0.4	1.19	2.35	0.61
Total	100	100	100	100	100	100	100	100	100
Ni	35	31	84	44	41	31	-20	153	*n.d.*
Cr	281	178	17	183	451	66	-5	347	24
Co	26	47	45	46	61	41	29	40	29
V	220	296	422	298	376	346	169	336	352
Sc	31	40	39	40	44	43	36	27	36
Cu	32	76	166	77	177	28	37	41	235
Zn	57	165	92	160	562	104	128	148	74
Mo	*n.d.*	*n.d.*	*n.d.*	*n.d.*	*n.d.*	*n.d.*	*n.d.*	*n.d.*	*n.d.*
W	1.4	*n.d.*	*n.d.*	*n.d.*	*n.d.*	*n.d.*	*n.d.*	*n.d.*	*n.d.*
Sb	0.8	0.3	*n.d.*	0.7	*n.d.*	1.0	0.7	*n.d.*	*n.d.*
Sn	*n.d.*	*n.d.*	*n.d.*	*n.d.*	*n.d.*	1.0	*n.d.*	*n.d.*	*n.d.*

Group	G3								
Reference	Beaumont-Smith, 2007								
Sample	103-00-1270	103-00-1244	103-00-1267	103-00-1267	103-00-1268	103-01-1612	103-01-1680	94-00-67	95-01-3
Ba	42	296	224	283	57	230	145	300	295
Cs	*n.d.*	0.9	1.9	0.9	*n.d.*	0.9	*n.d.*	*n.d.*	0.7
Rb	*n.d.*	*n.d.*	*n.d.*	*n.d.*	*n.d.*	*n.d.*	*n.d.*	*n.d.*	*n.d.*
Sr	208	198	285	201	131	287	229	422	172
Pb	*n.d.*	5	5	6	*n.d.*	6	*n.d.*	7	*n.d.*
Ga	18	19	21	20	21	18	19	16	15
Zr	93	83	111	84	93	92	93	72	29
Hf	2.7	2.3	3.0	2.2	2.8	2.6	2.5	1.8	0.9
Nb	6.8	4.8	7.9	4.6	5.9	5.1	4.4	3.3	2.4
Ta	0.4	0.3	0.5	0.3	0.4	0.3	0.4	0.2	0.2
Th	0.9	0.5	0.9	0.5	0.7	1.1	0.6	0.8	0.5
U	0.6	0.2	0.4	0.2	0.4	0.5	0.4	0.3	0.1
Y	26	31	32	31	21	37	25	27	9
La	7.1	8.2	9.3	8.0	7.1	9.9	6.8	9.1	3.8
Ce	21.0	20.2	22.8	19.6	18.1	23.0	17.5	20.6	8.6
Pr	3.29	2.88	3.25	2.79	2.60	3.24	2.57	2.66	1.14
Nd	15.9	14.0	15.5	13.7	12.6	16.0	13.1	12.0	5.3
Sm	4.4	3.9	4.4	3.8	3.7	4.3	3.7	3.2	1.4
Eu	1.01	1.50	1.56	1.43	1.36	1.57	1.63	1.11	0.59
Gd	4.6	4.8	5.0	4.6	4.2	5.0	4.2	3.9	1.6
Tb	0.8	0.8	0.9	0.8	0.7	0.9	0.8	0.7	0.3
Dy	4.8	5.4	5.7	5.4	4.4	6.0	4.9	4.3	1.7
Ho	1.0	1.1	1.2	1.1	0.8	1.3	1.0	0.9	0.3
Er	2.9	3.3	3.3	3.2	2.3	3.9	2.8	2.7	1.0
Tm	0.42	0.47	0.49	0.48	0.33	0.60	0.42	0.41	0.15
Yb	2.7	3.1	3.2	3.1	2.1	3.7	2.6	2.7	0.9
Lu	0.40	0.50	0.49	0.48	0.30	0.55	0.39	0.41	0.14

Group	G3								
Reference	Beaumont-Smith, 2007								
Sample	103-00-1270	103-00-1244	103-00-1267	103-00-1267	103-00-1268	103-01-1612	103-01-1680	94-00-67	95-01-3
La/Sm_{CN}	1.03	1.35	1.38	1.37	1.25	1.49	1.18	1.84	1.80
Gd/Yb_{CN}	1.43	1.26	1.28	1.23	1.69	1.13	1.36	1.19	1.43
La/Yb_{CN}	1.89	1.87	2.07	1.87	2.47	1.92	1.91	2.44	2.87
Eu/Eu*	0.68	1.05	1.02	1.05	1.06	1.04	1.26	0.97	1.21
Ce/Ce*	1.07	1.02	1.01	1.02	1.03	1.00	1.03	1.02	1.01
Zr/Y	3.5	2.7	3.4	2.7	4.4	2.5	3.7	10.8	30.5
Ti/Zr	65	119	109	117	111	132	80	109	125
Al_2O_3/TiO_2	12	9	7	9	9	7	14	16	22
Zr/Nb	14	17	14	18	16	18	21	22	12
Zr/Zr*	0.64	0.64	0.78	0.67	0.79	0.64	0.76	0.68	0.64
Zr/Sm_{PM}	0.84	0.84	1.01	0.88	1.01	0.86	0.98	0.90	0.86
Zr/Nd_{PM}	0.72	0.72	0.87	0.75	0.91	0.71	0.87	0.74	0.68
Ti/Ti*	0.71	0.93	1.08	0.96	1.09	1.09	0.71	0.96	0.95
Ti/Gd_{PM}	1.07	1.48	1.76	1.50	2.38	1.57	1.36	1.39	1.85
Ti/Sm_{PM}	0.49	0.89	0.98	0.92	1.01	1.02	0.70	0.88	0.97
Nb/Nb*	0.97	0.90	1.01	0.86	0.98	0.56	0.81	0.44	0.65
Nb/Th_{PM}	0.97	1.38	1.21	1.28	1.16	0.62	1.02	0.53	0.66
Nb/La_{PM}	0.96	0.59	0.84	0.57	0.83	0.51	0.63	0.36	0.64
Mg#	46	44	34	45	47	40	36	44	41
ΣLREE	57.35	55.46	61.81	53.93	49.64	63.02	49.59	52.60	22.35
ΣHREE	39.41	45.41	47.38	45.68	32.06	53.69	37.71	39.19	14.07

Group					**G3**				
Reference					**Beaumont-Smith, 2007**				
Sample	103-04-2163	95-00-37	95-01-61	95-01-148	12-77-687	95-01-58	103-04-2238	32-77-2116	95-00-21
Easting (m)	375980	381390	375784	373323	335201	376343	375720	392659	380931
Northing (m)	6303503	6307071	6304158	6301701	6276322	6304633	6303552	6313314	6308282
DDH	Outcrop	Outcrop	Outcrop	Outcrop	Outcrop	Outcrop	Outcrop	Outcrop	Outcrop
Depth (m)	-	-	-	-	-	-	-	-	-
SiO_2	56.36	49.13	50.05	46.75	48.46	51.30	51.64	48.72	52.34
Al_2O_3	21.65	12.16	17.72	16.88	18.22	19.85	20.49	21.15	14.86
TiO_2	0.58	1.54	0.49	1.32	2.55	0.83	0.92	0.55	1.61
Fe_2O_3	6.31	13.82	9.17	15.36	11.15	10.73	10.16	9.95	14.78
MnO	0.13	0.19	0.13	0.23	0.10	0.18	0.17	0.14	0.19
MgO	1.64	9.86	7.59	4.17	3.77	3.68	3.56	4.41	3.90
CaO	9.47	10.35	10.76	11.50	10.57	9.35	10.70	13.10	8.89
Na_2O	3.20	2.65	3.11	3.31	4.45	3.78	1.33	1.61	2.51
K_2O	0.47	0.16	0.90	0.30	0.42	0.20	0.89	0.30	0.60
P_2O_5	0.19	0.14	0.09	0.18	0.32	0.11	0.14	0.07	0.31
LOI	0.41	0.88	0.97	2.15	3.22	0.61	0.39	1.41	1.45
Total	100	100	100	100	100	100	100	100	100
Ni	*n.d.*	266	132	25	*n.d.*	28	*n.d.*	28	*n.d.*
Cr	7	718	206	23	*n.d.*	6	8	38	*n.d.*
Co	11	60	59	41	59	26	29	47	31
V	40	317	212	387	553	215	175	186	306
Sc	14	49	42	40	*n.d.*	32	23	*n.d.*	31
Cu	44	145	85	69	13	86	44	117	*n.d.*
Zn	59	78	71	116	151	80	82	84	221
Mo	*n.d.*	*n.d.*	*n.d.*	*n.d.*	*n.d.*	*n.d.*	*n.d.*	*n.d.*	*n.d.*
W	5.1	*n.d.*	*n.d.*	*n.d.*	22	0.6	*n.d.*	177	0.6
Sb	*n.d.*	1.0	0.9	*n.d.*	0.7	*n.d.*	*n.d.*	0.9	*n.d.*
Sn	*n.d.*	1.0	*n.d.*	*n.d.*	1.2	*n.d.*	*n.d.*	3.3	1.2

Group	G3								
Reference	Beaumont-Smith, 2007								
Sample	95-01-15	95-01-16	95-01-17	95-01-32	95-01-51	103-03-1901	103-00-1270	103-00-1270	95-00-21
Ba	116	256	332	198	90	46	227	17	169
Cs	0.3	0.9	0.8	0.8	*n.d.*	*n.d.*	*n.d.*	*n.d.*	1.3
Rb	*n.d.*	*n.d.*	*n.d.*	*n.d.*	*n.d.*	*n.d.*	*n.d.*	*n.d.*	*n.d.*
Sr	124	119	253	135	290	200	214	246	66
Pb	*n.d.*	*n.d.*	4	7	6	33	6	6	*n.d.*
Ga	16	19	19	12	23	21	23	23	20
Zr	68	95	127	49	123	127	121	102	93
Hf	2.0	2.8	3.7	1.4	3.4	3.6	3.2	2.8	2.8
Nb	3.9	5.2	6.9	4.2	7.0	15.3	15.7	6.7	6.2
Ta	0.3	0.3	2.5	0.3	0.4	1.0	0.9	0.4	0.5
Th	0.9	1.1	1.2	1.0	1.6	1.4	1.7	0.9	0.6
U	0.5	0.5	0.5	0.8	0.6	0.4	0.9	0.6	0.3
Y	17	21	34	11	28	24	28	33	21
La	6.9	6.5	11.4	6.4	14.0	16.6	18.8	12.7	8.1
Ce	15.9	13.0	27.6	14.0	31.5	38.4	44.1	33.4	21.4
Pr	2.07	1.53	3.63	1.71	3.94	4.84	5.77	4.66	2.93
Nd	9.7	6.6	16.7	7.0	17.6	21.3	25.2	21.2	14.4
Sm	2.5	1.7	4.4	1.6	4.5	5.3	6.0	5.4	3.9
Eu	0.83	0.87	1.26	0.59	1.59	1.84	1.99	1.64	1.21
Gd	2.9	2.3	5.2	1.8	5.1	5.2	5.7	5.8	4.2
Tb	0.5	0.5	0.9	0.3	0.9	0.8	0.9	1.0	0.7
Dy	3.0	3.6	6.0	2.0	5.3	4.4	5.4	6.2	4.0
Ho	0.6	0.8	1.3	0.4	1.0	0.8	1.0	1.3	0.7
Er	1.8	2.5	3.9	1.3	3.2	2.3	2.8	3.6	2.0
Tm	0.27	0.40	0.62	0.19	0.48	0.31	0.38	0.52	0.27
Yb	1.7	2.5	3.8	1.2	3.0	1.8	2.3	3.3	1.6
Lu	0.25	0.37	0.55	0.18	0.43	0.26	0.33	0.51	0.23

Group	G3								
Reference	Beaumont-Smith, 2007								
Sample	95-01-15	95-01-16	95-01-17	95-01-32	95-01-51	103-03-1901	103-00-1270	103-00-1270	95-00-21
La/Sm_{CN}	1.81	2.43	1.69	2.58	2.02	2.01	2.04	1.52	1.33
Gd/Yb_{CN}	1.39	0.76	1.12	1.26	1.41	2.38	2.01	1.44	2.13
La/Yb_{CN}	2.87	1.88	2.15	3.84	3.36	6.58	5.80	2.74	3.60
Eu/Eu*	0.94	1.33	0.81	1.05	1.02	1.07	1.05	0.90	0.91
Ce/Ce*	1.03	1.01	1.05	1.04	1.04	1.05	1.04	1.07	1.08
Zr/Y	23.0	17.8	20.9	33.4	15.1	6.5	8.4	8.8	4.5
Ti/Zr	57	61	39	68	58	95	88	91	97
Al_2O_3/TiO_2	14	20	14	12	8	13	16	16	9
Zr/Nb	18	18	18	12	18	8	8	15	15
Zr/Zr*	0.81	1.63	0.86	0.85	0.81	0.69	0.57	0.55	0.71
Zr/Sm_{PM}	1.10	2.18	1.16	1.21	1.10	0.95	0.81	0.75	0.94
Zr/Nd_{PM}	0.86	1.76	0.93	0.86	0.86	0.73	0.59	0.59	0.79
Ti/Ti*	0.63	1.04	0.49	0.81	0.63	0.98	0.80	0.76	1.02
Ti/Gd_{PM}	1.06	1.11	0.61	1.31	1.13	3.15	2.18	1.33	2.65
Ti/Sm_{PM}	0.56	1.20	0.40	0.74	0.57	0.81	0.64	0.62	0.82
Nb/Nb*	0.55	0.71	0.69	0.61	0.53	1.13	1.00	0.70	1.03
Nb/Th_{PM}	0.55	0.64	0.79	0.58	0.57	1.40	1.21	0.95	1.41
Nb/La_{PM}	0.55	0.80	0.60	0.65	0.50	0.92	0.83	0.52	0.76
Mg#	55	49	37	36	36	45	46	36	47
ΣLREE	40.87	32.52	70.16	33.18	78.21	93.41	107.54	84.76	56.13
ΣHREE	24.76	32.01	51.53	16.21	41.85	35.13	41.24	49.80	30.40

Group	G3								
Reference	Beaumont-Smith, 2007								
Sample	103-04-2100	95-00-75	103-00-1270	103-00-1244	103-00-1267	103-00-1267	103-00-1268	103-01-1612	103-01-1680
Easting (m)	348241	378239	353453	358975	353140	353140	352910	357203	350639
Northing (m)	6281322	6305905	6285720	6288612	6285339	6285339	6285022	6288794	6280568
DDH	Outcrop	Outcrop	Outcrop	Outcrop	Outcrop	Outcrop	Outcrop	Outcrop	Outcrop
Depth (m)	-	-	-	-	-	-	-	-	-
SiO_2	50.69	49.77	50.21	47.94	48.30	47.99	55.71	54.33	52.95
Al_2O_3	16.13	11.99	12.91	14.99	14.64	14.90	14.88	13.61	17.75
TiO_2	1.30	1.59	1.06	1.65	2.03	1.65	1.75	2.05	1.26
Fe_2O_3	13.06	14.06	14.42	16.20	17.21	16.23	12.81	14.19	12.00
MnO	0.19	0.17	0.22	0.24	0.22	0.24	0.13	0.18	0.24
MgO	5.95	8.93	6.08	6.55	4.50	6.57	5.70	4.84	3.37
CaO	7.80	9.98	11.97	7.98	9.06	8.00	3.66	6.20	8.43
Na_2O	4.41	3.18	2.88	3.48	3.30	3.44	5.10	3.42	3.24
K_2O	0.27	0.19	0.12	0.58	0.51	0.61	0.05	0.54	0.57
P_2O_5	0.20	0.14	0.15	0.38	0.24	0.37	0.21	0.63	0.20
LOI	1.38	0.79	3.81	0.66	1.51	0.69	0.53	0.4	1.19
Total	100	100	100	100	100	100	100	100	100
Ni	104	272	35	31	84	44	41	31	-20
Cr	267	689	281	178	17	183	451	66	-5
Co	47	62	26	47	45	46	61	41	29
V	278	328	220	296	422	298	376	346	169
Sc	36	50	31	40	39	40	44	43	36
Cu	95	159	32	76	166	77	177	28	37
Zn	83	76	57	165	92	160	562	104	128
Mo	*n.d.*	*n.d.*	*n.d.*	*n.d.*	*n.d.*	*n.d.*	*n.d.*	*n.d.*	*n.d.*
W	*n.d.*	*n.d.*	1.4	*n.d.*	*n.d.*	*n.d.*	*n.d.*	*n.d.*	*n.d.*
Sb	*n.d.*	0.4	0.8	0.3	*n.d.*	0.7	*n.d.*	1.0	0.7
Sn	*n.d.*	*n.d.*	*n.d.*	*n.d.*	*n.d.*	*n.d.*	*n.d.*	1.0	*n.d.*

Group	G3								
Reference	Beaumont-Smith, 2007								
Sample	103-04-2100	95-00-75	103-00-1270	103-00-1244	103-00-1267	103-00-1267	103-00-1268	103-01-1612	103-01-1680
Ba	44	222	44	343	74	121	56	104	45
Cs	*n.d.*	*n.d.*	*n.d.*	0.2	0.1	*n.d.*	0.1	0.9	*n.d.*
Rb	*n.d.*	*n.d.*	*n.d.*	*n.d.*	*n.d.*	5.6	*n.d.*	*n.d.*	2.8
Sr	200	337	336	190	181	181	255	197	197
Pb	*n.d.*	*n.d.*	*n.d.*	6	*n.d.*	*n.d.*	*n.d.*	*n.d.*	0.4
Ga	18	20	15	14	21	25	20	22	17
Zr	41	71	94	23	53	149	45	73	36
Hf	1.4	2.0	2.2	0.7	1.5	4.2	1.3	2.0	1.0
Nb	2.6	4.3	9.0	2.0	4.1	9.3	4.9	4.9	4.2
Ta	0.2	0.3	0.7	0.1	0.2	0.6	0.2	0.3	1.0
Th	0.4	0.6	0.9	0.5	0.8	2.2	0.7	0.6	0.3
U	0.2	0.3	0.2	0.2	0.3	1.6	0.1	0.4	0.4
Y	25	19	21	10	19	44	15	18	11
La	7.8	5.9	7.4	4.1	6.2	10.5	4.4	5.0	3.2
Ce	16.7	15.4	18.3	9.2	14.8	26.8	10.6	12.1	7.1
Pr	2.11	2.02	2.53	1.19	1.98	3.74	1.32	1.50	0.96
Nd	10.0	9.9	11.6	5.4	9.4	17.4	6.3	7.4	4.7
Sm	2.9	2.9	3.3	1.5	2.6	5.2	2.0	2.1	1.4
Eu	1.20	1.13	1.22	0.55	1.06	1.70	0.86	0.84	0.61
Gd	3.6	3.1	3.8	1.7	3.0	6.3	2.7	2.4	1.5
Tb	0.7	0.5	0.7	0.3	0.6	1.1	0.5	0.4	0.3
Dy	4.0	3.1	4.0	1.9	3.4	7.0	3.0	2.7	1.7
Ho	0.8	0.6	0.8	0.4	0.7	1.5	0.6	0.6	0.4
Er	2.3	1.9	2.2	1.1	2.0	4.5	1.8	1.7	1.1
Tm	0.31	0.27	0.32	0.17	0.30	0.67	0.27	0.25	0.16
Yb	1.8	1.7	2.1	1.1	1.9	4.3	1.6	1.6	1.1
Lu	0.27	0.25	0.29	0.16	0.29	0.69	0.23	0.24	0.16

Group	G3								
Reference	Beaumont-Smith, 2007								
Sample	103-04-2100	95-00-75	103-00-1270	103-00-1244	103-00-1267	103-00-1267	103-00-1268	103-01-1612	103-01-1680
La/Sm_{CN}	1.72	1.31	1.45	1.81	1.56	1.31	1.41	1.54	1.48
Gd/Yb_{CN}	1.62	1.57	1.50	1.32	1.31	1.21	1.40	1.23	1.21
La/Yb_{CN}	3.05	2.55	2.50	2.76	2.34	1.74	1.94	2.23	2.16
Eu/Eu*	1.13	1.15	1.05	1.07	1.17	0.91	1.12	1.15	1.28
Ce/Ce*	1.00	1.10	1.04	1.02	1.04	1.05	1.08	1.09	1.00
Zr/Y	1.7	3.8	4.4	2.3	2.7	3.4	2.9	4.0	3.2
Ti/Zr	129	49	97	124	146	99	110	76	90
Al_2O_3/TiO_2	20	37	8	36	13	7	24	22	39
Zr/Nb	16	17	11	12	13	16	9	15	9
Zr/Zr*	0.44	0.76	0.88	0.48	0.62	0.91	0.72	1.07	0.81
Zr/Sm_{PM}	0.56	0.97	1.14	0.63	0.82	1.15	0.88	1.38	1.03
Zr/Nd_{PM}	0.51	0.87	0.99	0.53	0.68	1.05	0.86	1.20	0.94
Ti/Ti*	0.65	0.46	1.07	0.75	1.08	1.13	0.80	0.98	0.84
Ti/Gd_{PM}	1.37	0.99	2.05	1.28	1.92	1.61	1.43	1.63	1.45
Ti/Sm_{PM}	0.65	0.43	1.00	0.70	1.07	1.01	0.87	0.94	0.83
Nb/Nb*	0.54	0.86	1.23	0.51	0.66	0.70	1.04	1.01	1.46
Nb/Th_{PM}	0.89	1.02	1.25	0.55	0.67	0.55	0.97	1.05	1.63
Nb/La_{PM}	0.33	0.73	1.21	0.47	0.65	0.88	1.11	0.97	1.31
Mg#	41	34	59	62	35	40	40	41	47
ΣLREE	44.44	40.44	48.13	23.69	39.10	71.57	28.34	31.26	19.48
ΣHREE	35.08	27.19	31.46	15.28	28.37	63.42	23.30	25.58	15.94

Group	G3		G3U						
Reference	Peck, 1986		Beaumont-Smith, 2007						
Sample	160	144	103-02-1801	95-00-75	103-01-1614	103-04-2127	95-00-24	95-00-25	103-04-2127
Easting (m)	-	-	373431	378239	357075	382363	380707	380650	382363
Northing (m)	-	-	6302347	6305905	6289003	6307116	6307529	6307528	6307116
DDH	Outcrop	Outcrop	Outcrop	Outcrop	Outcrop	Outcrop	Outcrop	Outcrop	Outcrop
Depth (m)	-	-	-	-	-	-	-	-	-
SiO_2	54.35	47.43	48.66	48.56	45.35	45.79	48.59	46.34	45.47
Al_2O_3	13.67	15.99	10.59	7.55	11.83	10.87	8.10	10.43	8.93
TiO_2	1.19	0.77	1.43	1.18	0.97	1.38	1.18	1.50	1.94
Fe_2O_3	13.88	12.98	13.04	12.92	13.12	14.17	14.49	14.96	14.40
MnO	0.21	0.18	0.27	0.21	0.21	0.27	0.23	0.22	0.20
MgO	4.57	8.90	12.91	18.37	17.00	17.07	12.93	11.69	17.55
CaO	7.34	10.79	11.96	10.49	10.30	9.90	12.91	13.11	10.94
Na_2O	4.12	2.52	0.61	0.52	0.89	0.31	1.31	1.43	0.30
K_2O	0.41	0.24	0.31	0.10	0.15	0.10	0.14	0.19	0.07
P_2O_5	0.25	0.21	0.22	0.10	0.19	0.15	0.13	0.14	0.20
LOI	0.33	3.15	2.05	3.56	2.87	3.71	3.19	3.61	3.82
Total	100	100	100	100	100	100	100	100	100
Ni	21	135	172	943	543	666	2400	572	533
Cr	33	293	581	1550	1350	876	1710	1180	273
Co	64	59	45	86	76	76	87	71	66
V	331	157	280	227	268	246	222	325	298
Sc	49	34	35	28	38	23	31	36	25
Cu	51	90	47	75	71	*n.d.*	150	116	*n.d.*
Zn	111	93	220	97	103	140	89	116	89
Mo	-	-	6.2	*n.d.*	*n.d.*	*n.d.*	*n.d.*	*n.d.*	*n.d.*
W	-	-	*n.d.*	*n.d.*	*n.d.*	*n.d.*	*n.d.*	*n.d.*	*n.d.*
Sb	-	-	0.6	0.4	2.2	*n.d.*	0.8	1.0	*n.d.*
Sn	-	-	*n.d.*	*n.d.*	*n.d.*	*n.d.*	*n.d.*	*n.d.*	1.2

Group	G3		G3U						
Reference	Peck, 1986		Beaumont-Smith, 2007						
Sample	160	144	103-02-1801	95-00-75	103-01-1614	103-04-2127	95-00-24	95-00-25	103-04-2127
Ba	143	145	26	14	21	9	37	187	14
Cs	*n.d.*	*n.d.*	*n.d.*	*n.d.*	*n.d.*	*n.d.*	0.1	0.6	*n.d.*
Rb	5.0	2.0	*n.d.*	*n.d.*	*n.d.*	*n.d.*	*n.d.*	*n.d.*	*n.d.*
Sr	164	366	55	31	52	72	144	281	33
Pb	-	-	9	*n.d.*	5	*n.d.*	*n.d.*	22	8
Ga	-	-	16	11	16	17	15	17	16
Zr	82	15	70	62	54	84	81	145	119
Hf	2.4	0.9	2.1	1.9	1.6	2.4	2.0	2.5	3.3
Nb	6.0	3.0	4.9	5.6	4.3	8.8	5.2	5.6	12.6
Ta	*n.d.*	*n.d.*	0.5	0.4	0.3	0.6	0.4	0.4	0.9
Th	0.9	0.4	0.5	0.6	0.8	0.9	0.6	0.7	1.3
U	0.8	0.2	0.2	0.1	0.2	0.3	0.1	0.2	0.3
Y	35	15	16	7	16	18	18	21	24
La	10.5	5.8	6.4	8.0	5.9	9.8	6.6	8.0	11.7
Ce	26.0	14.0	15.9	18.2	14.0	23.6	15.6	19.7	29.0
Pr	-	-	2.37	2.61	1.95	2.92	2.24	2.78	3.60
Nd	14.0	7.0	11.6	12.0	9.2	14.1	10.9	13.7	17.5
Sm	3.7	2.0	3.0	3.0	2.4	3.6	3.0	3.7	4.5
Eu	1.32	0.73	0.69	1.12	0.83	0.81	1.18	1.29	1.66
Gd	-	-	3.3	3.3	2.6	3.6	3.6	4.1	4.6
Tb	1.0	0.4	0.5	0.5	0.5	0.6	0.6	0.7	0.7
Dy	-	-	3.2	2.8	2.9	3.2	3.5	4.2	4.3
Ho	-	-	0.6	0.5	0.6	0.6	0.7	0.8	0.8
Er	-	-	1.8	1.4	1.7	1.7	1.8	2.2	2.3
Tm	-	-	0.25	0.19	0.24	0.24	0.25	0.29	0.31
Yb	4.1	1.7	1.5	1.2	1.4	1.4	1.5	1.7	1.8
Lu	0.61	0.24	0.24	0.15	0.19	0.20	0.18	0.23	0.25

Group	G3		G3U						
Reference	Peck, 1986		Beaumont-Smith, 2007						
Sample	160	144	103-02-1801	95-00-75	103-01-1614	103-04-2127	95-00-24	95-00-25	103-04-2127
La/Sm_{CN}	1.86	1.91	1.36	1.74	1.58	1.74	1.40	1.41	1.68
Gd/Yb_{CN}	-	-	1.86	2.39	1.53	2.16	2.02	1.98	2.17
La/Yb_{CN}	1.85	2.43	3.10	4.97	3.00	5.09	3.24	3.33	4.77
Eu/Eu*	-	-	0.66	1.09	1.01	0.69	1.10	1.01	1.11
Ce/Ce*	-	-	1.00	0.97	1.01	1.09	0.99	1.02	1.09
Zr/Y	2.3	1.7	4.3	8.8	3.5	4.7	4.4	6.9	5.0
Ti/Zr	87	185	119	108	103	95	84	59	94
Al_2O_3/TiO_2	11	21	7	6	12	8	7	7	5
Zr/Nb	14	8	14	11	13	10	15	26	9
Zr/Zr*	0.66	0.39	0.68	0.60	0.67	0.68	0.81	1.17	0.77
Zr/Sm_{PM}	0.89	0.51	0.92	0.83	0.90	0.93	1.06	1.56	1.05
Zr/Nd_{PM}	0.72	0.44	0.75	0.64	0.73	0.73	0.91	1.29	0.83
Ti/Ti*	-	-	1.39	0.88	0.96	1.18	0.83	0.93	1.02
Ti/Gd_{PM}	0.83	1.28	2.65	2.75	1.88	2.74	2.20	2.34	3.01
Ti/Sm_{PM}	0.70	0.84	0.98	0.81	0.83	0.79	0.80	0.83	0.89
Nb/Nb*	0.71	0.71	1.04	0.93	0.69	1.06	0.96	0.88	1.17
Nb/Th_{PM}	0.88	0.99	1.42	1.25	0.66	1.26	1.17	1.11	1.29
Nb/La_{PM}	0.57	0.51	0.76	0.69	0.72	0.89	0.79	0.70	1.07
Mg#	39	58	66	74	72	70	64	61	71
ΣLREE	-	-	43.41	48.28	36.81	58.40	43.02	53.37	72.54
ΣHREE	-	-	24.53	13.89	23.14	26.00	26.57	31.20	34.39

Group					**G3U**				
Reference	**C.B.-S., 2007**					**Chapter 2**			
Sample	95-00-26	103-00-1269	MG11-003	MG11-013	MG11-015	MG11-028	MG11-033	MG11-050	MG11-051
Easting (m)	380643	351902	383386	380934	380952	380302	380302	380048	380048
Northing (m)	6307441	6284281	6306386	6307519	6307492	6307261	6307261	6307163	6307163
DDH	Outcrop	Outcrop	Outcrop	Outcrop	Outcrop	MG11-15	MG11-15	MG11-38	MG11-38
Depth (m)	-	-	-	-	-	257.57	305.86	84	83
SiO_2	48.48	44.93	46.50	47.28	48.14	61.42	45.77	52.48	48.81
Al_2O_3	8.76	10.84	12.04	8.53	9.84	5.54	8.69	8.77	6.71
TiO_2	1.27	0.75	1.56	1.27	1.52	0.90	1.35	1.18	0.98
Fe_2O_3	13.98	13.85	14.78	13.30	14.09	14.23	14.48	16.78	16.31
MnO	0.20	0.19	0.21	0.29	0.22	0.17	0.22	0.34	0.42
MgO	14.05	14.89	12.76	17.83	13.59	10.87	19.62	13.57	14.63
CaO	12.00	13.71	10.40	11.05	11.56	5.94	9.38	4.74	11.09
Na_2O	1.14	0.55	1.48	0.28	0.68	0.25	0.32	0.17	0.24
K_2O	-0.01	0.18	0.12	0.05	0.23	0.59	0.04	1.84	0.68
P_2O_5	0.11	0.11	0.16	0.13	0.14	0.09	0.13	0.12	0.12
LOI	1.76	8.14	2.44	5.05	2.08	3.12	4.64	4.33	6.57
Total	100	100	100	100	100	100	100	100	100
Ni	992	456	530	930	530	380	770	340	390
Cr	1610	1430	1040	1480	990	1010	1460	920	1300
Co	93	62	76	85	66	59	89	49	68
V	251	214	307	248	296	162	268	221	189
Sc	32	29	32	27	31	19	28	25	21
Cu	292	17	60	130	20	200	140.0	1110	1380
Zn	76	157	200	380	280	2080	200	920	670
Mo	*n.d.*	*n.d.*	*n.d.*	*n.d.*	*n.d.*	*n.d.*	*n.d.*	*n.d.*	*n.d.*
W	*n.d.*	*n.d.*	*n.d.*	1.0	*n.d.*	1.0	4.0	*n.d.*	*n.d.*
Sb	0.7	2.1	0.9	3.2	7.9	0.8	0.8	*n.d.*	*n.d.*
Sn	*n.d.*	*n.d.*	1.0	*n.d.*	*n.d.*	*n.d.*	*n.d.*	*n.d.*	*n.d.*

Group					G3U				
Reference	C.B.-S., 2007					Chapter 2			
Sample	95-00-26	103-00-1269	MG11-003	MG11-013	MG11-015	MG11-028	MG11-033	MG11-050	MG11-051
Ba	78	53	42	8	52	111	3	79	115
Cs	0.1	*n.d.*	*n.d.*	*n.d.*	*n.d.*	1.2	*n.d.*	4.6	1.3
Rb	*n.d.*	*n.d.*	*n.d.*	*n.d.*	4.0	19	*n.d.*	40	18
Sr	234	126	137	58	137	86	41	79	121
Pb	*n.d.*	*n.d.*	*n.d.*	*n.d.*	6	46	6	14	10
Ga	13	13	17	12	16	9	13	12	10
Zr	86	54	95	68	83	49	71	61	52
Hf	2.0	1.4	2.3	1.7	2.1	1.2	1.8	1.5	1.3
Nb	5.0	2.6	7.0	6.0	8.0	4.0	5.0	4.0	4.0
Ta	0.4	0.2	0.5	0.5	0.6	0.3	0.4	0.3	0.4
Th	0.5	0.4	0.8	0.7	0.8	0.4	0.6	0.4	0.5
U	0.2	0.1	0.4	0.2	0.2	*n.d.*	0.1	0.2	0.2
Y	29	14	17	10	14	7	10	9	8
La	6.6	4.5	6.8	6.7	9.6	3.7	7.0	5.9	5.2
Ce	15.7	10.8	17.8	17.3	22.1	10.0	17.4	14.8	13.2
Pr	2.21	1.52	2.40	2.28	2.93	1.35	2.29	1.89	1.69
Nd	10.4	7.3	11.1	10.7	13.4	6.5	10.9	8.7	8.0
Sm	2.8	2.0	3.1	2.8	3.4	1.8	3.0	2.1	2.2
Eu	0.96	0.73	1.10	1.01	1.19	0.65	1.11	0.56	0.78
Gd	3.7	2.3	3.4	3.0	3.6	1.7	3.0	2.1	2.2
Tb	0.6	0.4	0.6	0.5	0.6	0.3	0.5	0.3	0.3
Dy	3.3	2.5	3.5	2.5	3.1	1.5	2.7	2.0	1.9
Ho	0.6	0.5	0.7	0.5	0.6	0.3	0.5	0.4	0.4
Er	1.8	1.4	1.9	1.2	1.5	0.7	1.3	1.0	1.0
Tm	0.25	0.20	0.30	0.19	0.22	0.11	0.19	0.15	0.14
Yb	1.5	1.3	1.9	1.1	1.4	0.7	1.2	0.9	0.9
Lu	0.19	0.19	0.28	0.16	0.21	0.11	0.18	0.15	0.14

Group					G3U				
Reference	C.B.-S., 2007					Chapter 2			
Sample	95-00-26	103-00-1269	MG11-003	MG11-013	MG11-015	MG11-028	MG11-033	MG11-050	MG11-051
La/Sm_{CN}	1.52	1.48	1.42	1.54	1.82	1.33	1.51	1.81	1.53
Gd/Yb_{CN}	2.09	1.49	1.48	2.26	2.13	2.01	2.07	1.93	2.02
La/Yb_{CN}	3.27	2.58	2.57	4.37	4.92	3.79	4.18	4.70	4.14
Eu/Eu*	0.91	1.06	1.04	1.07	1.04	1.14	1.13	0.82	1.08
Ce/Ce*	1.00	1.01	1.08	1.09	1.02	1.10	1.07	1.09	1.09
Zr/Y	3.0	3.9	5.6	6.8	5.9	7.0	7.1	6.8	6.5
Ti/Zr	87	76	95	107	107	107	108	109	104
Al_2O_3/TiO_2	7	14	8	7	6	6	6	7	7
Zr/Nb	17	21	14	11	10	12	14	15	13
Zr/Zr*	0.92	0.82	0.94	0.72	0.71	0.83	0.72	0.83	0.72
Zr/Sm_{PM}	1.21	1.08	1.22	0.97	0.97	1.08	0.94	1.16	0.94
Zr/Nd_{PM}	1.01	0.90	1.05	0.78	0.76	0.92	0.80	0.86	0.80
Ti/Ti*	0.99	0.80	1.17	1.05	1.08	1.25	1.06	1.55	1.04
Ti/Gd_{PM}	2.41	1.54	2.24	3.12	3.01	3.53	3.02	3.50	2.84
Ti/Sm_{PM}	0.94	0.74	1.04	0.93	0.93	1.03	0.91	1.13	0.87
Nb/Nb*	0.95	0.70	1.09	1.00	1.04	1.19	0.88	0.94	0.90
Nb/Th_{PM}	1.21	0.87	1.15	1.13	1.32	1.32	1.10	1.32	1.05
Nb/La_{PM}	0.75	0.56	1.02	0.89	0.83	1.07	0.71	0.67	0.76
Mg#	67	68	63	73	66	60	73	62	64
ΣLREE	42.31	29.14	45.70	43.79	56.22	25.70	44.70	36.05	33.27
ΣHREE	36.95	20.17	26.18	16.15	21.63	10.72	16.57	13.90	12.78

Group		**G3U**	
Reference		**Chapter 2**	
Sample	MG11-054	MG11-056	MG11-113
Easting (m)	379973	380048	378578
Northing (m)	6307114	6307163	6306250
DDH	MG11-25	MG11-38	MG11-48
Depth (m)	118	89	314
SiO_2	46.19	46.37	46.63
Al_2O_3	8.17	8.01	7.78
TiO_2	1.19	1.15	1.23
Fe_2O_3	13.63	13.86	13.56
MnO	0.34	0.33	0.24
MgO	19.86	18.72	17.57
CaO	10.27	11.11	12.54
Na_2O	0.21	0.25	0.24
K_2O	0.04	0.05	0.11
P_2O_5	0.11	0.16	0.12
LOI	6.8	6.19	5.99
Total	100	100	100
Ni	890	820	730
Cr	1500	1470	1330
Co	79	74	82
V	220	231	233
Sc	24	27	24
Cu	90.0	100	150
Zn	500	310	240
Mo	*n.d.*	*n.d.*	2.0
W	*n.d.*	*n.d.*	44.0
Sb	0.5	0.6	0.6
Sn	1.0	*n.d.*	1.0

Group		G3U	
Reference		Chapter 2	
Sample	MG11-054	MG11-056	MG11-113
Ba	3	6	17
Cs	*n.d.*	*n.d.*	*n.d.*
Rb	*n.d.*	*n.d.*	*n.d.*
Sr	91	75	143
Pb	*n.d.*	*n.d.*	9
Ga	13	13	14
Zr	60	61	67
Hf	1.6	1.8	1.7
Nb	6.0	6.0	5.0
Ta	0.4	0.4	0.4
Th	0.6	0.6	0.6
U	0.1	0.2	0.2
Y	10	12	11
La	6.5	8.6	6.0
Ce	17.3	21.5	15.8
Pr	2.39	2.83	2.09
Nd	11.1	13.8	10.3
Sm	2.7	3.4	2.8
Eu	1.00	1.00	0.91
Gd	2.8	3.3	2.8
Tb	0.4	0.6	0.4
Dy	2.4	3.0	2.6
Ho	0.5	0.6	0.5
Er	1.2	1.5	1.5
Tm	0.18	0.20	0.17
Yb	1.2	1.2	1.0
Lu	0.18	0.19	0.16

Group		G3U	
Reference		Chapter 2	
Sample	MG11-054	MG11-056	MG11-113
La/Sm_{CN}	1.55	1.63	1.38
Gd/Yb_{CN}	1.93	2.27	2.32
La/Yb_{CN}	3.89	5.14	4.30
Eu/Eu*	1.11	0.91	0.99
Ce/Ce*	1.08	1.07	1.09
Zr/Y	6.0	5.1	6.1
Ti/Zr	109	105	101
Al_2O_3/TiO_2	7	7	6
Zr/Nb	10	10	13
Zr/Zr*	0.64	0.52	0.72
Zr/Sm_{PM}	0.88	0.71	0.95
Zr/Nd_{PM}	0.66	0.54	0.80
Ti/Ti*	0.99	0.89	1.07
Ti/Gd_{PM}	2.59	2.52	3.21
Ti/Sm_{PM}	0.87	0.67	0.86
Nb/Nb*	1.10	0.96	0.95
Nb/Th_{PM}	1.32	1.32	1.10
Nb/La_{PM}	0.92	0.69	0.83
Mg#	74	73	72
ΣLREE	43.79	54.43	40.70
ΣHREE	16.06	19.29	17.33

VITA AUCTORIS

Name:	Michael William Philip Glendenning Jr.
Place of Birth:	Windsor, Ontario
Year of Birth:	1985
Education:	University of Windsor, Windsor, Ontario 2005 to 2011 B.Sc. University of Windsor, Windsor, Ontario 2011 to 2014 M.Sc